GAS CONTAMINATION IN DISCHARGE EXCITED KRF AND ATOMIC FLUORINE LASERS

T. Govindanunny

A Thesis Submitted for the Degree of PhD
at the
University of St Andrews

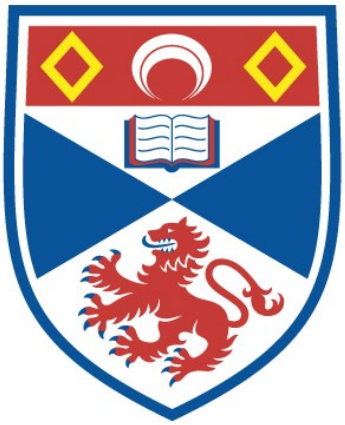

1984

GAS CONTAMINATION IN DISCHARGE EXCITED KrF AND ATOMIC FLUORINE LASERS

A thesis presented by

Govindanunny T, MSc

to the

University of St Andrews

in application for the degree of

Doctor of Philosophy

July 1983

ProQuest LLC.
789 East Eisenhower Parkway
P.O. Box 1346
Ann Arbor, MI 48106 – 1346

DECLARATION

I hereby certify that this thesis has been composed by me, and is a record of work done by me, and has not previously been presented for a higher degree.

This research was carried out in the Physical Sciences Laboratory of St Salvator's College, in the University of St Andrews, under the supervision of Dr A Maitland.

CERTIFICATE

I certify that Govindanunny T MSc has spent nine terms at research work in the Physical Science Laboratory of St Salvator's College, in the University of St Andrews, under my direction, that he has fulfilled the conditions of Ordinance No16 (St Andrews) and that he is qualified to submit the following thesis in application for the Degree of Doctor of Philosophy.

A Maitland

Research Supervisor

AUTHOR'S CAREER

Born in Kerala, South India, in 1953. Primary and secondary education in schools in Kerala. Pre-degree (1968-1970) in Maharaja's College of the University of Kerala, and BSc (1970-1973) in Union Christian College, University of Kerala. Masters degree in Science (1973-1975) from the Indian Institute of Technology, Madras, specialising in Laser Technology, Operations Research, and with Physics of Semiconductors as the elective subject. From 1975 till 1979, research work in the Physics department of the Indian Institute of Technology, Madras, in nitrogen and dye lasers. Part of this work was done in the capacity of Research Assistant for the Department of Science and Technology of the Government of India. From 1980 onwards, the author has been working in the department of Physics, University of St Andrews, in the field of discharge excited excimer lasers.

ACKNOWLEDGEMENT

I wish to thank Dr A Maitland for all his help, encouragement, and advice throughout this work. I gratefully acknowledge many helpful discussions with members of the Physics department, in particular, with Ms B Duval, R McRaw, M Whyte, and M Robertson. Finally, I would like to thank the University of St Andrews for the award of the University Research Scholarship, without which this work would not have been possible.

ABSTRACT

This thesis deals with gas contamination problems in atomic fluorine and KrF lasers. Five different versions of transverse electric discharge lasers were constructed using different materials, geometries, and discharge circuits. Three of these were investigated in detail for lifetime performance of a single fill of $He-F_2$ mix (atomic fluorine laser) and of $He-Kr-F_2$ mix (KrF laser). This was done using an on-line quadrupole mass spectrometer. The evolution of the various gas components appearing in the mix was calculated from the mass spectra of the gas mixture recorded at intervals when the laser was operated at one pulse per second. The impurity or contaminant species (ie species other than He, Kr, F_2) were found to be the same in all the lasers, differing only in their concentrations. The major contaminants found were CO_2, N_2, O_2, COF_2, CF_4, SiF_4, HF, CO, NO, SF_6, and H_2O. Of these, CO_2 was identified as the most deleterious impurity for both atomic fluorine and KrF lasers, reducing their output energy and the fluorine content, thereby reducing the single fill lifetime of the mix. A simple cold trap decreased the partial pressures of most of the detected impurities in the gas mixture and resulted in a marked increase in the number of shots to half energy and a decrease in the depletion rate of fluorine by half in both KrF and atomic fluorine lasers. To isolate and quantify the effects of individual contaminant species, they were deliberately added singly to the pure gas mix. These experiments confirmed that CO_2 was the most important impurity and that H_2 and CF_4 were the least harmful. Since the impurities were found to influence arcing of the discharge, they must affect preionization and/or discharge processes. Absorption effects were found to be insignificant in the regions of the laser wavelengths (248 nm,

730 nm). In order to quantify the effect of the impurities an effectiveness constant for each contaminant has been defined and used in a simple model which successfully calculates the laser output energy. This model has circumvented the problems arising from the physical complexity of the system and the lack of data on the various kinetic processes. The calculations show that CO_2 impurity depletes the energy output of the KrF laser at the rate of 0.9 mJ/ppt(wrt He).

CONTENTS

1 INTRODUCTION 1

1.1 Spectroscopy of KrF and fluorine 3

1.2 Pumping Schemes 5

1.2.1 E-beam pumping 5

1.2.2 E-beam controlled discharge pumping 7

1.2.3 Avalanche discharge pumping 9

1.3 Formation and quenching kinetics 13

1.3.1 KrF laser 13

1.3.2 Atomic fluorine laser 20

1.4 Stable species and gas-fill lifetime 21

1.5 Theoretical and experimental studies 23

1.5.1 Theoretical studies of KrF 23

1.5.2 Experimental studies of KrF 25

1.5.3 Theoretical and experimental studies on F2 lasers 26

1.6 Applications 27

1.7 Outline of the thesis 27

REFERENCES 29

CONTENTS

2 DESIGN CONSTRUCTION AND PERFORMANCE OF TEA LASERS 34

2.1 The fast transverse electric discharge 35

2.2 The LCI and uCT circuits 36

2.3 Preionizing methods 38

2.4 Design of the laser body 40

2.5 Constructional details and performance 41

2.5.1 Laser version 1 41

2.5.2 Laser version 2 43

2.5.3 Laser version 3 44

2.5.4 Laser version 4 46

2.5.5 Laser version 5 47

2.6 Gas handling system 47

2.7 Power supply and trigger circuits 48

2.8 Diagnostic instrumentation 49

REFERENCES 50

CONTENTS

3 THEORY AND INTERPRETATION OF MASS SPECTRA 51

3.1 The quadrupole mass spectrometer 52

3.2 Gas sampling technique 54

3.3 Interpretation of mass spectra (theory) 56

3.3.1 Cracking patterns and sensitivities 56

3.3.2 Background mass spectrum 57

3.3.3 Identification of compounds in the gas sample 57

3.4 Practical interpretation of mass spectra 59

3.4.1 Mass spectrometer background spectra 60

3.4.2 Cracking patterns in the Supavac 62

3.4.3 Measurement and reproducibility errors 65

3.5 Fluorine passivation of the Supavac 67

3.6 Presentation of results 68

REFERENCES 69

CONTENTS

4 IMPURITY FORMATION IN ATOMIC FLUORINE LASERS 70

4.1 The nature and effect of impurities 71

4.2 Impurities in pure He discharges 71

4.2.1 He fill without discharge 72

4.2.2 He fill with discharge 74

4.3 Impurity species in He-F2 gas fills 75

4.3.1 Variability of impurity in an initial fill 75

4.3.2 Impurity evolution in He-F2 fills without discharge 78

4.3.3 Impurity evolution in He-F2 fills with discharge 80

4.4 Effect of cold traps on He-F2 gas lifetime 87

4.4.1 Impurity evolution in LV3 with cold trap 87

4.4.2 Impurity evolution in LV4 with cold trap 89

4.4.3 Comparison of cold trapped LV3 and LV4 91

4.4.4 Mass spectral analysis of cold trap contents 92

4.4.5 IR analysis of cold trap contents 93

4.5 Conclusions 93

REFERENCES 96

CONTENTS

5 GAS LIFETIME AND IMPURITY EVOLUTION IN KrF LASERS 97

5.1 Impurity evolution in He-Kr-F2 mixtures 98

5.2 Effect of cold trap on He-Kr-F2 mix lifetimes 101

5.2.1 Lifetime of a He-Kr-F2 mix with a cold trap 102

5.2.2 Cold trap temperature dependence of KrF laser energy 106

5.2.3 Mass spectrum of cold trap contents 108

5.3 KrF laser revival by addition of fluorine 109

5.4 Comparison of KrF laser in versions LV4 and LV5 110

5.5 Conclusions 111

REFERENCES 113

CONTENTS

6 PERFORMANCE OF FLUORINE AND KrF LASERS WITH ADDED IMPURITIES 114

6.1 Impurity addition to He-F2 mixtures 115

6.1.1 Impurity evolution in doped He-F2 mixtures 115

6.1.2 Effect of dopants on F2 laser energy output 122

6.2 Impurity addition to He-Kr-F2 mixtures 124

6.2.1 Impurity evolution in doped He-Kr-F2 mixes 125

6.2.2 Effect of dopants on the KrF laser energy and lifetime . . .128

6.3 Role of impurities in the gas mixtures 129

6.4 Calculation of effectiveness constants for the impurities 133

6.5 Conclusions 138

REFERENCES 140

CONTENTS

7 CONCLUSIONS 141

7.1 The mass spectrometer as an analytical tool 142

7.2 Choice of construction materials for a laser 144

7.3 Use of cold traps to extend laser lifetime 145

7.4 Impurity addition to study impurity evolution 146

7.5 Impurity evolution and pulse repetition rate 147

7.6 Theoretical analysis of experimental results 148

REFERENCES 150

CONTENTS

Appendix A.1 i

Appendix A.2 viii

Appendix A.3 xi

Appendix A.4 : Design of a long lifetime single fill laser xiv

REFERENCES xviii

CHAPTER 1

INTRODUCTION

The KrF rare gas laser is the most efficient excimer laser reported to date. The laser action in rare gas monohalides was predicted by Ewing and and Brau (1975a) and by Velasco and Setser (1975) and was observed in 1975 by Ewing and Brau. The KrF and other excimer lasers show promises of being scalable to higher powers and energies. The KrF laser has been made to operate by electron beam and discharge pumping, with pulse repetition rates reaching 1kHz. The laser output occurs at 249 nm. With e-beam pumping efficiencies of over 9% and energies of a few hundred Joules are possible. This makes it a more attractive pump source than the low energy nitrogen laser for pumping dyes to extend the tunability into the uv and to increase tunable output energies. Much research has been carried out on the KrF and other rare gas halide lasers since they promise to be potential candidates for high energy high efficiency lasers. The growth of excimer technology has been faster than any other laser technology. The reliability and cost effectiveness of excimer lasers, including the KrF laser, make them ideal candidates for applications in chemistry, plasma and fusion physics, remote sensing, spectroscopy, material processing etc. One type of excimer laser uses a transverse electric (TE) discharge to pump the gas mix. This method is simple, reliable and is capable of exciting many other

gas mixes apart from excimer mixes. The atomic fluorine laser uses a two component gas mix (F_2 and Helium) and can be excited using the same TE discharge laser used for the KrF excimer mix. The output wavelengths are in the 700-750 nm region and pulse energies of a few mJ are possible. The F_2 laser is a cheap, reliable and reasonably efficient pump source for near IR dye lasers.

Despite vast improvements in their performance and reliability, the basic disadvantage of KrF and F_2 lasers is the limited lifetime of the gas mix, which necessitates refilling the laser with fresh mix after several hours of operation. This is mainly due to the high reactivity of the halogen donor, which is usually pure F_2 in the case of KrF laser. Extension of single fill lifetimes of the gas mix can be achieved if one knows what stable impurities are produced in the gas mix as a result of the discharge. In this thesis we report on the studies of stable species production in the laser gas mix for the F_2 and KrF laser using F_2 as the halogen donor. The quadrapole mass spectrometer is chosen as the diagnostic tool to identify the gas impurities formed in the laser and to measure their partial pressures as a function of time. Changes in the power output and single fill gas lifetime after deliberate introduction of some of the impurities thus identified are also studied for both lasers. Such systematic investigations have not been reported before in the literature.

This chapter is introductory and outlines KrF, F_2 laser principles, design, excitation mechanisms, reaction kinetics, stable impurity formation and the diagnostic methods used to study them.

1.1 Spectroscopy of KrF and fluorine

The spectra of rare gas monohalides were reported in 1974 by Golde and Thrush. Ewing and Brau (1975a) predicted the uv spectrum of KrF by comparison with the spectrum of the corresponding alkali halide RbF. Theoretical calculations of KrF has been carried out using ab initio methods (Dunning and Hay 1976, Hay and Dunning 1977). The KrF emission was experimentally studied by Tellinghuisen et al (1976). The spectroscopy of rare gas halide molecules has been treated in detail by Brau (1979). The schematic potential energy diagram is given in fig.1.1 . The ^1S rare gas and ^2P halogen atoms covalently bond to form the ground state. The upper level is derived from the ^2P rare gas positive ion and ^1S halogen negative ion and forms an ionically bound charge transfer state. As the internuclear distance decreases, the states split into 2Σ and 2Π states. The structure of the ground level and upper level manifold is similar due to the similarity in the species forming the upper and ground levels. The levels are labelled X,A,B,C,... in terms of increasing energy. Laser transition is from $B\ ^2\Sigma_{1/2}$ to $X\ ^2\Sigma_{1/2}$.

The fluorescence lifetime T of $B\,^2\Sigma \rightarrow X\,^2\Sigma$ transition for KrF has been theoretically calculated to be 6.5 nsec by Dunning and Hay (1976) and 7 nsec by Hay and Dunning (1977). This agrees well with the experimental value of 9 nsec (Burnam and Searles 1977) measured in a pulsed photolysis experiment.

Calculation of the stimulated emission cross section σ has been carried out using experimental data for o T and T by Tellinghuisen et al (1976). They got a value of 2.6×10^{-16} cm for σ(KrF) using T = 6.5 nsec. Using the measured value of 9 nsec we get σ(KrF)=2×10^{-16} cm. This is a large value compared to o for other laser transitions. For transitions to the A state the matrix elements and hence the cross sections were found to be very small. They are of negligible importance, especially for small laser systems (Dunning and Hay 1976, Hay and Dunning 1977). Other transitions in KrF are mainly due to excited state absorptions and will be discussed later.

The atomic fluorine laser transitions occur in the $2p^4 3p \rightarrow 2p^4 3s$ manifold of F^* and was shown to be stimulated in pulsed discharges of fluorine donors in helium (Kovacs and Utlee 1970, Jeffers and Wiswall 1970, Florin and Jensen 1971, Sutton et al 1975). There are 27 different transitions to the $2p^4 3s$ state allowed by selection rules and differing in wavelength (Sadighi-Bonabi et al 1982). They cover the red end of the spectrum from 623.9 to 780.0 nm. Transition probabilities for 3s -> 3p in fluorine have been experimentally determined (Bengtson et al 1971).

Table 1.1 Spectroscopic Data for KrF

Transition wavelength:		249nm (Tellinghuisen et al 1976)
Internuclear sep.	:	2.3Å (Brau and Ewing 1975)
B state vibr. rreq.	:	310 cm^{-1} (Tellinghuisen et al 1976)
σ T	:	17 Ånsec (" ")
T	:	9 nsec (Burnam and Searles 1977)

1.2 Pumping Schemes

The gas composition, kinetics, energy inputs and efficiencies of rare gas halide lasers depend upon the pumping scheme used to create the excited state rare gas halides. There are three main ways of pumping rare gas halides: 1. e-beam pumping, 2. e-beam controlled discharge pumping and 3. avalanche discharge pumping.

1.2.1 E-beam pumping

This can be called a brute force method. Relativistic high energy e-beams are used to pump a mixture of Argon, Krypton and F_2 at a total pressure of 1-3 atm and typical composition of 90% Ar,<10% Kr and <0.5% F_2. Ewing and Brau (1975) were the first to use e-beam pumping with KrF, and they initially got an efficiency of 0.4% (Ar:Kr:F_2 as 98.9:1.0:0.1). Other rare gas halides were also pumped using the same scheme (Searles and Hart 1975, Brau and Ewing 1975, Ault et al 1975). Pumping by e-beam is relatively

straightforward and eliminates problems of discharge stability compared to discharge pumped lasers. But because of the low pressures (1 - 3 atm) used, the stopping power of the gas on the electrons is less, and a lot of the incident energy is wasted on the container walls. To increase energy deposition, externally applied magnetic fields have been used (Hoffman et al 1976). Another cause of reduced efficiencies is the way in which the excited state excimer halides are formed. Electron beam pumping favours the ionic route for the formation of KrF^* states whereas discharge pumping favours the metastable route. The latter requires less excitation energy per molecule and is more efficient. The higher energy route for e-beam pumping limits the quantum efficiency of formation of KrF to about 25% in e-beam pumped lasers (Hutchinson 1980). The best efficiency for e-beam pumping has been obtained with a KrF laser: 15% intrinsic, 1% overall (Bhaumic et al 1976). They obtained 125 nsec pulses of 1.5 J using a coaxial e-beam laser. The highest energy obtained by e-beam pumping was again for KrF - 350 J using transverse excitation (Hunter 1977).

The schematic of an e-beam laser is given in fig 1.2 . A cold cathode electron source is connected to a pulsed high voltage supply, usually a Marx bank generator. The current density of the e-beam is around 10 amp/sqcm. The anode is a slotted metal structure carrying a thin metal or plastic foil to isolate the diode vacuum from the laser cavity. In this configuration the gas mixture is transversly excited. Mirrors M1 and M2 form the laser cavity.

The main limitations which prevent the scaling up of e-beam pumped devices are foil heating, diode closure and beam pinching. Beam pinching can be reduced using external magnetic fields (Hoffman et al 1976). Foil heating and diode closure cannot be overcome easily.

In the cavity itself there are losses due to the formation of rare gas ions which absorb in the uv. Thus considering all the losses the efficiency is restricted to about 6% for e-beam pumped lasers compared to about 15% for pure discharge lasers (Ewing 1978).

1.2.2 E-beam controlled discharge pumping

The first rare gas halide laser to be pumped using an e-beam controlled discharge was KrF (Mangano and Jacob 1975). These lasers are potentially more efficient and can be scaled up to higher powers compared to pure e-beam excited lasers. They can also be worked at higher repetition rates. The efficiency is higher because beam energy losses are less, electron losses due to scattering in the foil and gas are reduced, and there is a possibility of producing metastable states more efficiently. This is because a volumetrically stable discharge is produced by using e-beams as the ionising source in the discharge. A discharge model for the e-beam controlled discharge was proposed by Jacob and Mangano (1976). Their model predicted that rare gas metastables could be produced with 75% efficiency and rapid ionisation in rare

gas halogen mixtures could be balanced by attachment to give long stable discharge pulses. Daugherty et al (1976) derived this stability criterion for discharges where two step ionization is important. In KrF they found that two step ionization is dominant. If equilibrium is to be maintained in a discharge, the attachment rate has to be greater than or equal to twice the ionization rate. In the e-beam controlled discharge the difference is made up by the e-beam which acts as the external ionising source. The pumping power can then be increased by a factor of 5 to 10 compared to e-beam pumping (Daugherty et al 1976). For KrF, the efficiency is ~ 0.5%, about twice that achieved by e-beam pumping alone. The plasma impedence is constant, which makes for efficient coupling between the discharge circuit and the plasma (Hutchinson 1980). For high output energies and long pulses of usec duration, this pumping scheme is better than e-beam pumping.

A schematic diagram of the e-beam sustained discharge laser is given in fig 1.3 .

The highest pulse energy reported with the e-beam controlled discharge type of excitation is 50 J in KrF (0.3 usec pulse) with an efficiency of 3% (Hunter 1977).

1.2.3 Avalanche discharge pumping

The main advantages of discharge pumped lasers are their simplicity in construction and potential high efficiencies in operation. However, discharges are fundamentally unstable due to the growth of non-uniformities in the discharge to form steamers and arcs. For a successful laser these non-uniformities should be either suppressed or all the required energy should be fed into the gas before the arcs and streamers can develop. Fast transverse discharges attempt to do the latter, and can be constructed in a relatively simple way. Burnam et al (1976) first tried fast discharges on XeF using a transverse pulsed discharge with risetimes of 20 nsec. Sutton et al (1976) obtained 0.8 mJ in 25 nsec FWHM laser pulses from a fast discharge in KrF using a Blumlein type construction. McKee et al (1977) achieved diffraction limited performance in a KrF laser excited by a fast Blumlein circuit with stored energy of 5 J. The output energy was 50 mJ and power was 5 MW. Wang (1976) used a fast Blumlein device with a discharge duration of 10 nsec and an output of 1.6 mJ, obtaining an efficiency of 0.5%. Goddard and Vannier (1976) used relatively low voltages (<10 KV) in a Blumlein type fast discharge and obtained 1 MW, 4 nsec pulses using KrF, with a repetition rate of 100 pps and wallplug efficiencies of ~ 0.4%. Sze and Scott (1976) used a fast helical-pin discharge to get high quality beams from KrF with an average energy of 50 μJ.

The technique of preionization has been used in various ways to inhibit the growth of discharge non-uniformities. Burnam et al (1976a) used a simple preionising wire along the length of the discharge. Burnam and Djeu (1976) used a sparkboard to produce uv photons just before the initiation of the discharge. These photons caused volume preionization of the laser gas mixture. A flash board was used by Andrews et al (1977) to uv preionize the discharge volume. Sutton et al (1976) and Hasson et al (1977) used a corona discharge technique to preionize the gas. The corona blades formed part of the main electrodes, and the discharge started as soon as the electron density in the gas and the voltage across the main electrodes reached a sufficiently high value. Ishchenko et al (1977) used an auxilary discharge to produce the photons for uv preionization outside the cavity and optical coupling to the gas was through the cavity walls. A 1/4 J KrF laser was designed by Fahlen (1979) with corona preionization. He also used a hydrogen thyratron to get high pulse repetition rates (Fahlen 1978). The main difference between flashboard preionization and corona preionization is in the absence of an auxilary spark gap and time delay techniques for the latter, thus making its construction easier. Another preionising technique was used by Hasson and von Bergman (1979) to excite excimer halide lasers. The preionizer, made out of fibreglass-epoxy circuit board, was capacitively coupled to the main electrodes in their device. It required no separate switching or timing circuits. Schemes similar to the ones described above have been used by Watanabe et al (1979), Sze and Scott (1978), McKee et al (1979),

Taylor et al (1978) and Hsia (1977). The main disadvantage of corona and flashboard preionization is their low penetration depth. This decreases the volume of gas efficiently preionized. To overcome this defect preionization using x-rays and surface discharges has been used to get larger volume discharges and thus larger output energies (in the joule range). Levatter and Lin (1980) used x-ray preionization along with a water capacitor Blumlein discharge circuit and a fast rail gap switch to get energies of several joules in 100 nsec pulses from a XeCl laser. Dielectric surface discharges have been used by Baranov et al (1981) to yield large volume KrF discharges with specific output energies of 5.8 J/litre and total energies of 7 J at 1.5% efficiency.

The mechanism of preionization is still not clearly understood. The impurities in the gas can be ionized by uv photons formed near the preionizer, and the electrons attach to the halogen to form negative ions (Seguin et al 1974, Babcock et al 1976). The more uniform discharge could then be started by the unattached electrons and negative ions (Sze et al 1976, Hsia 1977). Without preionization the pulse length is limited to about 30 nsec for pressures less than 2 atm and less for higher pressures (Burnam et al 1976, Hasson et al 1977, Sutton et al 1976, Wang 1976, Mckee et al 1977). The output power from a KrF laser was shown to depend upon the number of electrons initially present in the discharge despite the fact that the energy deposited in the gas mix was independent of the preionization energy (Sumida et al 1981, Sze and Loree 1978).

Superradiant emission from the atomic fluorine system can be obtained by using the same excimer setup as for KrF by changing the gas mix. Many lines are emitted and there is little control over their relative intensities.

Because of difficulties in coupling the energy from the electrical source to the discharge, efficiencies of more than 2% are difficult to obtain in the case of a KrF laser (Burnam and Djeu 1976). Fahlen (1979) obtained an overall efficiency of 1.3% at a pulse rate of 2 pps and an output of 250 mJ for a KrF laser with corona preionization. Burnam and Djeu (1976) obtained 1.4% intrinsic efficiency in a 130 mJ KrF laser using a lumped element L-C inversion voltage doubling circuit. As yet there are no reports on efficiencies obtained for atomic fluorine lasers excited using a TE discharge.

1.3 Formation and quenching kinetics

1.3.1 KrF laser

In general one would expect the formation and quenching of KrF^* molecules to depend on the gas mix ratios, pressures, the type of buffer gas, the halogen donor gas, and the type of excitation used to produce the discharge. Studies so far indicate that the basic channels of energy transfer into the KrF^* state from the electron beam or discharge remain the same for a wide range of gas compositions and pressures. Rokni et al (1978), Brau (1979), and Hutchinson (1980) have reviewed the kinetics of KrF lasers under electron beam and discharge pumped conditions. A detailed study of the physics of the KrF laser has been published by Johnson and Hunter (1980). They describe the KrF laser as essentially a one level laser since it has several entrance channels to the upper level and a negligible population in the lower level. A typical electron beam pumped KrF laser mixture consists of about 90% of the buffer gas (Ar, Ne or He) , about 10% of Kr and about 0.5% of F_2 at total pressures of a few atmospheres. The upper level can be formed either directly from the ionic Kr^+ and F^- or by curve crossing from the ionic states into the KrF^* covalent state at

large (0.5 - 1 nm) internuclear separations. The three dominant reactions of KrF^* formation are

1. Harpooning: $Kr^* + F_2 \rightarrow KrF^* + F$
2. Displacement: $ArF^* + Kr \rightarrow KrF + Ar$ (Ar buffer)
3. Neutralisation: $Kr^+ + F^- + M \rightarrow KrF^* + M$

The ionic channel 3 is less efficient than the neutral channels 1 and 2 since the latter require less energy to form the metastable Kr^* and Ar^*. It was shown by Johnson and Hunter (1980) that high energy e-beam pumping and high pressure (>3 atm) self sustained discharges favour the ionic channel to form KrF^* molecules. E-beam controlled discharges can be tailored to give the most efficient excitation conditions. Theoretical studies of KrF lasers in a uv preionized TE discharge using He buffer gas showed that the efficiency of excitation of Kr^* was sensitive to the discharge voltage, reaching a peak of about 45% at E/n of 1.5×10^{-16} V-cm^2. Sze and Scott (1976) used a fast helical pin discharge to excite a KrF laser with Helium as the buffer gas. They postulated that apart from a discharge stabilizing function, He^+ was also involved in charge exchange collisions with Kr and three body Thompson recombination collisions with F^-, which could be a dominant formation path for KrF.

Johnson and Hunter (1980) have compiled a detailed list of the various formation and quenching rates including absorption processes in a KrF laser. Schematic diagrams describing the neutral and ionic channels of formation of KrF^* are given in fig

1.4a and 1.4b respectively (Huestis and Lorents - see Lorents 1978). The rate constants for the reactions labelled in fig 1.4 are given in table 1.2.

Table 1.2

No	Reaction	Rate constant
1	$Kr^* + F_2 \rightarrow KrF^* + F$	8.1×10^{-10} cm^3/sec
2	$ArF^* + Kr \rightarrow KrF^* + Ar$	3.0×10^{-10} cm^3/sec
3	$Kr^+ + F^- \rightarrow KrF^*$	1.0×10^{-6} cm^3/sec
4	$Ar^* + F_2 \rightarrow ArF^* + F$	8.5×10^{-10} cm^3/sec
5	$Ar^+ + F^- \rightarrow ArF^*$	1.0×10^{-6} cm^3/sec
6	$Kr_2^+ + F^- \rightarrow KrF^* + Kr$	1.0×10^{-6} cm^3/sec
7	$Ar_2^+ + F^- \rightarrow ArF^* + Ar$	1.0×10^{-6} cm^3/sec
8	$ArKr^+ + F_2 \rightarrow KrF^* + Ar + F$	6.0×10^{-10} cm^3/sec
9	$KrF^* + 2Ar \rightarrow ArKrF^* + Ar$	8.0×10^{-10} cm^3/sec
10	$ArF^* + 2Ar \rightarrow Ar_2F^* + Ar$	5.0×10^{-10} cm^3/sec
11	$Kr + ArKrF^* \rightarrow Kr_2F^* + Ar$	2.0×10^{-11} cm^3/sec
12	$KrF^* + Kr + Ar \rightarrow Kr_2F^* + Ar$	6.5×10^{-31} cm^6/sec
13	$Kr_2^* + F_2 \rightarrow Kr_2F^* + F$	3.0×10^{-10} cm^3/sec
14	$Kr_2^* + F \rightarrow KrF^* + Kr$	3.0×10^{-10} cm^3/sec
15	$Ar_2^* + F_2 \rightarrow Ar_2F^* + F$	2.5×10^{-10} cm^3/sec
16	$Ar_2^* + F \rightarrow ArF^* + Ar$	3.0×10^{-10} cm^3/sec
17	$Ar_2F^* + F_2 \rightarrow 2Ar + F + F_2$	1.0×10^{-9} cm^3/sec
18	$Ar_2F^* + Kr \rightarrow ArKrF^* + Ar$	1.0×10^{-10} cm^3/sec
19	$ArKr^* + Kr \rightarrow Kr_2^* + Ar$	1.0×10^{-10} cm^3/sec
20	$Kr^* + 2Ar \rightarrow ArKr^* + Ar$	1.0×10^{-32} cm^6/sec
21	$Ar^* + 2Ar \rightarrow Ar_2^* + Ar$	1.14×10^{-32} cm^6/sec

22	$Kr^* + Kr + Ar \rightarrow Kr_2^* + Ar$	1.0×10^{-32} cm^6/sec
23	$Ar^* + Kr \rightarrow Kr^* + Ar$	6.2×0^{-12} cm^3/sec
24	$Ar_2^* + Kr \rightarrow Kr^* + 2Ar$	4.0×10^{-10} cm^3/sec
25	$Ar^+ + 2Ar \rightarrow Ar_2^* + Ar$	2.5×10^{-31} cm^6/sec
26	$Ar_2^+ + Kr \rightarrow Kr^+ + 2Ar$	7.5×10^{-10} cm^3/sec
27	$Kr^+ + 2Ar \rightarrow ArKr^+ + Ar$	1.0×10^{-31} cm^6/sec
28	$ArKr^+ + F^- \rightarrow ArKrF^*$	1.0×10^{-6} cm^3/sec
29	$ArKr^+ + Kr \rightarrow Kr_2^+ + Ar$	3.2×10^{-10} cm^3/sec
30	$Kr^+ + 2Kr \rightarrow Kr_2^+ + Kr$	2.5×10^{-31} cm^6/sec
31	$Ar^+ + Kr \rightarrow Kr^+ + Ar$	3.0×10^{-11} cm^3/sec
32	$Kr^+ + Kr + Ar \rightarrow Kr_2^+ + Ar$	2.5×10^{-31} cm^6/sec

The quenching of KrF^* molecules by various other constituents of the gas is one of the causes in reducing the efficiency of KrF^* lasers. From a study of the spontaneous emission spectra of KrF^* emission Rokni et al (1977) and Jacob et al (1975) have calculated the quenching constants for the KrF^* laser (See table 1.2). The three body quenching of KrF^* by Ar and Kr gives

$$KrF^* + Ar + Ar \rightarrow ArKrF^* + Ar$$
$$ArKrF^* + Kr \rightarrow Kr_2F^* + Ar \quad \text{or}$$
$$KrF^* + Kr + Ar \rightarrow Kr_2F^* + Ar \quad \text{or}$$
$$KrF^* + Kr + \{M\} \rightarrow Kr_2F^* + \{M\}$$

Brau (1979) estimated the direct formation of KrF^* to be quite fast and the formation of $ArKrF^*$ to be an order of magnitude slower. When He is used as a buffer gas, KrF^* can be quenched as follows (Greene and Brau 1978):

$$KrF^* + Kr + He \rightarrow F + 2Kr + He$$
$$KrF^* + Kr + He \rightarrow F + Kr + 2He$$

At lower pressures the halogen species rapidly quenches KrF^* by the reaction (Mangano et al 1977):

$$KrF^* + F_2 \rightarrow Kr + 3F$$

In the KrF laser, formation kinetics all start with F_2 molecules. Since the recombination rate of F to F_2 is relatively small, the laser pulse energy cannot exceed one photon per initial F_2 molecule (Brau 1979).

Apart from molecular quenching processes, reabsorption of KrF radiation due to other species also reduce the lasing efficiency. Rokni et al (1978) points out that NF_3 as a fluorine donor is not as efficient as F_2 despite the fact that NF_3 does not absorb KrF^* radiation. This is because Kr^+ can charge transfer to NF_3 to form NF_3^+ thus constituting a loss process.

Laser action has been observed with SF_6 and CF_4 as fluorine donors and He as the buffer gas despite the fact that rate constants for the reactions

$$Kr^* + SF_6 \rightarrow KrF^* + SF_5$$
$$Kr^* + CF_4 \rightarrow KrF^* + CF_3$$

are practically zero (Rothe and Gibson 1977). Rothe and Gibson proposed that, in the case of self sustained KrF^* or XeF^* lasers, the metastables play a less dominant role. Their results showed that adding up to 20% Ar to the KrF gas mixture using He as the buffer gas did not change discharge characteristics or increase lasing efficiency. The reactions

$$Kr^+ + F^- + He \rightarrow KrF^* + He$$

$Kr_2^+ + F^- \rightarrow KrF^* + Kr$

were proposed as possible KrF^* formation paths (see also Ischenko et al 1977).

Sze and Loree (1978) found that the addition of 1% Ar to a mixture of 0.2% F_2, 5% Kr and the rest He at a total pressure of 2 atm increased the lasing energy by 20%. The pulse-to-pulse reproducibility was improved when they added 1% Ne to the basic mix. Fahlen (1979) also found the use of Ne as the buffer gas increased the uniformity of the discharge and the power output. The laser breakdown voltage was 20% greater with He than with Ne. This apparent contradiction in discharge behaviour when compared to that observed by Rothe and Gibson could be due to the different halogen donor gas used.

1.3.2 Atomic fluorine laser

It is only recently (Collins et al 1980) that the excitation mechanism of the F_2 laser has become reasonably clear. The pumping sequence is:

$F_2 + e \rightarrow F^- + F$

$He_2^+ + F^- \rightarrow F^*(3p) + 2He$

No work has yet been reported on the quenching kinetics or absorption processes in an F_2 laser.

1.4 Stable species and gas-fill lifetime

In the case of "sealed-off" laser operation the lifetime of the gas mixture depends on the stable reaction products formed in the cavity. These products are formed mainly due to the interaction of halogen with the electrodes, the cavity walls and the output windows. The stable products are detrimental in four ways: (1) they can irreversibly deplete halogen concentrations; (2) they can absorb at the lasing wavelengths; (3) they can quench the excited states; and (4) they can interfere with discharge stability by absorbing preionizing photons. Very few studies have been carried out to analyse the stable reaction products in a sealed-off excimer laser cavity. Gower et al (1980) used spectroscopic methods to analyse the stable species formed during the laser discharge. They found that NO_2, arising from impurities in the gas, formed one source of optical absorpion at laser wavelengths. Fluorine was depleted by the formation of SiF_4 with the glass walls. They concluded that high purity F_2 and a more compatible laser tube than glass should be used for long lived sealed-off rare gas fluoride operation. McKee et al (1979) identified CF_2 emission bands in a KrF laser which used F_2 as the halogen source gas. They applied extensive passivation procedures before laser operation. The output energy dropped typically by about 0.1% for every shot after passivation. A decrease in pulse energy with pulse rate has been observed by Fahlen (1978) for a sealed-off KrF laser but has not been explained. Miller et al (1979) detected an increasing concentration of HF and CF_3 in a closed loop flow KrF laser using a quadrapole mass spectrometer. These constituents were reported as

being detrimental to laser performance. Akerman and Tennant (1979) studied the effect on KrF gas-fill lifetime of impurities created due to the insulator and metal parts exposed to the gas mix and impurities likely to be present in the gases. Their results showed that Kel-F, Teflon, Kynar and Alumina were the least reactive insulators used. Impurities like air, HF, CO_2, C_3H_8 affect the KrF lasing efficiency. It was also reported that without gas cleanup the KrF laser operates for 20 minutes at 4 pps before the output energy drops to half the original value. Attempts to increase the lifetime of the gas mix by using cold traps and heated Titanium getters have been made with varying degrees of success (Johnson et al 1978, Burlamacchi et al 1979, Kutschke et al 1981, Mandl et al 1982). Addition of H_2 as a scavenger gas to remove impurities in XeCl, KrCl lasers was tried by McKee et al (1980). The lifetime of the gas mix was extended from slightly less than a million shots to more than three million shots to half power.

No reports have been yet published on the lifetimes of atomic fluorine lasers.

1.5 Theoretical and experimental studies

1.5.1 Theoretical studies of KrF

Various models for the excimer laser have been proposed and attempts have been made to simulate the excimer laser by analytically examining the relevant rate equations or numerically solving them on a computer. Burnam et al (1976a) studied a simple LCR equivalent circuit for the Blumlein-type fast discharge circuit. Their computations predicted that 70 - 80% of the energy stored in the capacitors is deposited in the discharge. A more detailed study of the uv preionized fast discharge laser was carried out by Greene and Brau (1978). In their kinetics model a uniform constant preionization was assumed. Their results predicted the major features of laser behaviour. Photoabsorption processes were shown to play an important role in reducing the laser output. The improvement in discharge uniformity observed in pure electric discharge pumped rare gas halide lasers in the presence of preionization is explained by a model in which F^- ions formed by dissociative attachment after uv photoionization act as an electron reservoir for the main discharge (Hsia 1977). Watanabe et al (1979a) analysed the amplification of KrF and ArF discharge lasers by numerical calculation which accounted for absorpion, pumping and spontaneous decay. The pulsewidth broadening predicted by the analysis was verified experimentally. Levatter and Lin (1980) developed an analytical model for a high E/n pulsed

avalanche discharge that included the effects of preionization, finite voltage risetime and variation of avalanche rate with applied electric field strength. Numerical results were developed for a XeF laser mixture and compared with experimental observations. They predicted that as long as a uniform strong preionization is present, there is no inherent limitations to the maximum volume or time for a homogeneous discharge, apart from slow development of thermal instabilities.

Simulation of electron beam sustained discharge lasers have been carried out by several authors. Jacob and Mangano (1976) used rate constants predicted by the Boltzman code to develop a self-consistent kinetics code that, coupled with the differential equations for the electrical circuit, gave the temporal evolution of the discharge current, voltage, and KrF^* fluorescence for a given preionization level, capacitor charge voltage, and gas mixture. The normalised predictions compared favourably with experiment. Daugherty et al (1976) found that two-step ionization is dominant for a KrF laser. Their analysis showed that the discharge is stable if the attachment rate is greater than or equal to twice the equilibrium ionization rate.

Boltzmann analysis of a KrF laser by Bradford et al (1976) showed that KrF metastable densities should be $\sim 10^{-6}$ of ground state population density, and for higher densities of KrF metastables, excited state absorptions and ionization become predominant. They also found analytically that optimum E/n to produce Kr^* was $\sim 6\times10^{-17}$ $V.cm^2$. Long (1979), Long and Bradford (1979)

investigated the discharge stability and electrical characteristics of an e-beam controlled discharge using a simple rate equation model. Their results showed that electron drift velocities were independent of F_2 concentration up to 0.35% , which are in agreement with experimental measurements. Johnson et al (1979) combined the many models and equations describing the kinetic and discharge processes and the Boltzmann equations were then solved, along with the equations for the physical optics to predict KrF^* e-beam sustained discharge laser performance. The results obtained agreed remarkably well with the experimental observations.

The theoretical models and analysis give only approximate predictions because of lack of knowledge of some of the important rate constants required for an accurate simulation. Before the models can be further refined, more information is necessary on the fundamental kinetic processes in the gas discharge along with accurate values of the rate constants and absorption cross sections from the various excited states.

1.5.2 Experimental studies of KrF

There have been very few systematic studies of the discharge characteristics and laser output as a function of the electrical characteristics of the discharge circuit. In their experimental studies on the KrF and ArF discharge laser, Sze and Loree (1978) changed the circuit parameters and the degree of preionization to investigate their effects on energy deposition and lasing. They

used a flashboard for preionization and found that the gas-fill lifetime was affected by the flashboard driving energy, with an optimum of 0.1 J (10 nf at 14 Kv) for KrF. Other experimental studies have investigated the effect of different halogen donors on power output and efficiency (Andrews et al 1977) and the effect of different types of spark gaps on the efficient pumping of KrF lasers (Kunitomo et al 1982).

Measurements of laser gain give a direct, absolute evaluation of the state of the medium, unmodified by resonators and independent of spectral characteristics of the detector. Many parameters like saturation behaviour, line narrowing, laser threshold, and output coupling depend upon the gain of the medium. Gain studies on e-beam pumped and discharge lasers have been carried out by various groups (Hasson et al 1977, Hawryluk et al 1977, Watanabe et al 1979, Patterson et al 1980, Edwards et al 1981, Gower and Edwards 1982).

1.5.3 Theoretical and experimental studies on F_2 lasers

Investigations on the F_2 laser have been mainly confined to the excitation mechanisms and spectroscopic details of output wavelength (Lawler et al 1979, Sumida et al 1979, Miller and Morgner 1977, Collins et al 1980). Measurement of small signal gains for transitions at 745 and 635 nm were done by Sadighi-Bonabi et al (1982). They found the gain was high, reaching 0.44 and 0.31 cm^{-1} respectively.

1.6 Applications

The applications of KrF and other excimer lasers have been recently discussed by McKee and Nilson (1982). The strong point in favour of excimer lasers is their high efficiencies when compared to other uv laser sources. Thus excimer lasers can be incorporated in any application requiring such sources of radiation. Excimer lasers can be used as a pump source for dye lasers to generate high efficiency tunable uv output. The F_2 laser could find promising applications as an efficient pump source for near ir dyes. Excimer lasers have been used in the surface treatment of semiconductor materials to produce high quality solar cells (Deutsch et al 1981). Vitamin D synthesis has been improved by using a KrF laser and nitrogen laser for two stage photolysis of 7DHC. In this method, competing photoreactions are suppressed and yield is increased to better than 90% (Malatesta et al 1981). These new high energy uv sources have enormous potential for applications in photochemistry.

1.7 Outline of the thesis

The rest of the thesis is organised in six chapters. Chapter 2 deals with the design, construction, and performance of the F_2 and KrF lasers used in the experiments. Each laser version is discussed in detail. The gas handling system, power supply, and the diagnostic instrumentation are also covered. Chapter 3 deals with the quadrapole mass spectrometer used for analysing the gas

mix in the laser. The practical interpretation of mass spectra, error analysis, and reproducibility of the results are discussed with regard to gas mixtures containing F_2. Chapters 4, 5, and 6 deals with the results obtained in analysing the mass spectra and the laser energy output of He-F_2 and He-Kr-F_2 mixes in the various laser versions. Chapter 4 deals with the He-F_2 mix including mass spectral and ir spectral analysis of cold trap contents. The KrF laser is dealt with in chapter 5. Chapter 6 covers the results obtained for both atomic fluorine and KrF lasers when impurities are added to a pure laser mix. These results are used in a black-box model to quantify the deleterious effects of the impurities. The results presented in these three chapters are summarised and possible directions of further research discussed in the last chapter. Based on the results, a design for a long-life high repetition rate atomic fluorine and KrF laser is given in the last chapter.

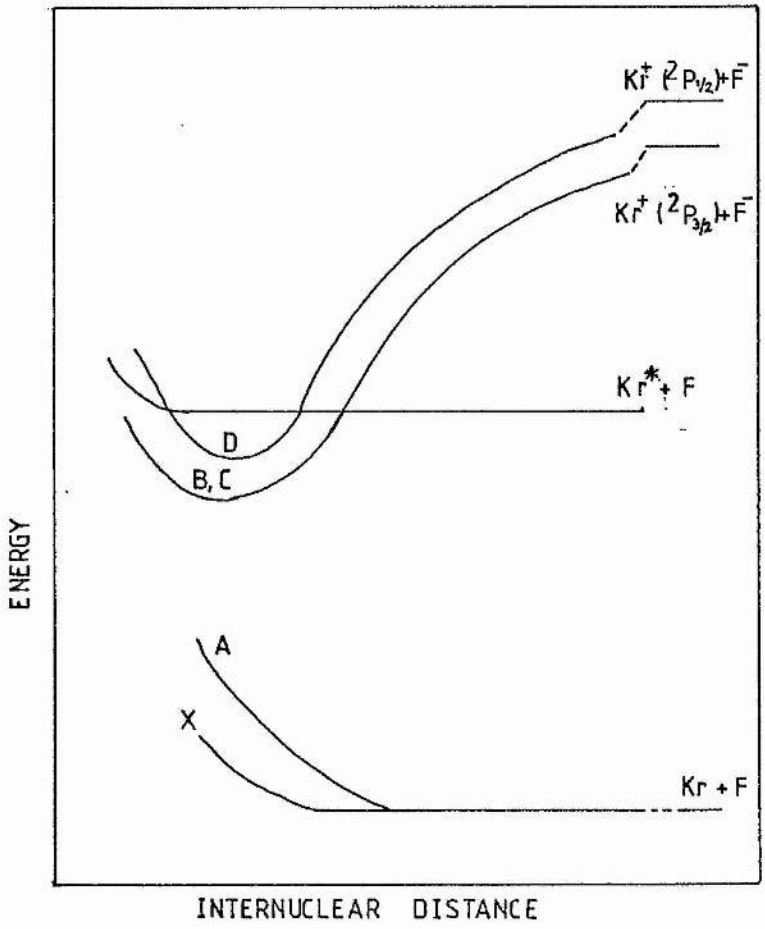

FIG 1.1 Energy level diagram for KrF^*

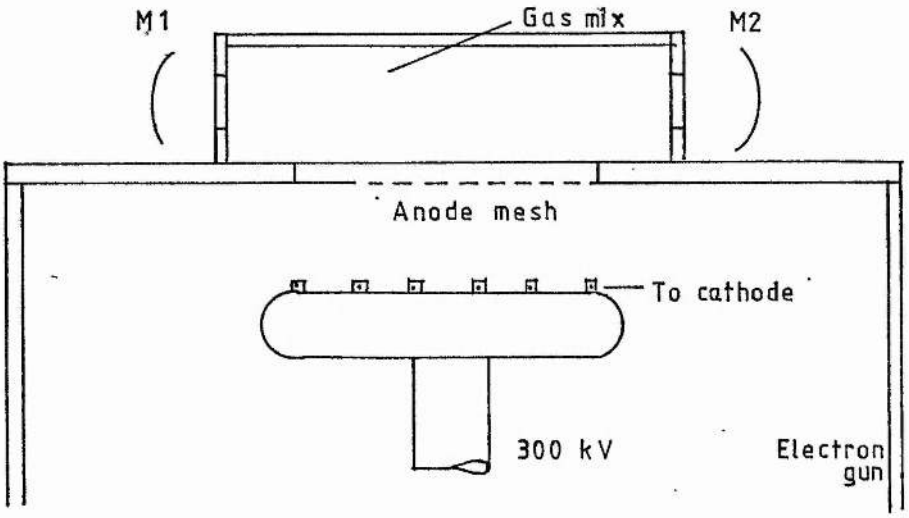

FIG 1.2 E-beam pumped laser (schematic).

FIG 1.3 E-beam controlled discharge laser (schematic).

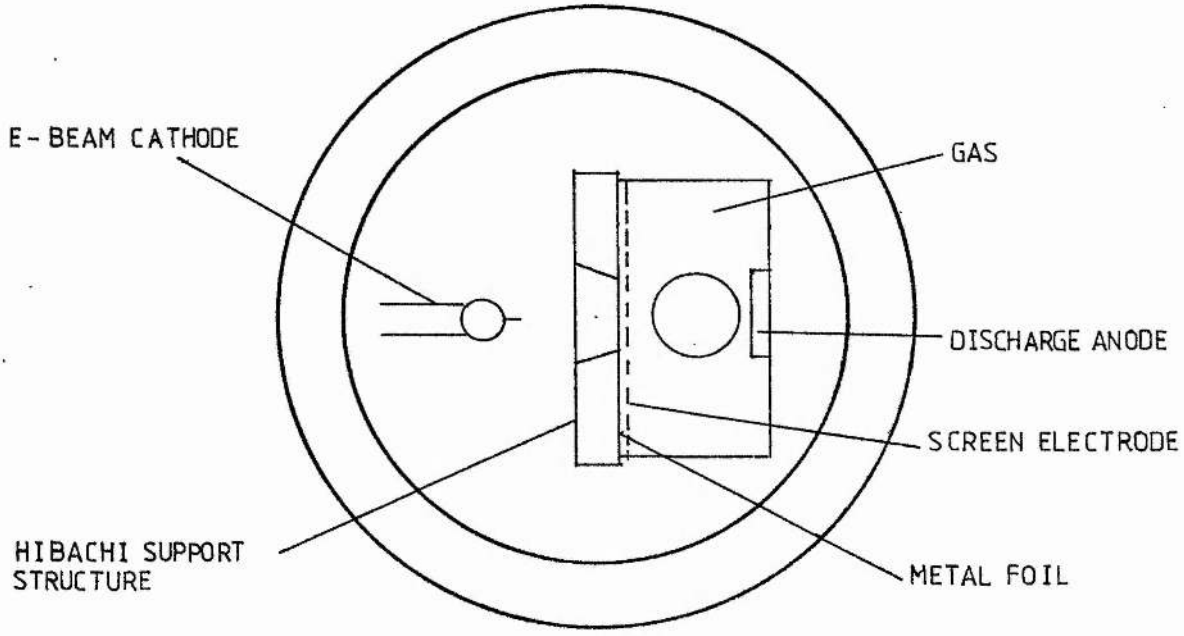

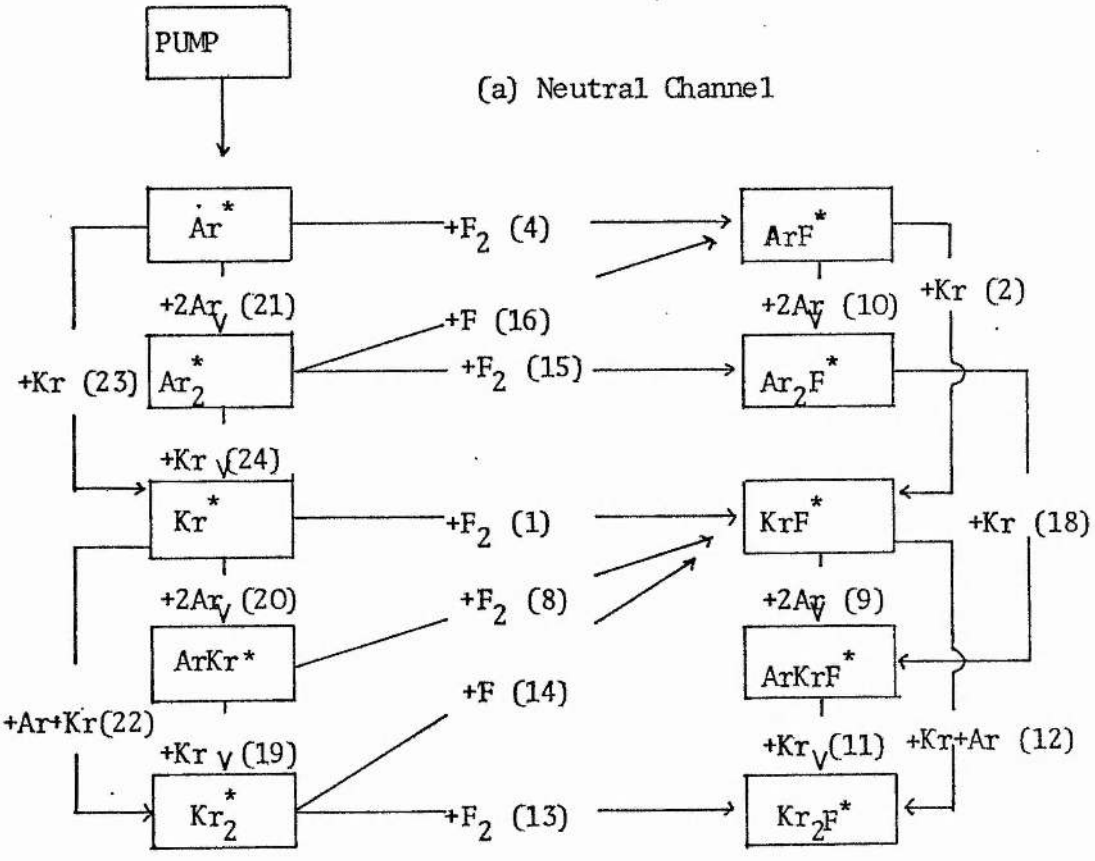

FIG 1.4 Formation of Krypton Fluoride.

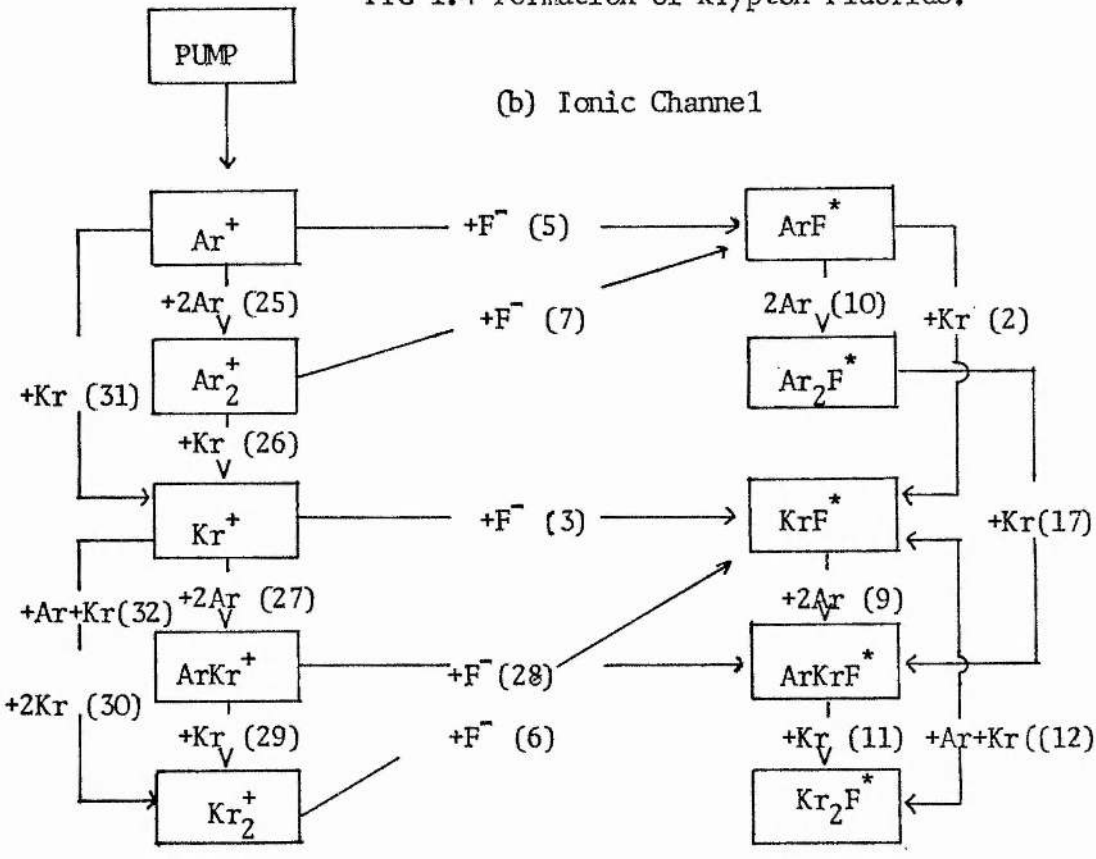

REFERENCES

Akerman M.A and Tennant R.A (1979) Topical Meeting on Excimer Lasers, Charleston, South Carolina.

Andrews A.J, Kearsly A.J, Webb C.E, and Hayden S.C (1977) Optics Commun. 20 265.

Ault E.R, Bradford Jr R.S, and Bhaumik M.L (1975) Appl. Phys. Lett 27 413.

Babcock R.V, Liberman I, and Partlow W.D (1976) IEEE J. Quantum Electr. QE12 29.

Baranov V.Yu, Borisov V.M, Davidovskii A.M, and Khristoforov O.B (1981) Sov. J. Quantum Electron. 11 42.

Bengston R.D, Miller M.H, Koopman D.W, and Wilkinson T.D (1971) Phys. Rev. A 3 16.

Bhaumic M.L, Bradford Jr R.S, and Ault E.R (1976) Appl. Phys. Lett. 28 23.

Bradford Jr R.S, Lancia W.B, Ault E.R, and Bhaumic M.L (1976) Optics Commun. 18 210.

Brau C.A and Ewing J.J (1975) J. Chem Phys. 63 4640.

Brau C.A (1979) in Excimer Lasers, Ed. Rhodes C.K, Springer Verlag, Berlin.

Burlamacchi L, Burlamacchi P, and Salimbeni R (1979) Appl. Phys. Lett. 34 33.

Burnam R and Djeu N (1976) Appl. Phys. Lett. 29 707.

Burnam R, Harris N.W, and Djeu N (1976) Appl. Phys. Lett. 28 86.

Burnam R, Powell F.X, and Djeu N (1976a) Appl. Phys. Lett. 29 30; Optics Commun. 18 118.

Burnam R and Searles S.K (1977) J. Chem. Phys. 67 5967.

Collins C.B, Lee F.W, and Carroll J.M (1980)
Appl. Phys. Lett. 37 857.

Daugerty J.D, Mangano J.A, and Jacob J.H (1976)
Appl. Phys. Lett. 28 581.

Deutsch T.F, Fan J.C.C, Turner G.W, Chapman R.L,
Ehrlich D.J, and Osgood Jr. R.M (1981)
Appl. Phys. Lett. 38 144.

Dunning Jr. T.H and Hay P.J (1976) Appl. Phys. Lett. 28 649.

Edwards C.B, O'Neill F, and Shaw M.J (1981)
Appl. Phys. Lett. 38 843.

Ewing J.J (1978) Physics Today, May, p32.

Ewing J.J and Brau C.A (1975) Appl. Phys. Lett. 27 350.

Ewing J.J and Brau C.A (1975a) Phys. Rev. A 12 129.

Fahlen T.S (1978) J. Appl. Phys. 49 455.

Fahlen T.S (1979) IEEE J. Quantum Electr. QE15 311.

Florin A.G and Jensen R.J (1971) IEEE J. Quantum Electr. QE7 472.

Godard B and Vannier M (1976) Opt. Commun. 18 206.

Golde M.C and Thrush B.A (1974) Chem. Phys. Lett. 29 486.

Gower M.C, Kearsley A.J, and Webb C.E (1980)
IEEE J. Quantum Electr. QE16 231.

Gower M.C and Edwards C.B (1982) Optics Commun. 40 369.

Greene A.E and Brau C.A (1978) IEEE J. Quantum Electr. QE14 951.

Hasson V, Lee C-M, Exberger R, Billman K.W, and Rowley P.D (1977)
Appl. Phys. Lett. 31 167.

Hasson V and von Bergmann H.M (1979) Rev. Sci. Instrum. 50 1542.

Hawryluk A.M, Mangano J.A, and Jacob J.H (1977)
Appl. Phys. Lett. 31 164.

Hay P.J and Dunning Jr. T.H (1977) J. Chem. Phys. 66 1306.

Hoffman J.M, Hays A.K, and Tisone G.C (1976)
Appl. Phys. Lett. 28 538.

Hsia J (1977) Appl. Phys. Lett. 30 101.

Hunter R (1977) 7th Winter Colloquium on High Power Visible Lasers, Park City, U.S.A.

Hutchinson M.H.R (1980) Appl. Phys. 21 95.

Ischenko V.N, Lisitysin V.N, and Razhev A.M (1977)
Appl. Phys. 12 55.

Jacob J.H, Rokni M, and Mangano J.A (1975)
Semi Annual technical Report, March 75 - Sept 76.

Jacob J.H and Mangano J.A (1976) Appl. Phys. Lett. 28 724.

Jeffers W.Q and Wiswall C.E (1970) Appl. Phys. Lett. 17 444.

Johnson P.M, Keller N, and Turner R.E (1978)
Appl. Phys. Lett. 32 291.

Johnson T.H, Palumbo L, and Hunter II A.M (1979)
IEEE J. Quantum Electr. QE15 289.

Johnson T.H and Hunter II A.M (1980) J. Appl. Phys. 51 2406.

Kovacs M.A and Ultee C.J (1970) Appl. Phys. Lett. 17 39.

Kunitomo K, Kaburagi M, Sumida S, Obara M, and Fujioka T (1982)
J. Phys. E. Sci. Instrum. 15 689.

Kutschke K.O, Hackett P.A, and Willis C (1981)
Rev. Sci. Instrum. 52 1655.

Lawler J.E, Parker J.W, Anderson L.W, and Fitzsimmons W.A (1979)
IEEE J. Quantum Electr. QE15 609.

Levatter J.I and Lin S.C (1980) J. Appl. Phys. 51 221.

Long Jr W.H (1979) J. Appl. Phys. 50 168.

Long Jr W.H and Bradford Jr R.S (1979)
IEEE J. Quantum Electr. QE15 327.

Lorents D.C (1978) in Electronic and Atomic Collisions,
Ed. Watel G, North-Holland, Amsterdam.

Malatesta V, Willis C and Hackett P.A (1981)
J. Amer. Chem. Soc. 103 6781.

Mandl A, Slater R, and Appel C.H (1982) Rev. Sci. Instrum. 53 301.

Mangano J.A and Jacob J.H (1975) Appl. Phys. Lett. 27 495.

Mangano J.A, Jacob J.H, Rokni M, and Hawryluk A (1977)
Appl. Phys. Lett. 31 26.

McKee T.J, Stoicheff B.P, and Wallace S.C (1977)
Appl. Phys. Lett. 30 278.

McKee T.J, Banic J, Jares A, and Stoicheff B.P (1979)
IEEE J. Quantum Electr. QE15 332.

McKee T.J, James D.J, Nip W.S, and Weeks R.W (1980)
Appl. Phys. Lett. 36 943.

McKee T and Nilson J.A (1982) Laser Focus, June, p51.

Miller W.H and Morgner H (1977) J. Chem. Phys. 67 4923.

Miller J, Dickie J, Davin J, and Kan T (1979)
Topical Meeting on Excimer Lasers, Charleston, South Carolina.

Patterson E.L, Rice J.K, and Tisone G.C (1980)
Appl. Phys. Lett. 36 188.

Rokni M, Jacob J.H, Mangano J.A, and Brochu R (1977)
Appl. Phys. Lett. 31 79.

Rokni M, Mangano J.A, Jacob J.H, and Hsia J.C (1978)
IEEE J. Quantum Electr. QE14 464.

Rothe D.E and Gibson R.A (1977) Optics Commun. 22 265.

Sadighi-Bonabi R, Lee F.W, and Collins C.B (1982)
J. Appl. Phys. 53 3418.

Searles S.K and Hart G.A (1975) Appl. Phys. Lett. 27 243.

Seguin H.J, Tulip J, and McKen D.C (1974)
IEEE J. Quantum Electr. QE10 311.

Sumida S, Obara M, and Fujioka T (1979) J. Appl. Phys. 50 3884.

Sumida S, Kunitomo K, Kaburagi M, Obara M, and Fujioka T (1981)
J. Appl. Phys. 52 2682.

Sutton D.G, Galvan L, Valenzuela P.R, and Suchard S.N (1975)
IEEE J. Quantum Electr. QE11 54.

Sutton D.G, Suchard S.N, Gibb O.L, and Wang C.P (1976)
Appl. Phys. Lett. 28 522.

Sze R.C and Scott P.B (1976) J. Appl. Phys. 47 5492.

Sze R.C, Loree T.R, Brau C.A, and Rockwood S.D (1976)
29th Gaseous Electronics Conference, Cleaveland, Ohio;
LASL Rep. LA-UR-76-1850.

Sze R.C and Loree T.R (1978) IEEE J. Quantum Electr. QE14 944.

Sze R.C and Scott P.B (1978) Rev. Sci. Instrum. 49 772.

Tayler R.S, Sarjent W.J, Alcock A.J, and Leopold K.E (1978)
Optics Commun. 25 231.

Tellinghuisen J, Hays A.K, Hoffman J.M, and Tisone G.C (1976)
J. Chem. Phys. 65 4473.

Velazco J.E and Setser D.W (1975) J. Chem. Phys. 62 1990.

Wang C.P (1976) Appl. Phys. Lett. 29 103.

Watanabe S, Obara A, Sato T, and Kashiwagi H (1979)
IEEE J. Quantum Electr. QE15 322.

Watanabe S, Obara A, Sato T, and Kashiwagi H (1979a)
Appl. Phys. Lett. 35 365.

CHAPTER 2

DESIGN CONSTRUCTION AND PERFORMANCE OF TEA LASERS

Transverse electric discharge pumping, as discussed in the previous chapter, is an efficient and simple way of pumping excimer and related gas lasers. At pressures greater than a few ten torrs this requires a preionization source in addition to the main discharge. One simple preionization source is a corona wire which, when a high voltage pulse is applied to it, provides uv photons to photoionize the gas between the electrodes. A homogeneous discharge is then produced by applying a fast rise time (10-100 nsec) high voltage (10-60 kV) pulse between the electrodes with a time delay with respect to the corona voltage pulse. Apart from holding off these high voltages the materials of the laser chamber and gas handling system are necessarily in contact with highly corrosive gases (F_2 in the case of KrF and F_2 lasers) in the presence of the ionizing uv photons from the discharge. This contact can lead to material damage, contamination of the gas mix and as a result, a limited lifetime over which a given gas mixture delivers useful laser power. The laser usually operates at a pressure in the range 1-10 atm and therefore must be constructed as a pressure vessel. The vessel must also be vacuum tight (rotary pump, 0.01 torr). Design of TE discharge excimer lasers has to take all these factors into account. In this chapter we outline the design and constructional details of the lasers built in our department using various materials and geometries. We studied such different versions utilizing different materials in construction in order to discover

the effect of the materials on the nature of the impurity species and to identify the impurity species common to all the versions. The materials and the electric design of these lasers are essentially similar to that of the varied commercial versions available. Understandably, the finer details of the materials used in the commercial versions are not available in open literature.

2.1 The fast transverse electric discharge

Self sustained volume electric discharges are initiated by the sudden (nsec risetime) application of a voltage pulse in excess of the breakdown potential of the gas mixture. This process starts an avalanche utilising the initial electrons present in the gas and leads to a breakdown of the gas and a sudden decrease in its impedence. Such discharges are inherently unstable and deteriorate into arcs after 30 to 40 nsec. The final plasma impedence is normally limited by the driving circuit impedence. Therefore the rate of excitation of the gas mix can be fixed by a proper choice of the driving circuit impedence. Onset of arcing is undesirable for two main reasons; it reduces the efficiency of lasing and spatial uniformity of the laser output, and the arcs produce such low impedence paths that the discharge could terminate or go into unstable oscillations, limiting again the laser output energy. In order to start a homogeneous volume discharge, an initial minimum electron density throughout the discharge volume is found to be necessary. Predictions for this density were made by Palmer (1974), and using a modified model of the discharge, by

Levatter and Lin (1980). These initial electrons - preionizing electrons - can be provided by various means as discussed in sections 1.2.2 and 1.2.3.

2.2 The LCI and CCT circuits

Production of a fast volume discharge can be achieved using either the Blumlein type LC inversion (LCI) circuit or the CC transfer (CCT) circuit (fig 2.1 a and b). The distributed inductance L1 in the ringing arm of the circuit determines the voltage risetime of the circuit and the distributed inductance L2 in the discharge arm controls the current risetime of the discharge current. For a given voltage risetime, more energy can be coupled into the discharge if the current risetime is kept short (Sze and Scott 1978). The CC transfer type is better suited for this purpose since the inductance in the discharge arm is lower, as seen from fig 2.1 a and b.

In both circuits the highest rate of rise of voltage is desirable to overvolt the discharge gap by the largest amount. For the LC inversion circuit this voltage risetime is determined by the ringing frequency of the ringing arm, which is

$$(1/2)\{(L_S + L_{C1})C1\}^{1/2} \quad (R2 \text{ very large})$$

Thus it is desirable to keep both the switching capacitance C1 and the total ringing arm inductance (which consists of the switch

inductance L_S and the inductance of the switching capacitor C1) low. Thus flat plate or coaxial transmission lines and spark gaps would be preferable to discrete capacitor arrays and thyratrons, provided the energy storage and repetition rate capability for the former combination are adequate.

In the case of the CC transfer circuit, the ringing frequency is

$(1/2\pi)\{(L_S+L_{C1}+L_{C2})C\}^{1/2}$ where $C = (C1\ C2)/(C1+C2)$.

The decreased voltage risetime due to the additional inductance L_{C2} is partly compensated for by a decrease in the capacitance C ($C < C1$). For a given charging voltage V, the discharge gap can have a potential difference maximum of $VC1/(C1+C2)$ in the case of a CC transfer circuit. Thus an LC inversion circuit is desirable when the highest overvolting is required.

Once the discharge is initiated the discharge resistance rapidly drops to values typically of the order of 0.2 ohms. Fast current risetimes in the discharge arm is desirable so that energy can be coupled into the discharge before the onset of inhomogeneities. The current risetime is proportional to L/R where L is the total inductance in the discharge loop and R the total (mainly discharge) resistance. Faster current risetimes are possible for the CC transfer circuit since the inductance in the discharge arm is less (see fig. 2.1). In practice the discharge current rises twice as fast in a CC transfer device compared to a similar LC inversion device (Sze and Scott 1978).

The inductances L_S, L_{C1} and L_{C2} must be as small as possible to give better voltage and current risetimes. The inductances (L_{C1} and L_{C2}) for parallel plate transmission lines and coaxial cables are less than for a parallel array of discrete capacitors. The physical sizes of the current loops also need to be kept as small as possible to keep these inductances low. Since the spark gap is usually of much smaller size than a thyratron, the inductance L_S for a spark gap is smaller. Thus fast risetime circuits are most easily designed using spark gap switched parallel plate transmission lines.

2.3 Preionizing methods

When discharge uniformity is required at pressures greater than a few hundred torr and for times greater than about ten nanoseconds, some kind of preionization is essential. Several types of preionization methods have been used as discussed in section 1.2.3. A simple method of automatic preionization is given in fig 2.2. The corona wires are a few cm away from the electrodes and parallel to them. They are connected to the capacitor C_p which is about 10% of C1. The same spark gap switch is used to switch C_p along with C1 to provide a high voltage spike to the corona wires which in turn produces a corona and uv photons which act as the primary preionizing source. The corona source can be mounted behind a mesh cathode and masked so that the discharge is constrained to the central uniform area of the electrodes. This

overcomes the need to machine electrodes to special uniform field profiles. Spatial control of discharges has been thus achieved by Hasson and von Bergmann (1980). More than one corona wire can be provided to increase the intensity and spatial distribution of preionizing radiation.

A time delay between the preionizing pulse and the main discharge is necessary for a uniform distribution of preionizing photons and species. This has been shown experimentally (Sze and Loree 1978) and theoretically (Hsia 1977). If discrete spark gap sources are used this time delay can be as high as a microsecond. For corona wires the uv source is more uniform spatially and time delays of about 50-100 nsec have been found adequate (Hasson and von Bergmann 1979). These time delays also bring in a short voltage rise-time requirement for the main discharge as was theoretically shown by Levatter and Lin (1980). The output energy from a KrF laser increases with the preionization electron density N_e according to the relation

$$E_o = a + b \ln(N_e)$$

where a and b are constants (Sumida et al 1980). This increase in energy has been found to be mainly due to an increase in laser output duration. The energy deposited in the gas by the discharge depend only on a minimum preionization density (Sze and Loree 1978). Lasers preionized with a corona wire can thus be expected to have lower energy output than those preionized with a spark array since the initial electron density in sparks is usually

much higher. We chose corona wire preionization because it is easier to construct and would not produce high energy sparks. Sparks can sputter material and form fresh surfaces for reaction with F_2, producing contaminants at a higher rate than in a corona discharge.

X-ray preionization, because of its greater penetration, is believed to be superior to either spark board or corona preionization. This preionization method would also minimize the chemical reactions in the laser since there is no electrical discharge in the gas mixture. We did not choose this method because of the increased complexity and expense it would entail.

2.4 Design of the laser body

Electrical, chemical and mechanical properties of the materials used in the construction of the laser body are critical. Figure 2.3 shows an exploded view of the laser body. The insulator must be good enough to hold off fields of about 20 kV/cm and be transparent (preferably) so that the discharge can be observed. It should be machinable, have good resistance to attack by F_2, not adsorb gases like CO_2, air or be permeable to helium. The insulator should not deteriorate under uv radiation. Expense is also a consideration. We have used polymethylmethacrylate (PMMA) and PTFE in various versions and their advantages and disadvantages are discussed later. The metal used is aluminium (containing traces of ~1% Si, Mn and traces of Cu, Fe, Zn and Cr) since it is

easily machinable, of adequate strength and forms a passive layer of aluminium fluorides when in contact with F_2. The electrodes were made of Al in two versions and Al and nickel mesh in another two versions; the final version has monel electrodes. O-rings are used between the insulator body and the metal electrode holder to seal the laser for both low and high pressures. The three pieces are held together using metal bolts either threaded into the plastic or insulated and passing through the plastic. The end window ports are sealed using 25 mm Silica or MgF_2 flats against O-rings. The capacitors of the energy transfer circuits are connected to this laser in various ways in the four versions as described below. The CCT circuit is used for the versions 2 to 5 since it is expected to produce higher laser energies due to faster discharge current risetimes. Another advantage is that the capacitors are pulse charged and thus should stand higher voltages for longer times than do the same capacitors in an LCI circuit. The gas inlet and outlet ports are connected to the gas handling system described in section 2.6.

2.5 Constructional details and performance

2.5.1 Laser version 1

A cross sectional diagram of this laser is given in fig 2.4a. The electrodes are attached to two aluminium plates 114 cm long. The gas cavity is formed between these plates by a PMMA box 25 mm thick with inner dimensions 1100 mm x 70 mm x 55 mm. The box is sealed against the aluminium plates using neoprene O-rings. Steel studs threaded into the PMMA are used to hold the whole structure together with nuts as indicated in the figure. The electrodes are

made of aluminium and stainless steel mesh (No.20). The solid aluminium anode with rounded edges is bolted onto one of the aluminium plates and the stainless steel mesh is bolted onto an aluminium support structure on the other plate. Two insulated stainless steel rods through this plate behind the mesh supports the corona wire (bare 0.1 mm stainless steel) 3 mm away from the mesh. The discharge gap is 25 mm. The cavity is completed by two adjustable quartz windows mounted on both ends, sealed with O-rings. Gas inlet and outlet ports are connected on the cathode plate.

The L-C inversion circuit for this version is given in fig 2.4(b). The capacitors are made of two flexible double copper clad Melinex sheets. The spark gap is integrated with the capacitor and has an inductance of less than 2 nH, calculated from the risetimes on the switching side.

This laser when tested produced quite homogeneous discharges and lasing in nitrogen up to 100 torr. Voltage risetimes on the anode, when measured using a high voltage probe (Tektronix P6015-1000X) and a CRO (Tektronix 7834) was found to be less than 25 nsec. Use of a slotted aluminium sheet behind the mesh was found to confine the discharge to the central portion of the electrodes. This helps in avoiding the use of specially contoured electrodes and is one of the advantages of a behind-the-electrode preionizing scheme.

We could not carry out further experiments on this laser because of the occurrence of frequent dielectric breakdowns in the melinex sheet above 15 kV.

2.5.2 Laser version 2

This version is a modified version of the previous one. The corona wire is replaced with a 0.5 mm dia copper wire insulated with PTFE. The insulation avoids arcing between the cathode and the corona wire. The melinex capacitors are replaced with barium titanate capacitors (working voltage of 30 kV) in a lumped element C-C transfer (CCT) configuration. The electrical circuit for this version is given in fig 2.5. This circuit increased the charging time of the charging capacitors to about 75 nsec compared to 25 nsec in version 1, as measured using the same set-up as described in sec 2.4. A mask with a 8 mm wide aperture was also used between the corona wire and the mesh. Use of barium titanate capacitors allowed the use of charging voltages to a maximum of 30 kV. Since the energy storage capacitors are pulse charged, their lifetimes are expected to be higher even when used beyond the specified voltage limits. The pulse charged energy storage section consists of 23 capacitors, each of 0.6 nf and made up of two 1.2 nf in series. Each capacitor has a maximum d.c voltage limit of 12 kV. The inductance L brings the cathode back to earth potential after each pulse, at the same time acting as an open circuit for the charging pulse from the charging capacitors.

The optical cavity consists of two aligned quartz windows on the laser (plane parallel) and an aligned external dielectric mirror of >99% reflectance at 248 nm with 2 m radius of curvature.

This laser when tried with a KrF laser mix (4 torr F_2 + 28 torr Kr + 730 torr He) gave a maximum power output of 19 mJ at 25 kV charging voltage. The output fell to half its initial value in 200 shots. The discharge looked uniform visually, with a few arcs at both ends at the termination of the masking aperture.

Mechanical problems in the system soon became evident after about three months of use. The threaded regions in PMMA started to crack and it became impossible to bolt the aluminium plates so as to maintain pressure and vacuum. Some experiments were conducted at atmospheric pressure but this version was soon abandoned.

2.5.3 Laser version 3

A cross sectional version of this laser is given in fig 2.6(a). The laser cavity is made of PMMA machined from a single block 50 mm thick. The internal dimension of the cavity is 840 x 89 x 50 mm. The aluminium electrodes are attached to two aluminium plates (90 x 46 x 13 mm) which have grooves for neoprene O-rings that seal against the PMMA. The plates are sealed down using studs embedded in the PMMA and bolts as in version 1. The solid electrodes are 710 mm long and 25 mm wide made of aluminium and contoured to a

semi circle. The discharge gap is 22 mm. Preionization is provided by two stainless steel corona wires (0.1 mm dia) symmetrically situated 34 mm away on both sides of the electrodes (see fig 2.6(a)). The cavity is sealed at both ends by 25 mm plane calcium fluoride windows which can be aligned. An external dielectric fully reflecting mirror completes the laser cavity. The CCT excitation circuit for this laser is given in figure 2.6(b). The capacitors and spark gap are mounted as close to the laser as possible to reduce the inductance of the various current loops. The peaking or energy storage capacitor (17 nf) is about 1/3rd the charging capacitor (60 nf). This keeps the pulsing voltage close in magnitude to the d.c charging voltage.

The materials used in the construction of this laser are aluminium (containing ~1% of Si, Mn) stainless steel, PMMA and neoprene rubber.

Electrical characteristics of this laser were not measured. Measurements of output energy as a function of krypton concentration were carried out for 4 torr F_2 and the rest helium to 990 torr. The results are given in fig 2.7.

2.5.4 Laser version 4

This version differs from the previous one in two essential aspects. The cavity is made from PTFE instead of PMMA and neoprene O-rings are replaced with viton O-rings. The cavity is sealed with steel bolts passing through the PTFE body. This gives much greater structural strength to the laser so that the gas mix pressure could be taken up to 5 atmospheres. The bolts also prevent the tendency of PTFE to creep under pressure. Nylon sleeves are provided around the bolts to insulate them against shorting the cathode and anode plates as seen in fig 2.8. The internal dimensions of the cavity are 50 x 90 x 870 mm. The electrode gap is 26 mm. The CCT discharge circuit used is the same as given in fig 2.6(b) except that C1 = 50 nf and C2 = 26 nf. The corona wires are stainless steel (0.1 mm dia) and mounted as in version 3 but from the side so that their distance from the electrodes could be adjusted. Three corona wires are used on each side instead of the one in version 3. The corona charging capacitors remain the same as in version 3. The cavity and optics are the same as in version 3.

This version has the following materials coming in contact with the gas mix: aluminium, PTFE, viton, stainless steel and calcium fluoride.

2.5.5 Laser version 5

This version is exactly the same as version 4 except that the aluminium electrodes are replaced by solid monel electrodes with circular contours and the stainless steel corona wires are replaced by nickel corona wires. Thus the active areas where the discharges occur are not aluminium and stainless steel but monel and nickel.

Laser versions 3, 4, and 5 have been used in the gas lifetime experiments described in the rest of this thesis.

2.6 Gas handling system

The gas handling system is made from 6 mm o.d. monel and stainless steel pipes, Swagelok valves and valve fittings (obtained from Glasgow valve fitting Co.). The schematic of the system is given in fig 2.9. The F_2, krypton and helium cylinders have their own regulators which bring the pressures down to about one atmosphere or less. The fourth inlet is for the addition of controlled amounts of impurity gases. Three gauges are used to monitor the pressure. The low pressure (0 - 50 torr) and medium pressure (0 - 760 torr) gauges are Capsulon gauges made by Edwards Vacuum Company. The high pressure (1 to 4 kg/cm^2)gauge is made by Matheson. The three gauges are F_2 passivated. The low and medium range gauges were calibrated against a mercury manometer before use. The circulating pump is a peristaltic type made by Vanton (trade name: Flex-I-Liner). The pump material in contact with the

gases is viton and the pumping speed is 2 litres/minute. This pump cannot be used in pressures in excess of about one atmosphere, so the gas mix pressure is kept around one atmosphere when this pump is used. The cold trap is made from 1.2 meters of 6 mm o.d. stainless steel tubing twisted into two spirals of about 50 mm dia. each. The gas handling system is connected to the laser using two 6 mm PTFE tubes. The circulating gas is sampled by the mass spectrometer via an adjustable needle valve.

2.7 Power supply and trigger circuits

The high voltage (0 - 30 kV) used to charge the capacitors in all the versions is an HML model 350 by Hartley Measurements Ltd. The output polarity can be changed to either positive or negative. The power supply is isolated from the laser by using a 1 Mohm charging resistor. The spark gap is triggered using an HML model 350 trigger unit and a step-up pulse transformer which yields trigger pulses of a few kV. The pulse repetition rate for the experiments described in this thesis is about one pps.

The laser is housed in an aluminium box with shielded lead-ins for the trigger and high voltage sources. This reduces the radiated noise from the laser discharge and pulsing circuits reaching noise sensitive diagnostic instruments.

2.8 Diagnostic instrumentation

The energy output from the laser is measured using a calibrated pyroelectric energy meter (Laser Precision model Rj 7200). The output from this is fed into a "home-made" sample-and-hold-circuit which leads to an x-t recorder to continuously record energy as a function of time. The gas mix in the laser is sampled at regular intervals during an experiment by the mass spectrometer at a constant pressure around 1.5×10^{-6} torr (monitored by a Mullard IOG 12 ion gauge). The mass spectrometer is described in detail in the next chapter. The mass spectra are recorded at different sensitivities on an x-y recorder (Bryans model 26000 A4). Continuous monitoring of the partial pressure of a single mass peak (usually m/e 38 of F_2) is also done using another x-t recorder during the experiment. A block diagram for the diagnostic set-up is given in fig 2.10. When using the system for F_2 laser studies the superradiant output is measured. When KrF mixtures are used the output coupler is a calcium fluoride window and the cavity is formed by the window and a 99.8% dielectric concave mirror of 2 meter radius.

In the next chapter the quadrupole mass spectrometer is described along with the measurement and interpretation of mass spectra.

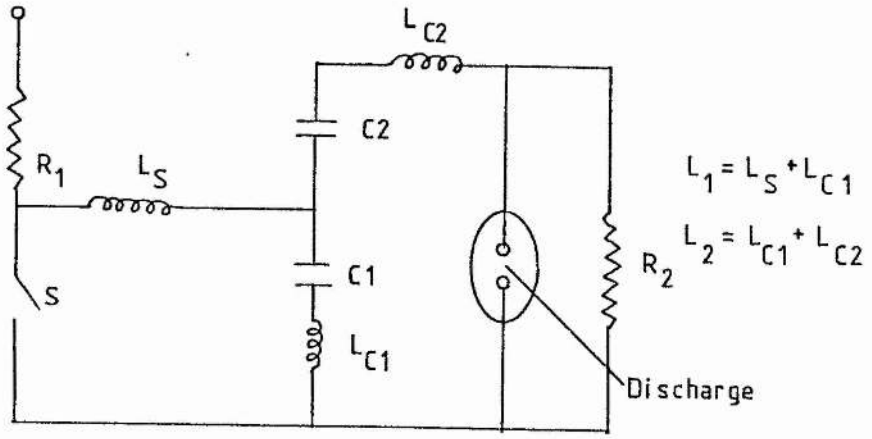

FIG 2.1a L-C Inversion discharge circuit.

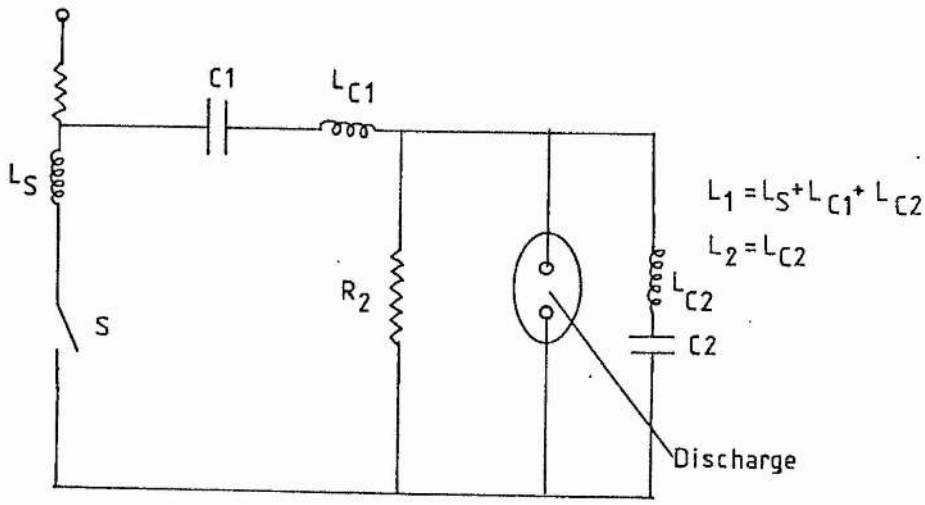

FIG 2.1b C-C Transfer discharge circuit.

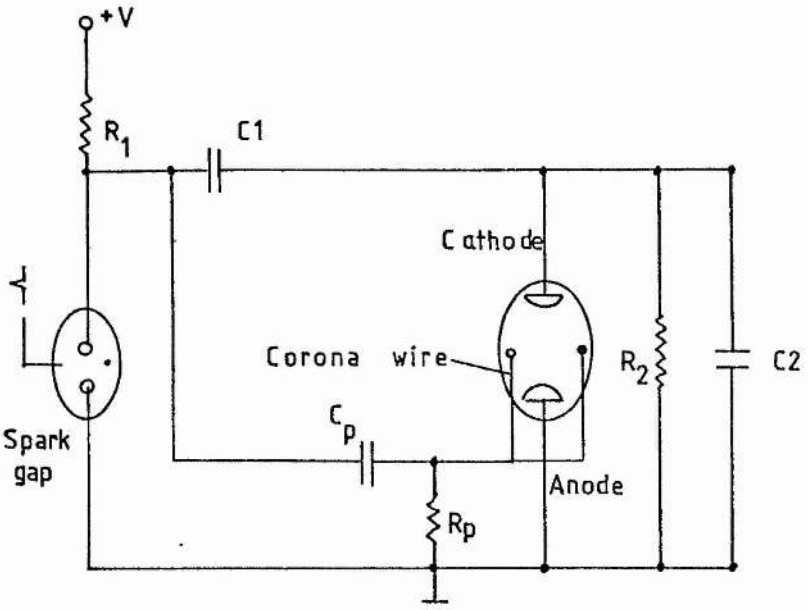

FIG 2.2 Automatic preionization circuit.

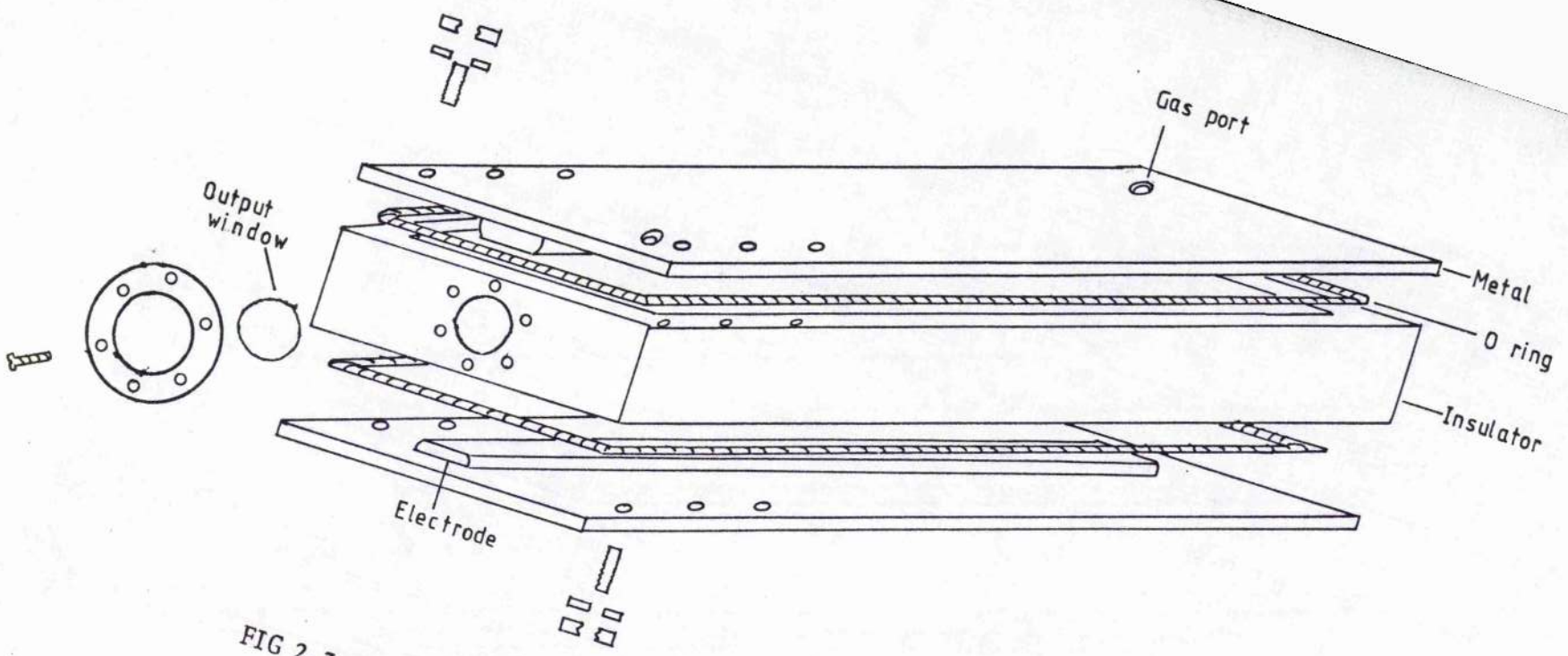

FIG 2.3 General laser body construction details.

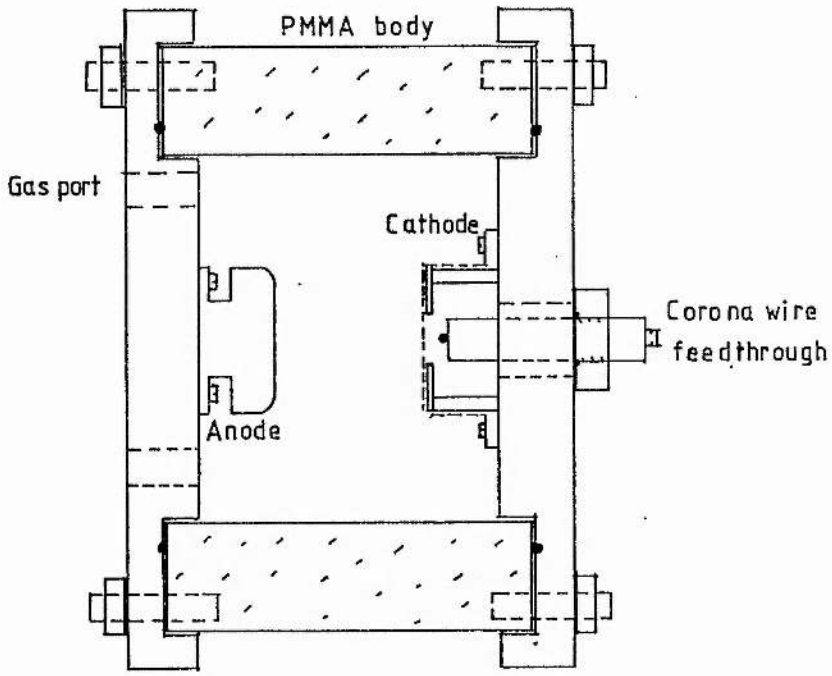

FIG 2.4a Laser Version 1.

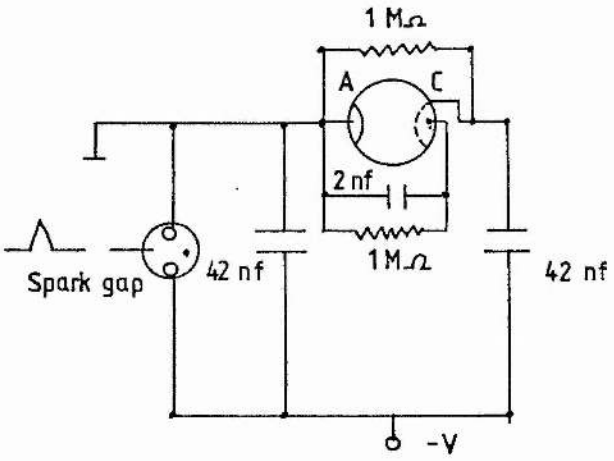

FIG 2.4b Electrical circuit for Laser Version 1.

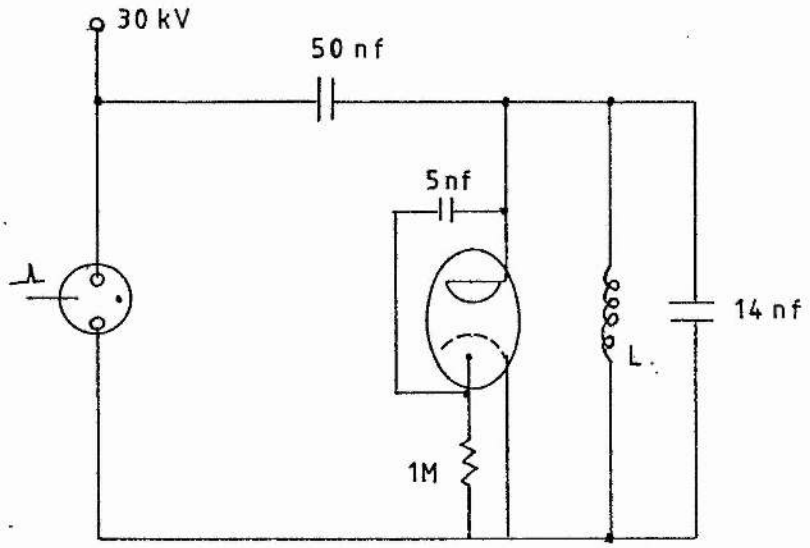

FIG 2.5 Laser Version 2 circuit diagram.

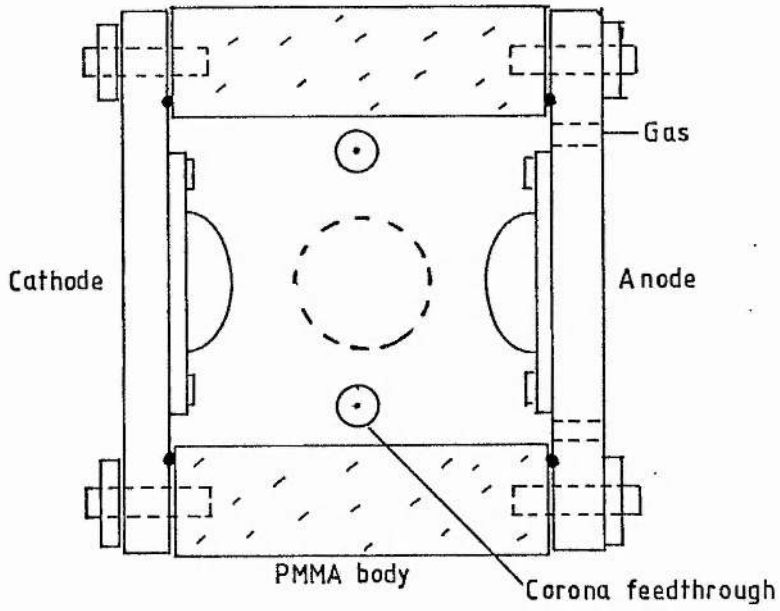

FIG 2.6a Laser Version 3.

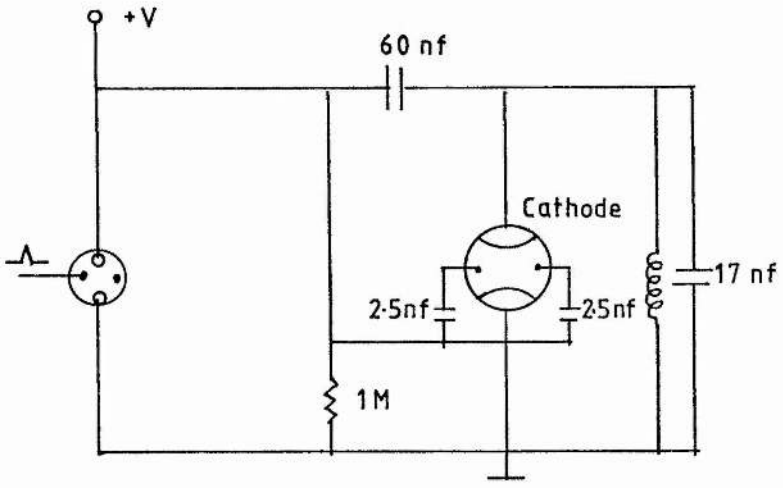

FIG 2.6b Electrical circuit for Laser Version 3.

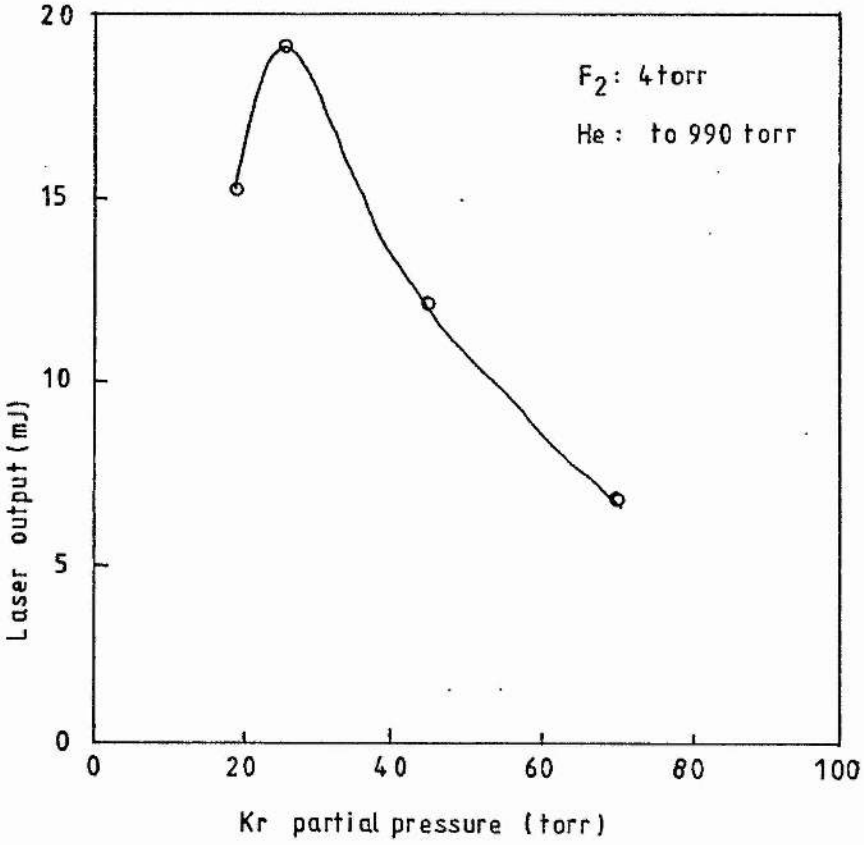

FIG 2.7 Laser output energy as a function of Kr partial pressure for Laser Version 3.

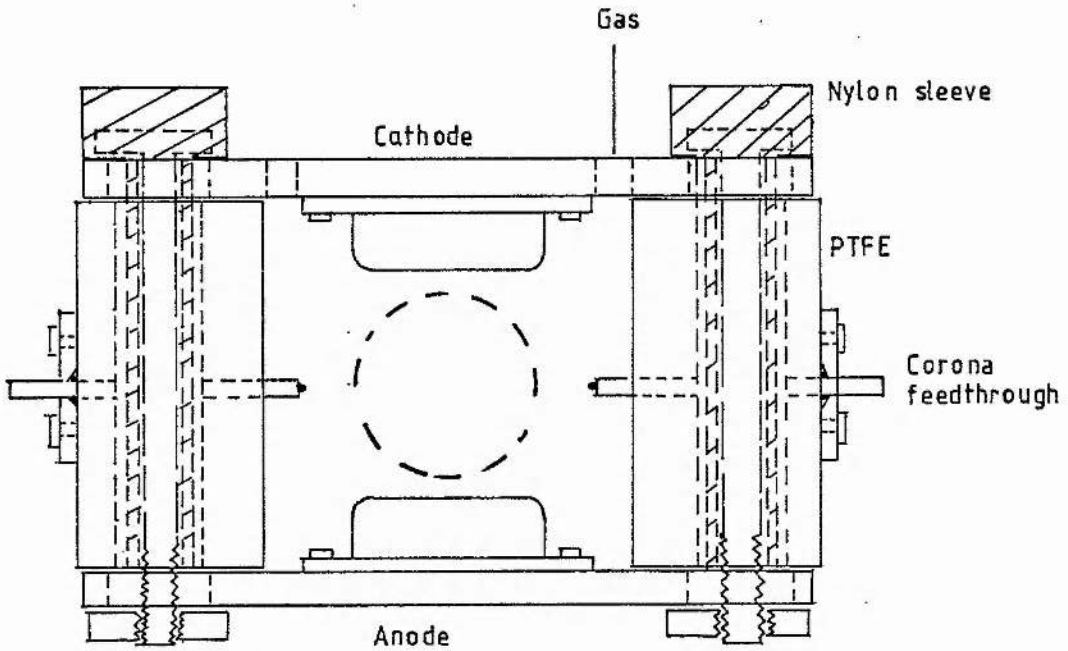

FIG 2.8 Laser Version 4 cross section.

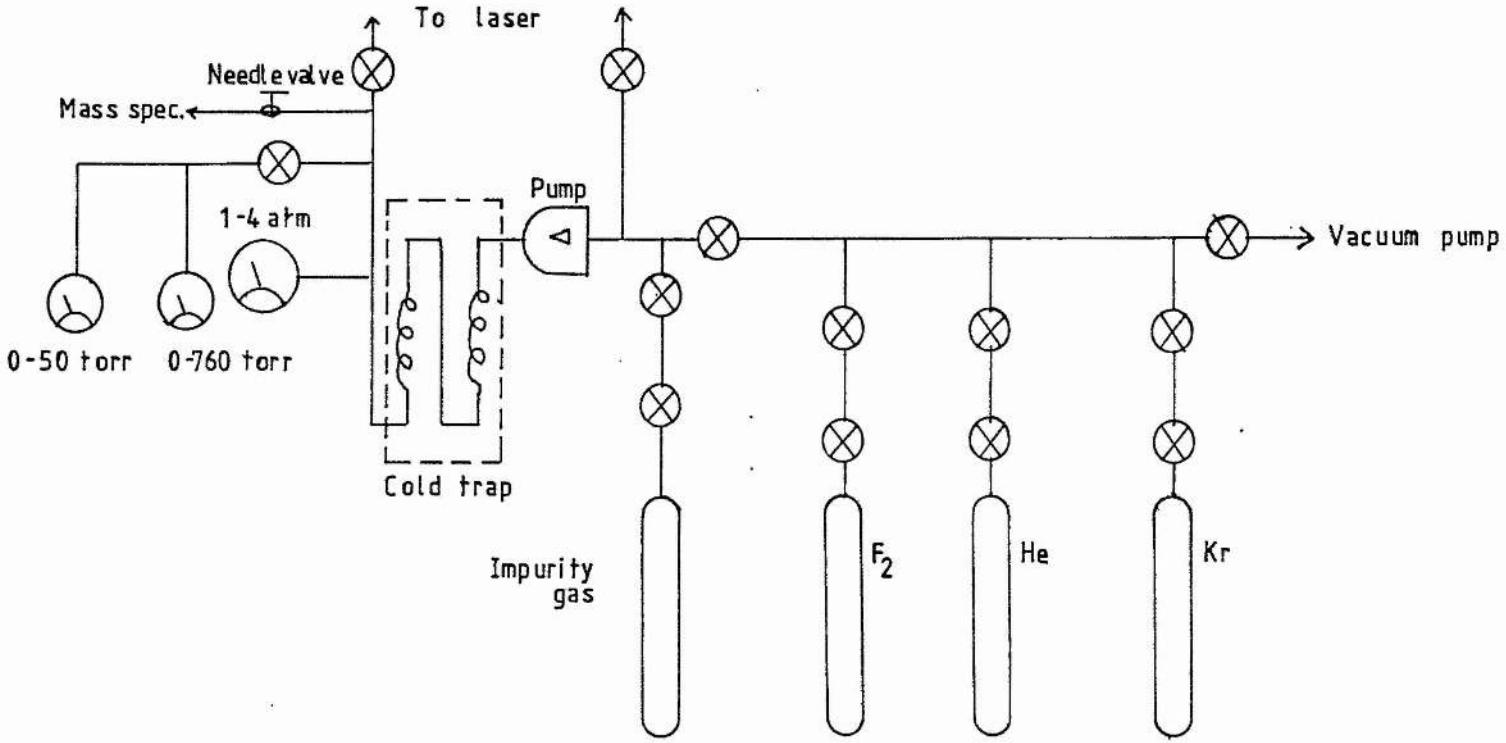

FIG 2.9 Gas handling system schematic diagram.

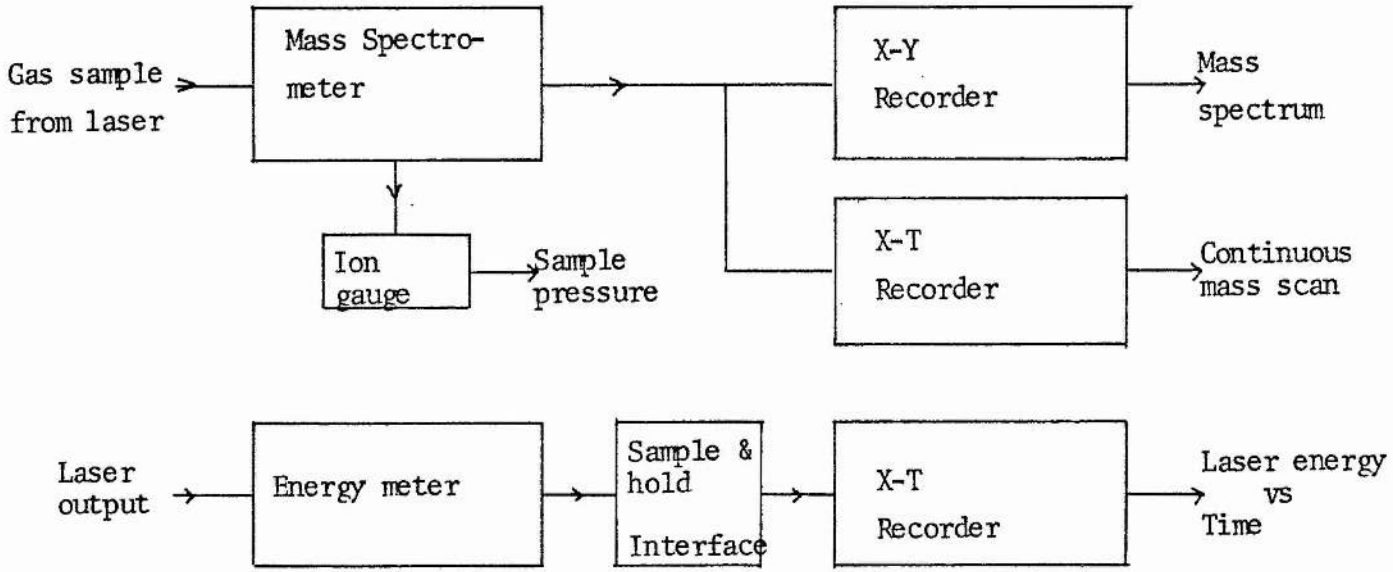

FIG 2.10 Diagnostic Instrumentation Schematic Diagram.

REFERENCES

Hasson V and von Bergmann H.M (1979) Rev. Sci. Instrum. 50 1542.

Hasson V and von Bergmann H.M (1980) J. Phys. E 13 632.

Hsia J (1977) Appl. Phys. Lett. 30 101.

Levatter J.I and Lin S.C (1980) J. Appl. Phys. 51 210.

Palmer A.J (1974) Appl. Phys. Lett. 25 138.

Sumida S, Kunimoto K, Kaburagi M, Obara M, Fujioka T,
and Sato K (1980) J. Appl. Phys. 52 2682.

Sze R.C and Scott P.B (1978) Rev. Sci. Instrum. 49 772.

Sze R.C and Loree T.R (1978) IEEE J. Quantum Electr. QE14 944.

CHAPTER 3

THEORY AND INTERPRETATION OF MASS SPECTRA

The analysis of a gas mixture to yield information about its composition can be done spectroscopically using uv, visible and ir absorption and emission spectroscopy. These methods are however more indirect and involved than methods like gas chromatography and mass spectrometry. Spectroscopic methods are useful when information on fast reaction kinetics is required because of the short response times (as short as 0.1 nsec) of spectroscopic detection. We are more interested in long lived species in the laser gas mixture. These species have lifetimes not less than a few minutes. The amount of a species produced in the laser is generally less than a few parts per thousand. At such low concentrations gas chromatography gives results with standard deviations greater than 100% (Krugers 1968). The quadrupole mass spectrometer is probably the best primary diagnostic instrument to study impurity formation in gas lasers since it has good sensitivity for most gases and molecules (down to one part per million), has fast scanning capabilities (60 atomic mass units per second) and is rugged enough to handle corrosive gases like F_2. In this chapter we describe the operation and characteristics of the quadrupole mass spectrometer. We also discuss the processing and interpretation of mass spectra and the special problems encountered in handling gas mixtures containing F_2 as one component.

3.1 The quadrupole mass spectrometer

A schematic view of the quadrupole mass spectrometer is given in rig 3.1 (Reed 1965). It consists of an ionization source where the sample is bombarded with electrons to produce positive ions and a mass filter. In the mass spectrometer (Supavac by Kratos Ltd.) we nave used in the experiments the electrons are emitted from a tungsten filament and accelerated to an energy of 62 eV. This energy is optimal for ionizing most molecules. The ion beam is then focused into the mass filter using a three element lens formed by the source plate (+0.5V) the focus plate (-57V) and the earth plate (0V, see Supavac instruction manual).

The mass filter consists of four cylindrical stainless steel rods (each 125 mm x 6.3 mm dia) aligned parallel to each other at distance of 2r as in fig 3.1 using two alumina collars. A combination of dc voltage U and rf voltage V is applied to these rods, opposite rods being connected together. This gives rise to a field inside the assembly whose potential at a point x,y is given by

$$\Phi = (U + V\cos\omega t)(x^2 - y^2)/r^2$$

where ω is the rf angular frequency. From this we can get

$$\ddot{y} = -(a + 2q\cos\omega t)x$$

$$\ddot{x} = (a + 2q\cos\omega t)y$$

where

$$a = 8eU/mr^2\omega^2$$

$$q = 4eV/mr^2\omega^2$$

and m/e is the mass to charge ratio of the ions. Solutions of these equations give the amplitude of oscillations performed by the particles in a direction perpendicular to the mass filter rods. This amplitude is finite only for a narrow range of masses of the ions. All the other ions with growing amplitudes are lost usually in collisions with the steel rods. Resolution of the mass filter becomes larger when the mass range gets narrower. Resolution can be shown to increase with increasing U/V ratio. At the same time sensitivity goes down since for higher resolution the number of ions passing through the mass range is decreased. The resolution defined as the percentage of valley height between adjacent peaks of equal height is 10% in the case of the Supavac. The sensitivity of the instrument is such that partial pressures down to $2x10^{-11}$ mbar at 2:1 signal to noise ratio are measurable. The mass scan is linear with respect to either U or V for a constant U/V. The Supavac scans the mass range 1 to 135 by changing the rf and dc voltages.

The ions after passing through the mass filter are collected by a Faraday plate. The ion current is further processed by solid state amplifiers to give the mass spectrum as a function of m/e in the range 1 to 135. The scan rate is adjustable from 60 amu/sec to 0.2 amu/sec. We have done all the scans at 1 amu/sec which was found

to be the best compromise between noise and scan rate.

In order to keep the background impurities low, the mass spectrometer is maintained at a pressure less than $3x10^{-8}$ torr. This is achieved by an oil diffusion pump incorporating a liquid nitrogen cold trap and backed by a rotary pump. The mass spectrometer which came in kit form was assembled into a portable unit along with the vacuum apparatus. Copper gaskets were used for seals on the high vacuum side to get the lowest possible pressures. After assembly the system was baked for a few hours at $200^{o}C$. The evacuated system pressure is generally $3x10^{-8}$ torr or lower.

3.2 Gas sampling technique

Our aim in using the mass spectrometer is to sample the gas contents in the laser continuously as a function of time. Since the gas mixture in the laser is at atmospheric pressure, a controlled leak is necessary to admit the gas sample into the mass spectrometer at the required pressure. This is achieved by a needle valve connected close to the circulating region of the gas handling system as shown in fig 2.9. The gas sample is then pumped through the mass spectrometer. The needle valve is adjusted to give the required sample pressure, which is about $1.5x10^{-6}$ torr in most experiments described in this thesis. The gas volume in the laser is about 4 liters at around 800 torr. Gas depletion due to sampling over a period of several hours was found to make no

difference in the laser gas pressure. The pressure on the mass spectrometer side of the needle valve is 1.5×10^{-6} torr which means the gas flow is molecular. The laser side of the needle valve has viscous flow due to the high (800 torr) pressure. This means that the recorded mass spectrum is a true representation of the gas in the laser, as long as enrichment effects of the sample due to differences in flow rate due to differences in molecular weight does not occur (Brittain 1975, pp 334). From the pumping speed of the system (5 litres/sec) it was calculated that over 100 minutes the depletion rate of gas components with a relative partial pressure with respect to helium of greater than 10^{-4}, is less than 3%. Thus the depletion over time of any component of the mixture in the laser can be neglected as long as its partial pressure is greater than 0.1 parts per thousand of helium, which is the usual lower limit for all the experiments reported in this thesis.

Experiments were done to find out how fast the mass spectrometer reacts to changes in gas composition in the laser. With circulator on, the mass spectrometer responded within one minute to the increase in oxygen concentration in the laser when the discharge was switched on. Another experiment in which helium and F_2 were circulated unmixed showed decaying oscillation of the mass peak at m/e of 38 (due to F_2) caused by the mixing of the two gases. The period of this oscillation was 45 seconds, which is the time taken for the gas to circulate once in the system.

3.3 Interpretation of mass spectra (theory)

3.3.1 Cracking patterns and sensitivities

When a compound is ionized in the mass spectrometer the ion fragments in principle give rise to a unique record of that compound called a cracking pattern. This pattern is a tabulation of the abundance ratio of the fragment ions at different m/e values. The highest peak in a cracking pattern is termed the base peak and is generally given a value of 100. Tables of mass spectral data have been published (Cornu and Massot (1966), Eight Peak Index). They can be utilised to identify compounds in a gas sample as is discussed later.

The ion current for a compound recorded at its base peak m/e generally varies from instrument to instrument and also depends upon the operating conditions of a given instrument. The relative sensitivity of the instrument is therefore more usually defined with reference to a standard compound like n-butane. Relative sensitivity values are generally given along with tabulations of cracking patterns (Cornu and Massot 1966).

3.3.2 Background mass spectrum

Even when no samples are admitted into the system the mass spectrometer gives rise to a spectrum due to the presence of background molecules. The main contribution to the background spectrum comes from water vapour, CO, CO_2, due to reaction on the hot filament and N_2 and O_2 due to background air. These background values are to be subtracted from any recorded mass spectrum to get the true mass spectrum. However we generally do not subtract background values since our main interest is in relative variations of the spectra.

3.3.3 Identification of compounds in the gas sample

The following assumptions are made in the analysis of mass spectra (Brittain 1975):

(1) The components of the gas sample gives rise to spectra that are linearly additive at any mass number.

(2) The ion currents recorded at any m/e values are proportional to the pressure of the sample. Under normal operating conditions this is true. It has been experimentally confirmed for the Supavac.

(3) The cracking patterns and sensitivities are invariant. This is not strictly true but any variation is taken into account as explained later.

These assumptions show that the resultant mass spectrum can be written as

$$
\begin{aligned}
H_1 &= h_{11}p_1 + h_{12}p_2 + \ldots\ldots + h_{1n}p_n \\
H_2 &= h_{21}p_1 + h_{22}p_2 + \ldots\ldots + h_{2n}p_n \\
&\vdots \\
&\vdots \\
H_m &= h_{m1}p_1 + h_{m2}p_2 + \ldots\ldots + h_{mn}p_n
\end{aligned}
\qquad \text{(3.1)}
$$

Here p_j is the partial pressure due to component j in the gas mix and h_{ij} is the ion current that would be recorded at m/e = i due to the component j if it were present at unit pressure.

In practice the m linear equations in n unknowns (equations 3.1) can be solved using least squares methods in a computer. The solution vector $[p_1 \ldots\ldots p_n]$ gives the partial pressures of the various components in the gas mix. The accuracy of the results can be checked by computing the standard deviation of the calculated spectrum from the measured spectrum. A more detailed account of the computer programme and its typical output is given in appendix A.1.

In theory, if all the cracking patterns are stored in the computer, a programme could be written to choose the compounds to be used in the equations (3.1). Such programmes have been written with varying degrees of success (for a review, see Chapman 1980).

However we did not attempt to write or use any such programmes because the specialised nature of the present problem suggested easier ways of solving the equations. The method adapted is as follows: A preliminary check of a mass spectrum is made for important peaks. They are then looked up in the catalogues of mass spectra (Cornu and Massot 1966, Eight Peak Index) and the possible compounds chosen. This choice is made easier because of previous knowledge of the main gas mix components. Cracking patterns for these components are then used in the programme to find the partial pressures. After two or three trials the calculated mass spectrum is found to agree with the measured spectrum within a standard deviation of 2% to 5% generally. When a peak could not be identified from published cracking patterns another computer programme, which generated all the possible combinations of a given set of elements to give ion fragments at the suspected m/e values is used to aid identification. Details of this programme are given in appendix A.2.

3.4 Practical interpretation of mass spectra

In this section we deal with the experimental results obtained in the Supavac mass spectrometer when typical gas mixtures used in the laser are analysed. An evaluation of the experimental errors is also carried out.

3.4.1 Mass spectrometer background spectra

Table 3.1 gives the partial pressure values for three background mass spectra taken over a 16 day period. Each spectrum in column (a) was taken at least 24 hours after the Supavac was used to analyse F_2 containing laser gas mixes. In the three cases the ion gauge read a background pressure of 1.5×10^{-8} torr. Comparison of this with the mass spectrum in column (b) taken after an interval of 19 hours after a F_2 mix was analysed shows that in the latter case m/e values at 85 (SiF_3^+), 20(HF^+), 19 (F^+) show a relative increase. Stable background readings can be thus taken only after waiting for at least 24 hours after the last sample is analysed. The stable background readings here show the permanent contamination of the system with HF and HCl apart from the usual presence of H_2O, CO, CO_2 and H. The table also shows that variation in the background spectrum is likely over a period of several hours after F_2 samples are analysed, especially at 19, 20 and 85 due to F_2 reactions inside the mass spectrometer.

Table 3.1

Background mass spectra for the Supavac mass spectrometer (arbitrary units).

m/e	Ion	(a)			(b)
		(1)	(2)	(3)	
2	H^+	20	84	94	3.5
12	C^+	2.3	2.5	2.7	1.4
14	N^+			1.0	
16	O^+	3.5	5.8	4.7	5.5
17	OH^+	8.5	19	15	12
18	H_2O^+	28	63	51	42
19	F^+	14	12.5	8.0	160
20	HF^+	43	54	52	153
28	CO^+, N_2^+	23	27	31	50
32	O_2^+	2.3	2.5	2.0	3.5
35	Cl^+	1.5	2.0	2.0	5.0
36	HCl^+	2.5	3.5	4.7	4.0
38	F_2^+		1.9	1.3	2.0
44	CO_2^+	38	15	19	24
47	COF^+				2.5
64	SO_2^+				1.5
66	COF_2^+				1.4
69	CF_4^+				1.5
85	SiF_3^+	1.3			12
Pressure(10^{-8} torr)		1.7	1.8	1.5	20

3.4.2 Cracking patterns in the Supavac

Even though cracking patterns are assumed invariant, published cracking patterns show variations. For example, the 16 peak of oxygen is given as 9%, 3% and 4% of the 32 peak in different tabulations (Eight Peak Index, Cornu and Massot 1966). We evaluated the cracking patterns of the following gases in the Supavac: H_2, O_2, N_2, CO, CO_2, CF_4, SF_6, Kr, and F_2. The results for four compounds along with published cracking patterns are given in table 3.2. The sensitivities with respect to helium were also determined and is given in table 3.3. The ratio of 66:47 heights for COF_2 was determined by reacting CO with F_2 in helium and recording the mass spectrum. This worked out to be 0.75 instead of the published 0.55.

We have used these measured results in analysing the mass spectra. Where measured results were not available published cracking patterns are used. However table 3.2 shows that drastic errors are not expected in using the published cracking patterns. Since we are more interested in the relative partial pressures of a compound, unique identification of its base peak alone is enough in many cases to evaluate the partial pressure of one compound.

Table 3.2

Compound	m/e values (row 1) and relative ion currents(row 2) as measured in Supavac. Values in bracket taken from Eight Peak Index and Cornu and Massot 1966.						
H_2	2	1					
	100	5.1					
	(100)	(2.1)					
O_2	32	16					
	100	6.9					
	(100)	(3.6)					
CO	28	12	14	16	30	29	
	100	2.3	0.3	0.5	0.24	1.13	
	(100)	(4.7)	(0.8)	(1.7)	(0.2)	(1.2)	
CO_2	44	32	28	16	22	12	29
	100	0.06	10.9	5.9	0.67	2.9	0.13
	(100)		(6.7)	(5.6)	(1.4)		(0.1)

Table 3.3

Sensitivities of the Supavac mass spectrometer to different gases.

Gas	Base m/e	Partial pressure wrt helium	Relative value of base peak wrt He 4 peak	Relative value of base peak per torr of gas (ppt of He)
(1)	(2)	(3)	(4)	(5)
H_2	2	.0093	0.0325	4.1
CO_2	44	0.0093	0.125	15.6
N_2	28	0.0093	0.10	12.5
CO	28	0.0066	0.088	14.7
O_2	32	0.0093	0.062	10.3
CF_4	69	0.0072	0.13	21.7
SF_6	127	0.0047	0.088	22.0

3.4.3 Measurement and reproducibility errors

The mass spectrometer reads ion currents directly in millibars with the assumption that all species are detected with equal sensitivity. The x-y recorder records this spectrum on an altered scale and the peak heights can vary according to the scan speed and inertia of the recording pen. An evaluation of this error was carried out by the stationary and scanned recording of the largest peak (which is expected to give the largest error). This error was found to be less than 2%, the scanned peak reading being always smaller than the stationary reading.

The linearity in response of the system was checked using helium and SF_6. Peak heights at 4 and 127 were recorded as a function of the total sample pressure as recorded by the ion gauge. The partial pressures increased linearly with the total pressure up to the maximum tested pressure of 2×10^{-6} torr.

The cracking patterns of SF_6 taken at three different times are given in table 3.4. The standard deviation for all the peaks is about 10%. Instrument reproducibility is thus found to be sastisfactory. However, analysis of gas mixtures may not show the same reproducibility in terms of the variation of partial pressures in two 'identical' experiments. Such variations are discussed in subsequent chapters when they arise.

Table 3.4

Reproducibility of cracking pattern of SF_6 in the Supavac.

m/e:	127	89	108	51	54	70	32	35
Trial 1	100	23.0	9.8	3.9	3.1	3.7	2.2	1.1
Trial 2	100	25.3	10.1	4.2	3.5	3.8	2.4	1.1
Trial 3	100	28.0	10.0	4.6	3.8	4.3	3.0	1.5
Mean of 3 trials	100	25.4	10.0	4.2	3.5	3.9	2.5	1.2
Published value	100	26.3	8.9	7.6	7.4	5.3	5.1	4.6

3.5 Fluorine passivation of the Supavac

Since the laser gas mixture contains elemental F_2 the Supavac mass spectrometer had to be first passivated with F_2. When the Supavac was tried at first with a helium-F_2 mix (760 torr:6 torr) the F_2 peak at 38 was hardly present (readings were less than 10^{-9} mbar). After several hours of use the F_2 response improved to 1.5×10^{-9} mbar indicating improved passivation of the instrument. Even after several months of use the reading at m/e of 38 for the same partial pressure of F_2 nas continued to increase slowly. In order to avoid large errors due to short term passivation by F_2, experiments on any day are preceded by at least half an hour of F_2 passivation using a 760 torr helium:6 torr F_2 mixture at 1.5×10^{-6} torr. Most of the experiments are carried out on a regular daily basis with the Supavac under less than 10^{-7} torr pressure whenever it is not used. Experiments after longer breaks (like weekends) are preceded by ıonger passivation runs. Since eaoh experiment normally ıasts only two hours, one does not expeot over this time interval any change ın the 38 peak reading due to loss of F_2 in passivation.

3.6 Presentation of results

The mass spectrum is processed by the computer as described in section 3.3.3. Usually each experiment results in three to four spectra taken at half hour intervals. The computed partial pressures of the gas components as a function of time is then passed on to a plotting subroutine which yields graphs of partial pressure vs time ror a requested list of the compounds on a hard copy plotter. The computer programme for this is given in appendix A.3.

The partial pressures are conveniently expressed as parts per thousand of the helium partial pressure (given by the magnitude of the peak at m/e of 4). Since helium concentration in the gas mix does not vary, this is a more reliable way of evaluating the results since the relative values are independent of the total sample pressure in the reservoir as long as the sample pressure does not vary over the duration of a scan. The sample pressure is kept around 1.5×10^{-6} torr. This is not an absolute value, since the ion gauge reading will, to an extent, depend upon the constituents of the gas mix.

In the following discussions the term impurity is used to indicate that the particular component of the gas mixture is unwanted or detrimental to laser performance. The rest of the thesis deals with experimental results obtained in the evaluation of the lasers described in chapter two utilising a helium-F_2 mixture (lasing at ~730 nm) and a helium-krypton-F_2 mixture (lasing at ~248 nm).

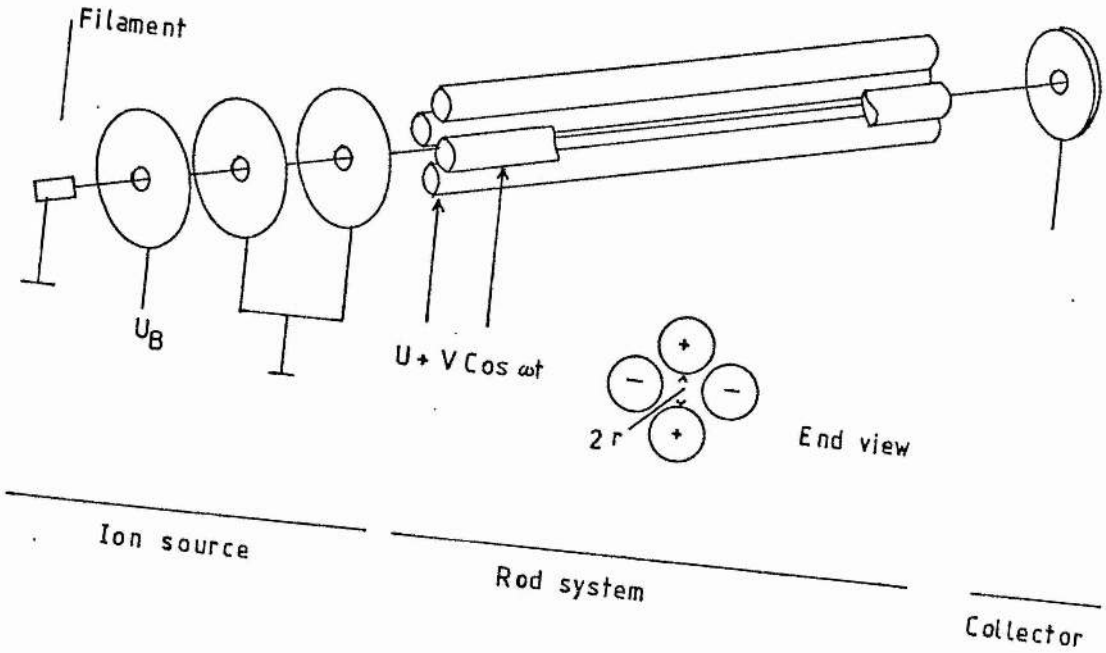

FIG 3.1 Schematic view of the quadrupole mass filter.

REFERENCES

Brittain, Ed. (1975) Introduction to Molecular Spectroscopy: Theory and Experiment, Academic Press.

Chapman J.R (1980) J. Phys. E 13 365.

Cornu A and Massot R (1966) Compilation of Mass Spectral Data, Hayden and Son Ltd with Presses Universitaries de France.

Eight Peak Index of Mass Spectra (1970) First edition, Mass Spectrometry Data Center, U.K.

Krugers J, Ed. (1968) Instrumentation in Gas Chromatography, Centrex Publishing Co., Netherlands, pp 11.

Reed R.I, Ed. (1965) Mass Spectroscopy, Academic Press, pp 48.

CHAPTER 4

IMPURITY FORMATION IN ATOMIC FLUORINE LASERS

The atomic fluorine laser output spans the wavelength range from 623.9 to 780.0 nm. There are 27 possible lines in this region arising from 3p -> 3s transitions in F^*. Of these, over half have been observed. These wavelengths are of practical interest in the excitation of dyes emitting in the near infra red. Investigations on the atomic fluorine laser have been mainly confined to its spectroscopic and discharge characteristics (Sadighi-Bonabi et al 1982, Sumida et al 1979, Lawler et al 1979). No reports on the lifetime of, or impurity formation in, He-F_2 mixtures have been published yet. Since the atomic fluorine laser is a two component system the mass spectra of the gas mix is not as cluttered as that of a three component system like KrF (He-Kr-F_2 mixtures). In KrF mixes the peaks at m/e of 41, 41.5, 42, 43, 78, 80, 83, 84 and 86 due to Kr are quite strong, which could mask the peaks at these masses due to the formation of small amounts of impurities or contaminants (that is, species other than the basic gas mix components). Mass spectrometric results from the F_2 laser mix can be compared to the results obtained for the three component KrF mix to gain more insight into the formation and effect of the impurities formed in the two different systems. In this chapter results obtained in the investigation of the F_2 laser in laser system versions 3, 4 and 5 are discussed.

4.1 The nature and effect of impurities

In He- F_2 mixtures the partial pressure of F_2 is around 6 torr in 850 torr of He. Since F_2 is highly reactive, this partial pressure is expected to drop in reactions with impurities in the gas mix, and with the electrodes and walls of the system. This limits the active lifetime of the gas fill. Apart from the loss of F_2 the laser output can decrease due to changes in the discharge characteristics and absorption at the laser wavelength caused by the impurities formed in the laser. In a closed system with a single fill of gas mix the loss of F_2 is more important since the impurities could be removed by appropriate filters and traps. Loss of F_2 in reactions would give rise to F_2 containing species like HF, SiF_4, COF_2, CF_4 etc. Subsequent sections in this chapter deal with the evolution of such impurities and those not containing F_2 but which could more readily react with F_2 to accelerate its loss. This is done for the various laser versions described in chapter 2.

4.2 Impurities in pure He discharges

Before looking at He F_2 mixtures we investigate the evolution of different species in a pure He fill in the two versions 3 (LV3- with the PMMA body) and 4 (LV4- with the PTFE body). This is done with and without a discharge in He. These experiments would give the outgassing rate of various gas components in the two systems. In both cases He at 850 torr is circulated in the laser at a rate

of 2 litres/minute. The pressure is kept slightly above atmospheric to prevent any possible leakage of air into the system even though the laser set-up was tested and found to be leak-tight. The mass spectra are recorded and processed as explained in chapter 3.

4.2.1 He fill without discharge

The solid lines (Δ) in figures 4.1 to 4.10 gives the uncorrected partial pressures of the various impurities in parts per thousand of He pressure as a function of time for He in LV3 and the dashed lines (X) with the discharge started at 27 minutes and continuing to the end of the experiment. The partial pressures for the various identified components in He in LV4 are given by curves marked (□). In this case the discharge is started in the same gas fill at 75 minutes till the end of the run so that the partial pressures from 0 to 75 minutes are for He without discharge in LV4. Comparison of the curves for the gas fill without discharge in LV3 and LV4 show the following. In LV3 concentrations of CO, and to a lesser extent, H_2 and HF remain steady, while that of CO_2, N_2, O_2 and Ar increase. The partial pressures of Ar, N_2, and O_2 in LV3 are more than that in LV4 at the beginning. The CO_2 background in LV4 is small (~0.3 ppt of He) compared to that in LV3 (~3 ppt of He) at start. The growth of CO_2 partial pressure in LV3 is larger than in LV4 over the same time period. The amounts of water vapour and hydrogen in LV4 are lower than in LV3. Species that are higher in LV4 are NO, SiF_4 and HF. Of these NO grows in LV4 whereas

hardly any NO was detected in LV3 (no significant signal at m/e of 30).

The partial pressure values of SiF_4 and HF depend upon the history of the mass spectrometer and laser. In the case of LV3 the mass spectrometer was not as passivated as it was for LV4 for which the readings were taken a few months later. The absolute values are therefore not easy to interpret, and have to be treated with caution. The same is true of the results for water vapour. In the case of water vapour the difference is large enough to suggest here that LV4 contains less background water vapour than LV3.

These observations suggest that on the whole LV4 with the PTFE body is 'cleaner' than LV3 with the PMMA body (as might have been expected). The higher initial values of O_2, N_2 and Ar in LV3 suggests that the background vacuum before filling with the mix is worse in LV3 than in LV4. The growing partial pressures of Ar, N_2 and O_2 suggest either the diffusion of air from outside or outgassing from the walls. This is higher for the PMMA system. The outgassing of CO_2 and water vapour from the walls is also higher for LV3 with the PMMA body. Large quantities of water vapour evolve from PMMA under vacuum (Beck 1964, pp232). The water retention of PTFE is zero (Beck 1964) so one expects less background water vapour pressure in the PTFE system (LV4) as is observed here. Outgassing rates for various plastics, including PTFE and PMMA are given in table 10 of Beck, 1964.

4.2.2 He fill with discharge

The partial pressures of various components when a discharge is established in He at 15 kV charging voltage and one pulse per second repetition rate show different rates of change in the two laser versions. In LV3, O_2 and CO decrease when the discharge is on. Other partial pressures remain about the same. One possible explanation for this is that in the presence of H_2O or H_2, CO reacts with O_2 to give CO_2 when the discharge is on (Kondratev 1964). Oxygen can also be used up in a reaction with C in the stainless steel preionizer wires. However, the CO_2 so produced has not significantly affected the rate of increase of CO_2 without discharge. In the case of LV4 the discharge, established from 75 minutes, mainly affects the increase in NO. It is probable that NO is converted into NO_2 even though no significant amount was detected. There is a slight increase in the rate of formation of CO_2 and CO and a slight decrease in the formation of HF. Reaction of O_2 with carbon in the corona wires could form CO_2 and CO. Another source of carbon is the plastic body itself, especially near the corona wire inserts where surface or near-surface arcing could produce CO and CO_2. Since the background H_2O vapour pressure is less in LV4, conversion of CO to CO_2 may not be as fast as in LV3.

The background values of SO_2 are higher in the PTFE system but remains below 0.1 ppt of He throughout. Small peaks in the 10^{-10} mbar range could be detected at m/e of 67, 69, 47, 48, 49, 50 etc but the partial pressures of compounds for these peaks are less

than 0.05 ppt of He and show no significant changes throughout the experiment.

4.3 Impurity species in He-F_2 gas fills

4.3.1 Variability of impurity in an initial fill

Before comparing the impurity levels in the various laser versions we first look at the variability in partial pressures of different species in three different initial mixes (that is, the laser mixture at the start of the experiment before any discharge) of 6 torr F_2 and 850 torr He in LV3 and LV4. Table 4.1 gives the calculated partial pressures and standard deviations for various species in LV3 and LV4 for three trials in each. The variation in initial pressures of CO_2 and N_2 are more for LV3 than LV4. Note the increased partial pressure of F_2 even though the mixes are identical. This is due to better passivation of the mass spectrometer. Laser version 4 (LV4) trials were done five months after LV3 trials. On the whole the initial levels of impurities are constant in both the versions. Their origin is mainly from the He and F_2 gases used in the experiments. The He is better than 99.9% pure but F_2 is only better than 98% pure. The SF_6 and SO_2 impurity comes from the F_2 sample. Other impurities possibly present in F_2 are HF, CF_4, and COF_2 even though it is difficult to decide how much of these arise in the reactions in the laser. Our

interest usually lies in the change in partial pressures of the various species during an experiment so the initial amounts are not that relevant as long as they are reproducibly present.

Table 4.1

Partial pressure variability of detected species in a He-F_2 gas mixture for three trials.

Compound	Partial pressures in ppt of He					
	LV3			LV4		
	Mean	σ	Coeff of Variance	Mean	σ	Coeff of Variance
N_2	8.4	7.0	82	1.33	0.06	4
H_2O	3.4	2.0	61	1.7	0.53	31
H_2	1.0	0.06	6	0.49	0.23	46
HF	3.6	1.4	39	5.0	0.42	8
SiF_4	0.4	0.35	80	1.1	0.15	13
COF_2	0.11	0.03	26	0.23	0.12	53
CF_4	0.29	0.08	26	0.33	0.14	43
O_2	1.5	1.1	78	0.2	0.01	6
CO_2	5.0	1.4	28	3.0	0.47	16
CO	1.6	0.8	48	1.5	0.15	10
NO	0.08	0.07	94	0.11	0.03	24
SF_6	0.14	0.04	31	0.15	0.07	47
SO_2	0.08	0.01	12	0.21	0.06	30
F_2	0.38	0.33	87	4.5	0.46	10
Ar	0.28	0.08	28			

Comparison of the initial fills in LV3 and LV4 shows that they follow the same pattern as He fills discussed in section 4.1, with LV3 containing higher background values of CO_2, O_2, Ar, N_2 and H_2O. Apart from these impurities, presence of F_2 gives rise to HF, SiF_4 and CF_4 in both the versions. There is a significantly higher level of SO_2 in LV4. Its origin is unknown.

The initial mix in LV5 behaves the same way as in LV4 as expected since the version LV5 is basically similar to LV4 except for the electrodes and corona wires, which would not significantly influence the impurities without discharge.

4.3.2 Impurity evolution in He-F_2 fills without discharge

Figures 4.11 to 4.22 show the evolution in time of the various species detected in the laser gas mixture of 6 torr F_2 to 850 torr He in LV3, LV4 and LV5 (curves marked Δ, x, and □ respectively). The gas was circulated without any discharge to obtain these results. Therefore the changes in concentration of the various species would be due to outgassing, adsorption, surface reactions and normal chemical reactions between the species and the walls of the laser body. The materials of construction of the three lasers are given in chapter 2. Versions LV4 and LV5 are practically identical except for a change of electrodes and corona wires from Al and stainless steel in LV4 to monel and nickel in LV5. Thus for a passive situation where a mix is circulated without a discharge

the changes in gas composition would be identical in LV4 and LV5. The variation in CO_2, N_2, O_2, H_2O, SiF_4, COF_2, CF_4, and SO_2 are similar in both lasers. The partial pressure of HF is higher in LV5 at the start, mainly because the experiment was done immedietely after the mass spectrometer had been used to sample a similar mix, leaving a higher HF background reading. The rises in HF and SiF_4 readings are due in part to the increase in mass spectrometric background of these species. The increase of NO partial pressure in LV5 is less than in LV4, whereas the CO partial pressure in LV4 is less, and drops, when compared to CO in LV5. The reasons for this are unknown. Fluorine partial pressure is higher in LV5 because it was taken later in time, after improved passivation of the system.

Comparison of these two PTFE laser systems with the less clean PMMA version LV3 show trends which agree with the previous observations using He alone. The most significant observation is the increase in CO_2 partial pressure in LV3, from 5ppt to 30 ppt in about 100 minutes whereas in LV4 and LV5 they hardly change. This increase, in absolute terms using the calibration table, is from 0.3 torr to 1.9 torr. This increase in LV3 is higher than in the pure He experiment (about 6 ppt in 100 minutes), showing the influence of F_2. Fluorine probably reacts with the PMMA to liberate CO_2. The initial increase in N_2 and O_2 are slightly higher in LV3. The background pressures of N_2, O_2, and H_2O are higher in LV3. Differences in partial pressures of F_2, SiF_4, and HF are mainly due to differences in passivation of the mass spectrometer.

The main differences between the PMMA and PTFE versions are therefore the increased production of CO_2 in the PMMA version and the higher background values of N_2, O_2, and H_2O. These are explained by the fact that PTFE is more inert to F_2 attack, and to outgassing of H_2O, etc (Beck 1964).

It is also seen that the F_2 partial pressure drops by one ppt over 100 minutes for LV5 even when the laser is not on. For LV4 and LV3 the drop is masked by inadequate passivation problems. This could mean than other fluorine carrying species (HF, COF_2, CF_4 etc.) are formed even without a gas discharge being present, thus limiting the gas lifetime of the mix even when the laser is left unused.

4.3.3 Impurity evolution in He-F_2 fills with discharge

Figures 4.23 to 4.34 give the evolution of the various detected species in the gas mix when the discharge is switched on after the first scan at the time indicated by L on the figures. The three scans were taken in the version LV4 (PTFE) under identical conditions; that is, the same mix ratio (6 torr F_2 to 850 torr He), the same discharge voltage (25 kV, one pulse per second) and the same flow conditions. The curves (Δ) were taken after the laser was passivated by a half-hour run using a similar mixture under similar conditions. The other two curves ($\times$) and ($\square$) were taken after the laser was used over a period of about two hours. Results of a run without discharge is given by curves ∇, for comparison.

The deviations of the curves Δ from curves X and □ are more than that between curves X and □ for CO_2, H_2O, O_2, and SiF_4. But, on the whole, the evolution rates of the impurities are the same in the three experiments. The changes are approximately linear for CO_2, SiF_4, and F_2. These curves give us an idea of the variability of evolution rates of the impurities as a function of the passivation of the laser. It has to be pointed out that the variations in SiF_4 and HF are only partly due to their partial pressure increases in the laser; the rest are due to their production in the mass spectrometer. Similarly, the variations in water vapour are also difficult to interpret, as was pointed out before.

The effect of changes in materials of construction of the laser on the constituents of the gas mix and the laser output energy is seen in the plots in figures 4.35 to 4.50. They give the evolution of impurities for laser versions 3 (LV3 - Δ), 4 (LV4 - X) and 5 (LV5 - □). The laser output energy is given in fig 4.51 for the three versions with the energy at start taken as 1.0 in each case. This measured energy is the amplified spontaneous emission (ASE) from the laser with 4% feedback from the aligned cavity windows but without any mirrors. These curves can be compared with the corresponding curves in figures 4.11 to 4.22 where the gas is circulated without discharge to find the effect of the discharge. The laser output curves show that the PMMA version, with only 780 pulses to half power, is a very poor performer when compared to the two PTFE versions. The output energy from LV4 and LV5 did not change over two hours of operation at one pulse per second. The

cause of the decrease in energy could be either depletion of F_2 or/and presence of absorbing or quenching impurities. A separate experiment was done with a fresh mix of 850 torr He and 3 torr of F_2 to find the output power of the laser when the F_2 concentration has depleted to half but without change in impurity levels from time 0. This showed an increase in energy from 1.67 (in arbitrary units) to 2.18. This shows that any decrease in the F_2 laser energy when the F_2 concentration has fallen to half is caused by impurities evolving in the laser and not by F_2 depletion.

The F_2 partial pressure in LV3 falls to half its initial value in just under 17 minutes. Over the same period of time the F_2 partial pressure in LV4 drops to 95% of its value at t=0 and in LV5 this drop is to 93%. Fluorine reactions in LV3 are therefore taking place at a far higher rate than in LV4 or LV5. This has to be due to the higher levels of impurities in LV3 compared to LV4 and LV5. The F_2 partial pressure drops in LV5 at a slightly higher rate than in LV4.

The impurities containing F_2 molecules detected by the mass spectrometer are COF_2, CF_4, HF, SiF_4, OF_2, SF_6, and SO_2F_2. Apart from these, the ion current at m/e of 119 is also found to grow, and is attributed to C_2F_5 group belonging probably to an organic fluorinated compound like hexafluoropentane. Of these COF_2 in LV3 at t= 40 minutes (when the laser energy has dropped to half its initial value in LV3) is 1.5 ppt of He, far higher than in LV4 or LV5. The rate of increase of COF_2 in LV3 is also much higher, probably due to the higher CO_2 partial pressures. The rate of rise

of CF_4 in LV3 is about the same as in LV4 but its value is slightly less than in LV4 at t= 40 min. The value of SiF_4 increases till the end even though F_2 is being used up. We would expect the SiF_4 pressure to go down if the contribution is only from inside the mass spectrometer since it would be proportional to the fluorine pressure. Fluorine is therefore being lost by reacting with Si (in Aluminium of the electrodes and the electrode plates) to yield SiF_4. The reaction path leading to the formation of SiF_4 may involve H_2O, HF, and H_2. When the SiF_4 curves in the two sets (with and without lasing - figures 4.16 and 4.40) are compared for LV4 and LV5, the amounts of SiF_4 are the same at t= 75 minutes but the rate of increase is slightly less when the laser is on. For LV3 the rate of increase of SiF_4 is higher when the laser is on. Thus the rate of production of SiF_4 in LV3 is higher than in LV4 or LV5. Since the H_2O, H_2 partial pressures in LV4 and LV5 are lower than in LV3 one would expect the production of SiF_4 inside the laser system to be higher in version LV3 than in LV4 or LV5. The rate of growth of HF is about higher in LV3 compared to LV4 and LV5 when there is no discharge. Since the H_2O partial pressure is higher in LV3, one would expect higher rates of increase of HF in LV3 due to the reaction

$$H_2O + F_2 \rightarrow 2HF + (1/2)O_2$$

However, the HF partial pressure falls in LV3 when the discharge is on. This seems to be mainly due to the drop in background HF in the mass spectrometer since F_2 concentration drops to 50% of its initial value in 17 minutes for LV3 whereas the drop is only about 5% for LV4 and LV5. On the whole, HF concentrations are lower when the discharge is on, showing that it is taking part in reactions in

the laser, probably with Si to produce SiF_4.

The amount of SO_2F_2 produced in times up to t= 80 minutes in LV4 and LV5 when the discharge is on is negligible but in LV3 it increases to 0.14 ppt of He from 0.0 at start. Without discharge there is no SO_2F_2 production. The source of S could be partly from SF_6 impurity in the gas mix and partly from the Neoprene O-rings in LV3. versions LV4 and LV5 use Viton O-rings.

The amounts of OF_2 and its increase in LV4 and LV5 are higher than in LV3. LV5 has a slightly higher rate of increase of OF_2 than LV4. After t= 50 minutes the rate of increase of OF_2 levels off indicating that it is taking part in other reactions. Sulphur hexafluoride, present as background impurity, is also taking part in reactions as seen by the drop in its partial pressure in LV3, LV4 and LV5 when the discharge is on.

Of the rest of the impurity species (which do not contain F atoms), CO_2 seems to be the most important. The high background pressure of CO_2 in LV3 compared to LV4 and LV5 can lead to a faster depletion of F_2 in a reaction

$CO_2 + F_2 \rightarrow COF_2 + (1/2)O_2$

Thus in LV3 we see a higher rate of increase of both COF_2 and O_2 compared to LV4 and LV5. Further reactions of COF_2 with F_2 yield CF_4 and O_2. However, the increase in CF_4 in LV3 is smaller than in LV4 or LV5 because of the rapid depletion of F_2 in LV3.

Comparing LV4 ad LV5, the rate of increase of O_2 in LV5 is higher. The continuously monitored rate of increase of CO_2 in LV4 and LV5 is given in figure 4.52. The curves show that CO_2 production in LV5 is lower than in LV4. In fact, the rate of increase of CO_2 seems to be balanced by the rate of loss of CO_2 in reaction with F_2 for the first 50 minutes. After 50 minutes, the rate of loss of CO_2 is less because the concentration of F_2 has decreased, and this results in the increase in CO_2 partial pressure. Since LV5 uses nickel corona wires, CO_2 production at the corona wire site will be zero (unlike the case of stainless steel corona wires containing carbon as used in LV4). Thus, O_2 is used up to a lesser extent in LV5, and CO_2 increases at a lower rate, compared to LV4.

The partial pressure of CO in LV3 drops faster when the laser is on compared to LV4 and LV5. In LV4 and LV5 the drop starts much later. Again this could be because CO generation inside the system is dependant on F_2 concentration. The concentrations of H_2O and H_2 are also higher in LV3, leading to higher rates of production of HF and SiF_4. The larger amounts of H_2 in LV3 could be from the increased amount of H_2O which can react with F_2 to yield HF, H_2, and O_2.

When subjected to repetitive discharges N_2 partial pressure falls in LV4 and LV5 at about the same rate, and rises at a slower rate in LV3, compared to the partial pressures in the unlased mix (fig 4.36). Apart from small concentrations of NO and NO_2 no other compounds such as NF_3, N_2F_2, N_2F_4, were detected in the mass scan.

The partial pressure of NO_2 decreases when the laser is on and that of NO increases at a slower rate compared to the unlased mix. The decrease in N_2 does not seem to be fully accounted for by the increase in NO. It is possible that N_2 forms non-volatile nitrides at the electrode site which are not detected in the gas mix.

The above analysis of the variation in partial pressures of the detected impurities in the gas mix shows that LV3, with its higher initial partial pressures of CO_2, H_2O, N_2, O_2 gives the worst gas and laser lifetime performance of the three versions. This is due partly to the faster rate of depletion of active F_2 and partly to the deleterious effects on the discharge of the impurities evolving in the laser. Since the F_2 laser output is in the red, and since the impurities are simple compounds without any absorption bands in the red region of the spectrum, their effect is primarily on the discharge and on the preionization. The gas mixtures in versions LV4 and LV5 show lesser amounts of CO_2, N_2, O_2, and H_2O and also lesser amounts of increase of COF_2, CF_4, OF_2, SiF_4, and HF. The laser output hardly changes over the time period studied, because the depletion of F_2 and the formation of impurities are on a much longer time scale. The higher levels of impurity production in the PMMA version (version LV3) shows that PMMA is chemically less suitable than PTFE as an insulator in F_2 lasers. The stainless steel corona wires are also less suitable than the nickel corona wires since CO and CO_2 production at the corona wire is more for LV4. The aluminium alloy is best replaced by another not containing silicon to avoid the formation of SiF_4. Neoprene O-rings in LV3 could have been one cause for the increased

evolution of SO_2F_2 in that version.

In the next section we study the effect of cold traps on the impurities in the laser mix and how it affects the lasing lifetime of a single fill.

4.4 Effect of cold traps on $He-F_2$ gas lifetime

In this section we compare LV3 and LV4 laser versions in which cold traps are used to condense out the impurities formed in the system. In version LV3 the cold trap is kept at $-150^{o}C$ and in version LV4 it is kept at liquid nitrogen temperature (LNT : $-195.8^{o}C$). It is found that the flow rate and cold trap size are such that the F_2 partial pressure is not affected by the LNT trap even though F_2 condenses at $-188.1^{o}C$.

4.4.1 Impurity evolution in LV3 with cold trap

Curves marked □ and ∨ in figures 4.53 to 4.68 give the changes in partial pressures of different species in the gas mix as a function of time in LV3 without and with the cold trap at $-150^{o}C$. The laser output energy in relative units is given in fig 4.69 (curves marked □ and ∨).

It is seen that the cold trap increases the life to half power of the gas mix in LV3 from 780 shots to 2800 shots. The cold trap is expected to condense the following species (with boiling points above -150°C): CO_2, SiF_4, HF, H_2O, COF_2, CF_4, SF_6, SO_2F_2, and SO_2. It is seen from fig 4.56 that the CO_2 partial pressure is much lower in the cold trapped version. The first scan was taken after the cold trap was at -150°C for 10 minutes, long enough for the CO_2 to reach the reduced partial pressure determined by the low temperature. The nett rate of increase in CO_2 is also reduced but the trap capacity is not enough to cope with the high rate of production of CO_2 in the laser. The N_2 partial pressure drops during the discharge compared to the change without the cold trap. This is not directly due to the cold trap since N_2 liquefies at -196°C. Of the other compounds the decrease in CO_2 has led to an expected decrease in O_2 production from CO_2. There is a slight increase in COF_2 and CF_4 partial pressures compared to the untrapped version. This could be due to the lower rate of depletion of F_2 in the trapped system. The partial pressure of F_2 drops to half its initial value in 17 minutes in the untrapped version and 31 minutes in the trapped version. The rate of drop of CO is smaller in the trapped version; this could be due to the smaller amount of background O_2, which leads to a decrease in the oxidising reaction with CO when H_2O is present. The absolute amounts of HF, and F_2 are higher in the cold trapped version but this is mainly due to lack of passivation when the experiments with the untrapped version were carried out. The partial pressure of HF drops at about the same rate in both experiments. However, the

partial pressure of SiF_4 is less in the cold trapped version even though one expects a higher background of SiF_4 because F_2 decay is less in the trapped version. This indicates that SiF_4 condenses in the cold trap (as expected from its boiling point).

The depletion rate of F_2 is almost halved when the cold trap is used. The drop in output energy in LV3 without the cold trap is not due to the drop in F_2 partial pressure (which takes 17 minutes to halve in value, during which time the laser output, if there were no impurities, would go up slightly) but due to the evolved impurities. The increased number of pulses to half power in the trapped version LV3 is mainly due to the decrease in background impurities, notably CO_2 , O_2 and N_2. Background partial pressures of HF, SiF_4, and H_2O can also be expected to be smaller even though this is not clear from the mass scans (due to background interference).

4.4.2 Impurity evolution in LV4 with cold trap

Curves Δ and X in figures 4.53 to 4.68 give the evolution of components in the gas mix in LV4 without and with the cold trap at $-196^{\circ}C$ (LNT). The state of passivation of the mass spectrometer is about the same when the two experiments were done so that the partial pressures of SiF_4, HF, and F_2 can be compared with a greater degree of confidence than for LV3. Comparison of the curves show that the partial pressures of all the major impurities drop dramatically when the cold trap is used. The amount of CO_2 is

seen to be less than in the untrapped version and to decrease with time. Oxygen production (inferred from partial pressure) is seen to decrease. This may be partly due to the drop in CO_2 and partly due to O_2 being trapped out (b.p. of O_2 is $-183^{\circ}C$). Water vapour is also expected to be trapped and, in fact a small decrease in the partial pressure of H_2O is recorded but it is not conclusive since the background variations are larger. However, one expects this decrease to lead to a fall in the partial pressures of HF and O_2. The partial pressures of HF and SiF_4 go down as seen in figures 4.57 and 4.58 since they appear to be efficiently trapped. Partial pressures of CO and NO decrease at about the same rate in both trapped and untrapped versions. The partial pressure of CO in the trapped version drops faster than in the untrapped version. Possibly this is due to a decreased production of CO at the corona wires due to a decreased amount of O_2 in the trapped version. The decrease in CO_2 and H_2O have lead to a reduced amount of F_2 being used up in the reactions which yield HF, SiF_4, COF_2, and CF_4. The F_2 partial pressure drops to half its initial value in 73 minutes without the trap, whereas with the trap, the time required is 140 minutes. The laser energy increases in time (see figure 4.69, curves marked Δ , X) since the impurities decrease over the same time. The number of shots could not be estimated since there was no drop in output energy over the time interval studied. The energy output from a fresh He-F_2 mix with 3 torr of F_2 is more than from a similar mix with 6 torr of F_2. In the cold trapped version the impurity levels are maintained at around that in the fresh mix. This causes an increase in output energy from the He-F_2 mix when the F_2 partial pressure goes down in time.

Of the rest of the impurities only NO and SO_2F_2 appear to have significant influence. The variation of NO is random as seen from the figure 4.68. At 48 minutes SO_2F_2 in LV3 without cold trap is 0.14 ppt of He and with the cold trap it is down to less than 0.09 ppt of He at 53 minutes (see figure 4.67). All other impurities except the constant background of HCl at about 0.1 ppt of He are less than 0.1 ppt of He. In LV4 the background SO_2 is about 0.1 ppt of He with and without the cold trap. The version without the cold trap nas about 0.1 ppt of SO_2F_2 at 115 minutes but with the cold trap this goes to zero. The background SF_6 impurity drops in all cases. Part of it is possibly converted to SOF_2 and SO_2F_2, especially in the runs without the cold trap.

4.4.3 Comparison of cold trapped LV3 and LV4

It is seen from the above results that a simple cold trap with liquid nitrogen as a coolant improves the lifetime performance of the atomic fluorine laser to a great extent. The temperature of the cold trap and its capacity are also seen to be important parameters. It is seen that for the flow rate used here and for the size of the cold trap, F_2 is not condensed out at -196^{o}C. However, this temperature is much lower than the boiling point of many of the other species appearing in the system and these are apparently removed efficiently. These improvements in the gas mixture result in an increased number number of pulses to half power for the PTFE version LV4. Also, F_2 is used up more slowly.

For the PMMA version LV3 the improvement is not so marked because of the less efficient (-150°C) cold trap and the higher background production rates for CO_2 and H_2O. Even in this case, the output falls to half its initial value in 2800 shots instead of the 780 shots without the trap. In both versions, the rate of drop of F_2 is halved when the cold trap is used.

4.4.4 Mass spectral analysis of cold trap contents

The contents in the cold trap of LV3 and LV4 were examined to find out the nature of the impurities trapped out. The analysis could not be done quantitatively since the amounts were small and reactive, thus changing their partial pressures in time. However a qualitative analysis shows the following:

Versions LV3 and LV4 have the same kind of impurities but the LV4 trap is more efficient in trapping them out. The strongest in LV3 was at 44 (CO_2) followed by 28, 12 (CO_2), 69 (CF_4), 85 (SiF_4), 47,66 (COF_2), 30 (NO) and smaller peaks at 119, 131, 100 assigned to halogenated compounds with $C_2F_4^+$ (100), $C_2F_5^+$ (119) groups. The peak at 131 could be due to a halogenated compound with $C_3F_5^+$. In LV4 the strong peaks are observed at 69 (CF_4), 47, 66 (COF_2), 44 (CO_2), 85 (SiF_4), 119 ($C_2F_5^+$), 127 (SF_6) and 131. The 119 peak is very prominent. Peaks with $>0.1\times10^{-9}$ mbar readings are found at 108 (SiF_4^+), 105 ($SO_2F_2^+$), 102, 100 ($C_2F_4^+$), 97, 93, 81, 83, 75, 62, 60, 33 etc, many of which can be assigned to CF_n groups. Their ratios suggest the presence of hexafluoroethane. This could be the

final stable product in many reactions with F radicals of the plastics PTFE and PMMA. The recorded mass spectrum of the cold trap contents is given in figure 4.70.

4.4.5 IR analysis of cold trap contents

The contents of the cold trap were transferred into an evacuated cell 10 cm long made of Al with NaCl windows for an infra-red analysis of the contents. The IR spectrum, taken on a Perkin Elmer spectrometer, is given in figure 4.71. The Na_2SiF_6 is probably formed by a reaction of NaCl with the trapped SiF_4. The other peaks are identified as due to SiF_4, COF_2, CF_4, NO_2, CO_2, NF_3, SF_6, and the CF_3-CF_2 group. These assignments confirm the mass spectral analysis of the cold trap contents.

4.5 Conclusions

The above study shows that the mass spectrometer is a very useful tool for the quantitative evaluation of the components of a laser gas mixture. The He-F_2 mixture used in the three different versions is seen to have mainly the following impurities: CO_2, H_2, HF, N_2, O_2, CO, SiF_4, COF_2, CF_4, SF_6, SO_2F_2, OF_2, and NO. Their evolution depends on the materials of construction of the laser. It is seen that PMMA is worse than PTFE as the insulator material due to its higher rates of outgassing and interaction with F_2. This results in higher partial pressures of CO_2, N_2, H_2O, etc in

the gas mix compared to the PTFE version. These impurities, especially CO_2, and H_2O, react with F_2 to produce COF_2, CF_4, HF, and O_2. The impurities reduce the output energy by interfering with the laser kinetics and preionization processes and reduce the lifetime of a single fill by removing the active F_2 molecules by converting them into compounds like COF_2, CF_4 and HF. These reactions reduce the gas lifetime of the mix in PMMA laser version to 17 minutes (for F_2 depletion to half its initial pressure) and the laser lifetime to 780 shots to half power. However, for the laser with PTFE as the insulator, the background levels of CO_2 and H_2O are smaller and this improves the gas lifetime to 31 minutes and the laser energy hardly drops in two hours of operation at one pps. The Si in the Al electrodes reacts with F_2 and HF to produce SiF_4, thus providing another depletion route for F_2. The production of CO and CO_2 impurity in the PTFE version is reduced by replacing the stainless steel corona wires in LV4 with nickel corona wires.

Use of a cold trap to liquify the impurity components of the gas mix and thus reduce their levels in the active volume of the laser is found to be successful in increasing the number of shots to half power and the F_2 lifetime. In the case of the PMMA version the gas lifetime is doubled and the number of shots goes up to 2800 when a $-150^{o}C$ cold trap is used. In the PTFE version the trap is more efficient, partly because it is colder ($-196^{o}C$) and partly because the evolution rates of the impurities are lower. This results in a doubling of the gas lifetime. Analysis of the cold trap contents reveals the presence of CO_2, SiF_4, HF, NO, NO_2, NF_3, CF_4, SF_6, etc,

basically the same components found in the gas mixture. An infra red spectral analysis of the cold trap contents confirms the identity of the compounds. It is also seen that the presence of the impurities reduces the energy output of the He-F_2 laser by interfering with the discharge processes. The loss of F_2 due to reactions with the impurities is only of secondary importance.

In the next chapter we look at the impurity evolution in a He-Kr-F_2 mixture in the PTFE laser version and how it affects the laser and gas lifetime of the KrF laser. The results are then compared with the results presented in this chapter.

Figures 4.1 to 4.10
Uncorrected partial pressures of the detected impurities in Helium:

—▽— Version LV3 without discharge -✕- with discharge

··□·· Version LV4, without discharge till 75 minutes, with discharge till end from 75 min.

L marks start of discharge.

FIG 4.1

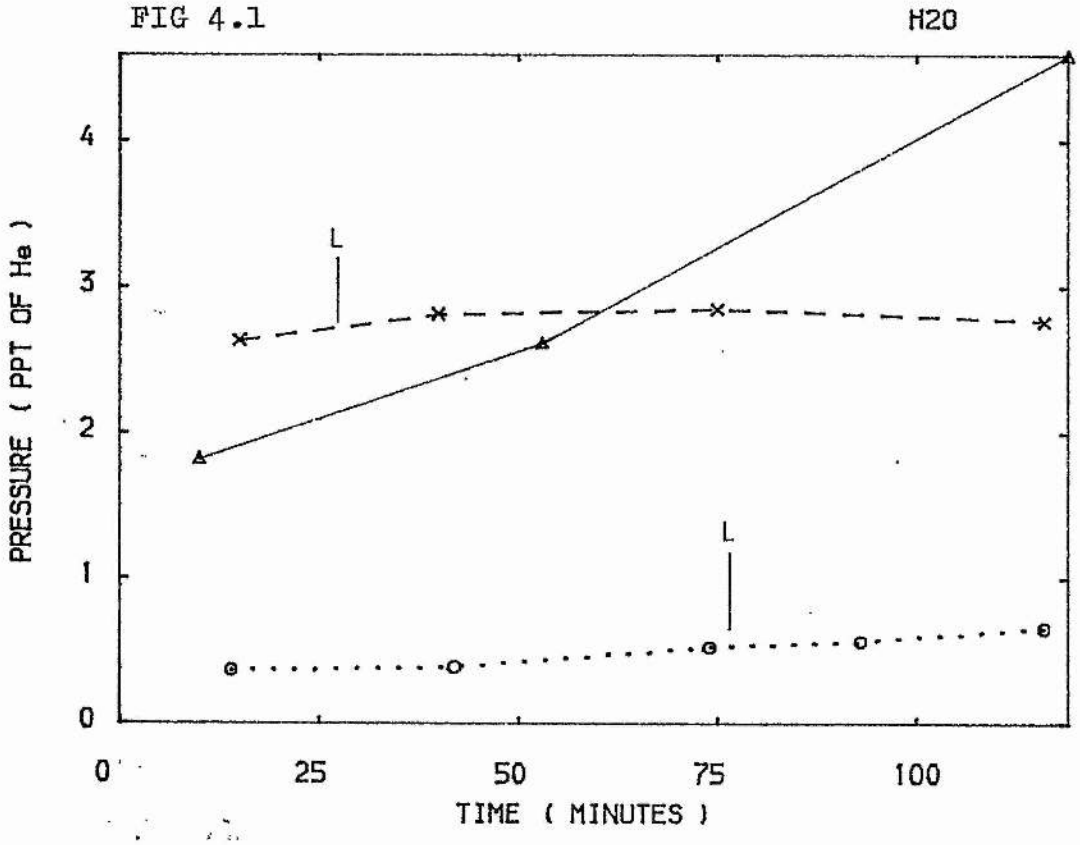
H20
PRESSURE (PPT OF He)
TIME (MINUTES)
L
L
0
1
2
3
4
0
25
50
75
100

FIG 4.2

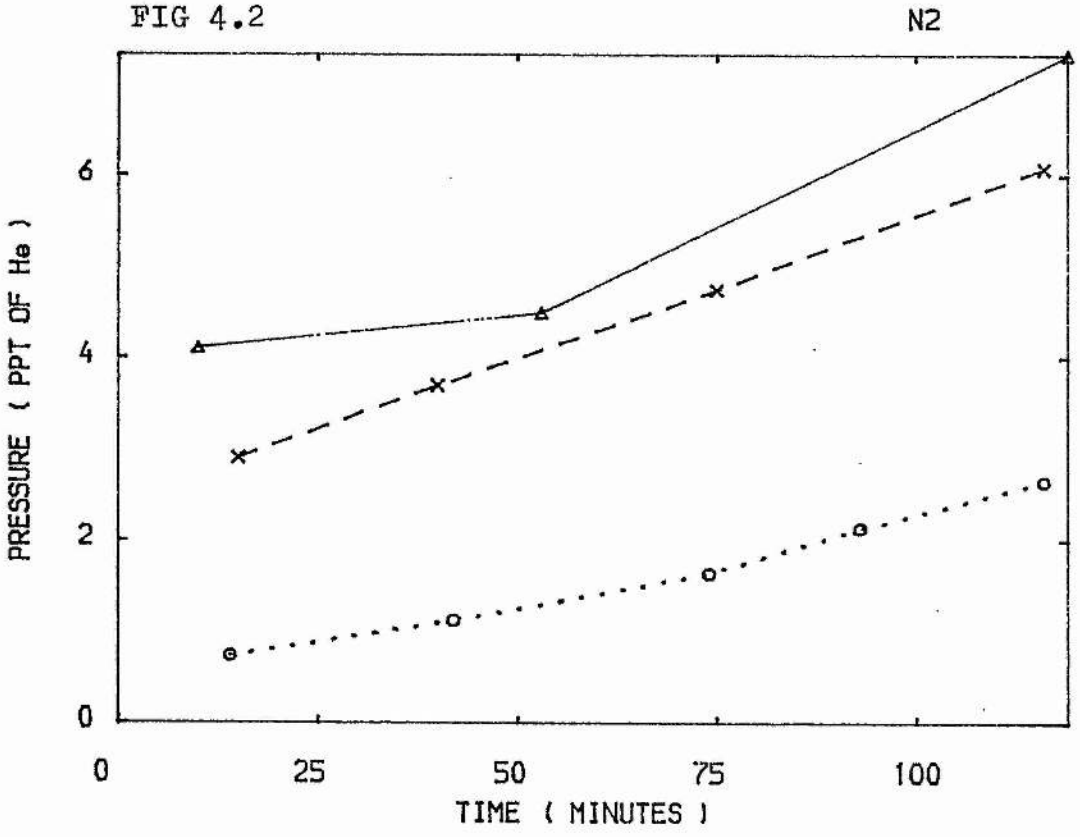
N2
PRESSURE (PPT OF He)
TIME (MINUTES)
0
2
4
6
0
25
50
75
100

FIG 4.3

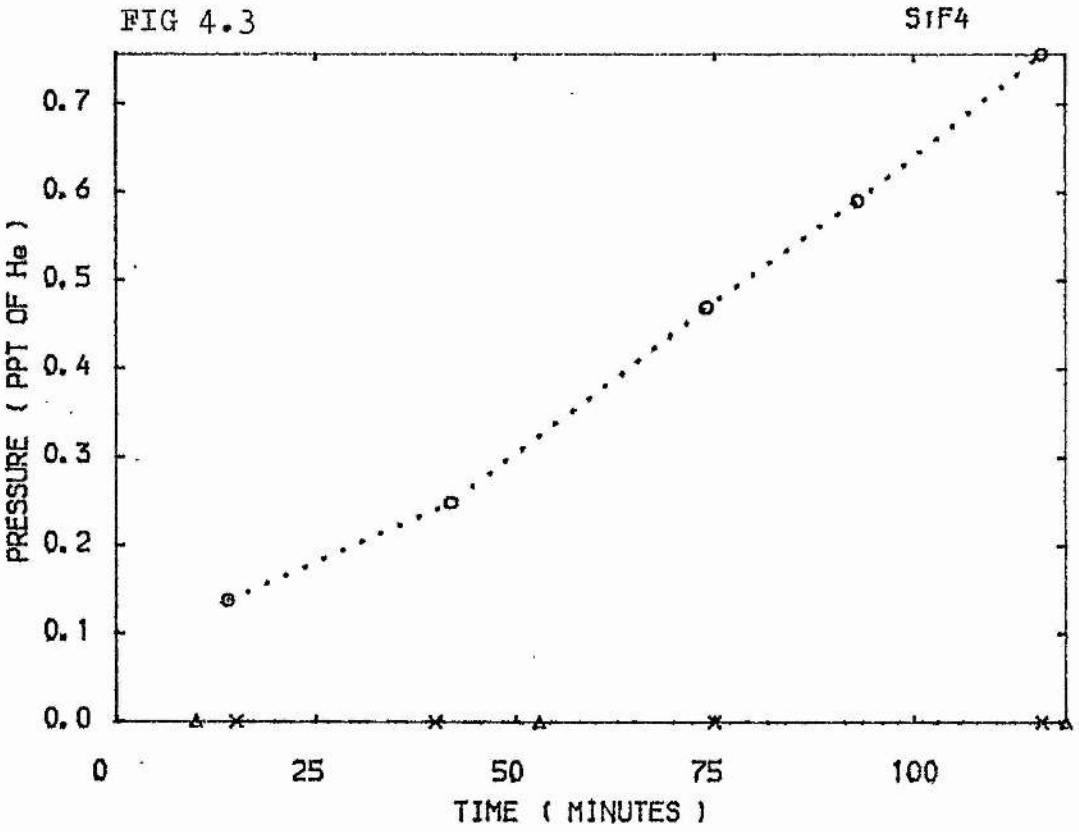
SiF4
PRESSURE (PPT OF He)
0.0
0.1
0.2
0.3
0.4
0.5
0.6
0.7
0
25
50
75
100
TIME (MINUTES)

FIG 4.4

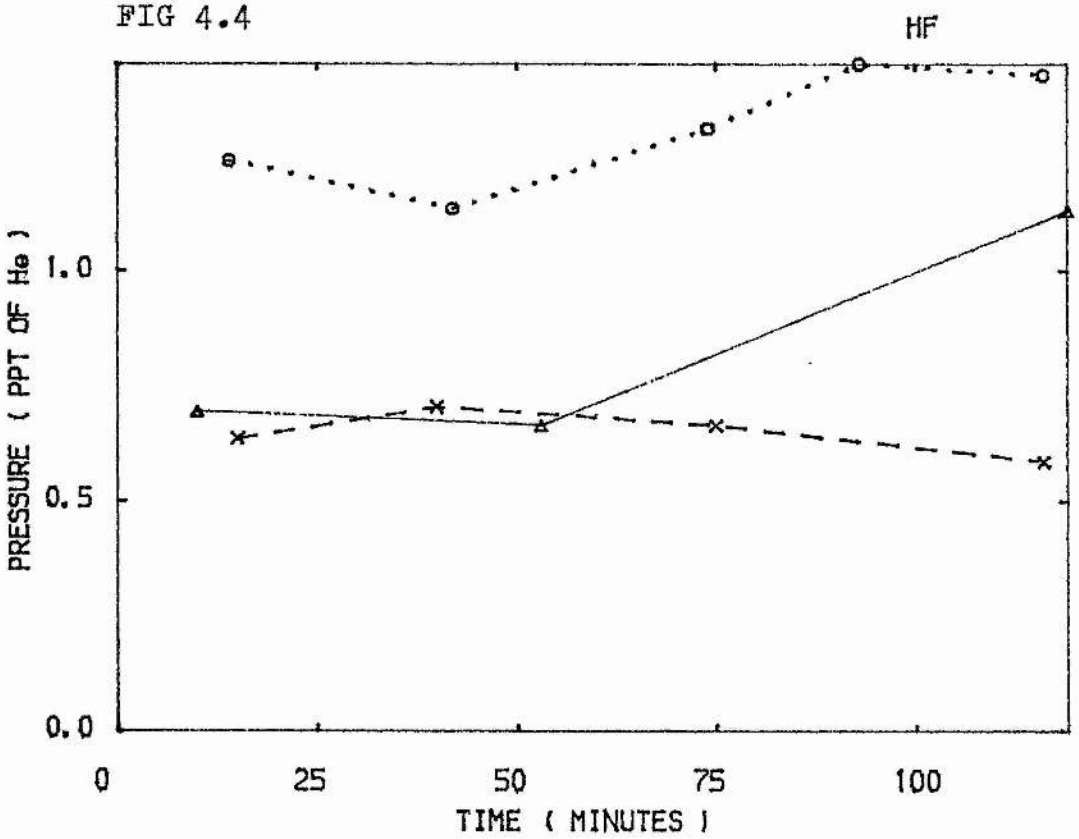
HF
PRESSURE (PPT OF He)
0.0
0.5
1.0
0
25
50
75
100
TIME (MINUTES)

FIG 4.5

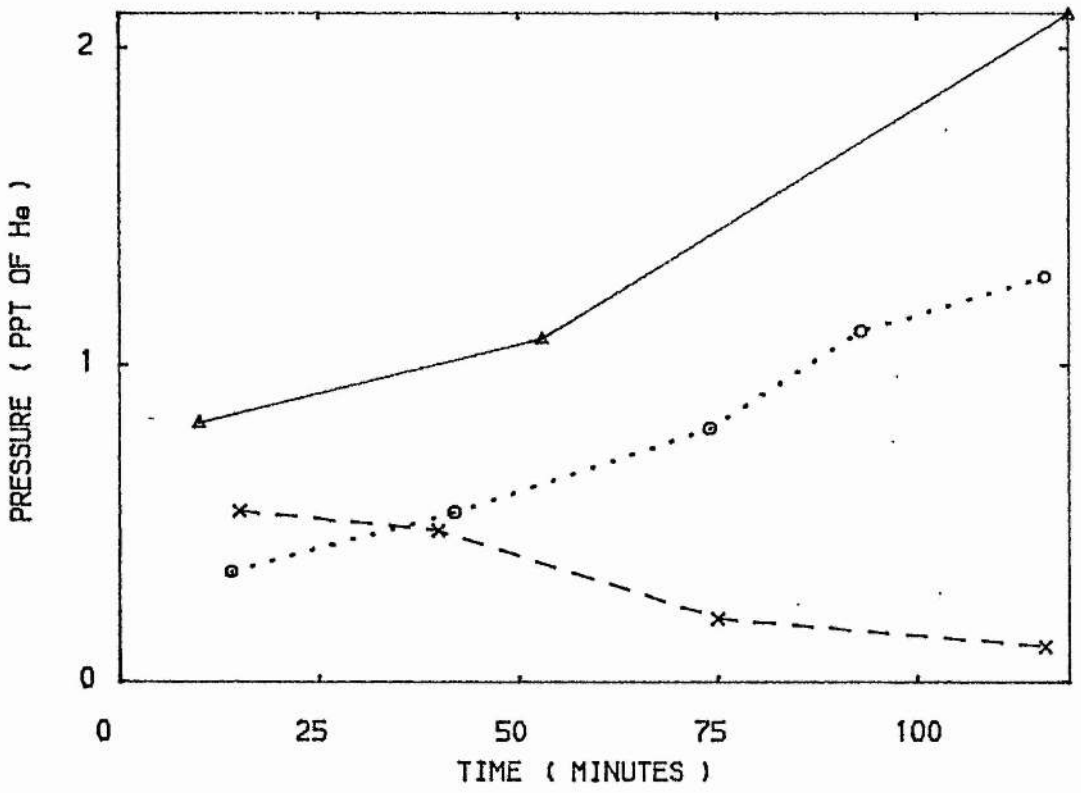
O2
PRESSURE (PPT OF He)
2
1
0
0
25
50
75
100
TIME (MINUTES)

FIG 4.6

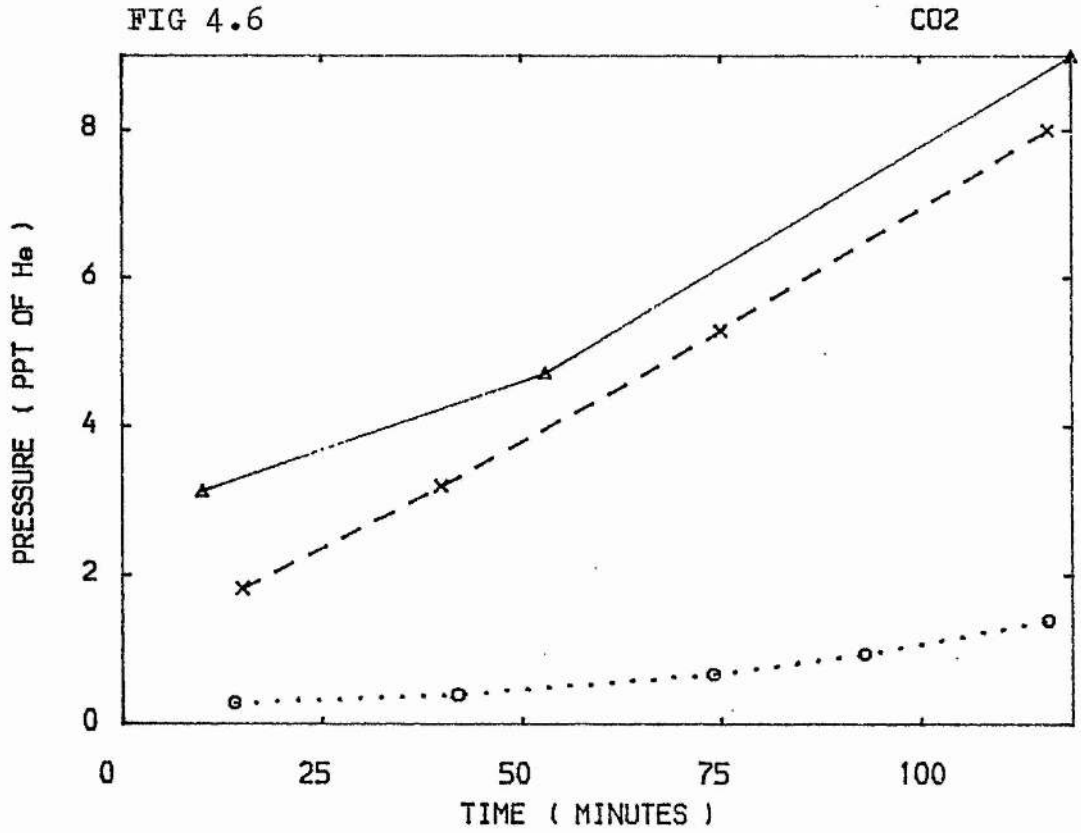
CO2
PRESSURE (PPT OF He)
8
6
4
2
0
0
25
50
75
100
TIME (MINUTES)

FIG 4.7

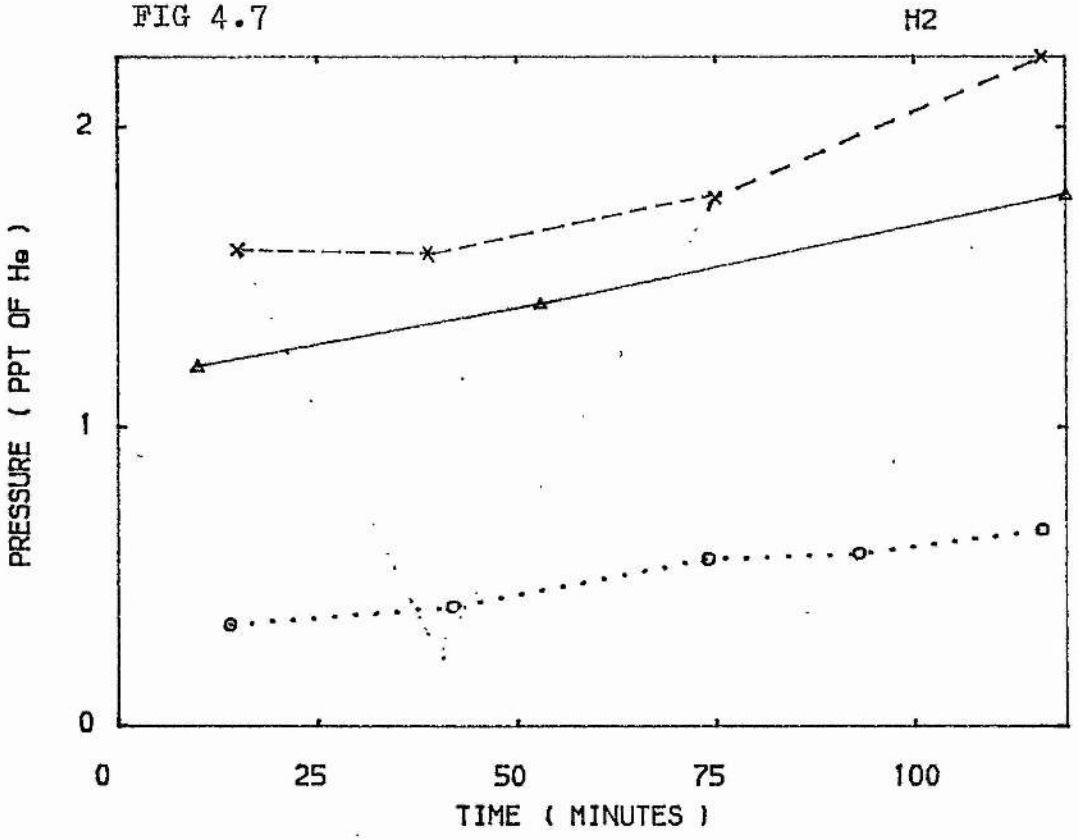
H2
PRESSURE (PPT OF He)
2
1
0
0
25
50
75
100
TIME (MINUTES)

FIG 4.8

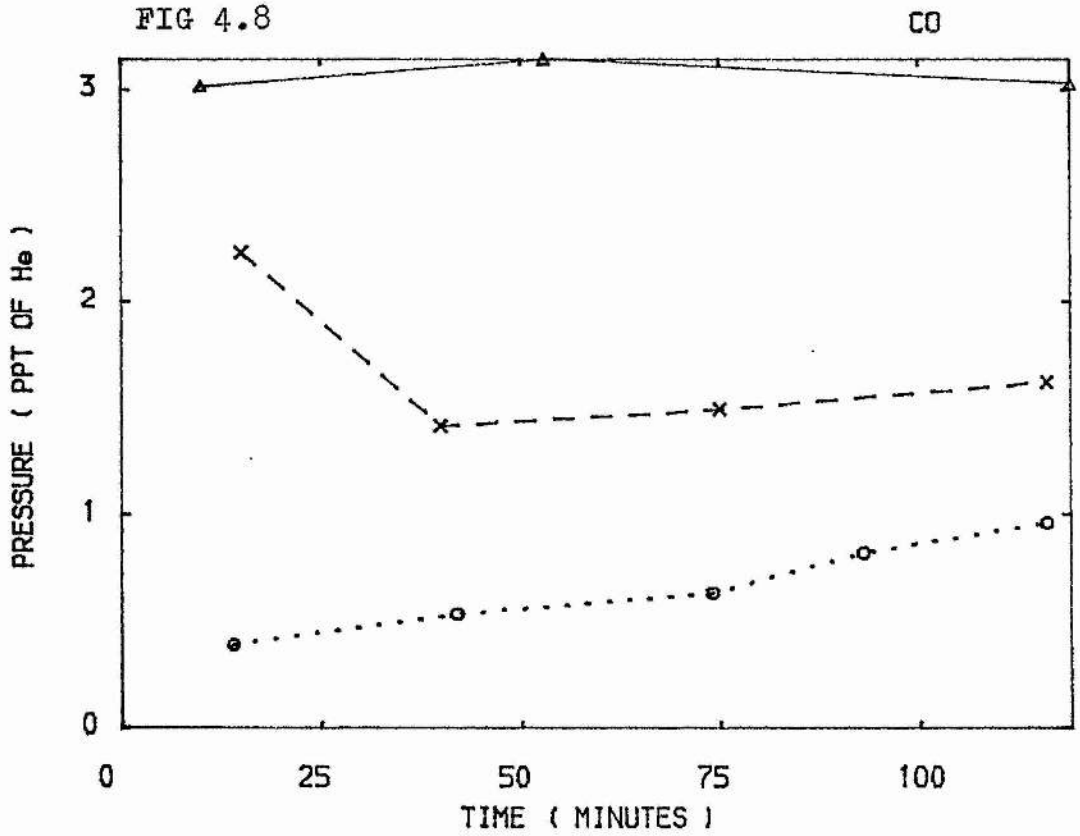
CO
PRESSURE (PPT OF He)
3
2
1
0
0
25
50
75
100
TIME (MINUTES)

FIG 4.9

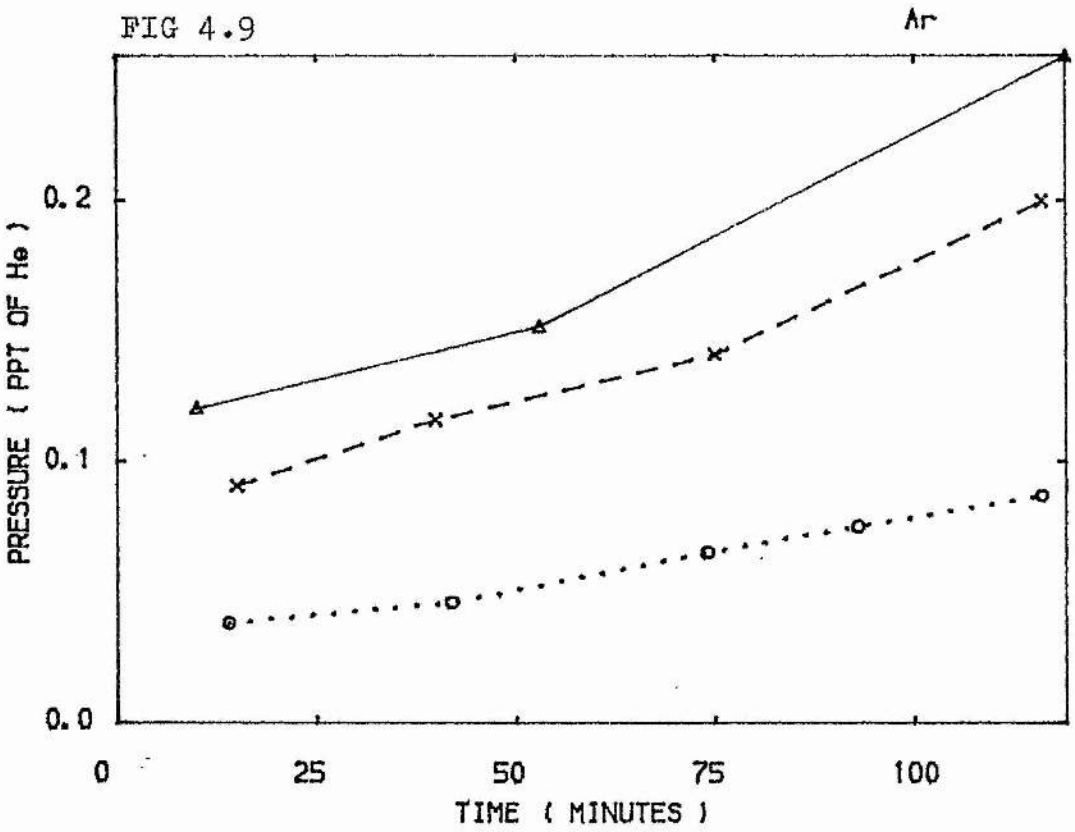

FIG 4.10

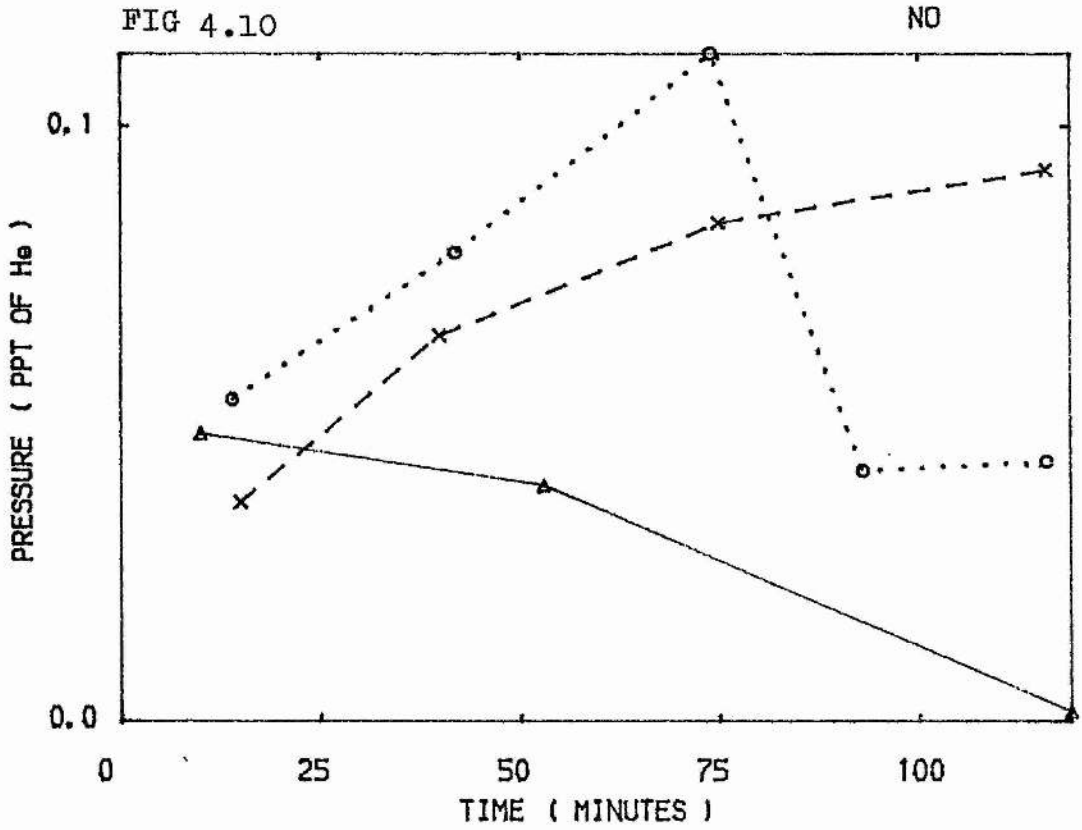

Figures 4.11 to 4.22
Evolution of various species in a He-F_2 mix
in:

—△— LV3
--X-- LV4
··□·· LV5

without discharge. Species names on top right.

FIG 4.11

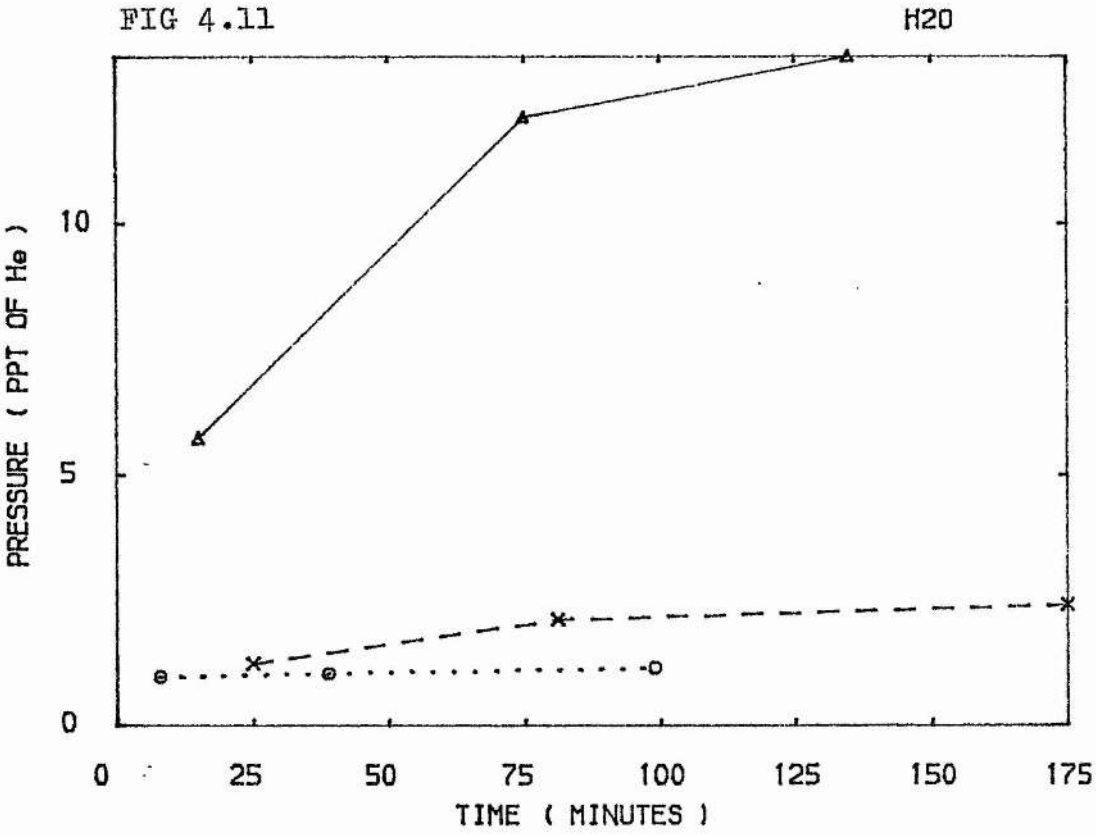

FIG 4.12

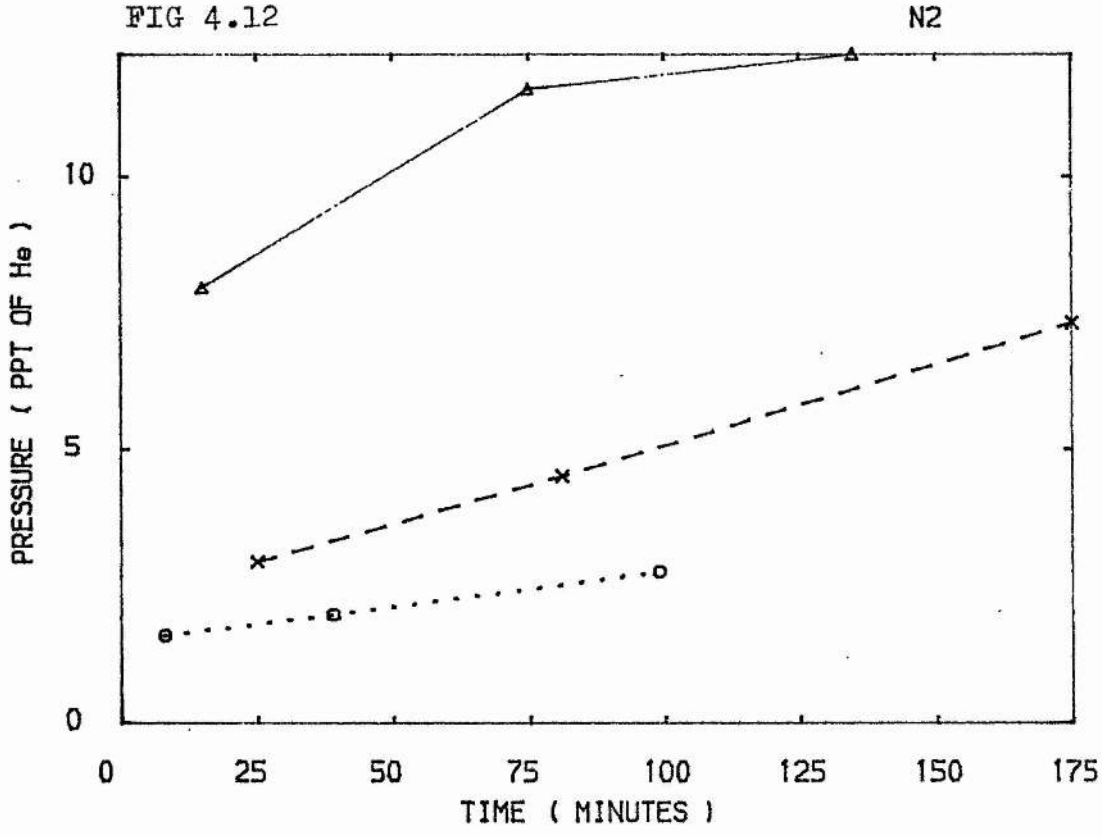

FIG 4.13

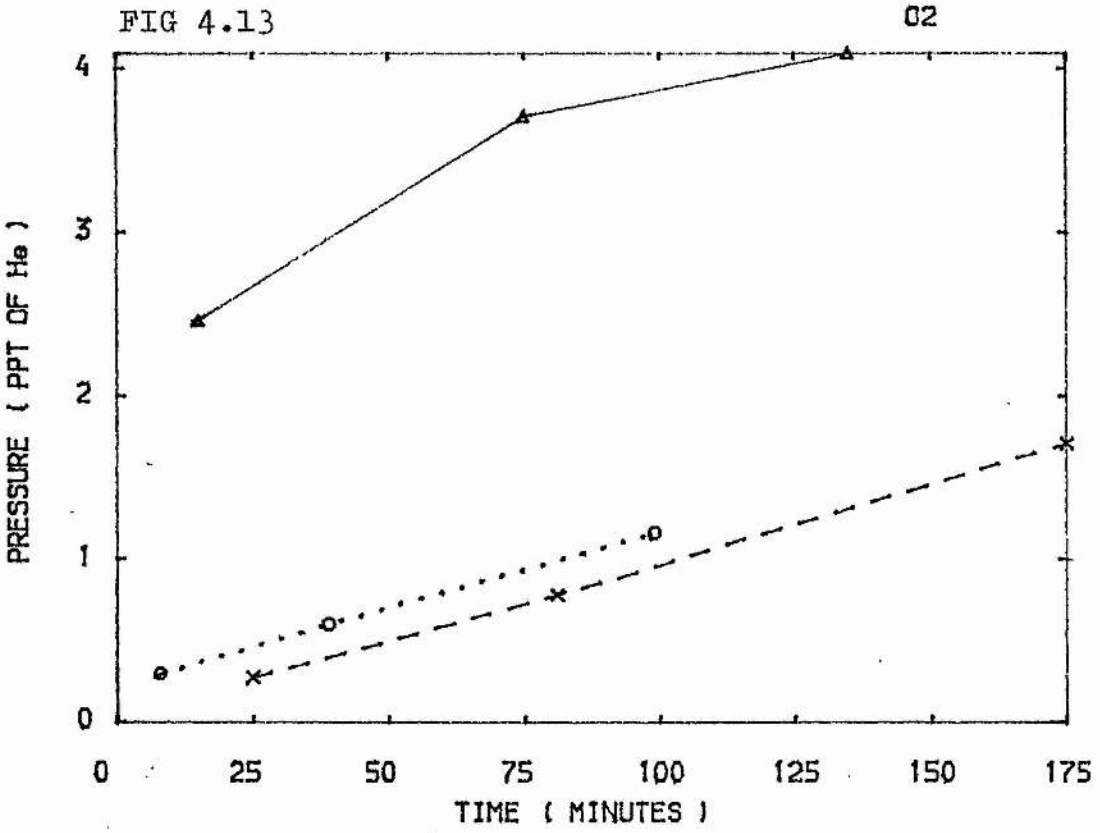

FIG 4.14

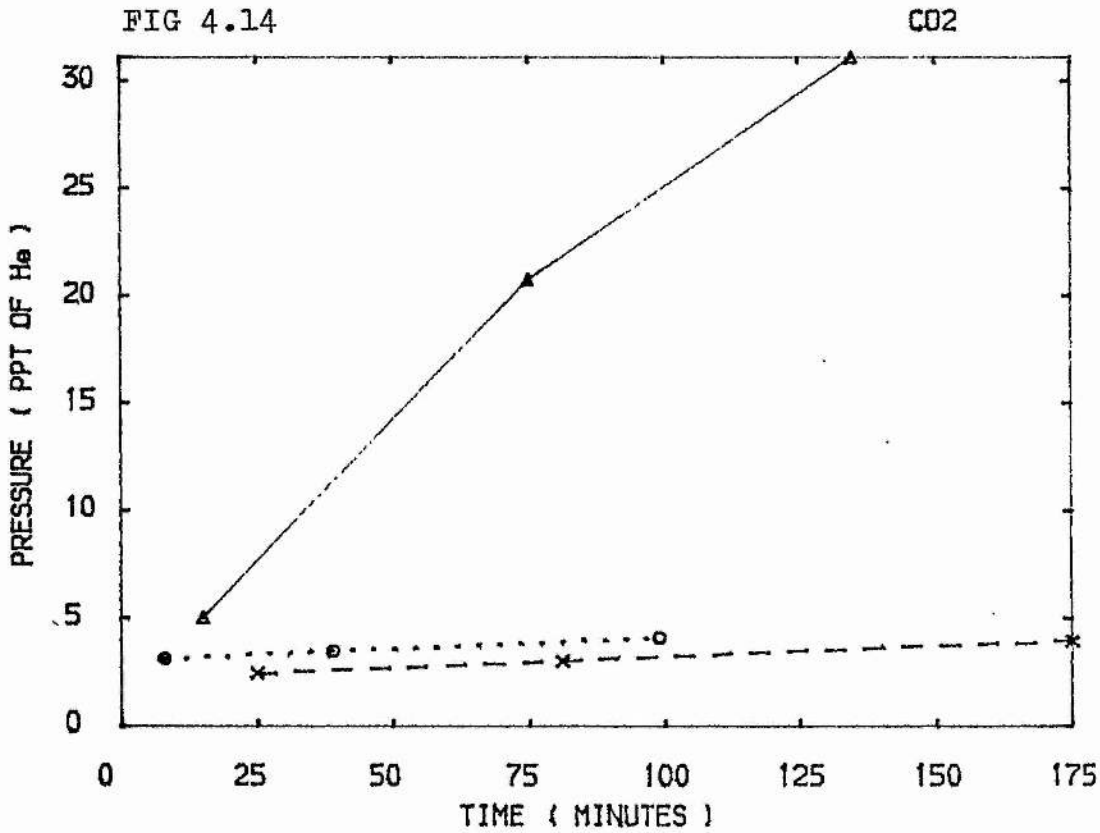

FIG 4.15

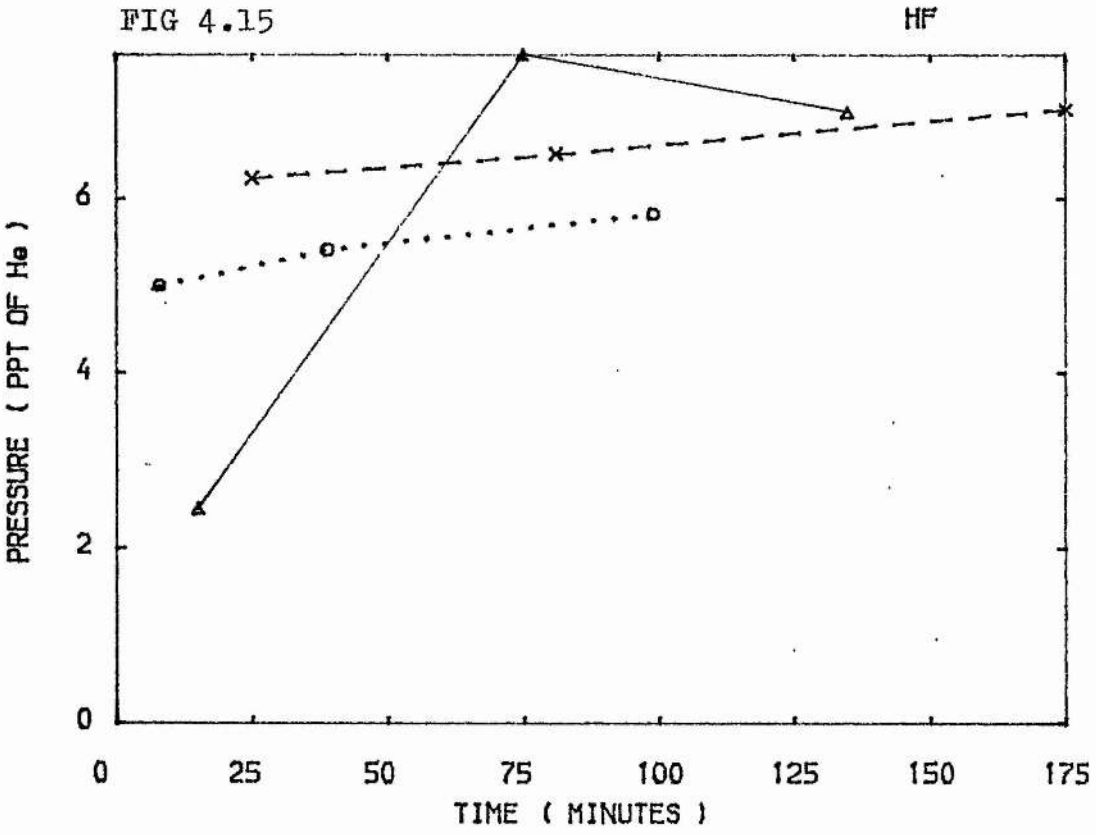

FIG 4.16

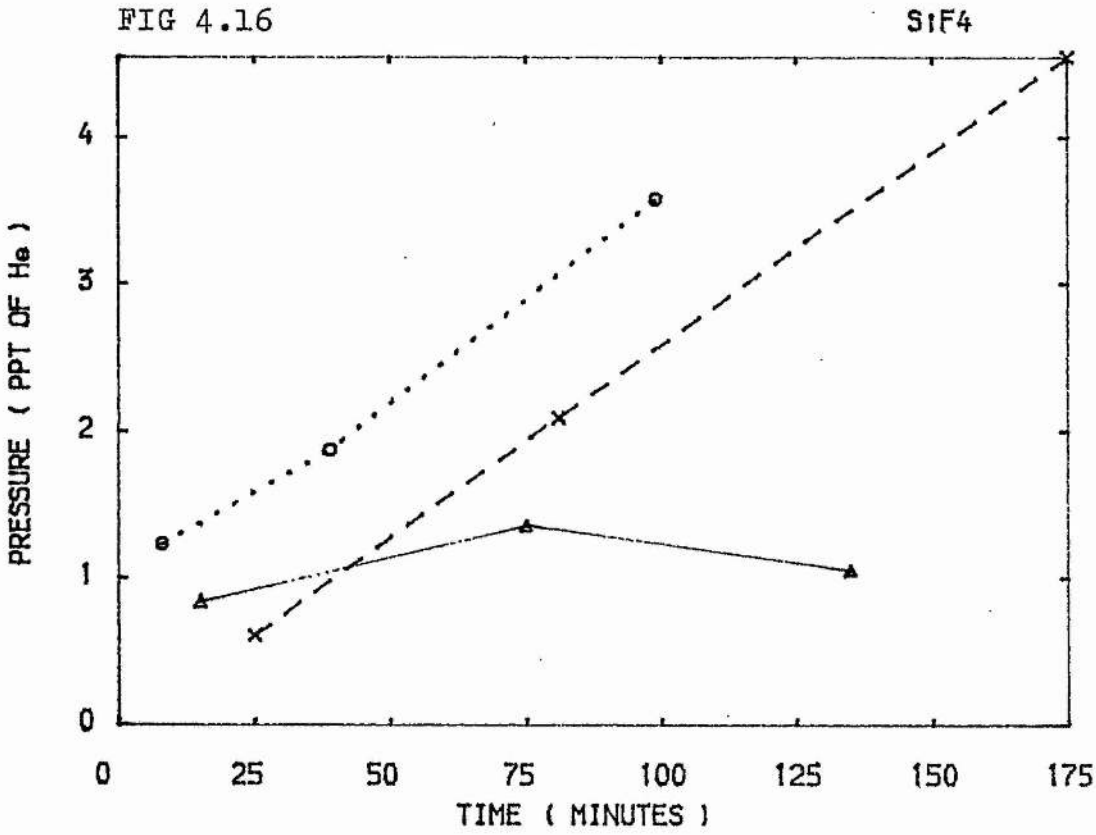

FIG 4.17

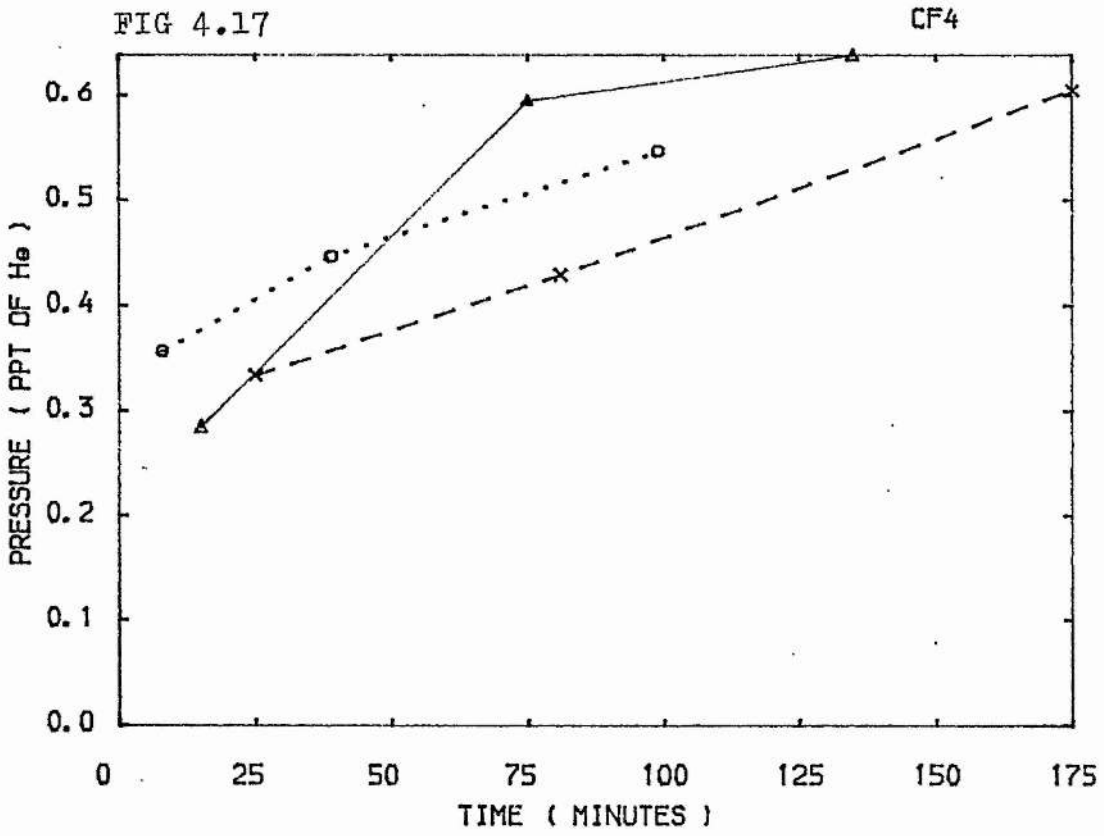

FIG 4.18

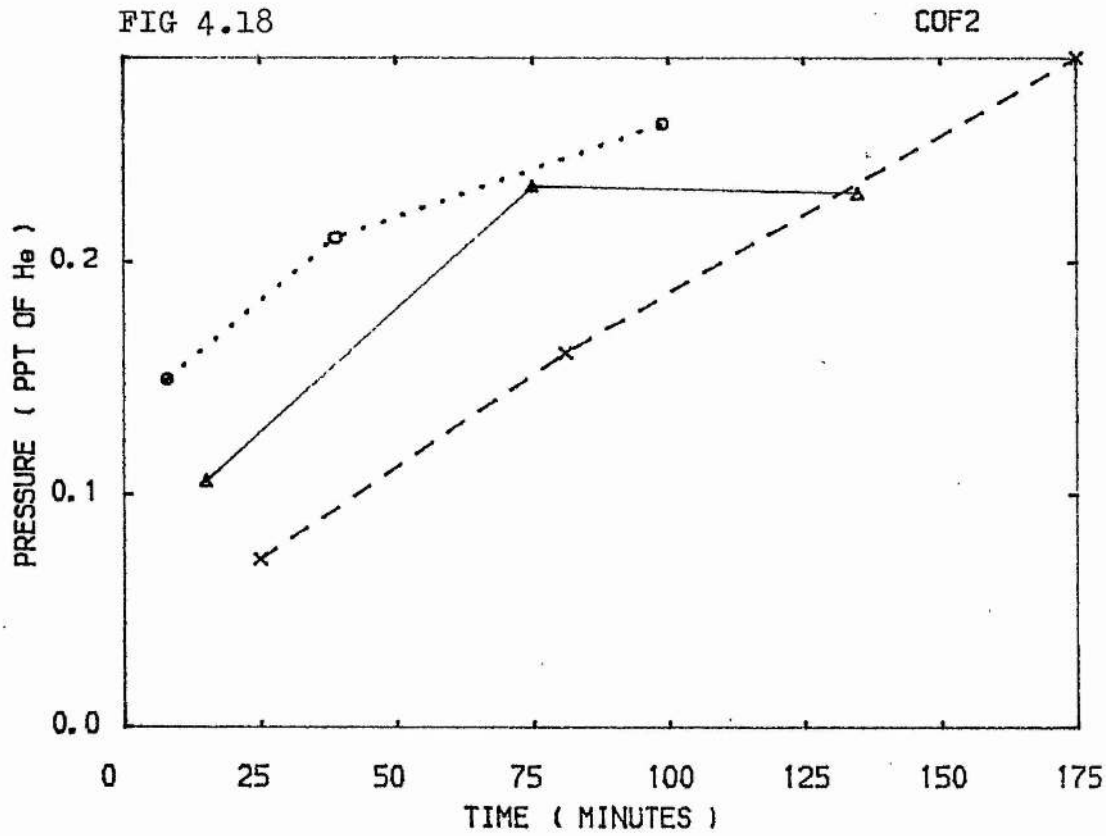

FIG 4.19

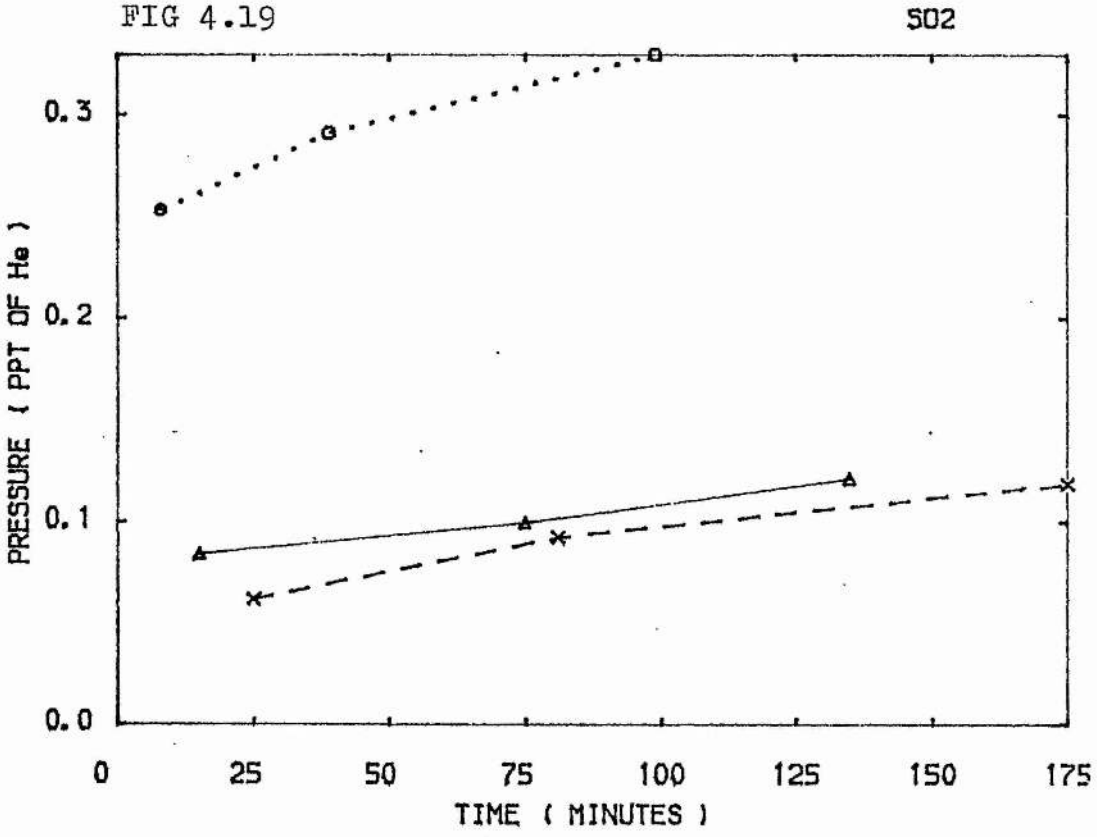

FIG 4.20

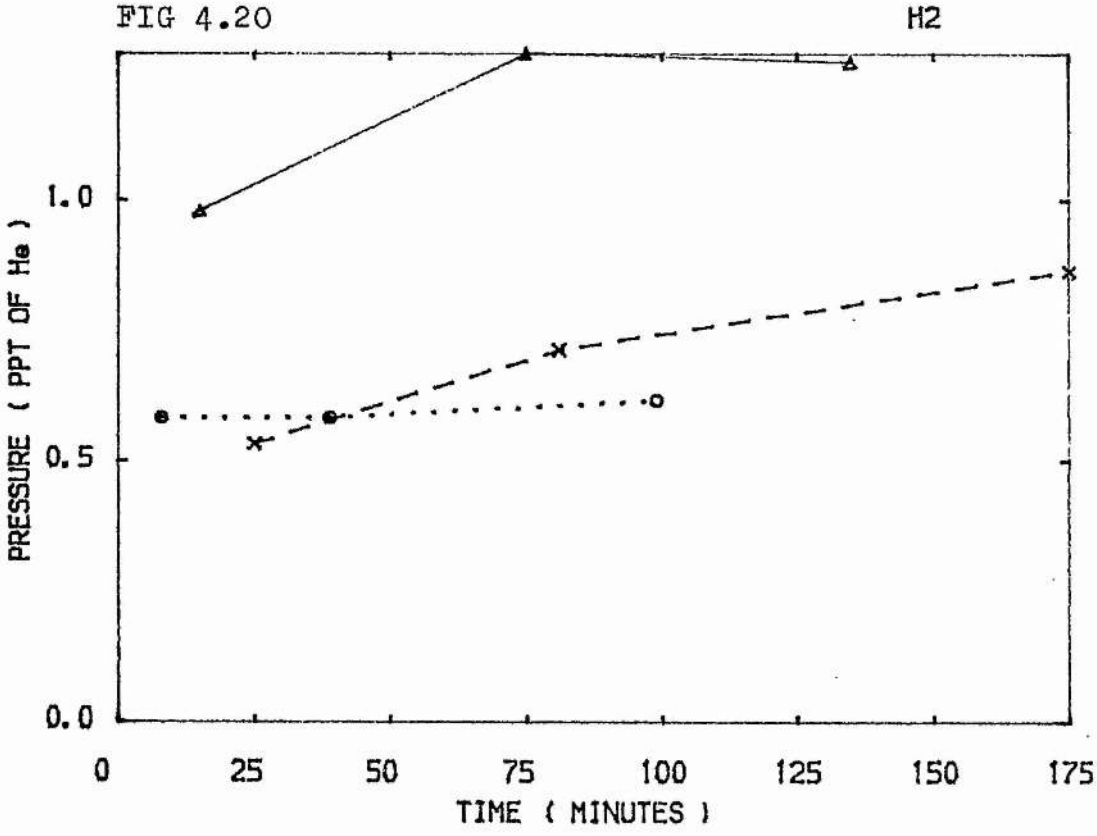

FIG 4.21

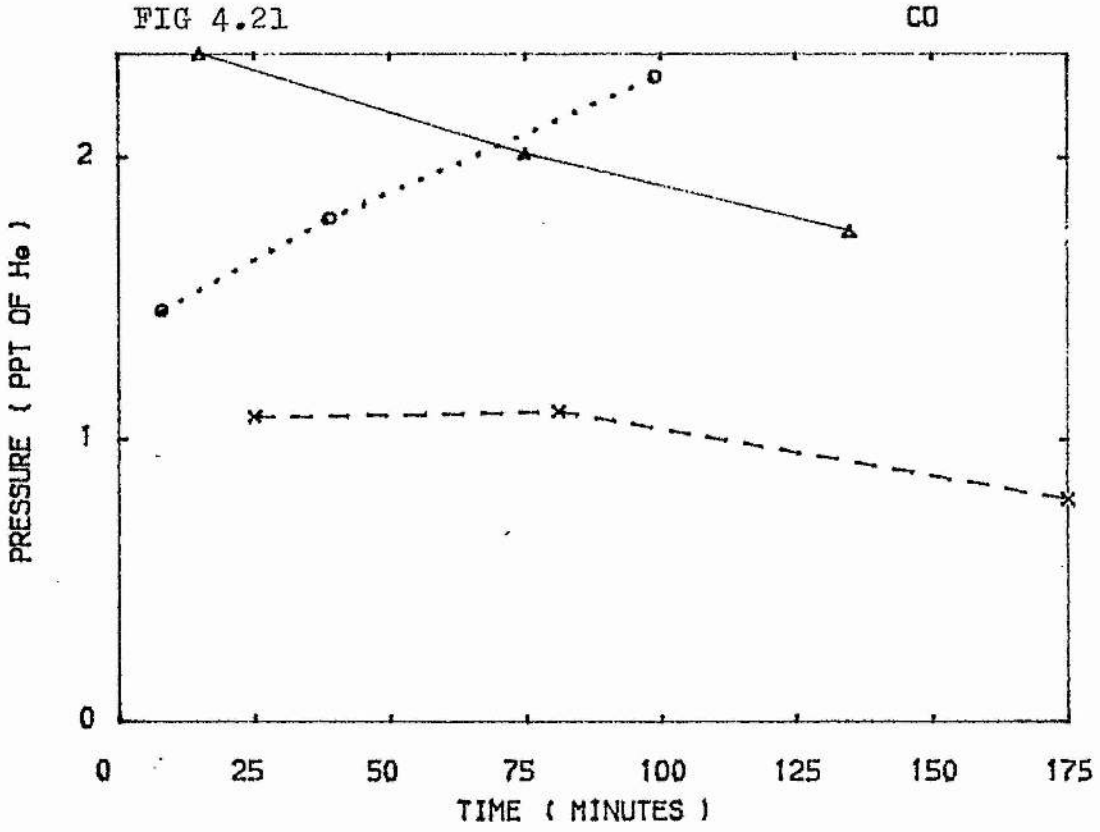

FIG 4.22

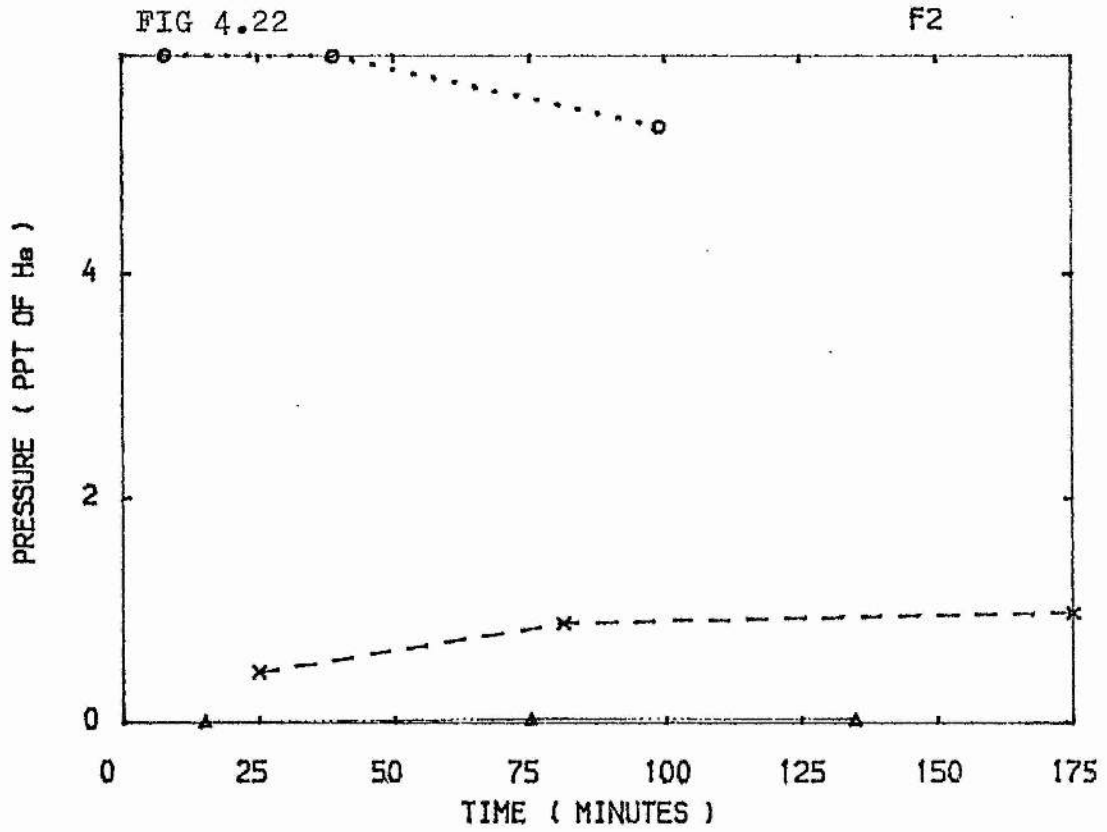

Figures 4.23 to 4.34
Evolution of various species in a He-F_2 mix,
laser on at time indicated by L in 4.23, in LV4

Curves -·v·- give a comparison run without discharge.

FIG 4.23

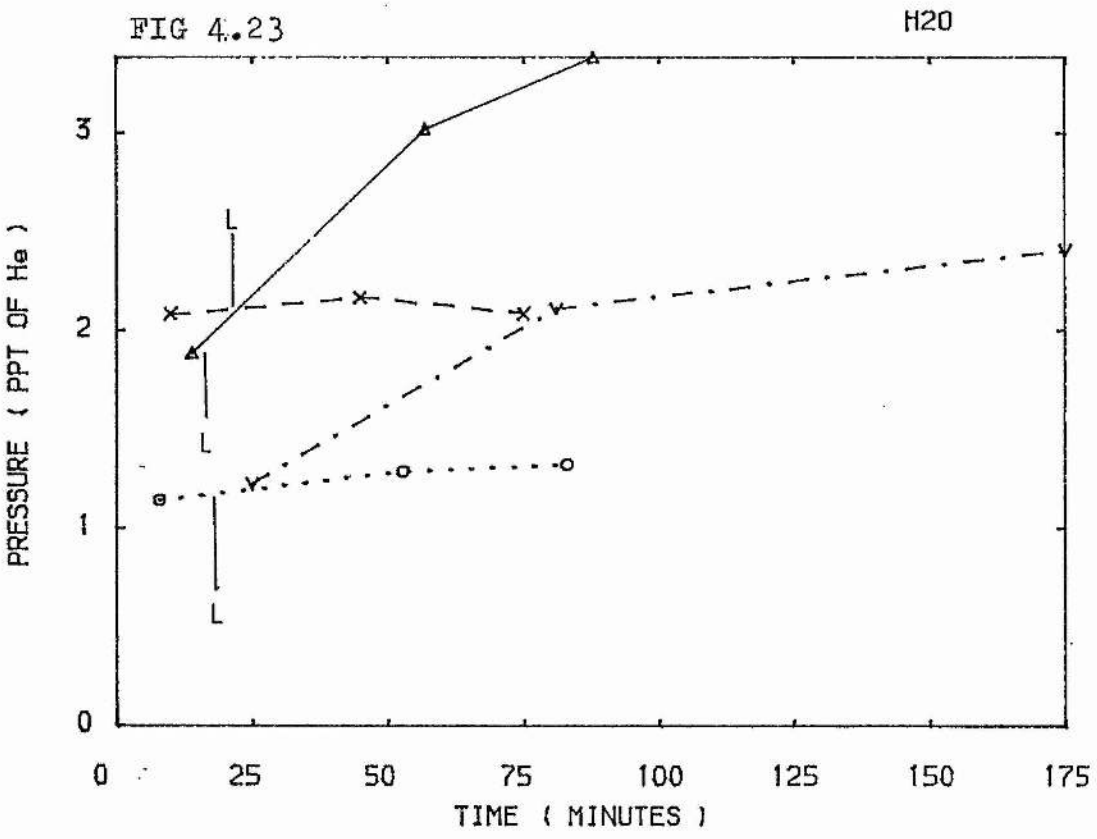

FIG 4.24

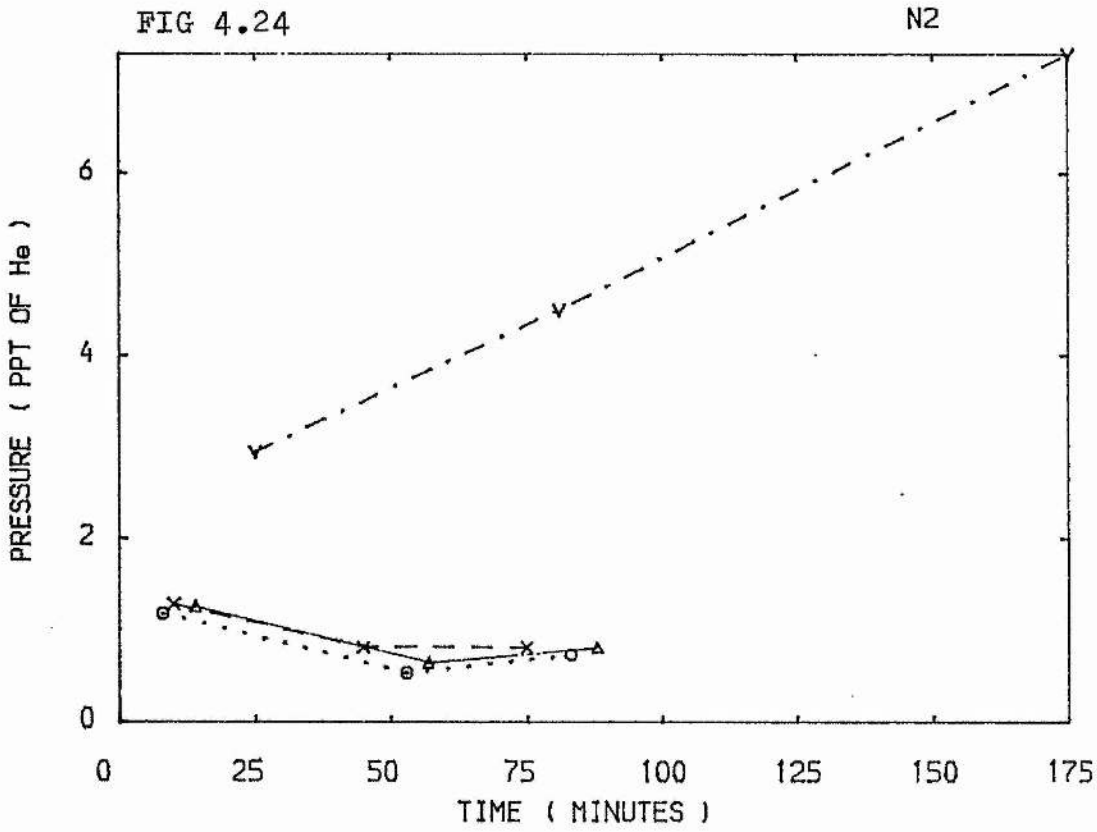

FIG 4.25

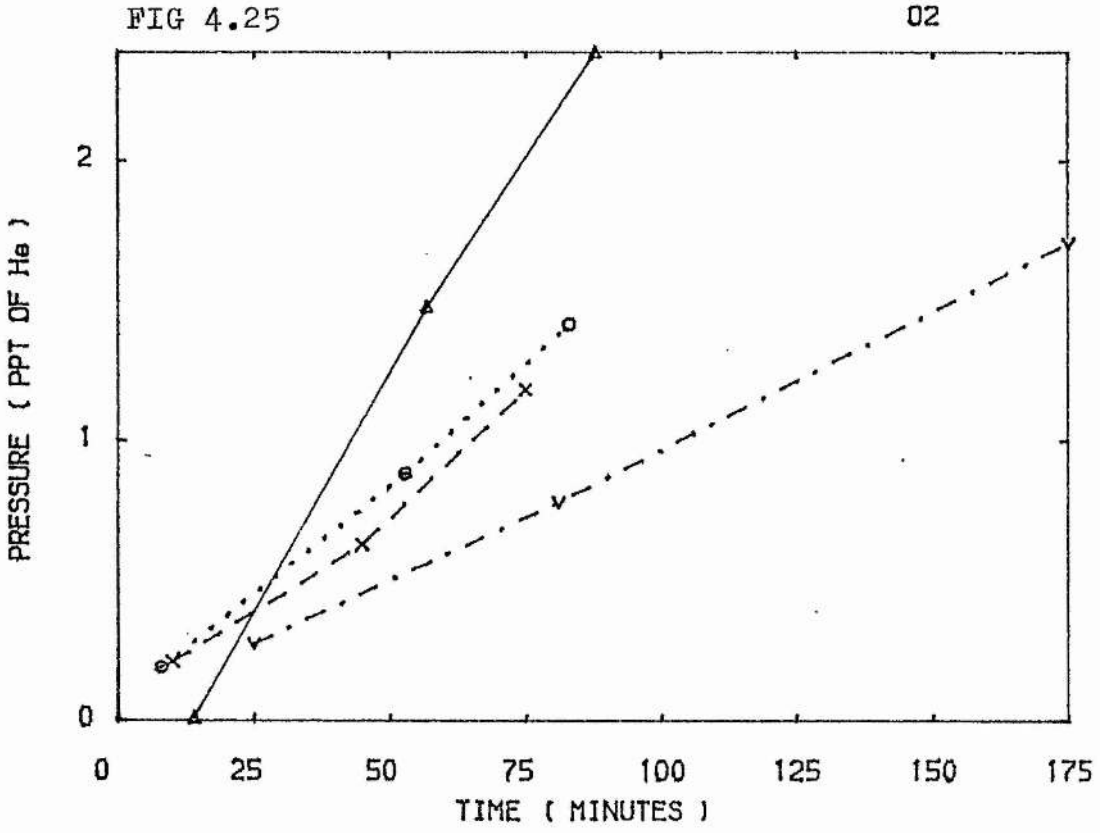

FIG 4.26

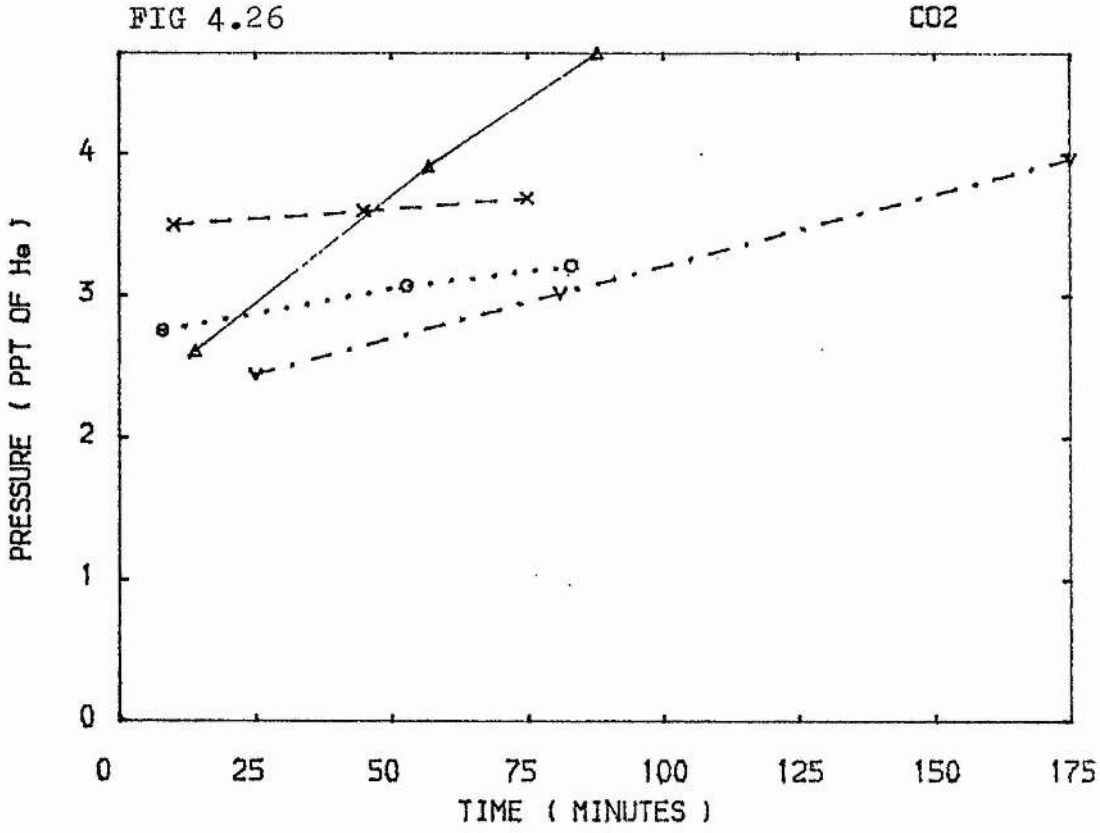

FIG 4.27

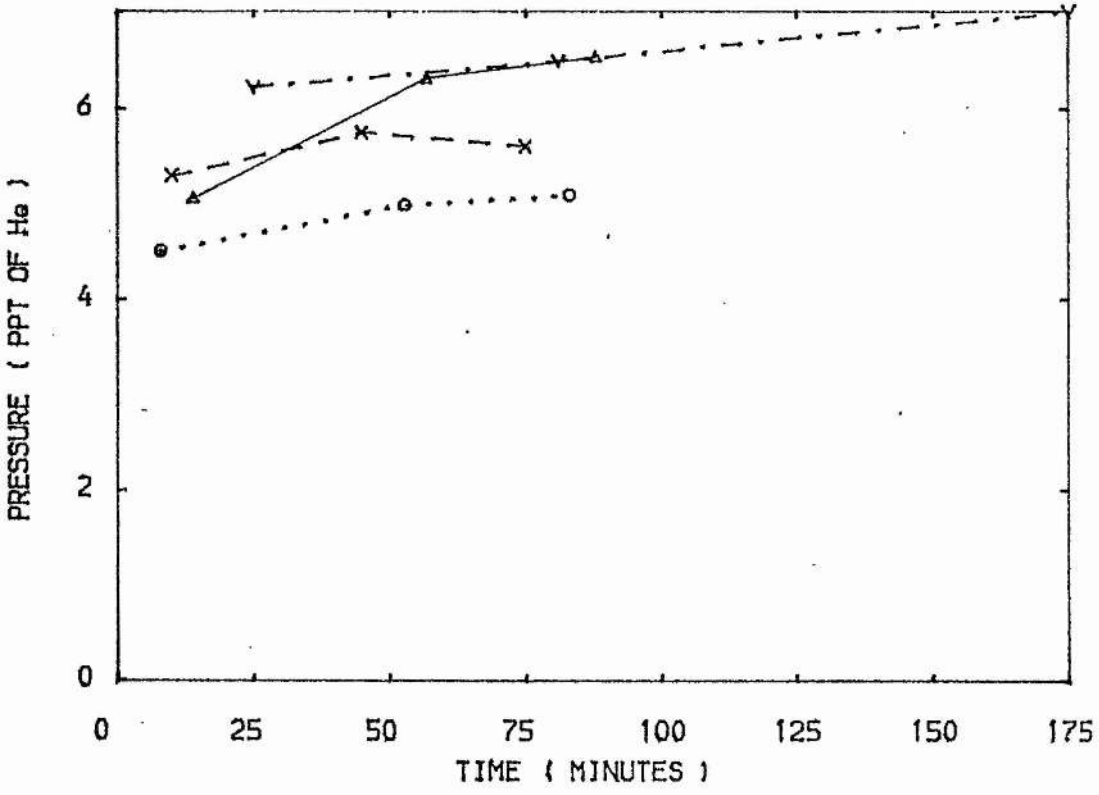

FIG 4.28

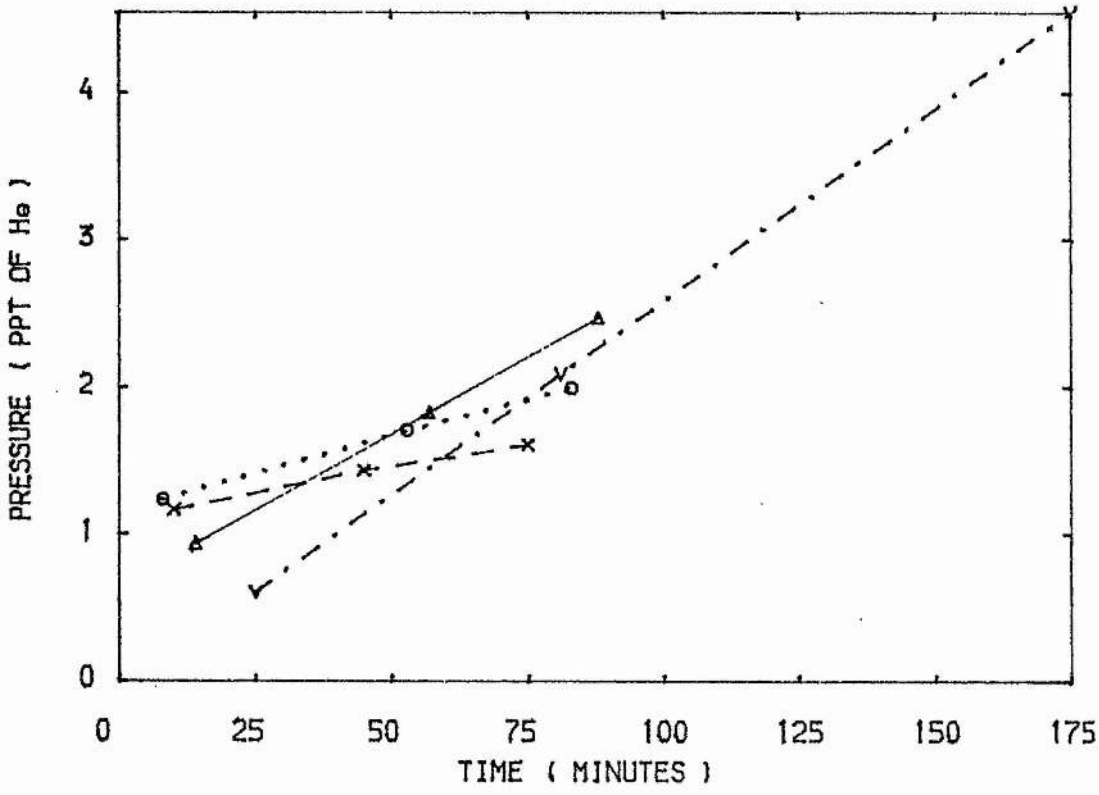

FIG 4.29

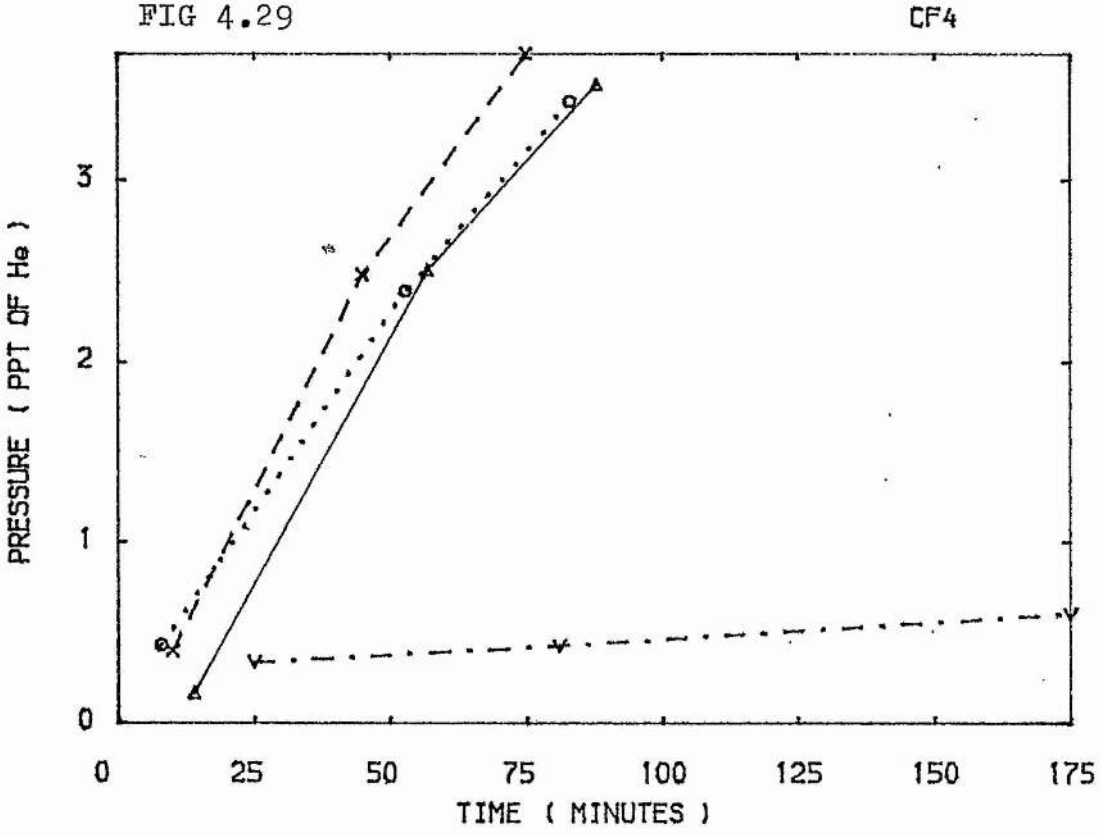

FIG 4.30

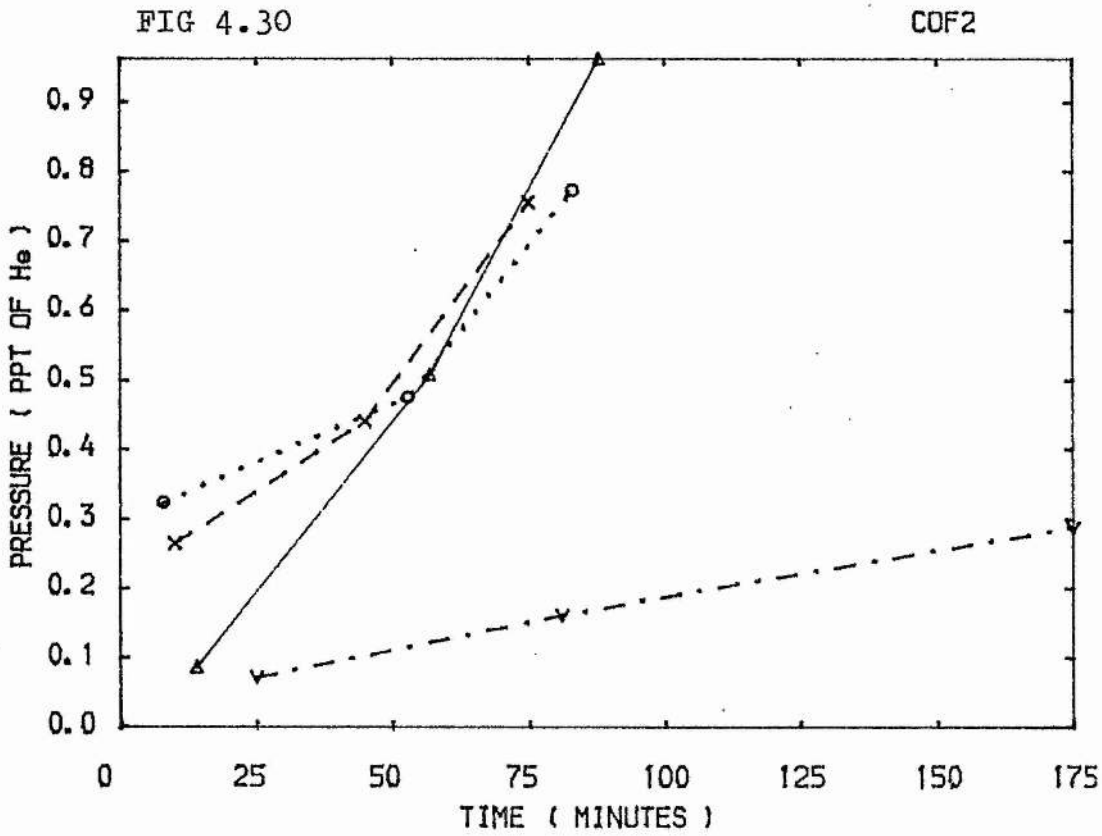

FIG 4.31

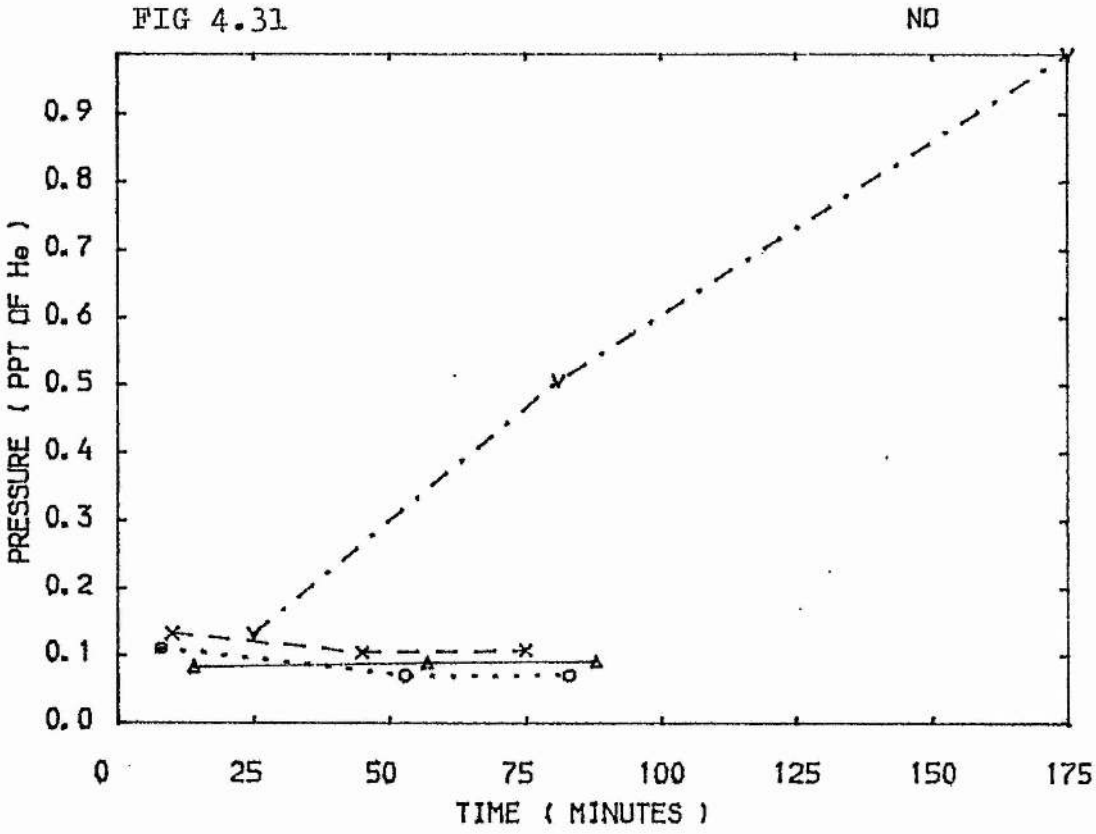

FIG 4.32

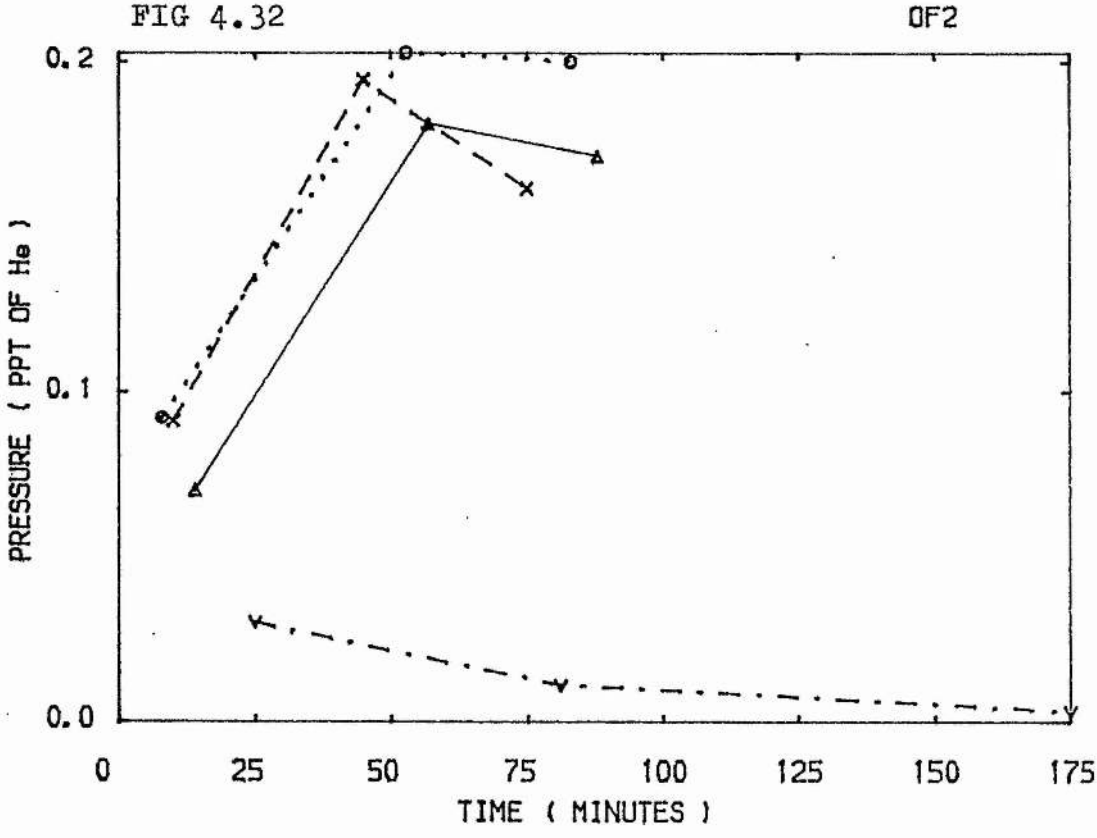

FIG 4.33

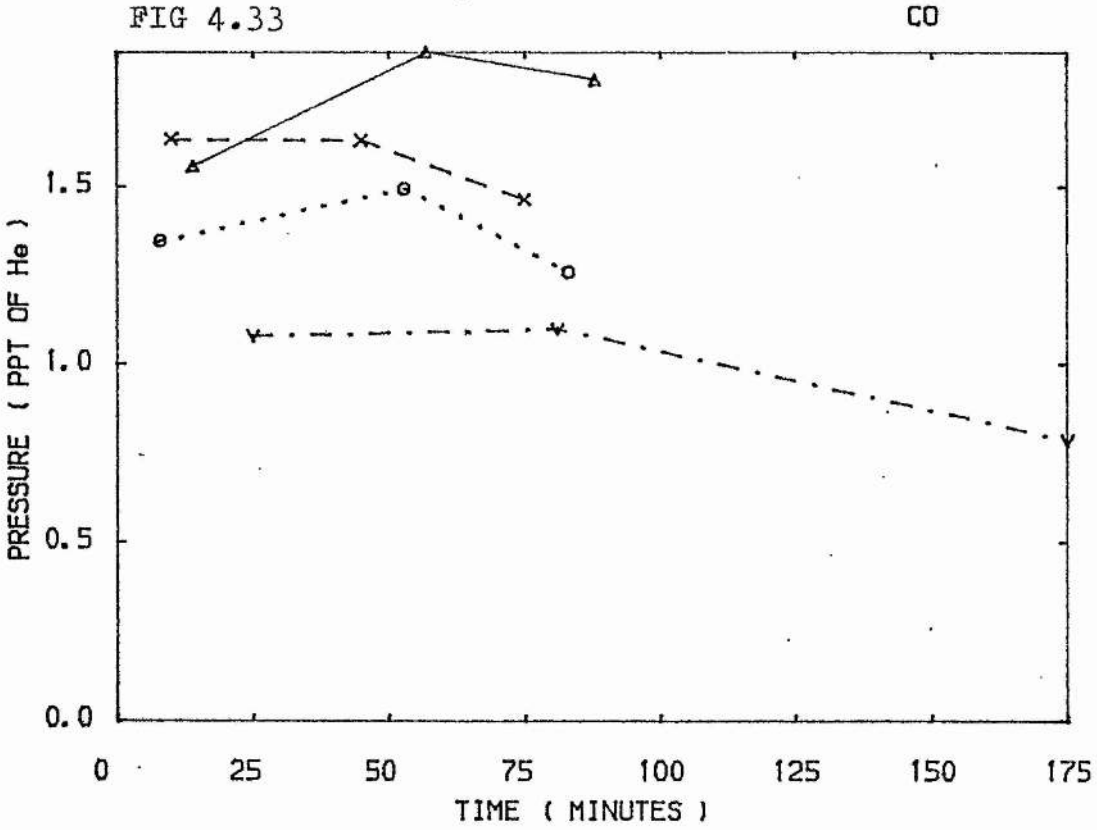

FIG 4.34

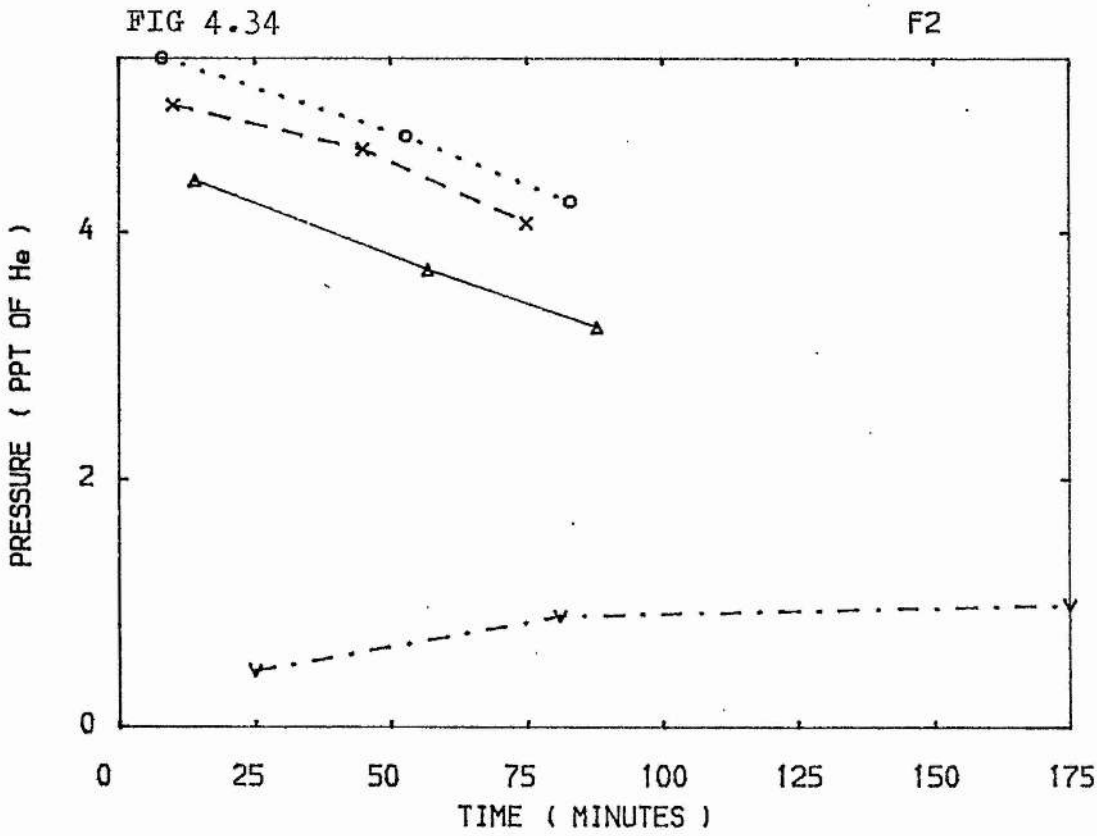

Figures 4.35 to 4.50
Evolution of various detected species in a He-F_2 mix, in:

—△— LV3
---X-- LV4
···□··· LV5

Start of discharge indicated by L.

FIG 4.35

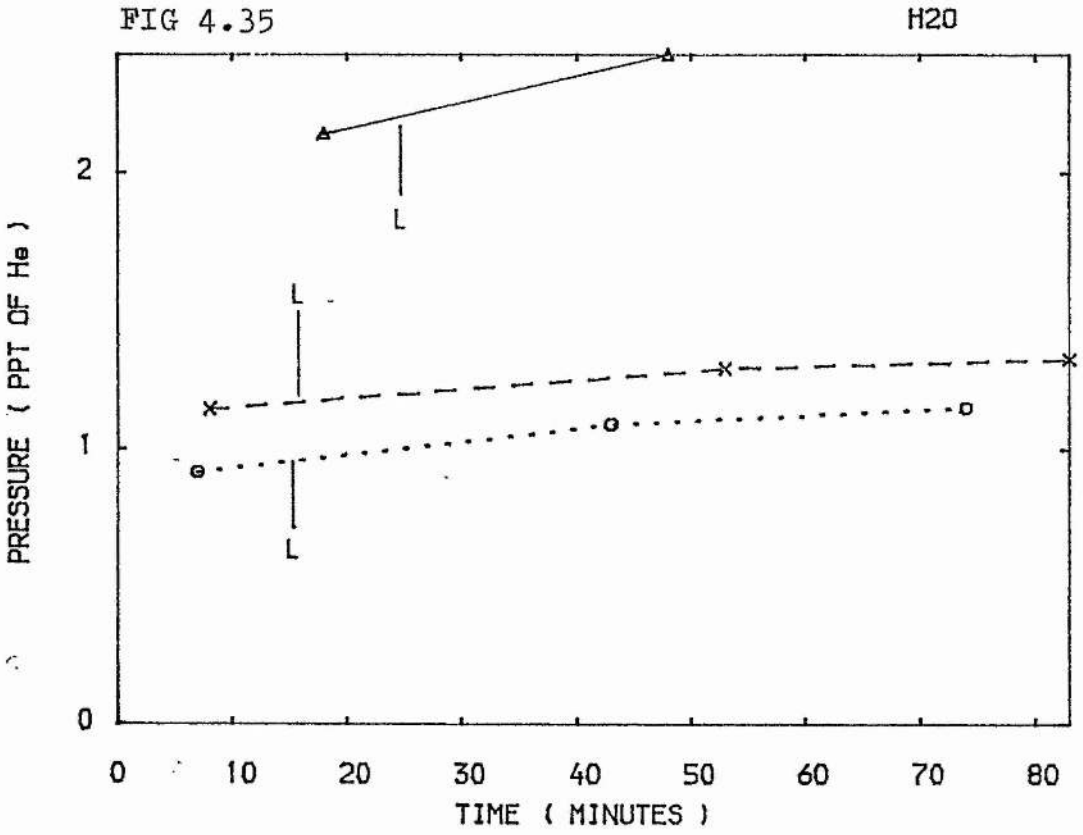

FIG 4.36

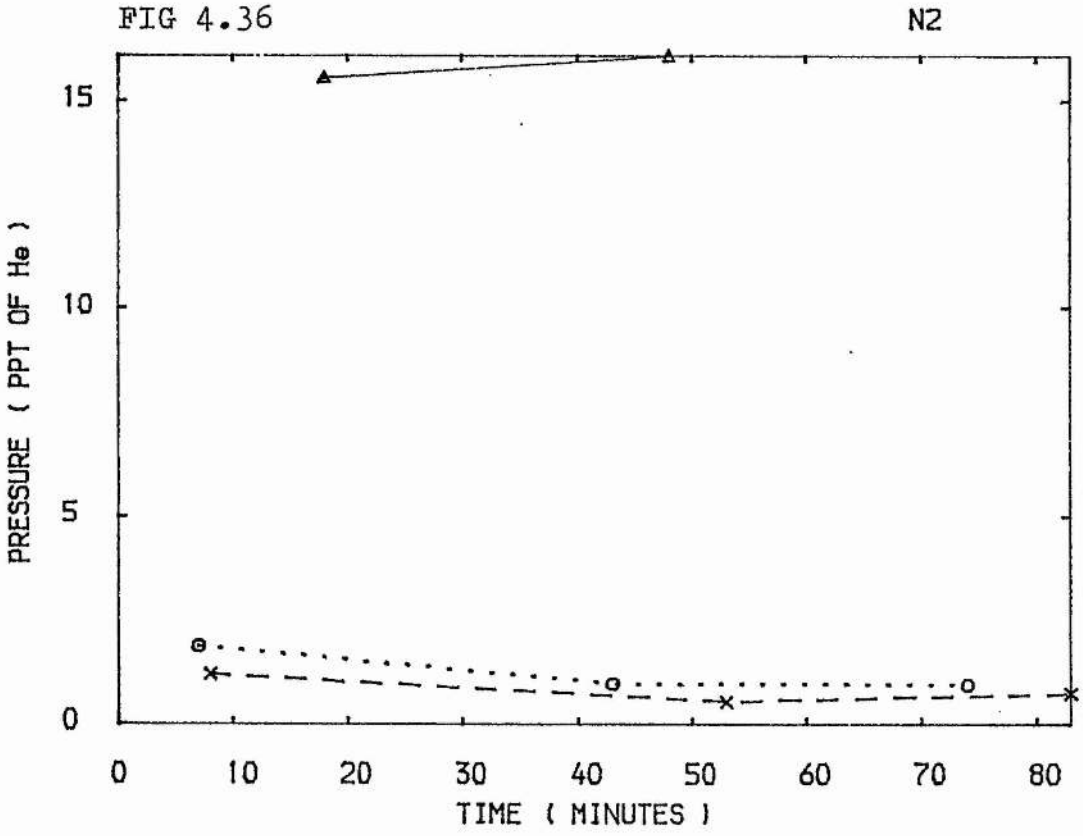

FIG 4.37

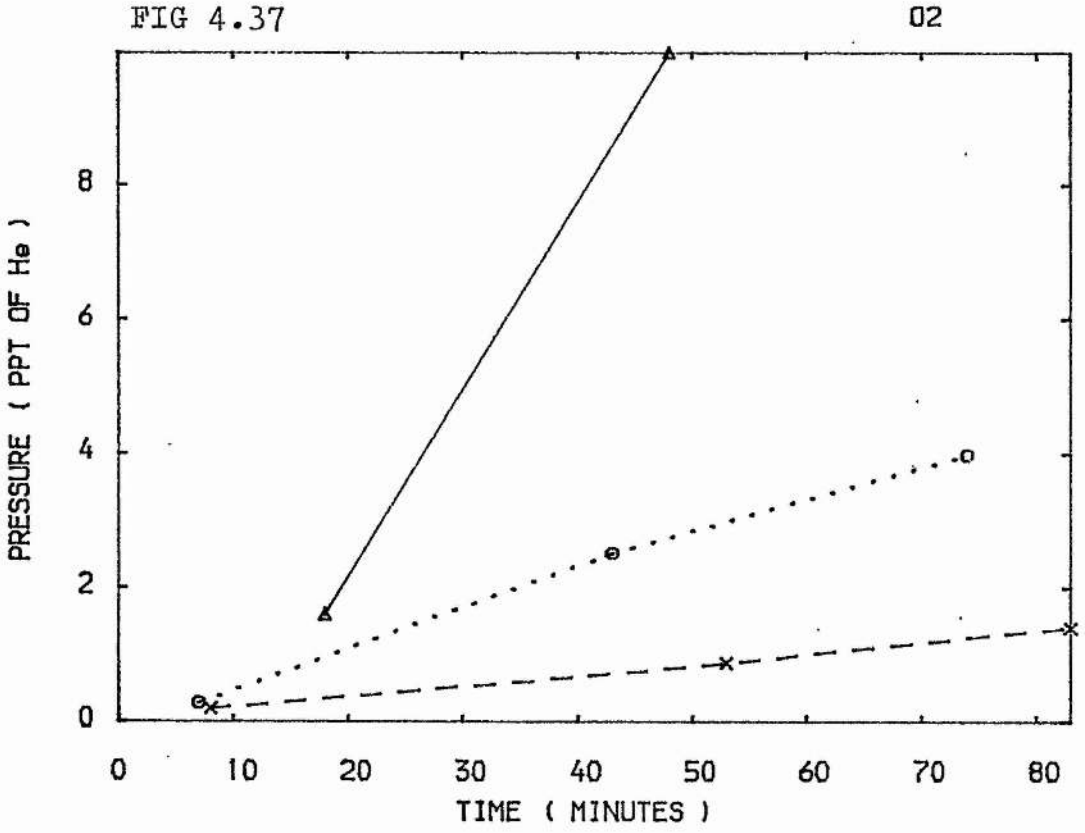

FIG 4.38

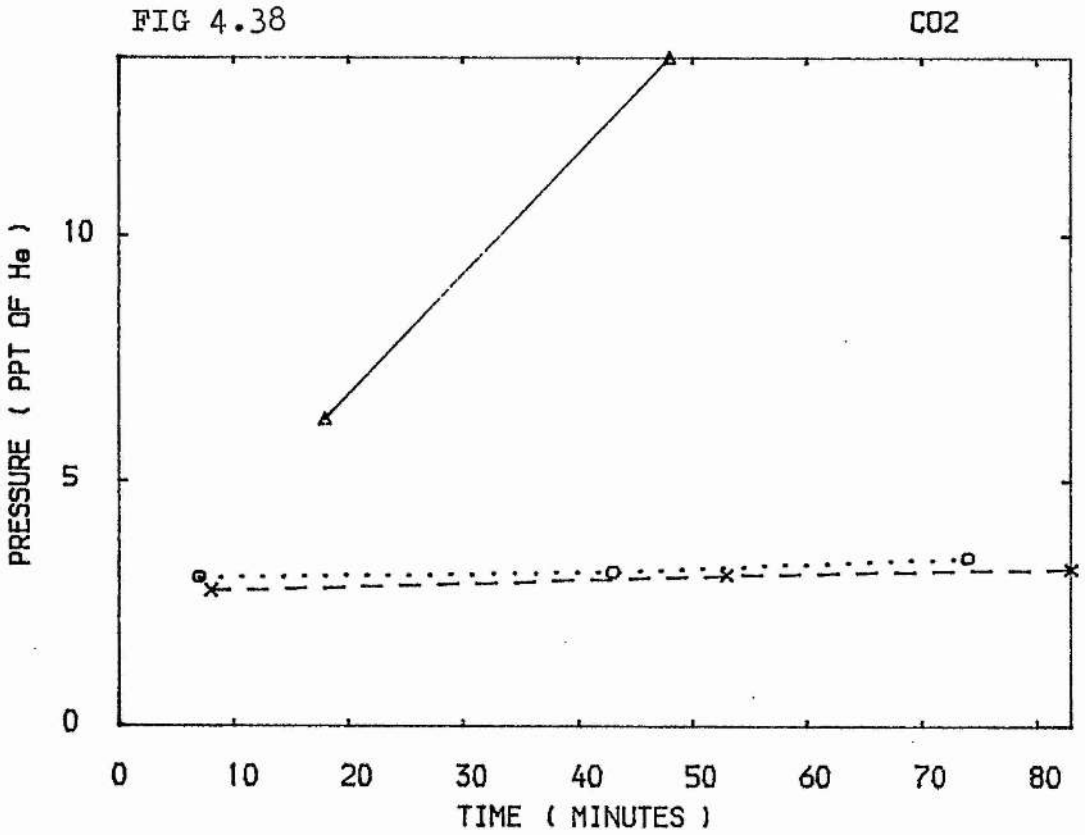

FIG 4.39

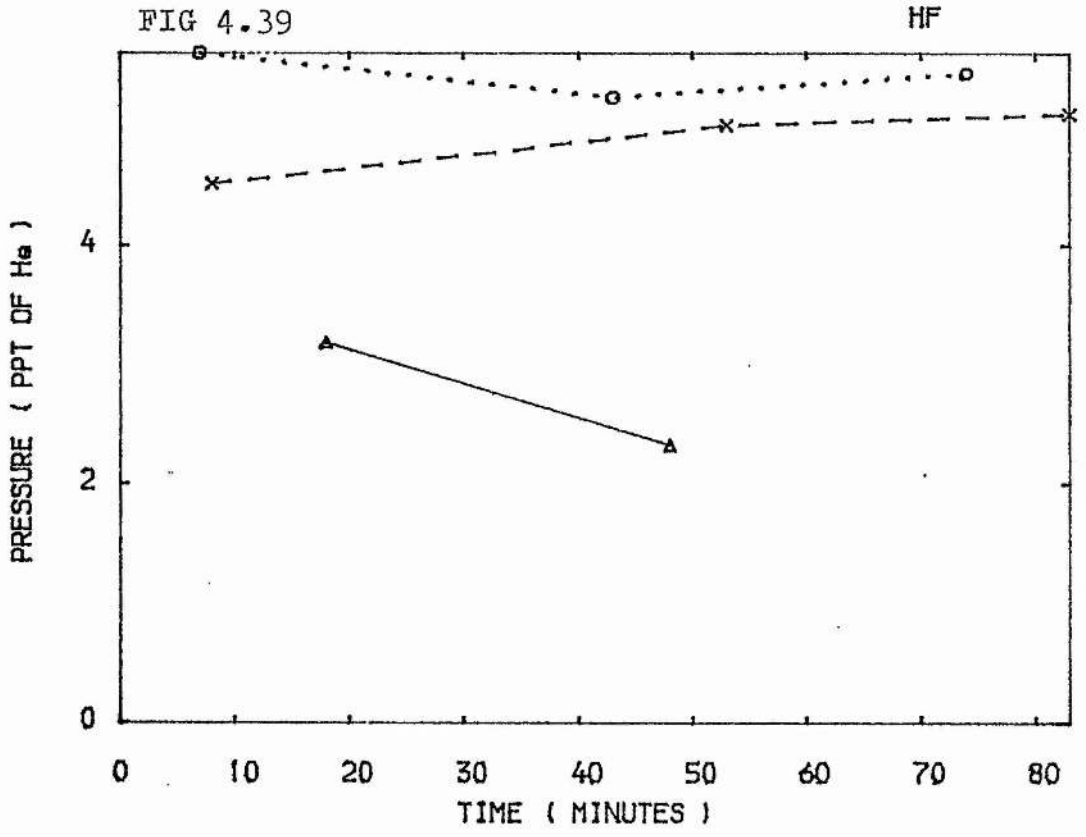

FIG 4.40

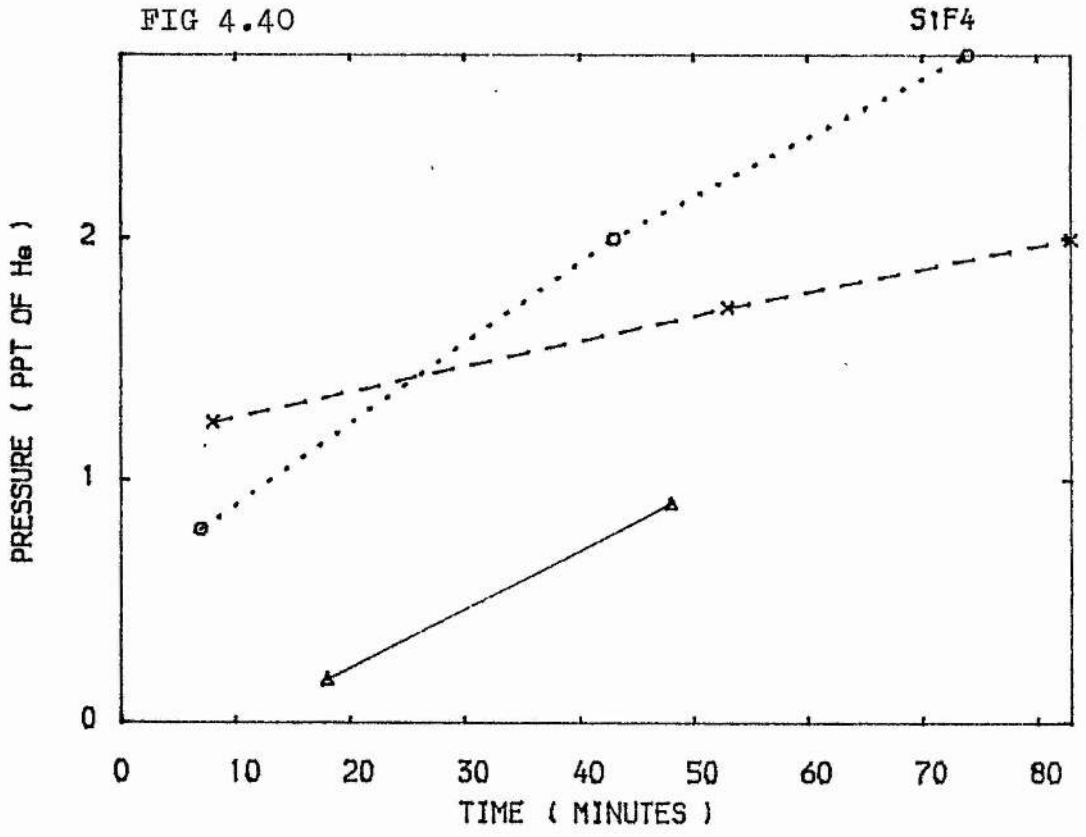

FIG 4.41

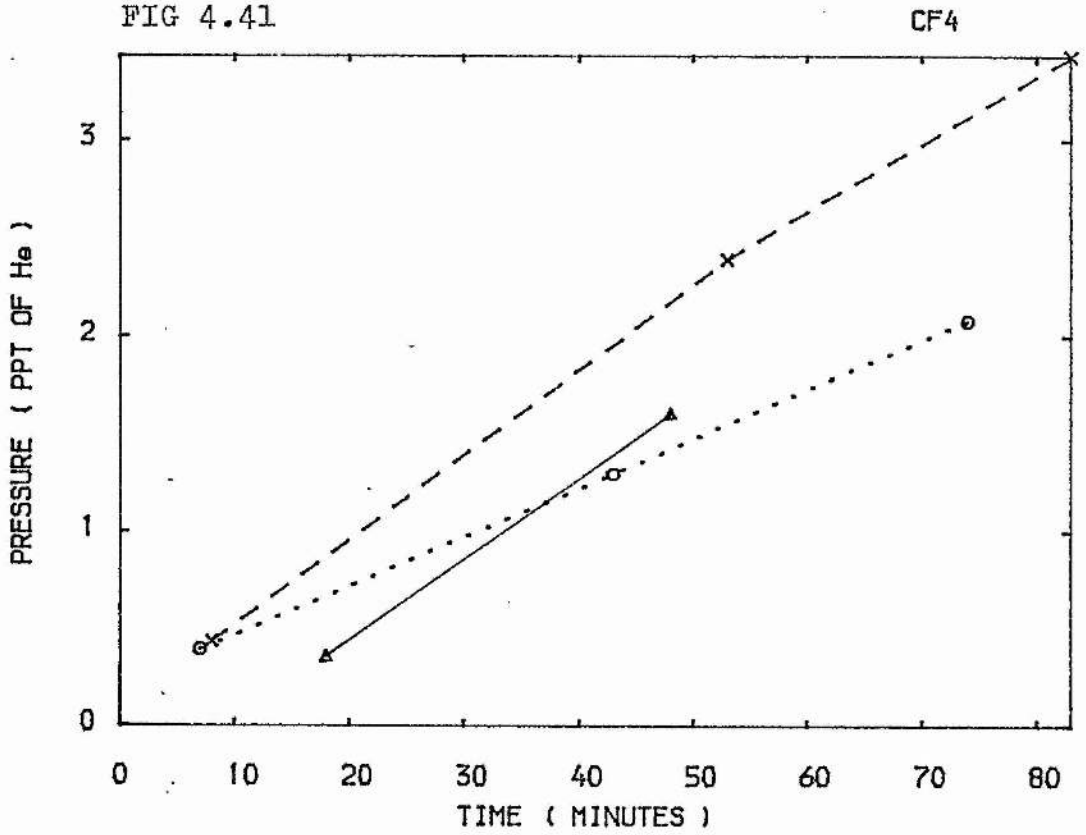

FIG 4.42

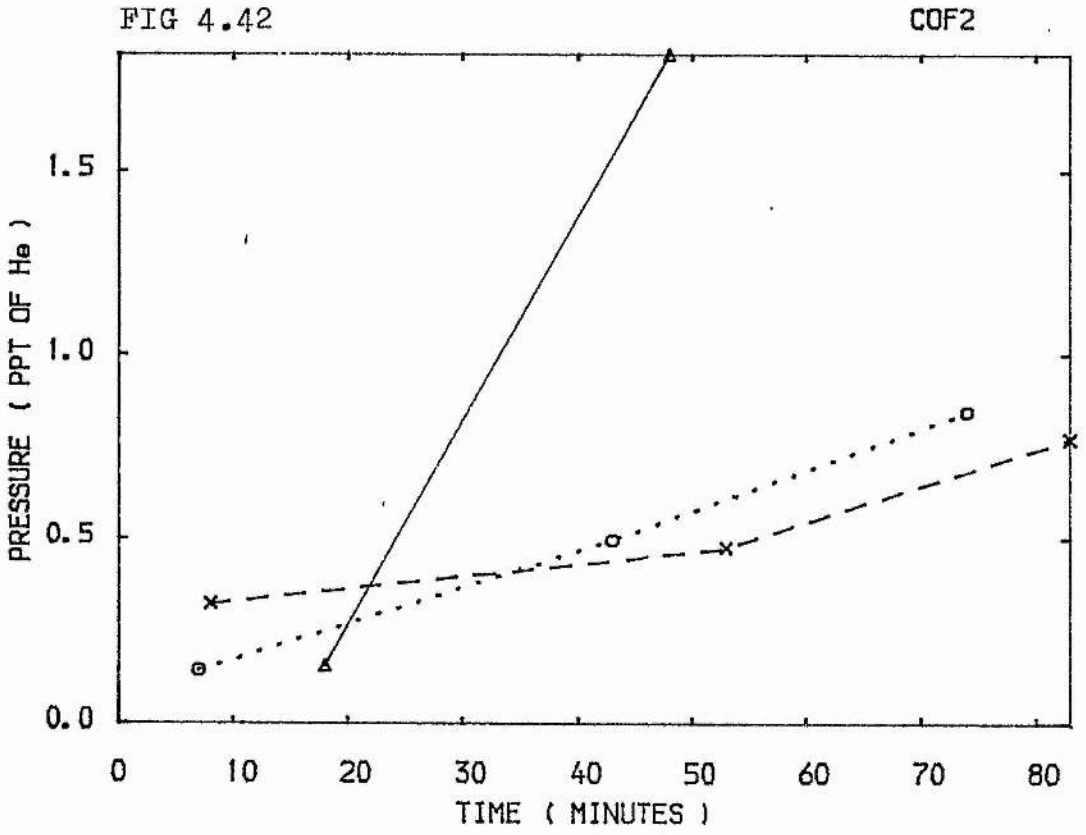

FIG 4.43

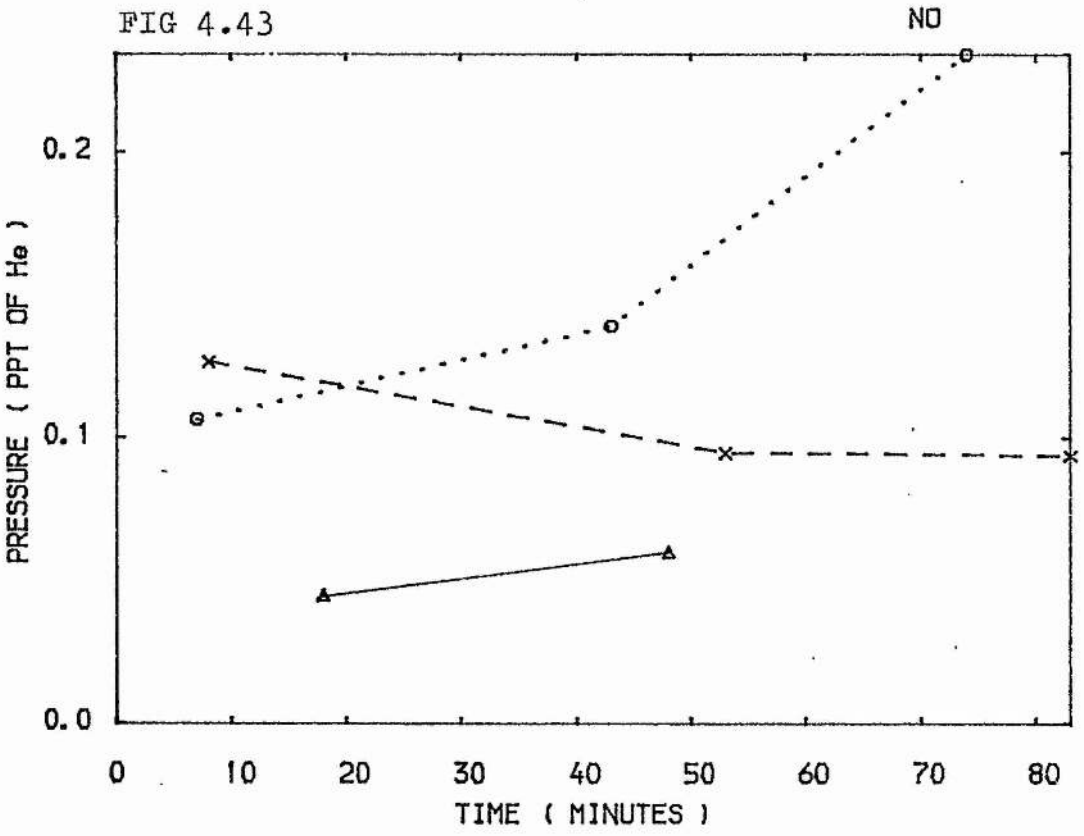

FIG 4.44

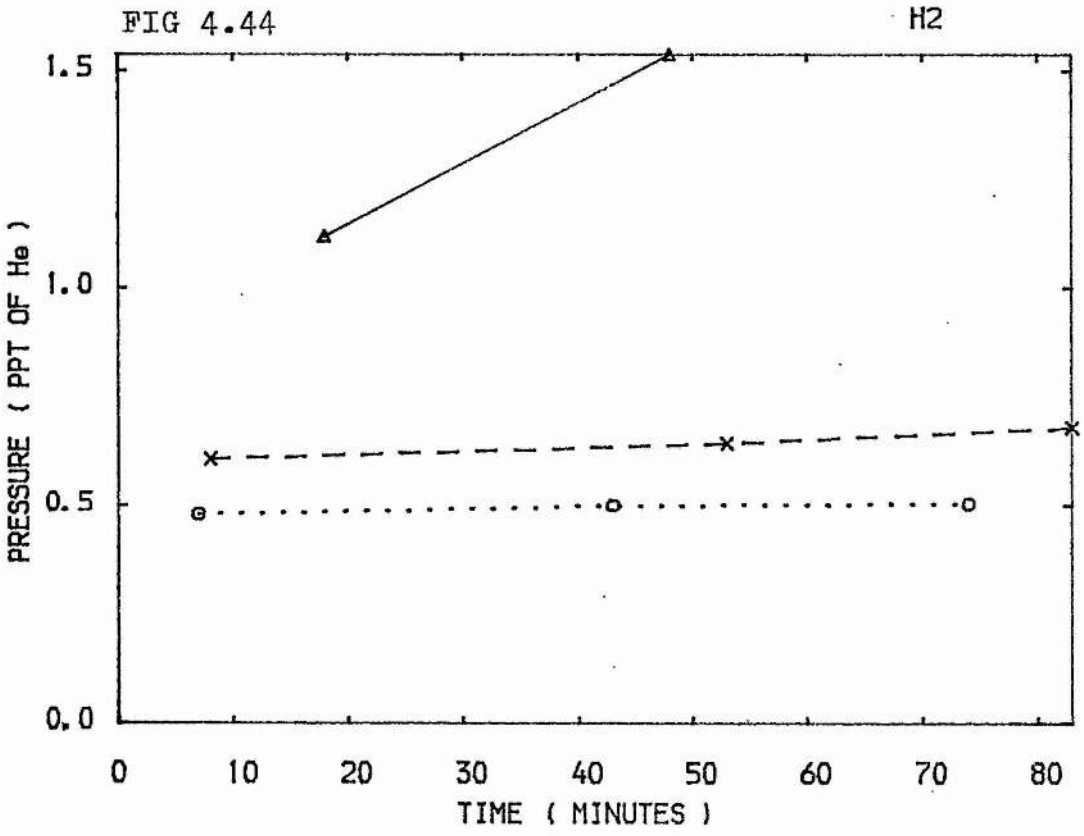

FIG 4.45

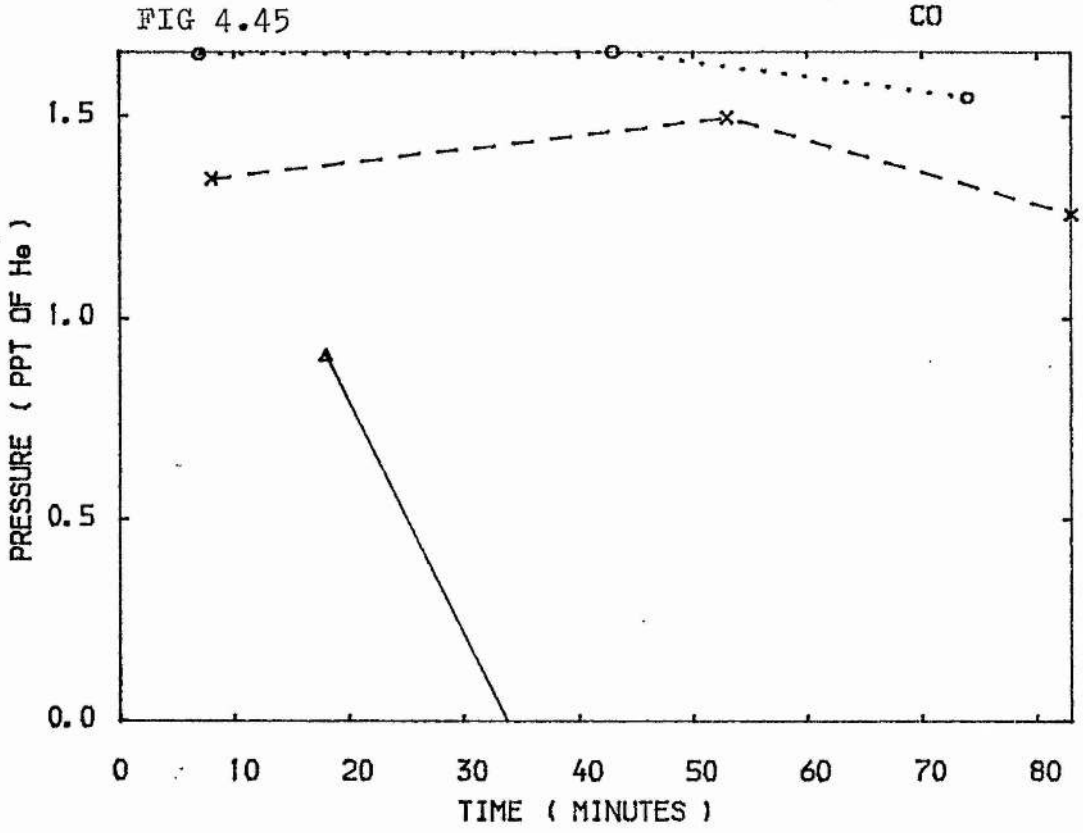

FIG 4.46

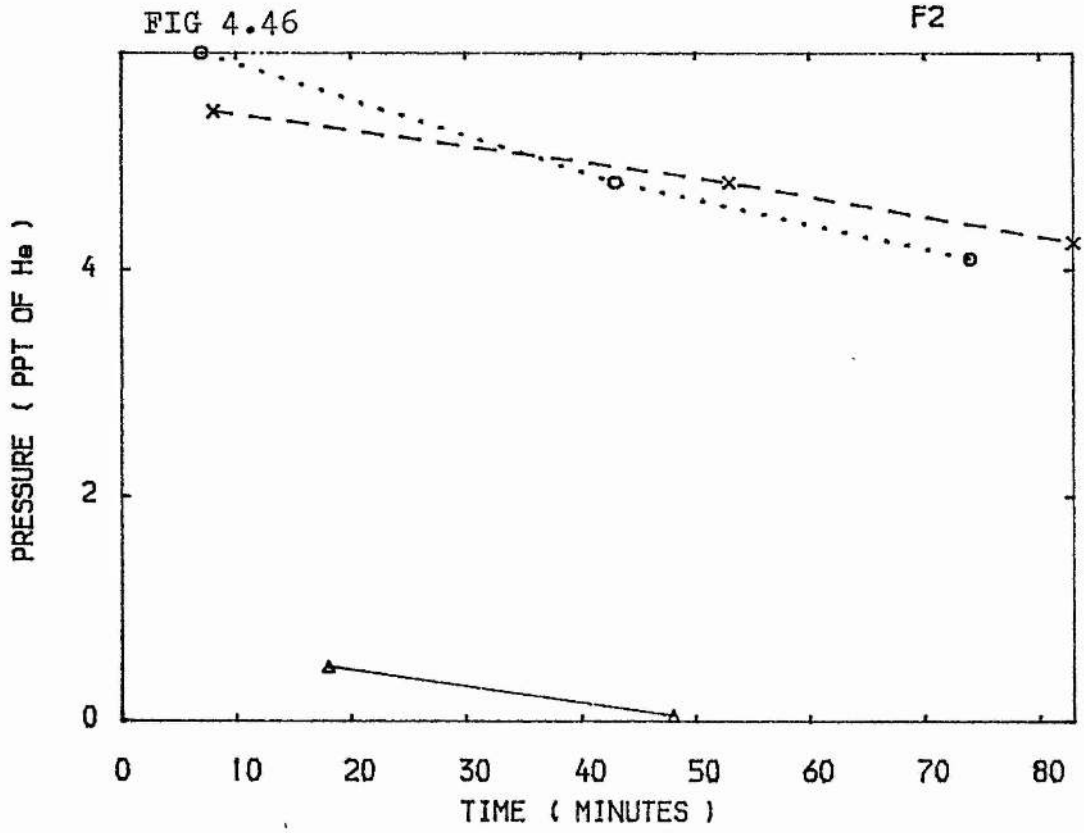

FIG 4.47

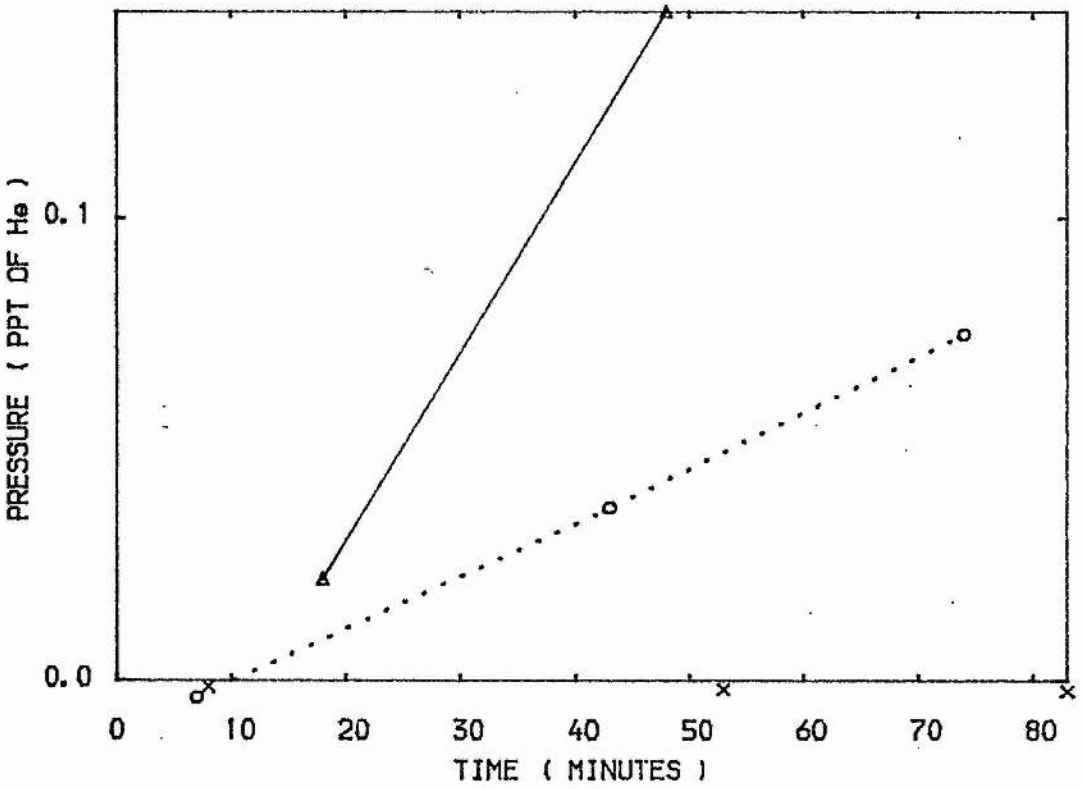

FIG 4.48

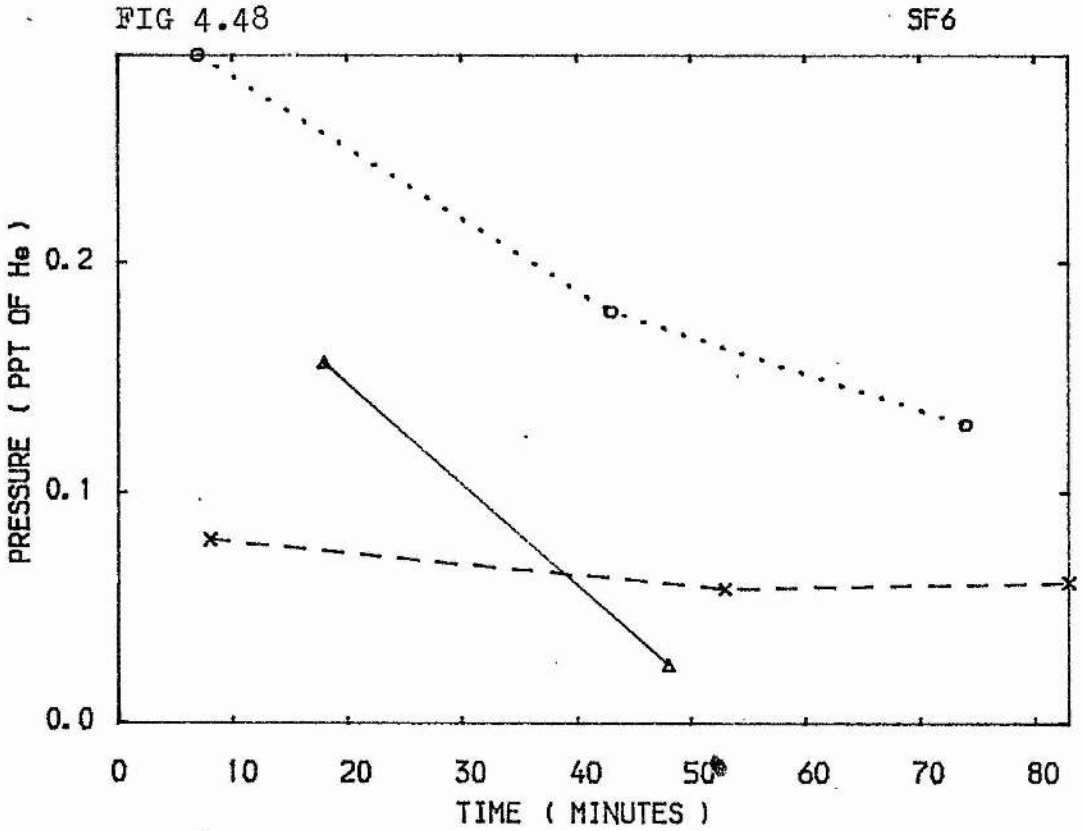

FIG 4.49

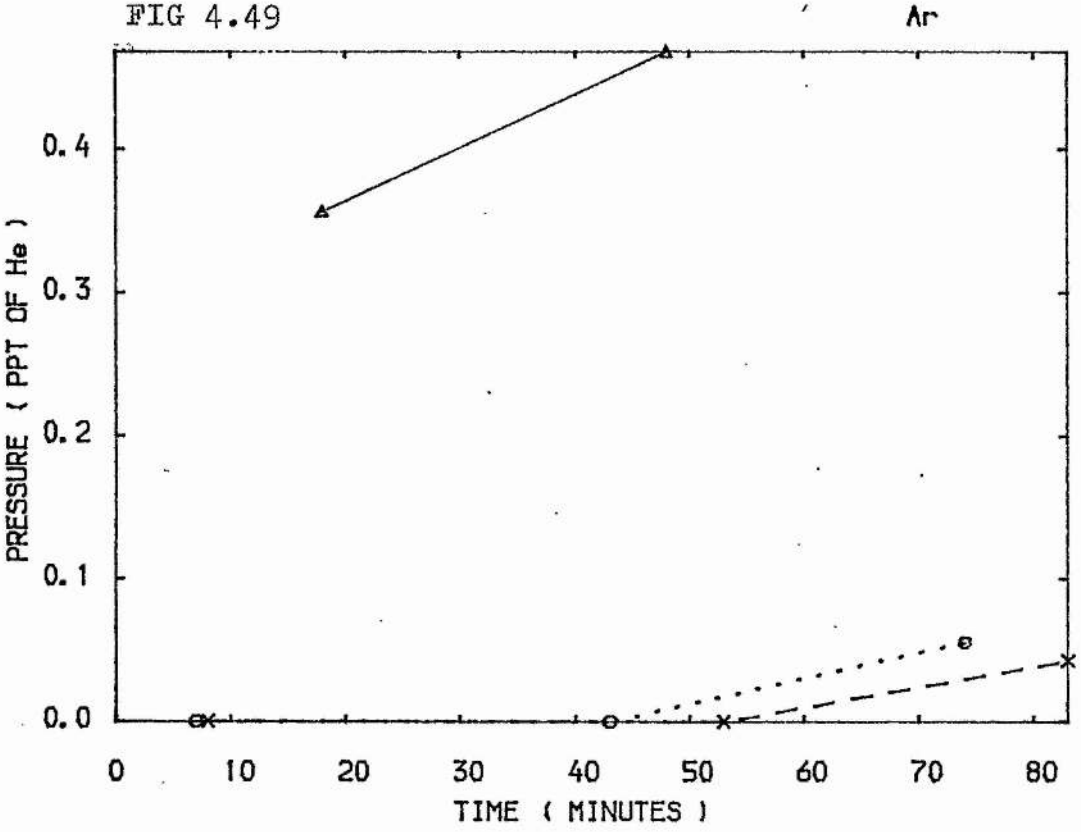

FIG 4.50

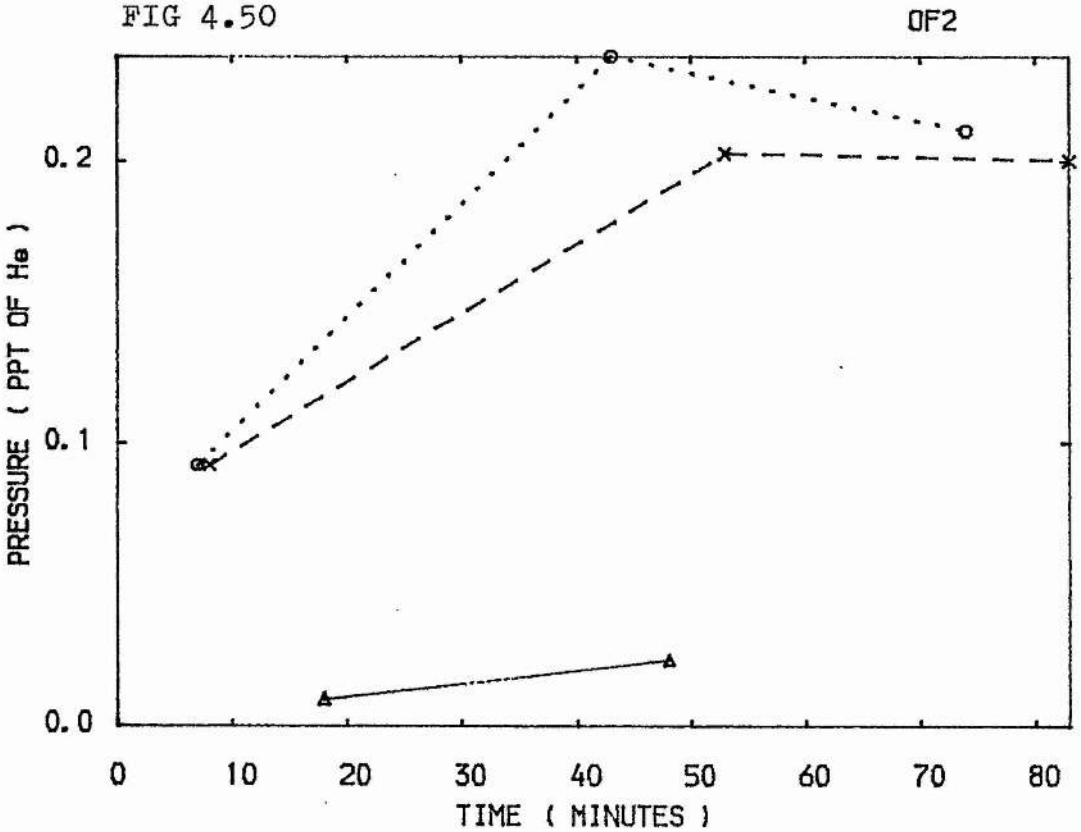

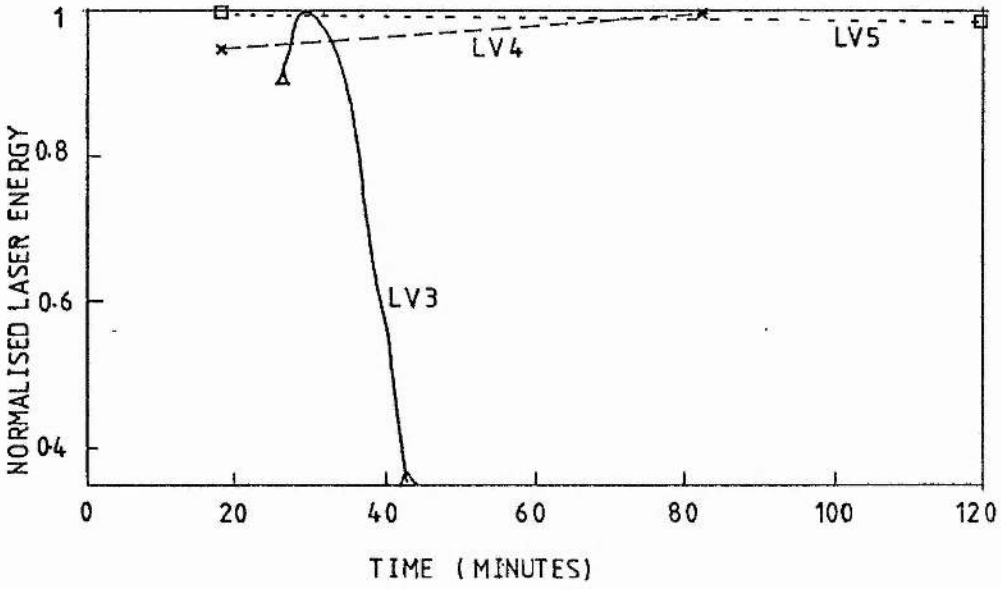

FIG 4.51 Laser output from He-F_2 mixes in LV3, LV4, and LV5.

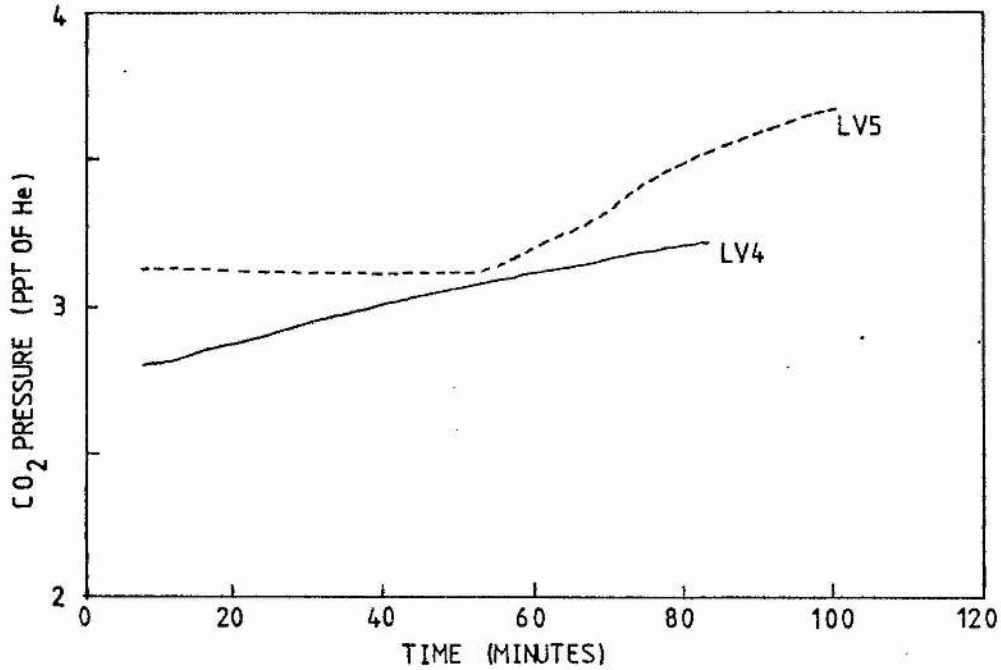

FIG 4.52 Continuous monitoring of CO_2 in LV4 and LV5.

Figures 4.53 to 4.68

Effect of cold traps on the evolution of impurities in He-F_2 mixes:

···□··· LV3 without cold trap

–·-▽-·– LV3 with cold trap at -150°C

—△— LV4 without cold trap

––X––LV4 with cold trap at -196°C

L indicates start of discharge; C indicates start of cold trap.

FIG 4.53

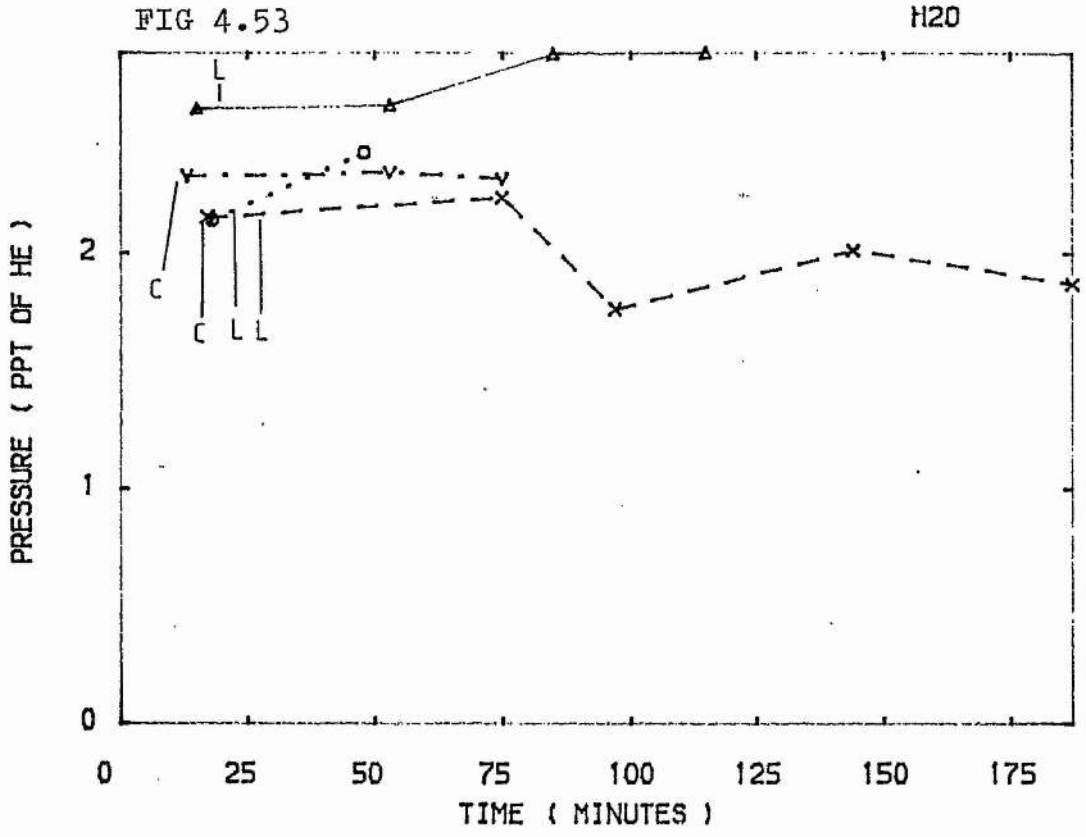

FIG 4.54

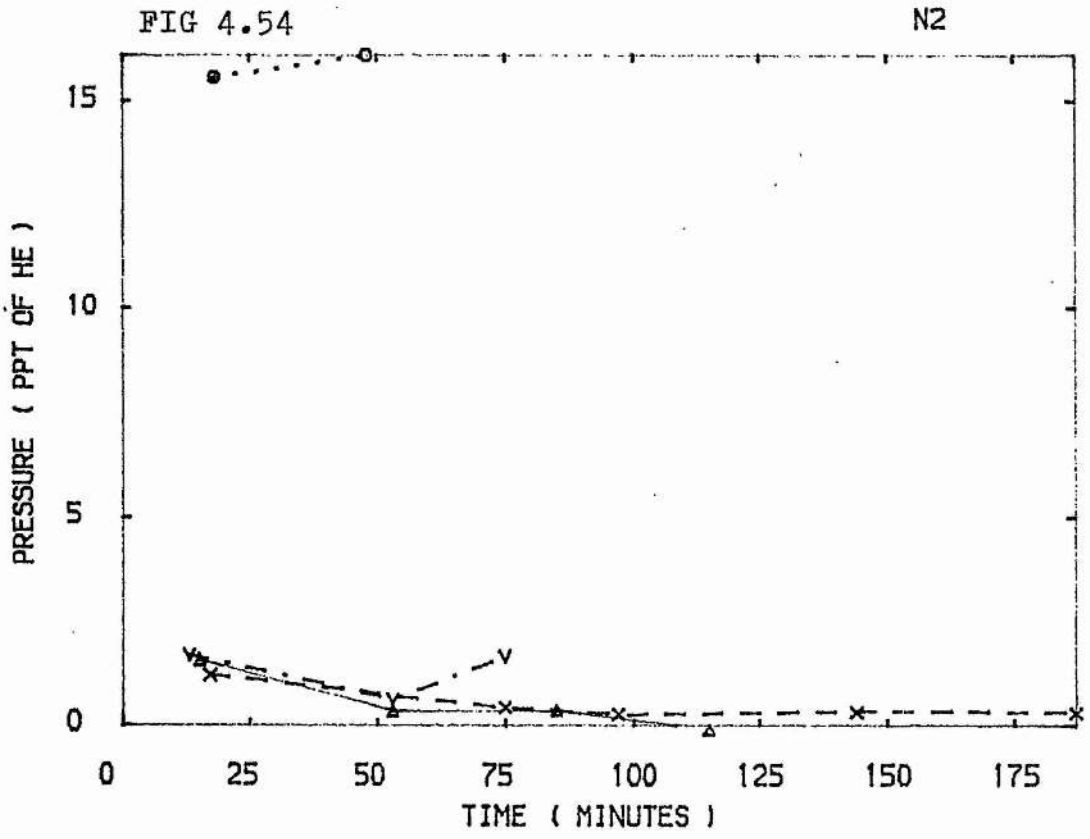

FIG 4.55

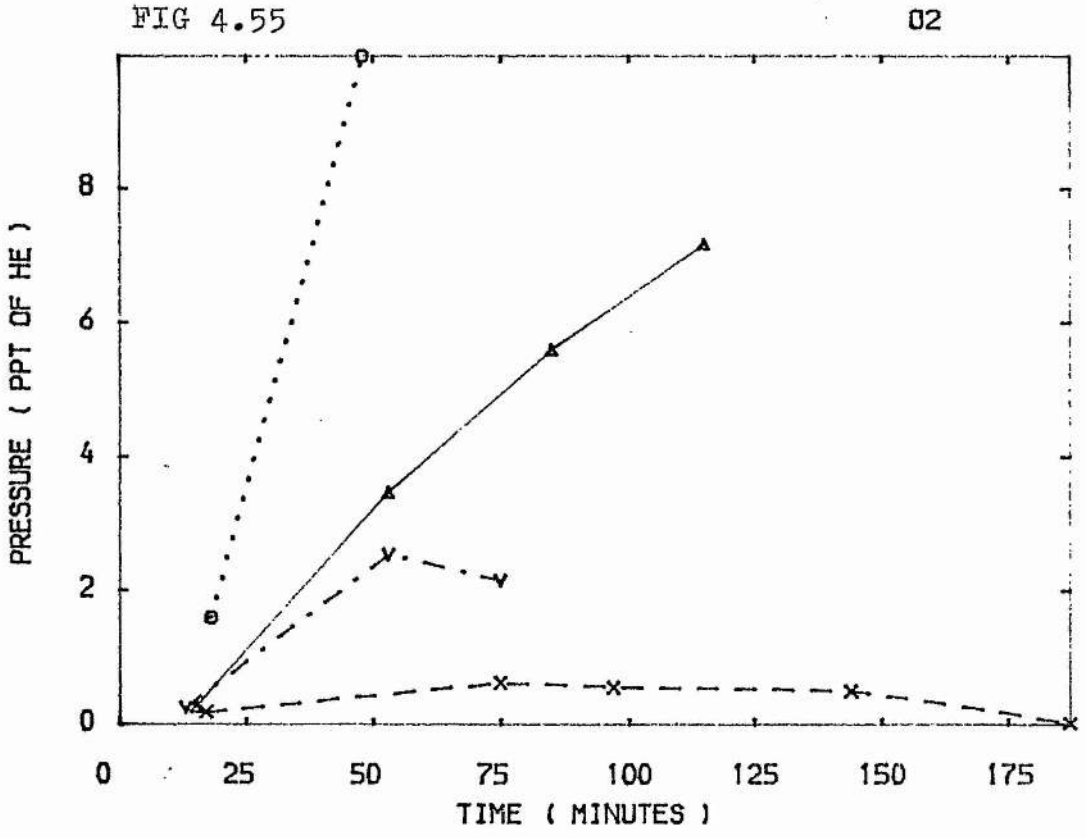

FIG 4.56

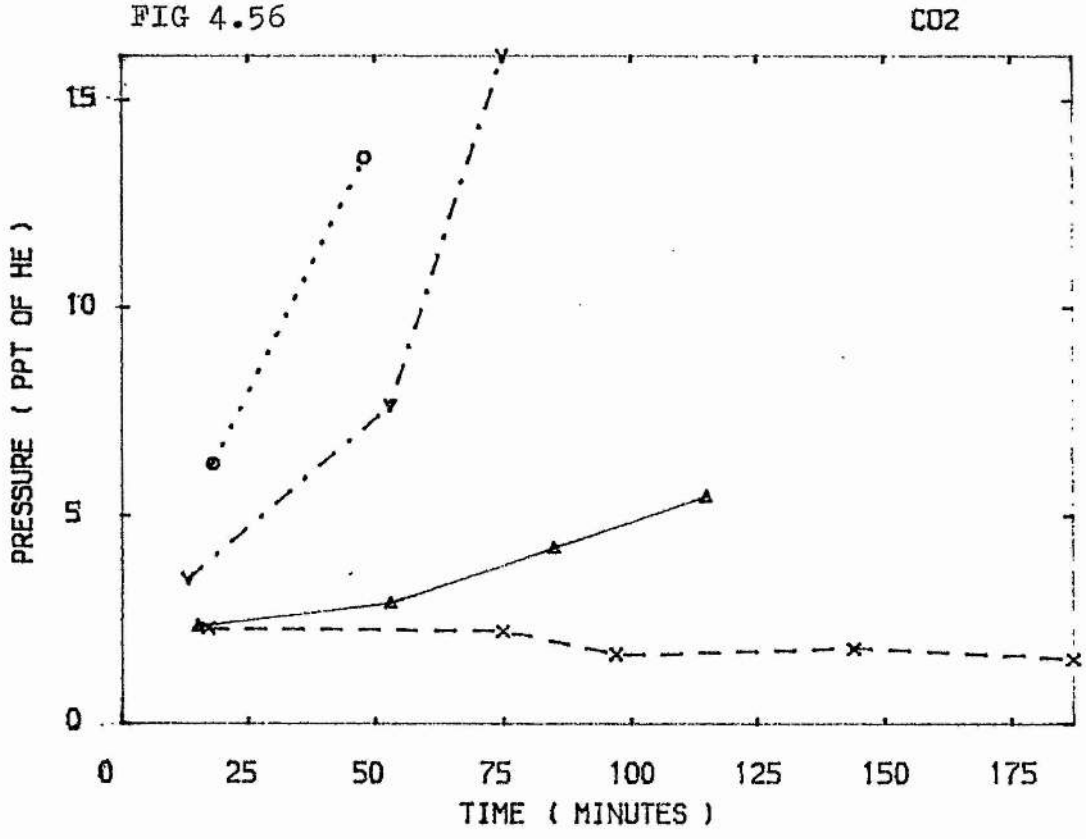

FIG 4.57

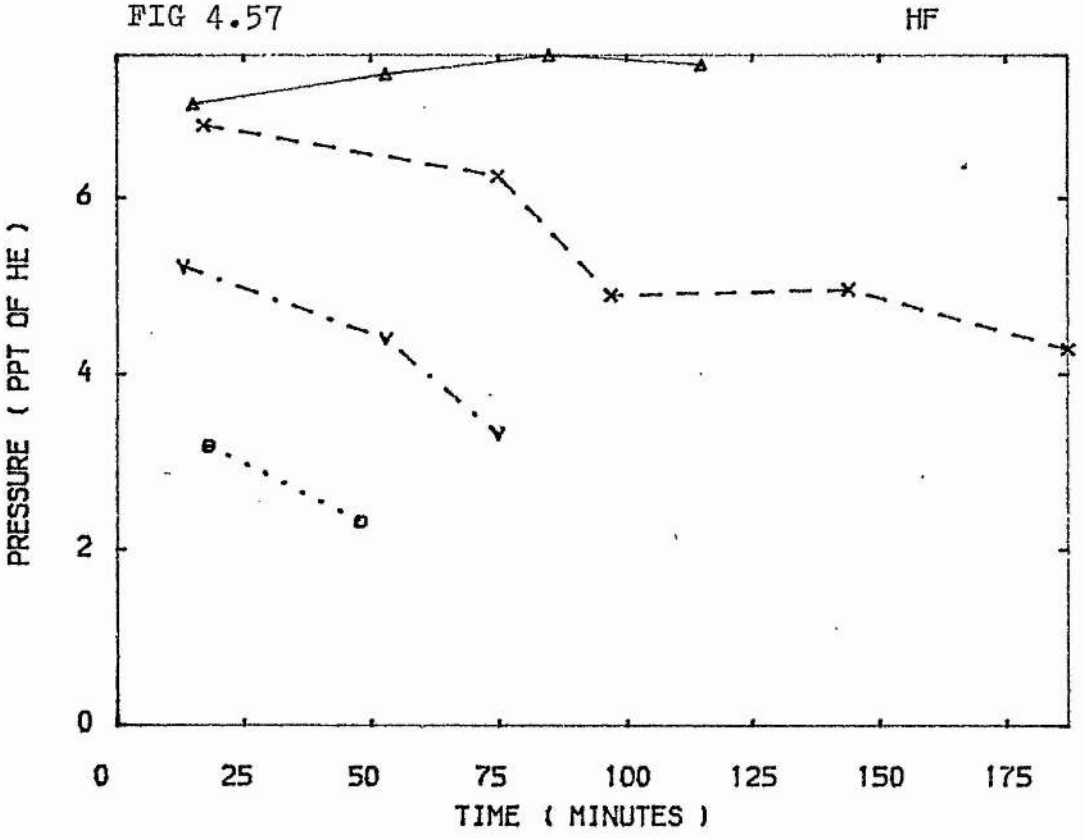

FIG 4.58

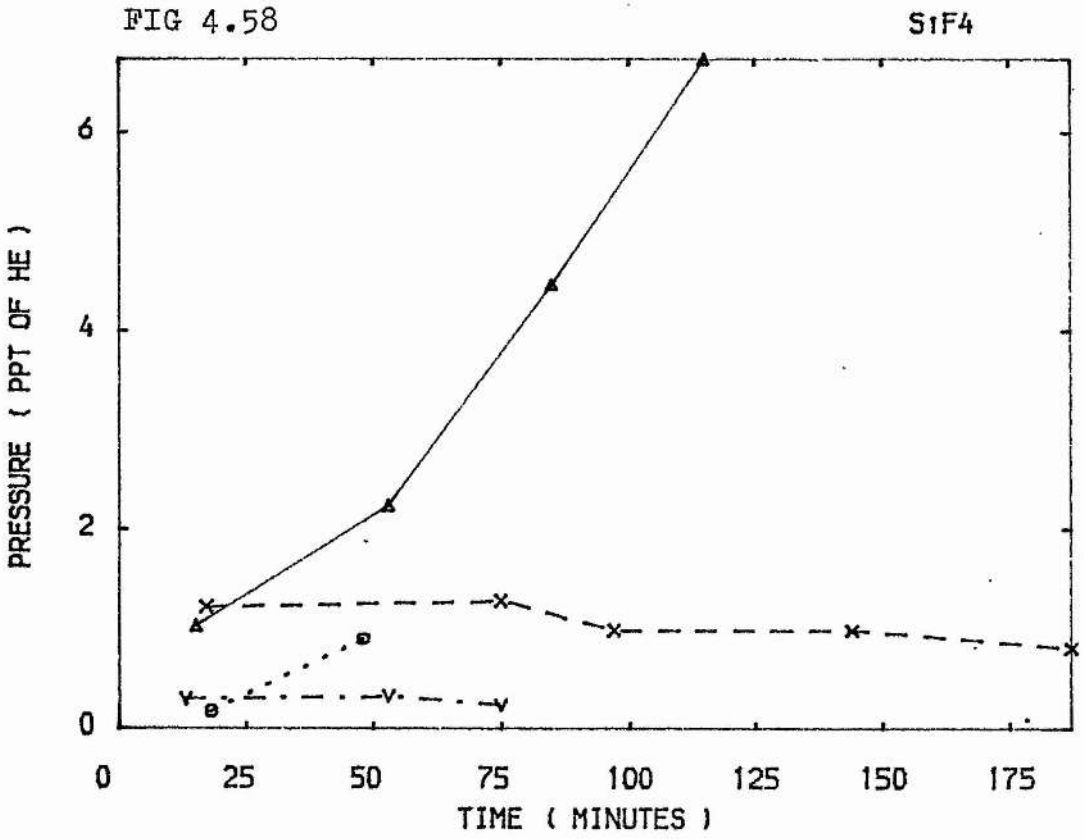

FIG 4.59

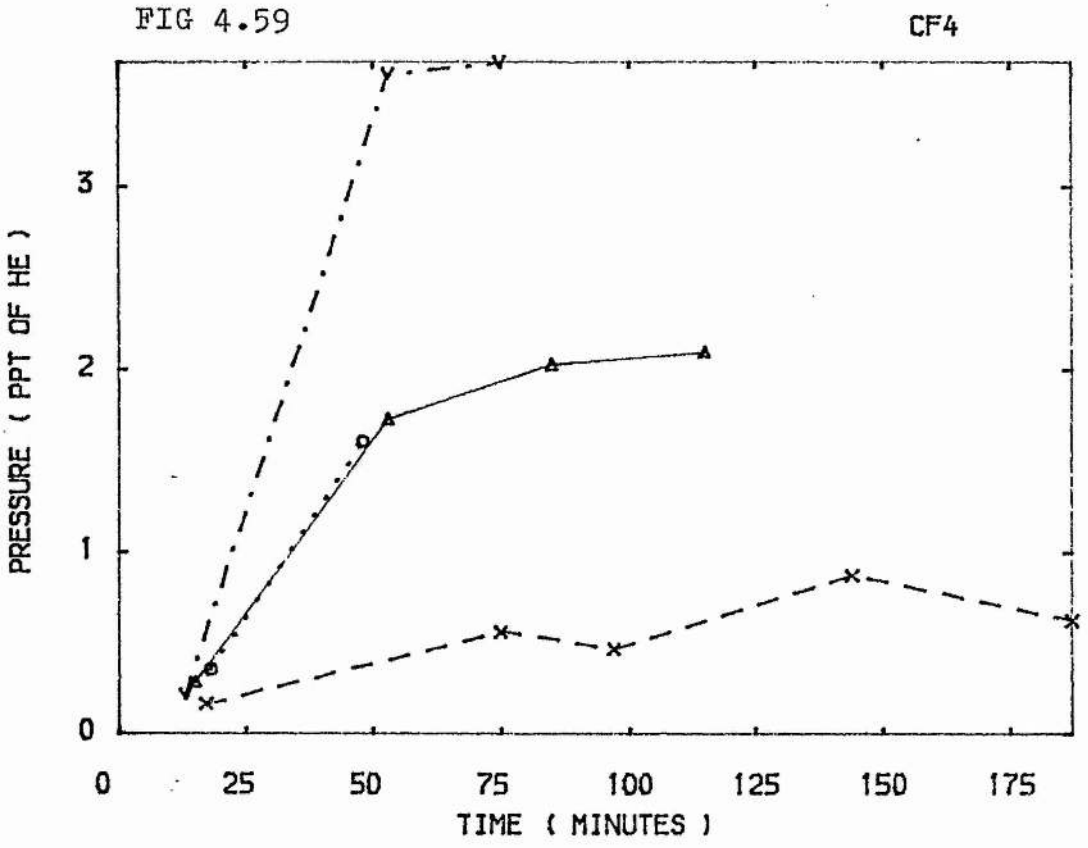

FIG 4.60

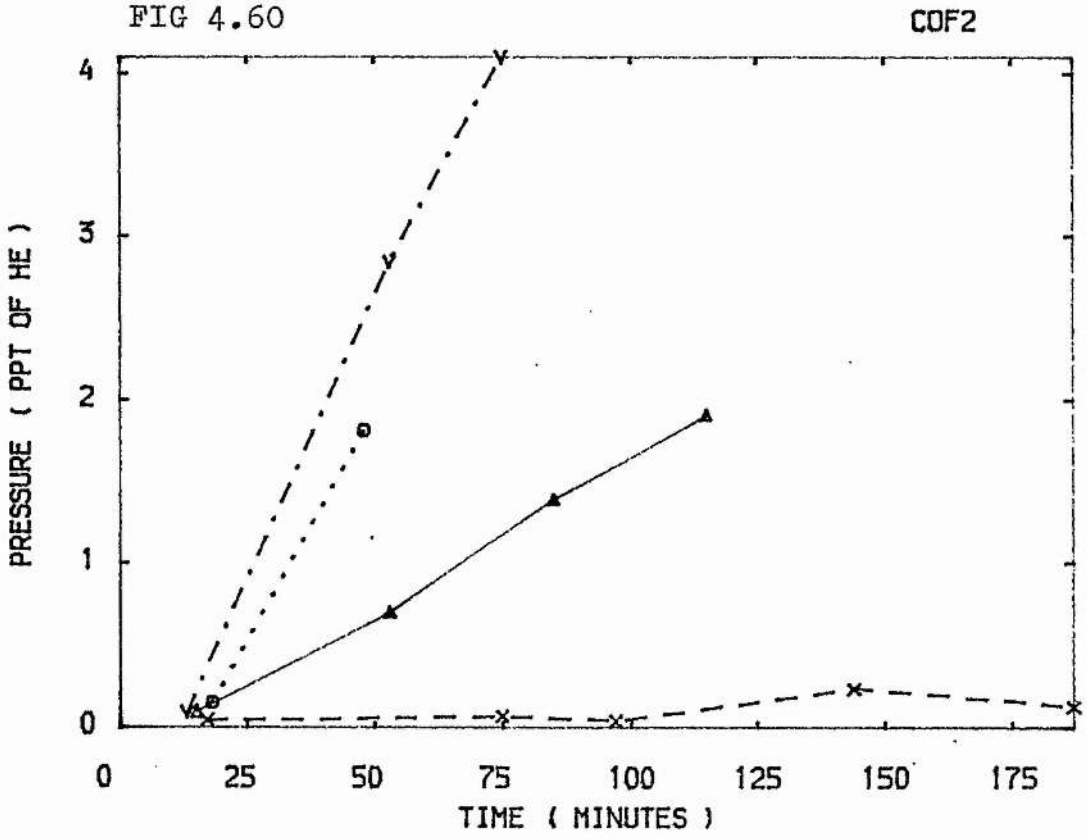

FIG 4.61

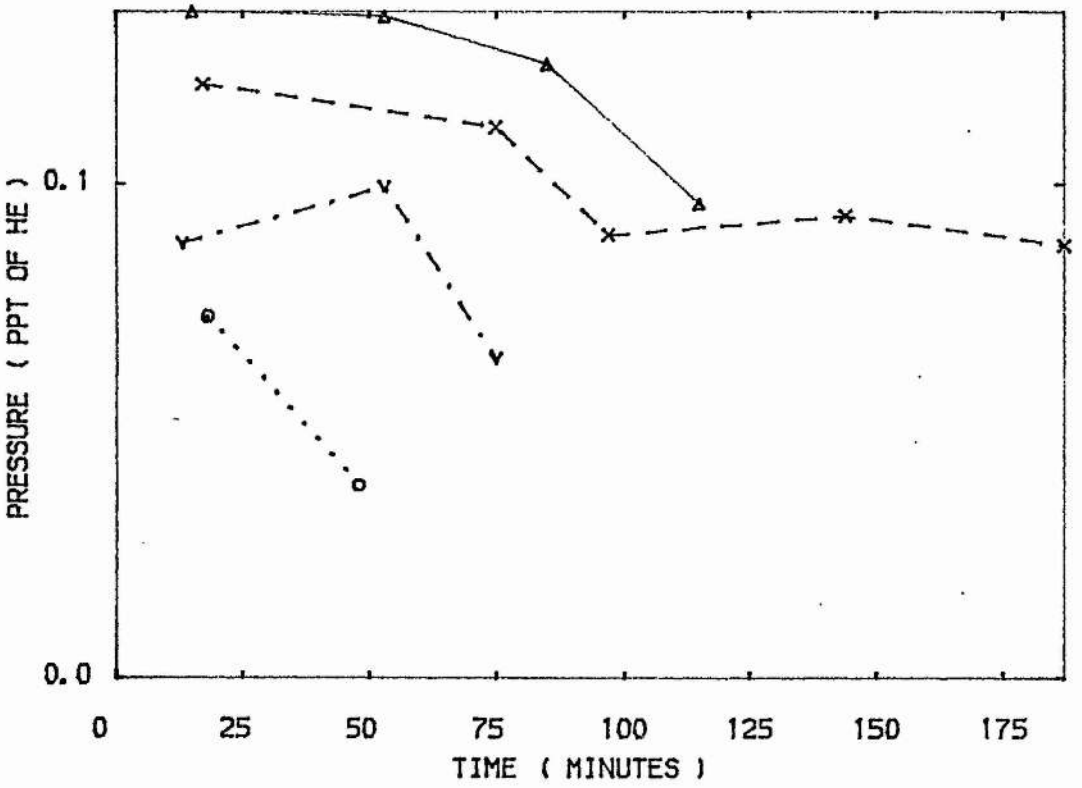

FIG 4.62

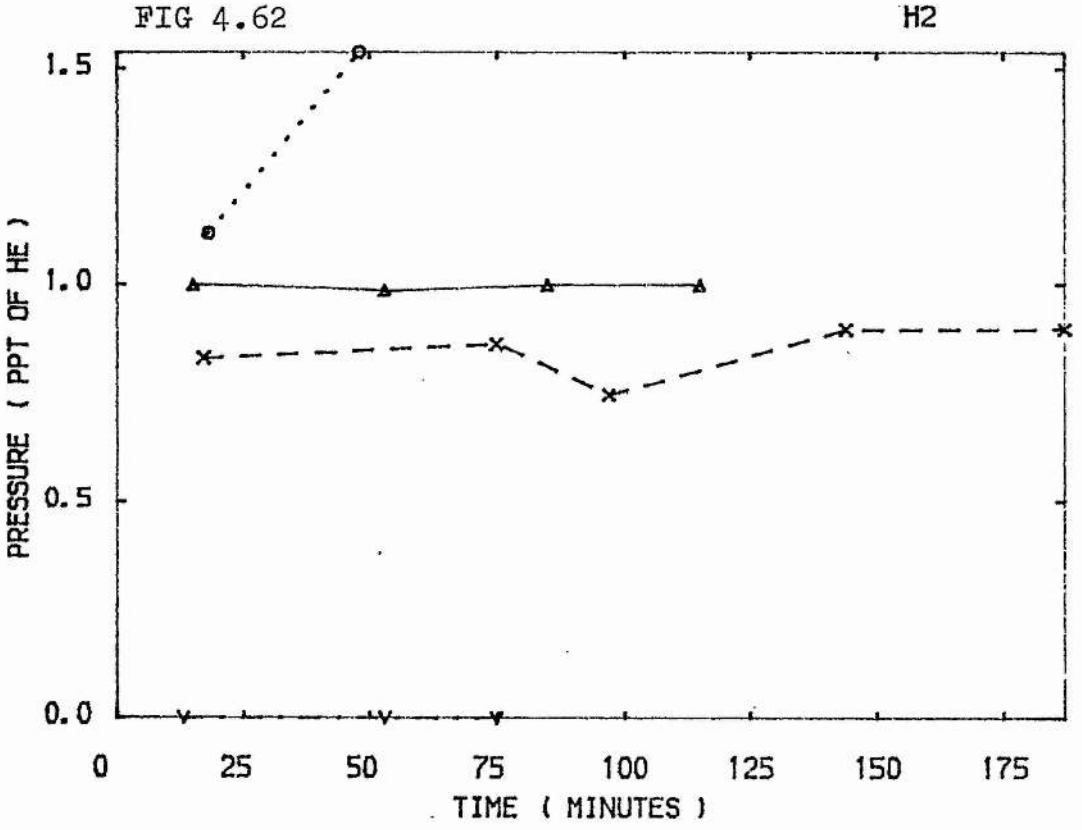

FIG 4.63

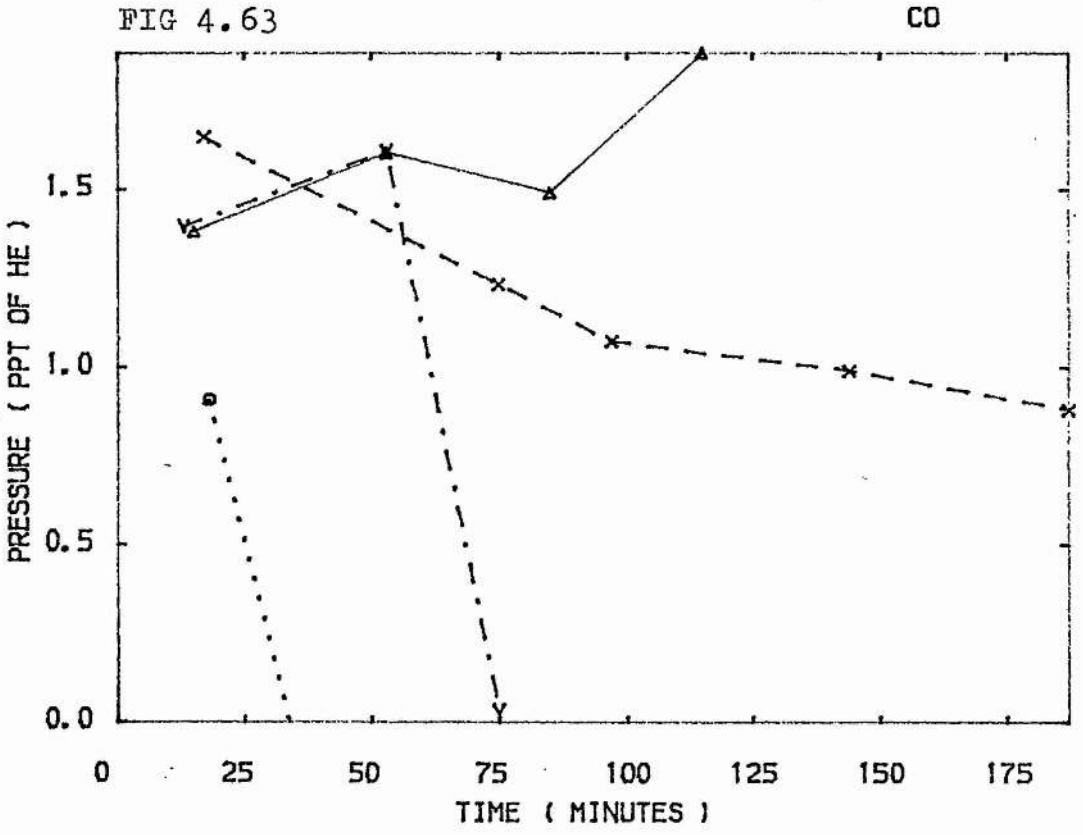

FIG 4.64

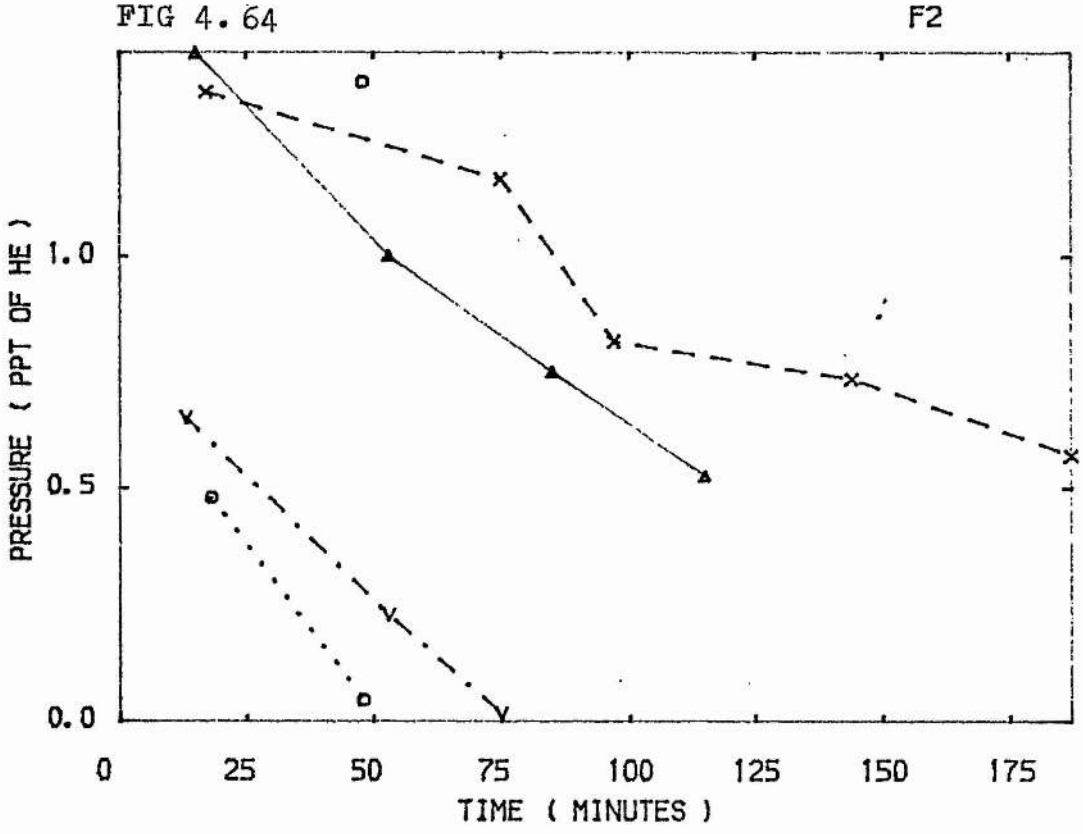

FIG 4.65

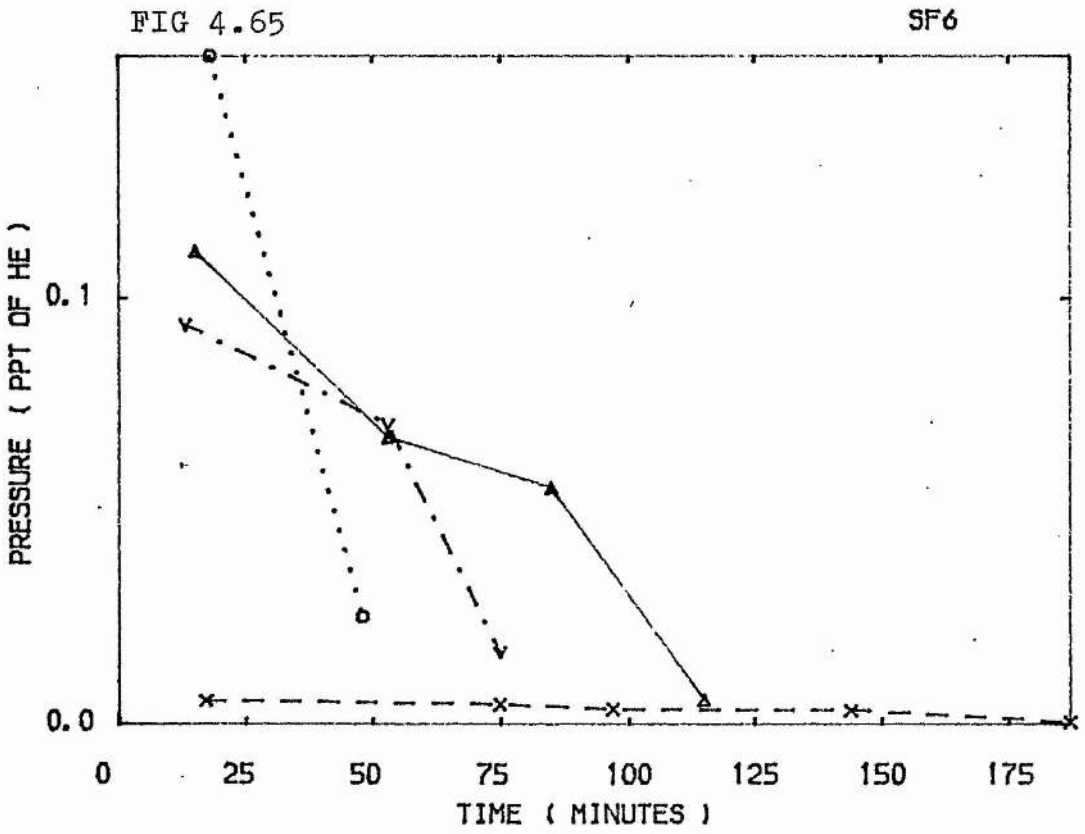

FIG 4.66

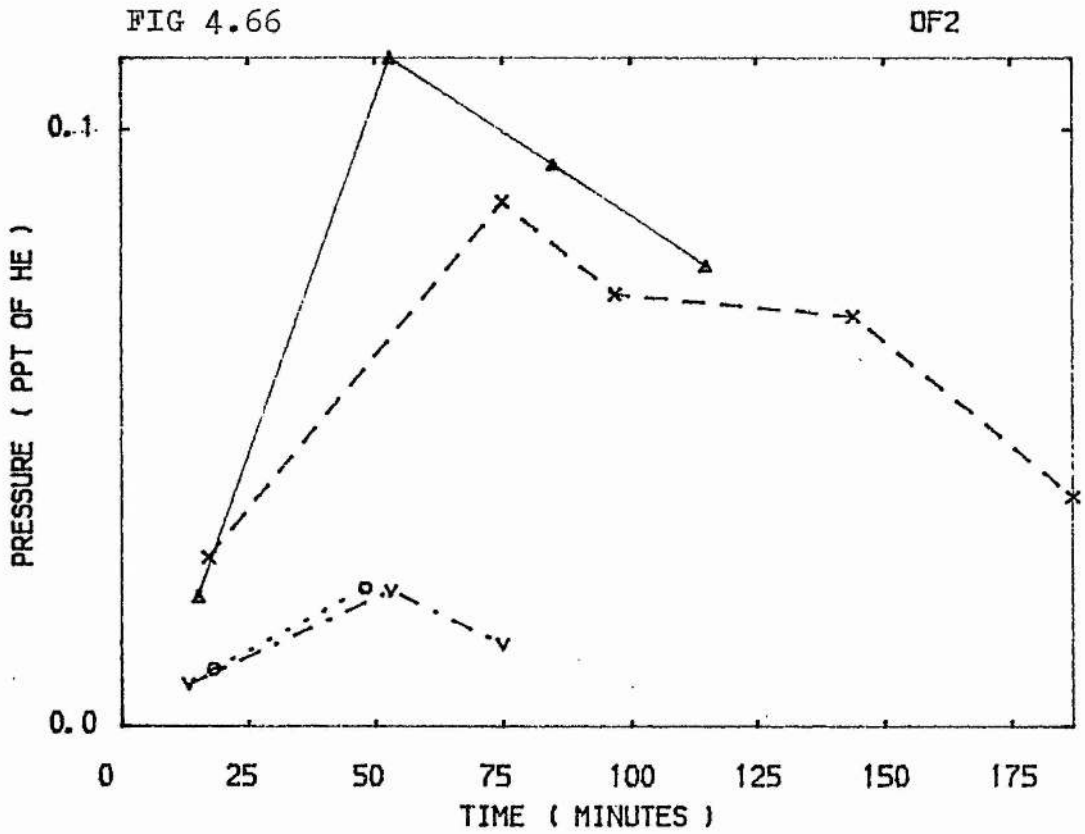

FIG 4.67

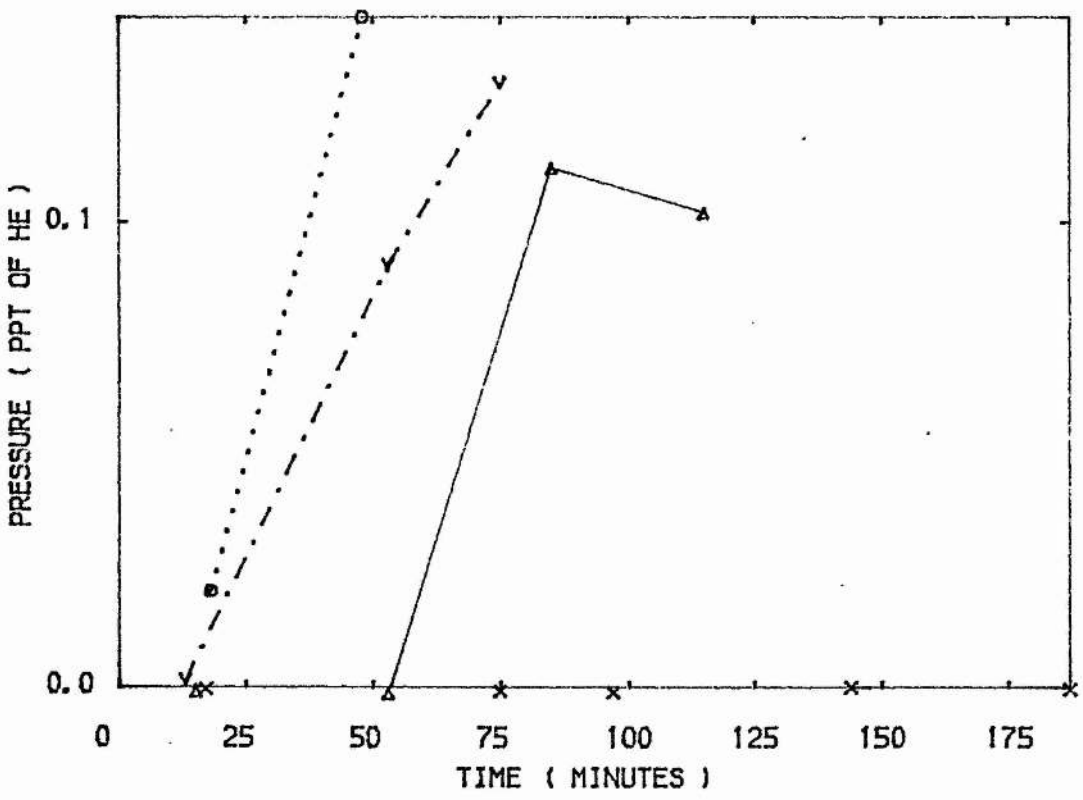

FIG 4.68

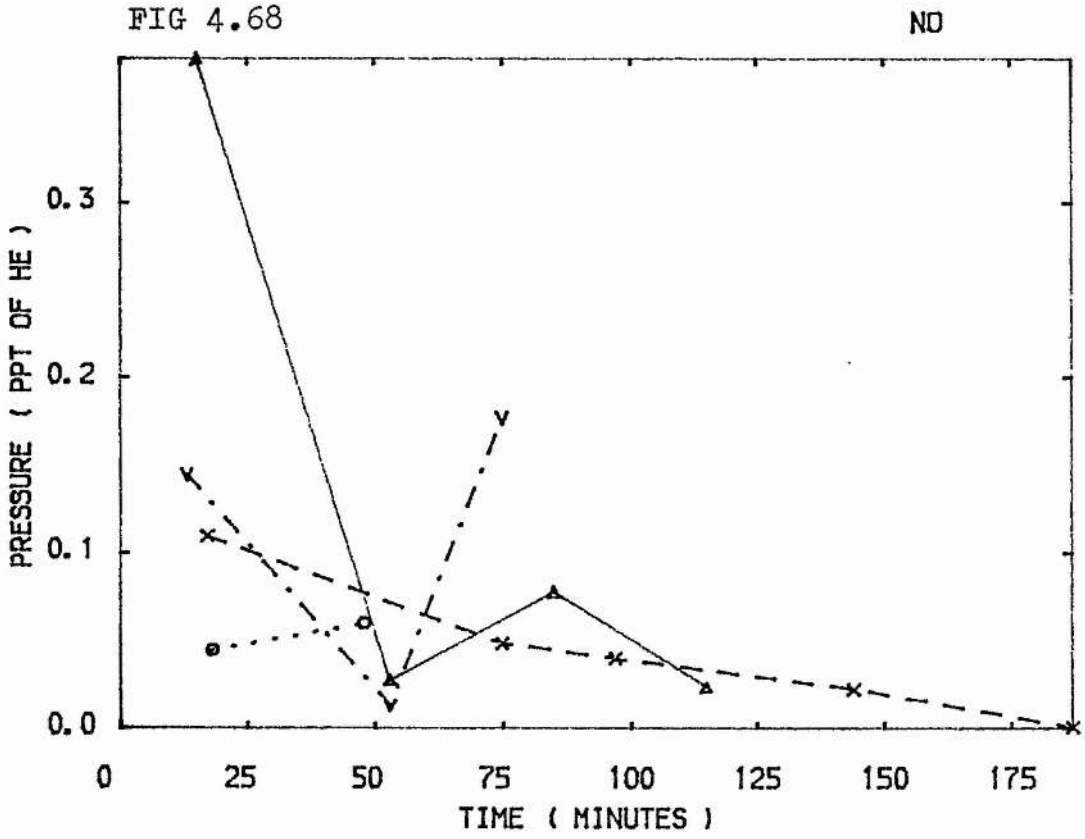

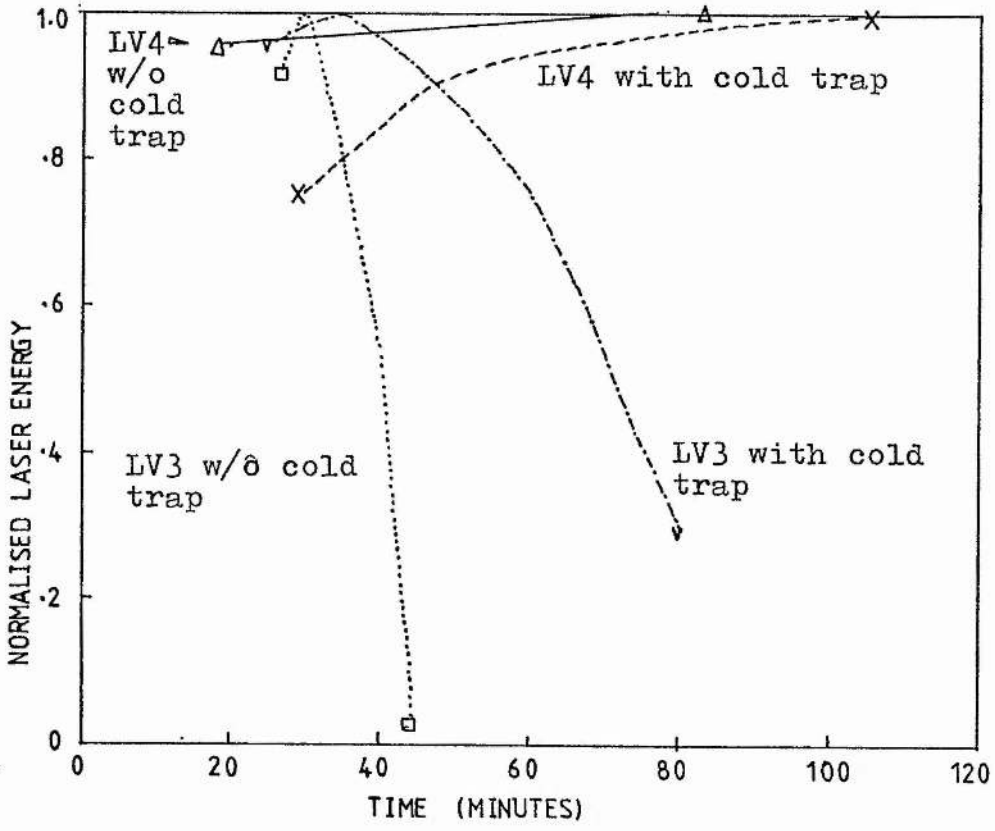

FIG 4.69 Laser output from a He-F_2 mix in LV3 and LV4 with and without cold trap.

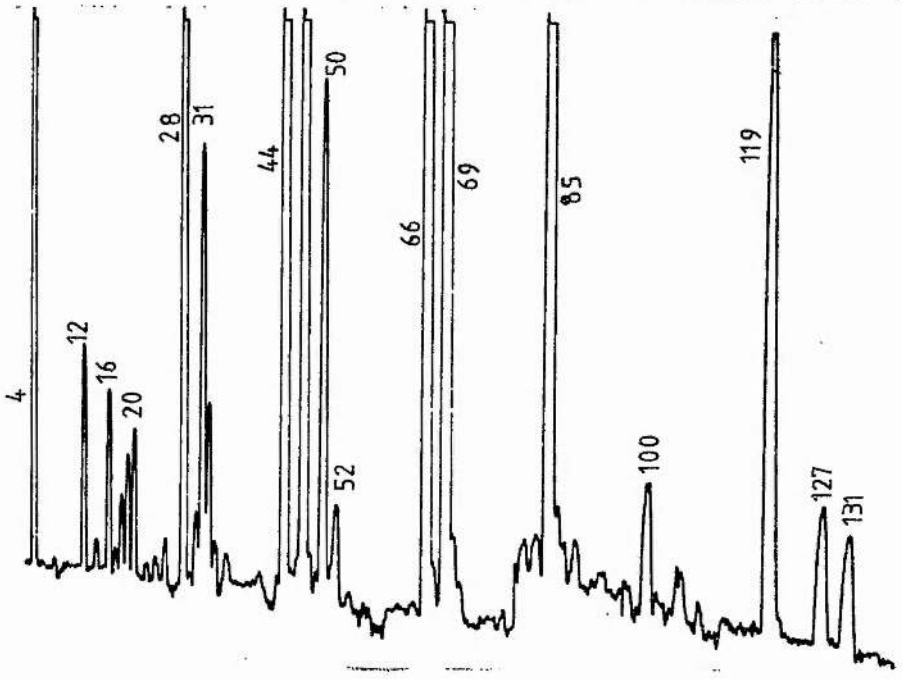

FIG 4.70 Mass spectrum of cold trap contents

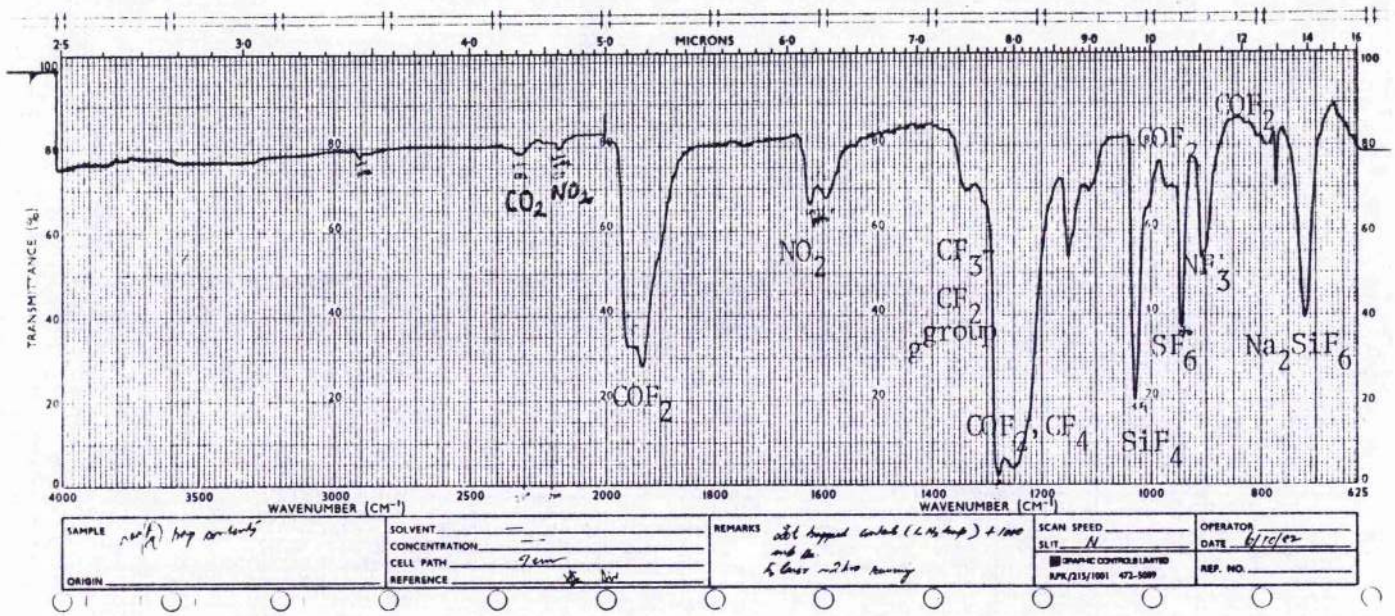

FIG 4.71 Infra-red spectrum of cold trap contents of a fluorine laser after 120 minutes.

REFERENCES

Beck A.H, Ed. (1964) Handbook of Vacuum Physics, Vol 3, part 4, Pergamon Press, Oxford.

Kondratev v.N (1964) Chemical Kinetics of Gas Reactions, Pergamon Press, Oxford.

Lawler J.E, Parker J.N, Anderson L.W, and Fitzimmons W.A (1979) IEEE J. Quantum Electr. QE15 609.

Sadighi-Bonabi R, Lee F.W, and Collins C.B (1982) J. Appl. Phys. 53 3418.

Sumida S, Obara M, and Fujioka T (1979) J. Appl. Phys. 50 3884.

CHAPTER 5

GAS LIFETIME AND IMPURITY EVOLUTION IN KrF LASERS

In the last chapter we saw an improvement of the single fill lifetime of a He-F_2 gas mix from 760 shots to half power to less than 1% drop in power output over 7200 shots. The rate of use of F_2 was correspondingly 17 ppt of He/min and 71 ppt of He/min in the two cases, for a drop in absolute partial pressure from 6 torr to 3 torr. It was also shown that the drop in power output was mainly due to the impurities present or evolving in the mixture. Compared to the atomic fluorine laser one expects the lifetime of a KrF laser to be different for several reasons. The kinetics leading to the formation of upper level of KrF could be more or less susceptible to impurity quenching. Absorption at the KrF laser wavelength of 248 nm due to species like COF_2, CF_4, etc., could be different from that at the laser wavelength of the atomic fluorine laser (730 nm). In this chapter we report measurements of the lifetime of a single gas fill and the impurities appearing in He-Kr-F_2 mixes used in the laser versions 3, 4, and 5. (See chapter 2 for details of construction of these versions.) We also study the effect of a cold trap at different temperatures on the output energy of the laser. The results are then compared with the He-F_2 experiments to ascertain whether there are any differences in

the nature and concentration of impurities and thus to understand more about the effects of impurities on the performance of each system.

5.1 Impurity evolution in He-Kr-F_2 mixtures

Figures 5.1 to 5.12 give the evolution of different compounds detected by the mass spectrometer in four different He-Kr-F_2 mixtures where the partial pressure of F_2 and Kr are 3 torr and 22 torr, respectively, and the rest is He to a total pressure of 890 torr. Curve V corresponds to the trial where the the system had not been subjected to discharges and the other three curves give the evolution of different impurities when the laser was operated at about one pulse discharge per second. repetition rate. Each experiment is preceded by passivation for about 30 minutes using 6 torr of F_2 in 890 torr of He. The laser energy outputs are given in fig 5.13.

The species detected are the same as in the He-F_2 mix, but generally in smaller quantities, as a comparison with figures 4.23 to 4.34 shows. The evolution of impurity species is also seen to be similar to that in the He-F_2 mixtures. The three scans with the laser on were taken within 14 days time and the scan without the laser taken six months afterwards. The response to F_2 over this time has increased from about 1ppt of He to about 2.5 ppt of He for an actual amount of F_2 of 3.3 ppt of He. The mass spectrometer is, however, sufficiently passivated such that no variation due to

passivation is expected over a few hours. The partial pressures of N_2, O_2, and CO_2 in the fill are higher at the beginning for curve (V) because of higher levels of initial background impurities. The scatter of curves corresponding to the three runs with the discharge on show the degree of reproducibility for the evolution of the different components.

The partial pressure of F_2 is seen to drop at about the same rate as in the run without the discharge. There is a slight increase in the partial pressure of CO_2 as for the He-F_2 mix in LV4 (compare fig 5.4 with 4.26). The partial pressures of O_2, COF_2, and CF_4 go up, again as in the He-F_2 mix. The amount of CO, N_2, and NO drop when the laser is on, as in the He-F_2 mix. The partial pressure of H_2 goes up when the discharge is on when compared with the mix without discharge. The variation in HF partial pressures is similar in He-Kr-F_2 and He-F_2 mixes but the scatter is too large for any definitive conclusions. So is the case with H_2O. The partial pressure of SiF_4 in the He-Kr-F_2 mix could not be measured because of the interference from the large peaks in the 10^{-7}-10^{-8} mbar range due to Kr. However, the above comparison shows that SiF_4 also seems to evolve in the same way as in a He-F_2 mix. The partial pressures of the other components like OF_2, SO_2F_2, etc are negligible (<0.05ppt of He). The HCl impurity is present as in the He-F_2 runs but does not change from its initial value of about 0.1 ppt of He in all cases. The increase of partial pressure at m/e of 119 is found to be similar to that in He-F_2 mixtures but at about half the magnitude (<0.005 ppt of He). Comparison of evolution of the impurities in the above described He-Kr-F_2 fills to that in the

$He-F_2$ fills in version LV4 show that the presence of Kr has not significantly affected the kinetics leading to the formation of the impurities, at least on a macroscopic time scale. The smaller rates of increase of partial pressures of the impurities, especially COF_2, CF_4, and O_2 in the $He-Kr-F_2$ mixes are in accordance with the decreased partial pressure of the reactive species F_2 to half its value (in corrected partial pressure units) in the $He-F_2$ mix. Thus the same kinds of reactions are probably occurring in the $He-Kr-F_2$ mix as in the $He-F_2$ mix discussed in section 3.3 but at reduced rates.

The laser output curves in normalised units show the effect of these impurities on the performance of the laser. The average number of shots to half power for the three curves is 2700 ± 300 shots. The shorter lifetime for the mix (X) seems to be due to an inhomogeneous discharge as indicated by the large pulse to pulse variation. The cause for this was probably the sparkgap, which was firing erratically. The variations in half-life of the three different mixes cannot be correlated to the variation in partial pressures of the impurities measured because of the scatter in the readings and the lack of more accurate values for the partial pressures of H_2O, HF, and SiF_4.

A separate experiment in which a fresh $He-Kr-F_2$ mix with half the partial pressure of F_2 than in the mixes used in the above described experiments showed that the output energy at the start was slightly greater (110%) than for the mix with 3 torr F_2. The absolute values of the output energy are about 10 mJ at start for

the He-Kr-F_2 mix used in the experiments. Thus, as in He-F_2 mixes, the decrease in power output is most likely due to the impurities evolved in the laser. In the case of KrF laser with the output at 249 nm, the shorter lifetimes of the mix to half-power compared to He-F_2 mixes suggest that the laser kinetics and the discharge are more sensitive to the impurities present. The absolute values of the impurities are generally less as explained before in the He-Kr-F_2 mix. More quantitative aspects of the role of the impurities are dealt with in chapter 6.

Even if the impurities evolved can be successively removed, loss of F_2 would ultimately limit the lifetime of a mix unless replenished with fresh F_2. In the above results it is seen that loss of F_2 is not much higher when the discharge is on when compared to the loss without any discharge. Thus the loss rate of F_2 in reactions with the background impurities and the vessel interior assumes equal significance whether the laser is on or off.

5.2 Effect of cold trap on He-Kr-F_2 mix lifetimes

It was seen in section 4.4 that a liquid nitrogen cold trap effectively removed many of the impurity species evolving in the laser cavity to increase the lifetime of the gas mix and the number of shots to half power. A liquid nitrogen trap is not feasible for a He-Kr-F_2 mix because of the far higher boiling point of Kr ($-152^{\circ}C$) compared to N_2 ($-196^{\circ}C$). Thus dry N_2 bubbled through a dewar containing liquid N_2 is used to cool the cold trap coils to

temperatures above -150°C by adjusting the flow rate as described in section 2.6. This trap is not expected to be as efficient as the liquid N_2 trap which operates at lower temperatures. However, the results can be compared with those from the He-F_2 mixes studied with the colder liquid N_2 cold trap.

5.2.1 Lifetime of a He-Kr-F_2 mix with a cold trap

Figures 5.14 to 5.25 give the evolution of different detected species in the laser mix under four different conditions. Curves labelled Δ give the partial pressures in the mix circulated without any cold trap or discharge. These serve as a basis for comparison for the other three curves, of which those marked X belong to a run with discharge, with the cold trap at -150°C from the beginning to the end of the experiment. Curves marked □ show the evolution of the impurities in a mix with discharge from the beginning, and the cold trap switched on later in time when the output energy has dropped to less than half the starting value. Curves marked V belong to a run with the mixture circulated and the cold trap at -113°C after 100 minutes. It is sampled for laser energy output at intervals. The corresponding curves in figure 5.26 give the normalised output energy as a function of time and the cold trap temperature at different times if they differ from the room temperature of 22°C. Arrows indicate the time when the laser is switched on.

Comparison of curves X from 50 minutes and the initial part of □ up to 60 minutes before the cold trap is on show the effect of a -150°C cold trap on the evolution of impurities and the half life of the mix. The number of shots to half power increases from 3000 to about 11000 (extrapolated value assuming linear fall) when the cold trap is present, as seen from fig 5.26. The rate of fall of F_2 and CO remain the same in both cases but O_2 does not rise above the initial value and N_2 falls more rapidly than without the cold trap. There is a fall in the partial pressure of CO_2 when the trap is on, whereas without the trap and with the laser on, the partial pressure of CO_2 shows a small rise. The partial pressures of COF_2 rise at the same rate in both cases while that of CF_4 is marginally higher in the trapped version. The production of NF3 in the cold trapped run is higher. Water vapour and HF does not show any significant changes, even though they are expected to be trapped.

Since the cold trap is at -150°C one expects the condensation of H_2O, HF, CO_2, COF_2, CF_4, NO, and NO_2 in the trap. From the partial pressure curves it is seen that COF_2 and CF_4 are produced at a greater rate than can be handled by the cold trap. In the case of the He-F_2 mixture, the liquid N_2 trap was able to reduce the partial pressure of CF_4 to values smaller than in the KrF laser. The absolute values of COF_2 are about the same in both the lasers (compare 4.60 with 5.21) but in the F_2 laser the drop in growth rate is quite dramatic. All the other species detected in the KrF mix change their partial pressures the same way in the F_2 laser when the cold trap is on. Since SiF_4 would condense at -150°C,

comparison with the He-F_2 curves show that a drop in SiF_4 partial pressure is expected, albeit to a lower extent, in the KrF laser mix too, when the cold trap is on.

The improved lifetime of the mix, as far as the number of shots to half power is concerned, can be attributed to the drop in the level of background impurities, notably N_2, O_2, CO_2, COF_2, CF_4 and also most probably, H_2O, HF, and SiF_4, even though the mass spectra do not indicate this drop due to reasons detailed previously. The fact that the cold trap is very effective in increasing the power output by trapping the impurities is seen from the power vs time curve for the curves marked □ after 60 minutes, when the cold trap is cooled to -150°C within 20 minutes. The laser power goes up from 44% to 75% of the initial value within minutes, showing that the output power is very sensitive to the small percentage of impurities present. However, no such rapid changes are seen in the partial pressures of the components except for a drop in the partial pressure of O_2 which is not large enough to fully explain the recovery of laser energy. Since O_2 itself cannot be condensed out at -150°C we infer that H_2O and CO_2, which are the two main O atom donor species in any breakdown in the laser, are condensed rapidly. The drop in O_2 partial pressure also indicates that it takes part in some reactions in the discharge, probably with H_2 and N_2 to produce H_2O, NO, and NO_2. Since CO_2 partial pressure changes do not seem to be large enough when the cold trap is down to -150°C, this leaves H_2O as the significant impurity which can condense out fast due to its higher boiling point. A sudden drop in the partial pressure of H_2 is also in keeping with this

hypothesis. The change in the measured partial pressure of H_2O is unfortunately not a reliable estimate of any such rapid changes in the laser. It is also seen from the curves marked □ that the amounts of COF_2, CO_2, and O_2 are higher than for the curves marked X obtained when the cold trap was on from the beginning of the discharge sequence.

Finally, the curves V give the component partial pressures when the gas mix is cold trapped after t=100 minutes but not used for lasing. The laser output from this mix, sampled at intervals, is given in figure 5.26 (curve V). The output falls from 8.5 mJ at start to 5.2 mJ at 100 minutes. This can be only due to the increased level of impurities since a fresh mix with F_2 down to 1.5 torr gives a slightly higher power output. The impurities that increase significantly are N_2, CO_2 and to a lesser extent, O_2, CO, H_2, and NO. The drop in F_2 is less than in the lasing mix, since F_2 is being used up to a lesser extend in the absence of a discharge. At 100 minutes, without the cold trap or the discharge, the energy output drops to 60% of the initial value, whereas when the laser is on, the extrapolated drop is to about 30%. Thus, even without the discharge there is a significant drop in the power output due to the impurities evolved in the laser. When the cold trap is switched on, the power output at t=140 minutes goes up to 6.2 mJ (78% of initial value) even though the recorded values of all the impurities except NO keep going up at about the same rate. This indicates that the significant impurity is H_2O and possibly HF. It is seen that the rate of growth of O_2 does not change when the trap is cooled to $-113^{\circ}C$ without the discharge, unlike the

curve □ or X. Thus the growth of O_2 in this instance is mostly due to the usual background growth, with a slight addition from the discharge when the laser energy is tested at intervals.

These observations show that the cold trap keeps the laser mix active over longer periods of time by condensing out the impurities formed in the gas mix due to outgassing and the discharge. However, for the KrF mix, the changes in partial pressures of the different components are not large enough to be satisfactorily correlated with the increase in the energy output of the laser when the cold trap is used. A more quantitative exploration of the role of impurities in the KrF laser is carried out in chapter 6. In the next section we try to get a better idea of the role of the cold trap by looking at the power output and impurity evolution at different cold trap temperatures in the range 22°C to -150°C.

5.2.2 Cold trap temperature dependence of KrF laser energy

As seen in the last section, the energy output of a KrF laser, after having fallen to about 50% of the initial value, recovers to about 78% of the initial value when the same gas mix is passed through a cold trap at -150°C. This shows that the major impurities have a boiling point below -150°C. It was also seen that the mass spectra did not give a satisfactory indication of the changes in the impurity species with time in the results given in the last section. Once the cold trap has collected enough of the impurity species, warming the trap slowly would let the impurities

back into the system one at a time, depending upon their boiling points, and by monitoring the power output as a function of temperature, the identity of the impurity species could be found.

The evolution of various detected impurities in a cold trapped gas mix is given in figures 5.27 to 5.38. The trap is at room temperature till t= 100 minutes, and at -150°C till t= 235 minutes. The laser is off till t= 190 minutes and working at one pps till the end of the run. The solid curve (Δ) is a comparison run without any cold trap or laser but with the same ratio of gas mix. The cold trap temperature and power output as a function of time is given in fig 5.39a. From these curves it is seen that there is a greater rate of increase in CO_2, COF_2, CF_4, and NO partial pressures after the cold trap is allowed to return to room temperature. The partial pressure of O_2 in the cold trapped mixture increases when there is no discharge, but decreases when there is a discharge. When the cold trap is warmed up to room temperature, the rate of fall of N_2 decreases and the partial pressure of F_2 increases slightly. These changes could be due to the condensed impurity products getting back into the laser mix and also reacting in the discharge. The laser energy does not recover the original value when the cold trap is cooled again to -150°C after warming it up to room temperature for a few minutes. This shows that once the reaction products are formed, it is difficult to recondense them to recover the original energy. However, when the cold trap is warmed up to -66°C from -150°C and then cooled again to -150°C after a few minutes, the energy recovers to the original value. It is also seen from figures 5.39a and 5.39b that

the energy drops rapidly when the cold trap reaches -80°C and there is also another rapid drop at the higher temperature of ~0°C. This shows that the condensed products evaporating back into the system with boiling points at these two temperatures are the important impurities in the KrF laser mix. Since the impurities detected in the system and their boiling points are known, these two impurities are seen to be CO_2 (sublimes at -78.5°C) and H_2O (melting point 0°C). The rest of the major impurities have boiling points well removed from these two temperatures. These results are in accordance with previous observations on the partial pressures of CO_2, O_2, COF_2, and CF_4 recorded in the previous sections.

5.2.3 Mass spectrum of cold trap contents

A mass spectrum of the cold trap contents of a cold trapped KrF laser is given in figure 5.40. This spectrum was taken at the end of 90 minutes of lasing with the cold trap at -150°C. Strong peaks are observed due to N_2(14, 28), NO(30), O_2(32, 16), CO_2(44, 12, 22), COF_2(47, 66), CF_4(69, 50), $C_2F_5^+$(119), $C_2F_4^+$(100), SiF_4(104, 85 lost in the Kr background), HF(20), peaks due to Xe impurity in Kr, due to Kr, and due to He. The peak at m/e of 51, which was found to grow in an unlased He-F_2 mix, could be due to O_2F. Of these compounds, N_2 and O_2 could not have been trapped out by the -150°C cold trap, rather they are reaction products of the cold trap contents such as H_2O, HF, CO_2, NO, NO_2, and COF_2 released as the trap warmed up to room temperature. All the compounds detected in the cold trap have been found in the mass spectra of the gases

taken from the laser. The compounds identified are also the same as found in the He-F_2 mixes discussed in chapter 4.

5.3 KrF laser revival by addition of fluorine

Various reports in the literature (Johnson 1978, Kutschke 1981, Mandl 1982) have given procedures for maintaining the power output of excimer lasers by trapping out the impurities and restoring the partial pressure of the halogen donor to the optimum value by adding it continuously. This is one way of overcoming the depletion of F_2 and the accumulation of impurities. Even though the system is not strictly sealed off any more, it is better than refilling with a completely fresh mixture.

In figure 5.41 the results of an experiment in which a cold trap was used for 20 minutes to remove the impurities accumulated in the laser is given. The laser is working at one pps for 150 minutes in which time the power output drops from 8.5 mJ to 1 mJ. The F_2 partial pressure drops from about 1.4 ppt of He to about 0.75 ppt of He during this time. The cold trap is then cooled down to -150°C and the impurities trapped for 20 minutes. When the laser is switched on again at 200 minutes the power is seen to be up to 2 mJ, indicating that some of the impurities have been trapped. Some fresh F_2 is then added so that the F_2 pressure is up to 1.05 ppt of He, enough to take the power back to the initial value if there were no impurities present. However the power recovers to 4 mJ (~50% of the initial value) indicating that the impurities are not

fully trapped out. This is in agreement with the previous results which showed that even with the cold trap, the accumulation of impurities could not be stemmed.

5.4 Comparison of KrF laser in versions LV4 and LV5

A KrF laser mix of 3 torr F_2 + 22 torr Kr + 850 torr He is used in the laser version LV5 to compare the half life of the mix with that in LV4. This comparison would show if replacement of the Al electrodes and the stainless steel corona wires help to increase the number of shots to half power. The output power variation is found to be larger than in LV4 (see figure 5.42) and the number of shots to half power is slightly less. The impurity evolution compared to that in LV4 is given in figures 5.43 to 5.54.

The main differences between LV4 and LV5 are seen to be the higher rate of evolution of O_2 and a lower rate of evolution of CF_4 in LV5. The same trend is found for a He-F_2 fill in LV4 and LV5 (see figures 4.37 and 4.41). Since the stainless steel corona wires are replaced by nickel corona wires in LV5, production of CO_2 at the corona wire site due to carbon in the stainless steel is eliminated. This leaves more unused O_2 in LV5 than in LV4. Since CO_2 production is lower in LV5, CF_4 production (from CO_2 and F_2) is also lower. However, CO_2 still grows in LV5, especially after a fall in the partial pressure of F_2. Initially the depletion of CO_2 in a reaction with F_2 would slow down the rate of growth of CO_2. However, it is seen that this growth picks up later, and is

accompanied by a slight drop in the growth of O_2, indicating that a reaction with O_2 and some carbon source, probably the PTFE near the corona wire, is taking place.

The energy output and F_2 depletion curves (figures 5.42 and 5.54) show that replacement of the corona wires and the electrodes by nickel and monel have not caused any significant change in the performance. The comparison of LV4 and LV5 with KrF mixtures show similar trends as was found in He-F_2 mixtures discussed in chapter 4.

5.5 Conclusions

From the above discussion of the results from experiments on the He-Kr-F_2 gas mixtures it emerges that the impurities evolved are similar to that in the He-F_2 mixtures discussed in chapter 4. Their partial pressures are, on the whole, lower due to the lower concentration of F_2 used in the initial mix. But they affect the laser lifetime of the KrF laser to a greater extent than does the atomic fluorine laser. With the use of a -150°C cold trap the impurities are trapped and the number of shots to half power goes up from 2700 shots to about 11000. The evolution of COF_2, O_2, and CF_4 are reduced by the cold trap as in the He-F_2 mix. Warming the cold trap after sufficient amounts of impurities are trapped suddenly lowers the laser energy at two distinct temperatures, around the sublimation point of CO_2 and the freezing point of H_2O. This shows that two of the main impurities are CO_2 and H_2O. The

laser energy does not recover its original value on subsequent cooling of the trap once it is warmed up to room temperature, but there is recovery if it is warmed up to -66°C for a few minutes and then cooled to -150°C. Revival of the laser by trapping out the impurities and adding fresh F_2 takes the energy up to 50% of the initial value from about 1% showing that the cold trap is not fully successful in trapping out all the impurities. The mass spectrum of the cold trap contents is found to be similar to the mass spectrum of the contents of the cold trap of a He-F_2 mixture. Comparison of versions LV5 and LV4 show trends similar to those found for a He-F_2 mixture.

The next chapter deals with the effects of some of the major impurities detected in the mixtures discussed in chapters 4 and 5 when they are individually added deliberately to the gas mixtures.

Figures 5.1 to 5.12

Impurity species detected in He-Kr-F_2 mixes:
Version LV4 with laser on at time indicated by L,
—·—V—·— LV4 without lasing.

FIG 5.1

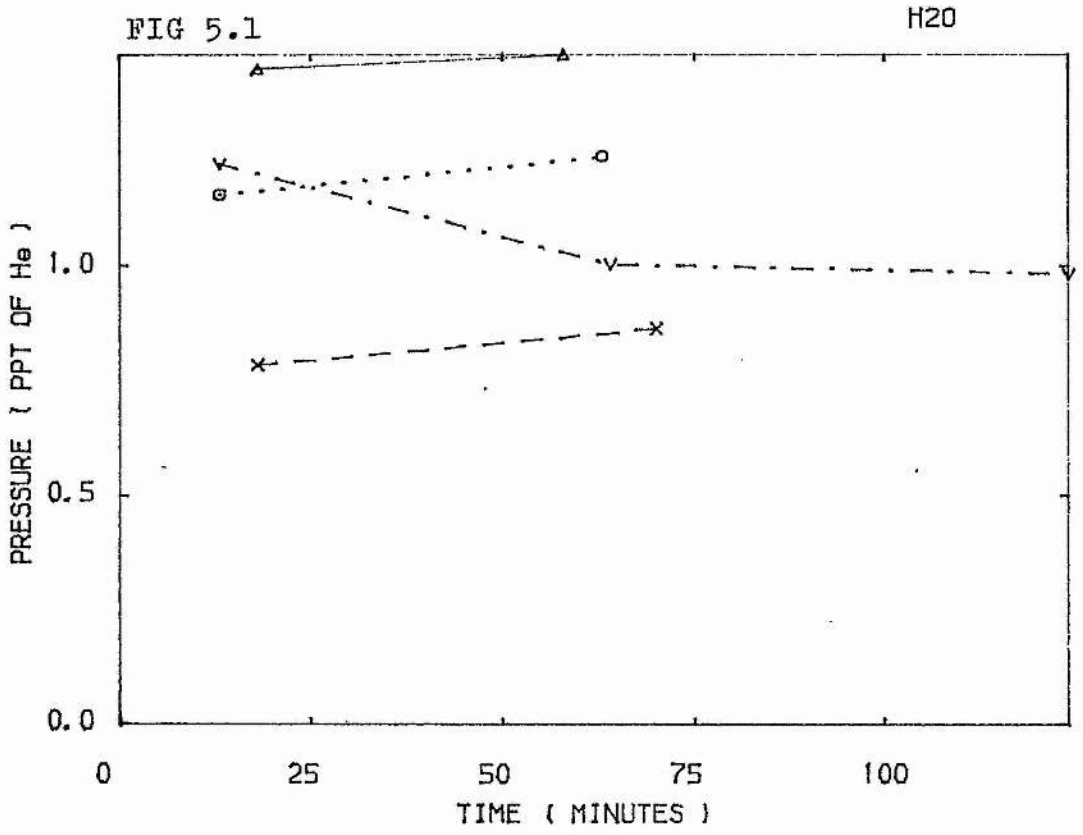
H20
PRESSURE (PPT OF He)
1.0
0.5
0.0
0
25
50
75
100
TIME (MINUTES)

FIG 5.2

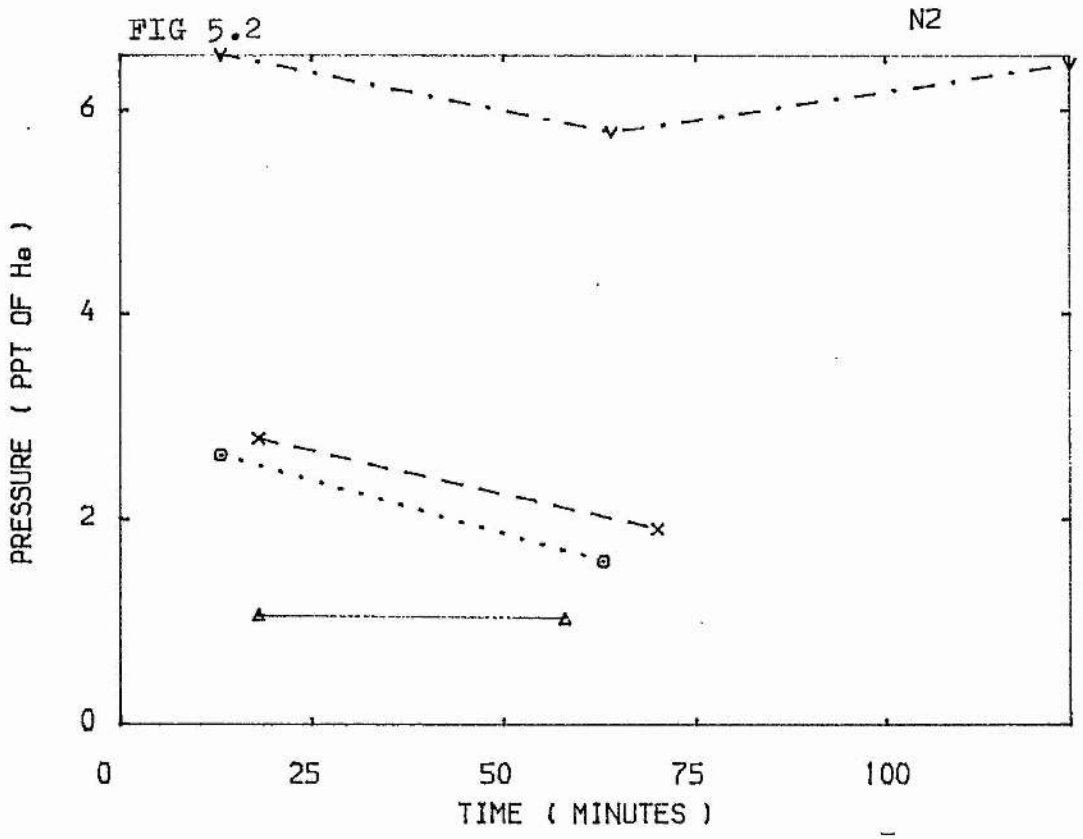
N2
PRESSURE (PPT OF He)
6
4
2
0
0
25
50
75
100
TIME (MINUTES)

FIG 5.3

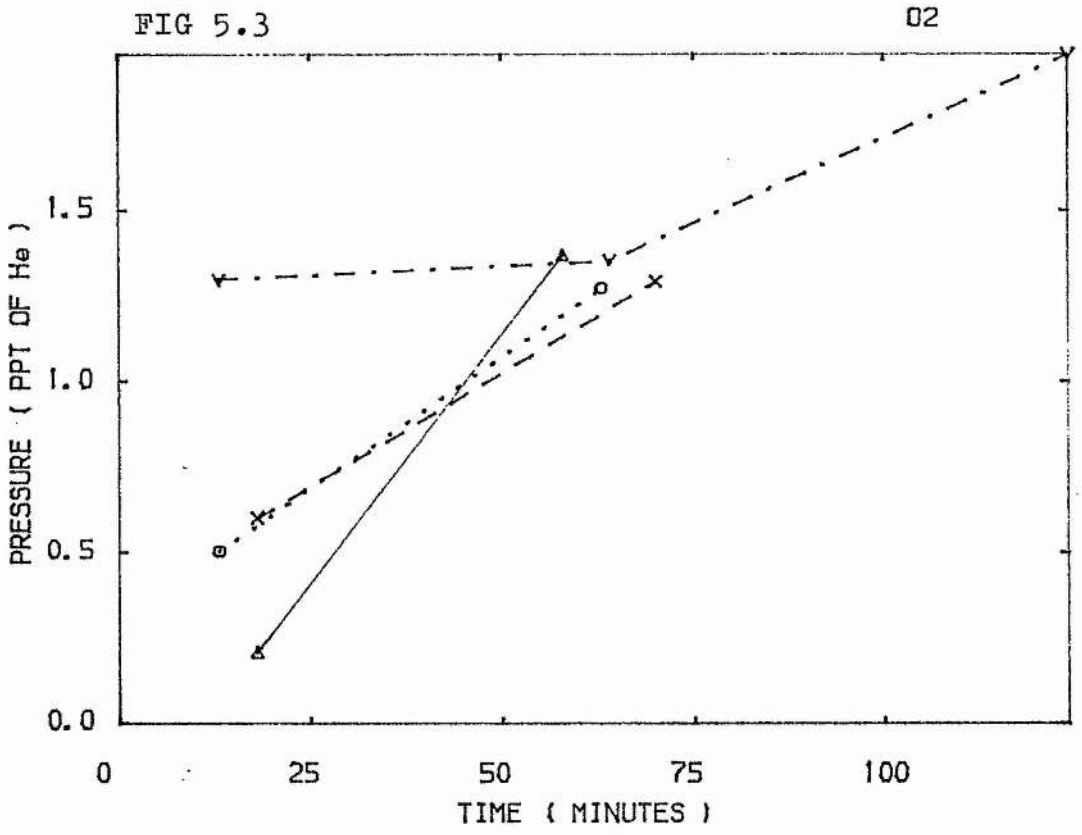
O2
PRESSURE (PPT OF He)
1.5
1.0
0.5
0.0
0
25
50
75
100
TIME (MINUTES)

FIG 5.4

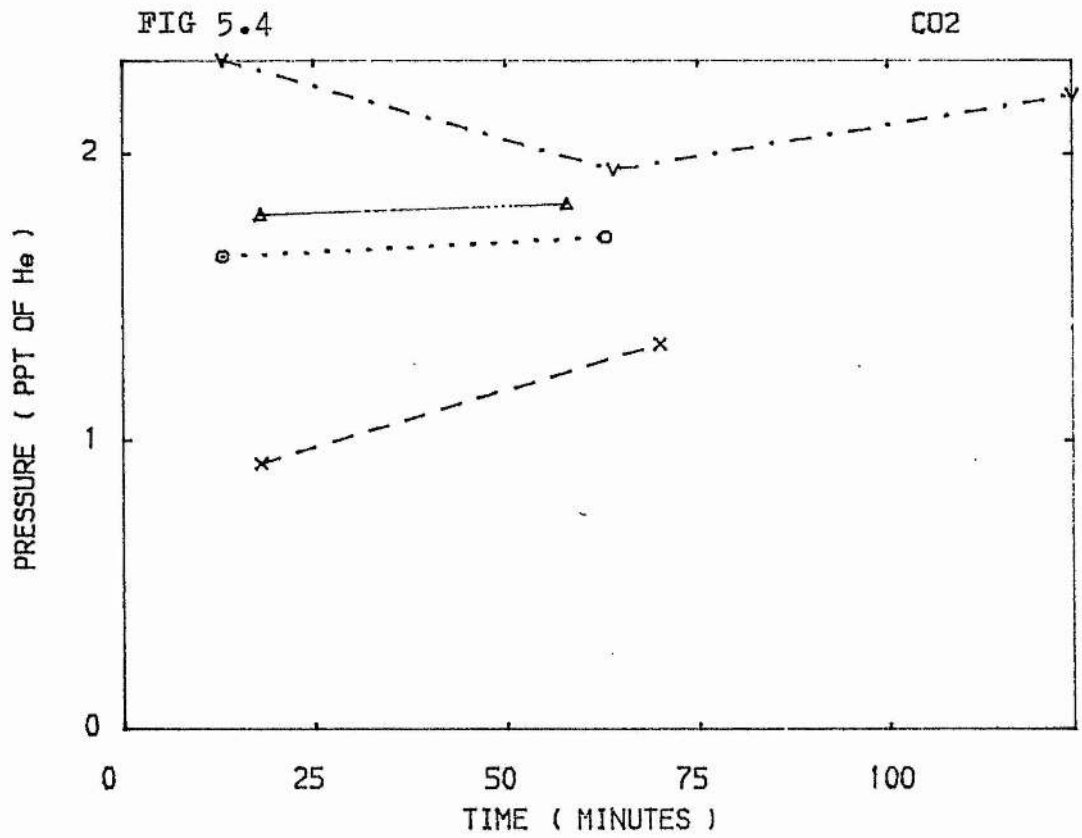
CO2
PRESSURE (PPT OF He)
2
1
0
0
25
50
75
100
TIME (MINUTES)

FIG 5.5

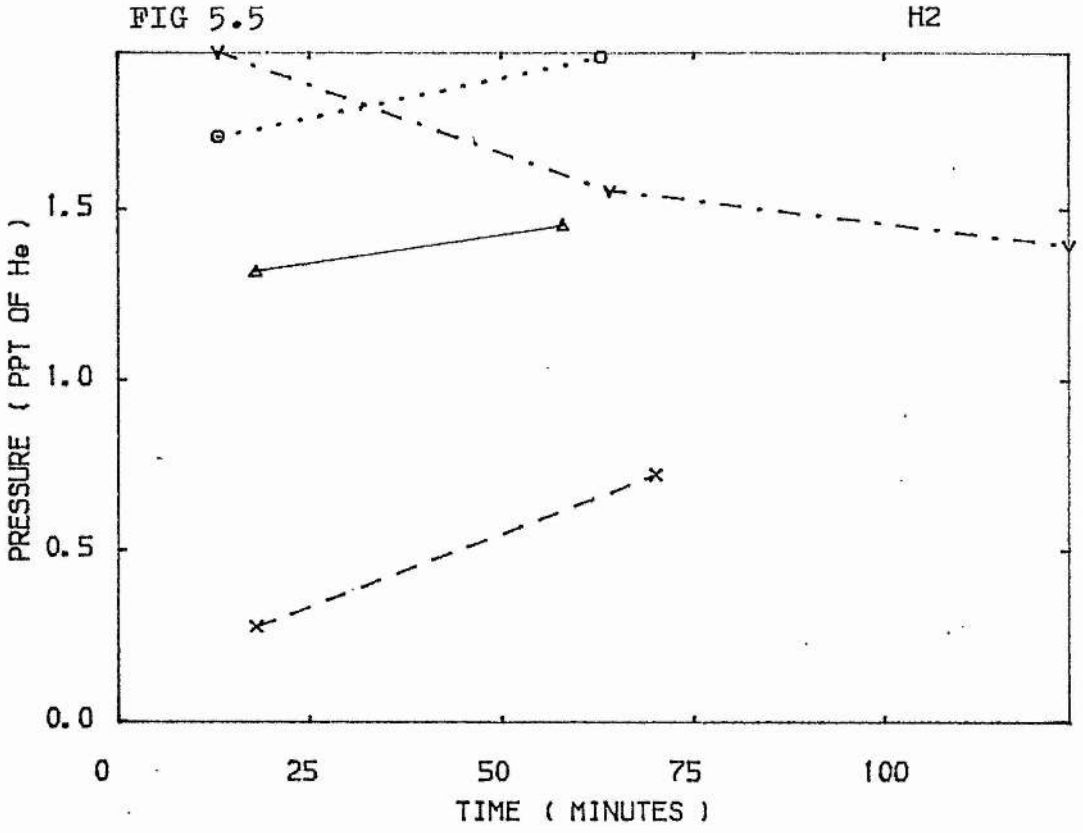
H2
PRESSURE (PPT OF He)
1.5
1.0
0.5
0.0
0
25
50
75
100
TIME (MINUTES)

FIG 5.6

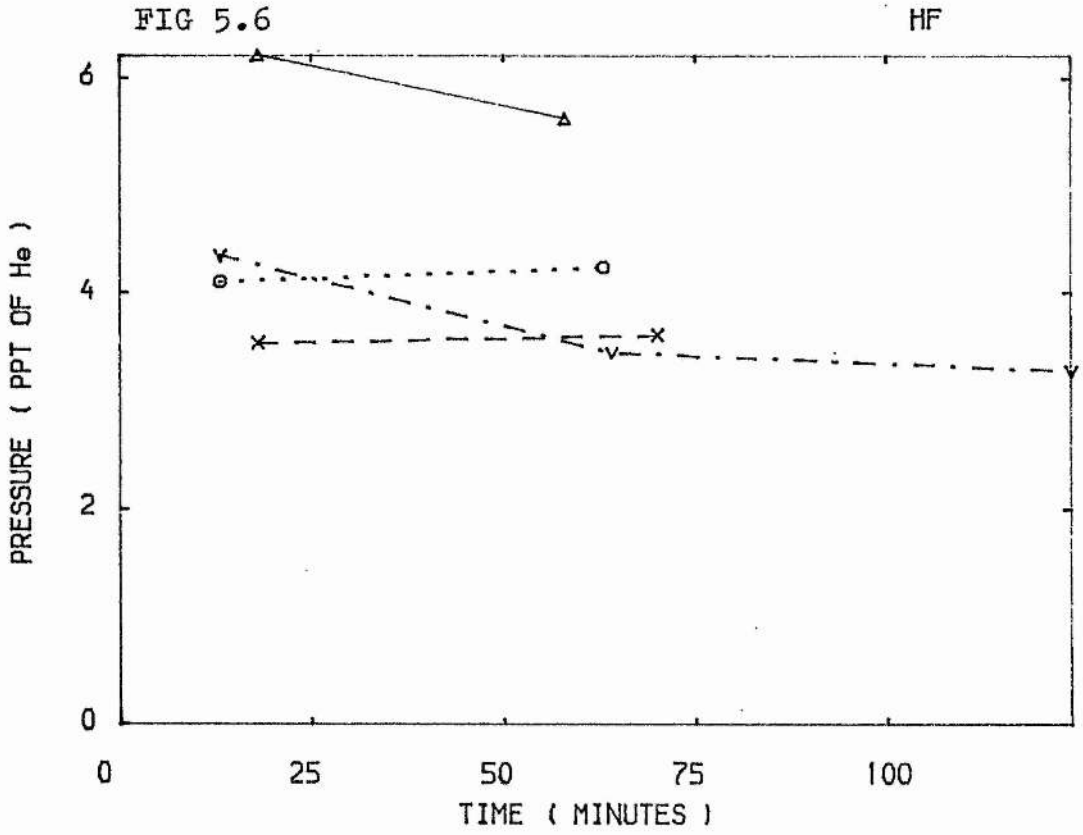
HF
PRESSURE (PPT OF He)
6
4
2
0
0
25
50
75
100
TIME (MINUTES)

FIG 5.7

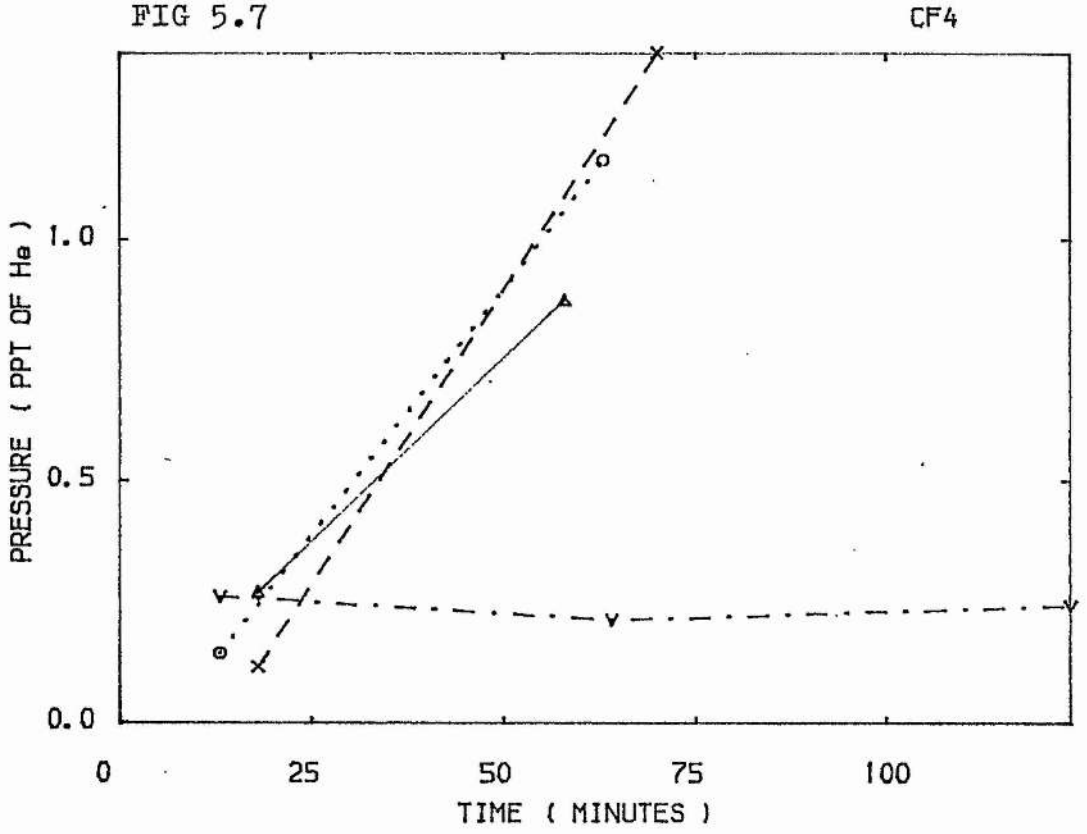
CF4
PRESSURE (PPT OF He)
1.0
0.5
0.0
0
25
50
75
100
TIME (MINUTES)

FIG 5.8

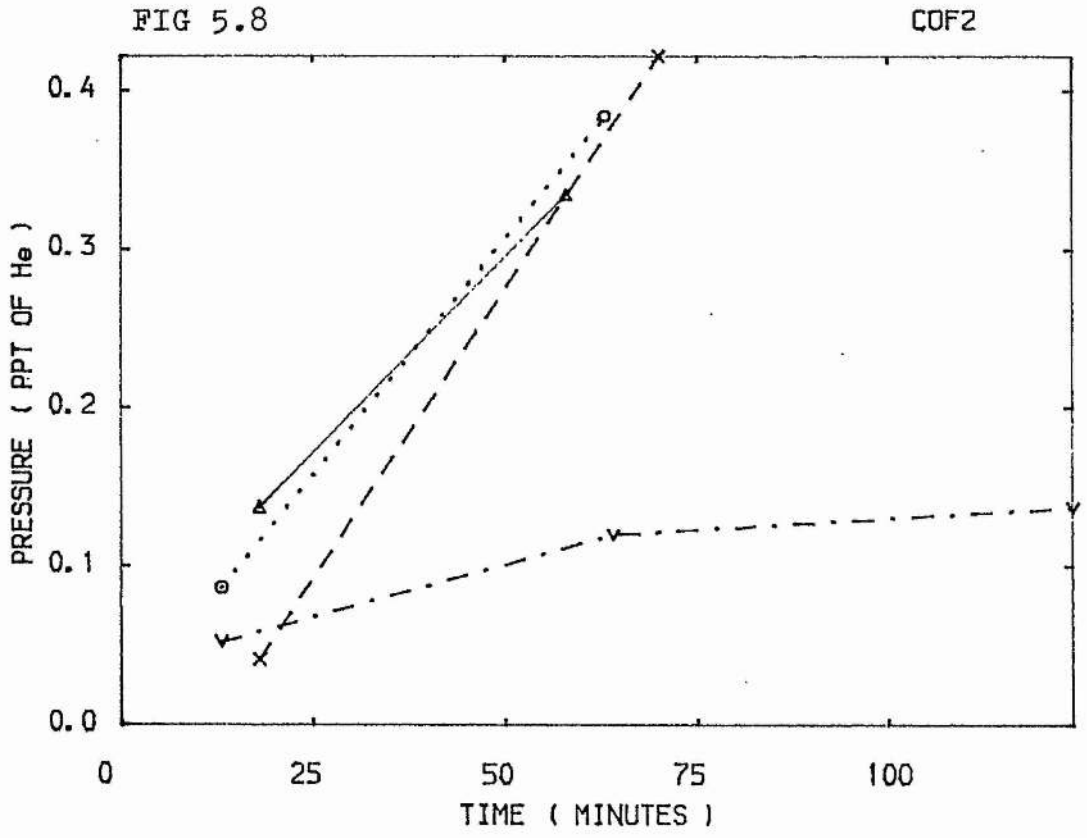
COF2
PRESSURE (PPT OF He)
0.4
0.3
0.2
0.1
0.0
0
25
50
75
100
TIME (MINUTES)

FIG 5.9

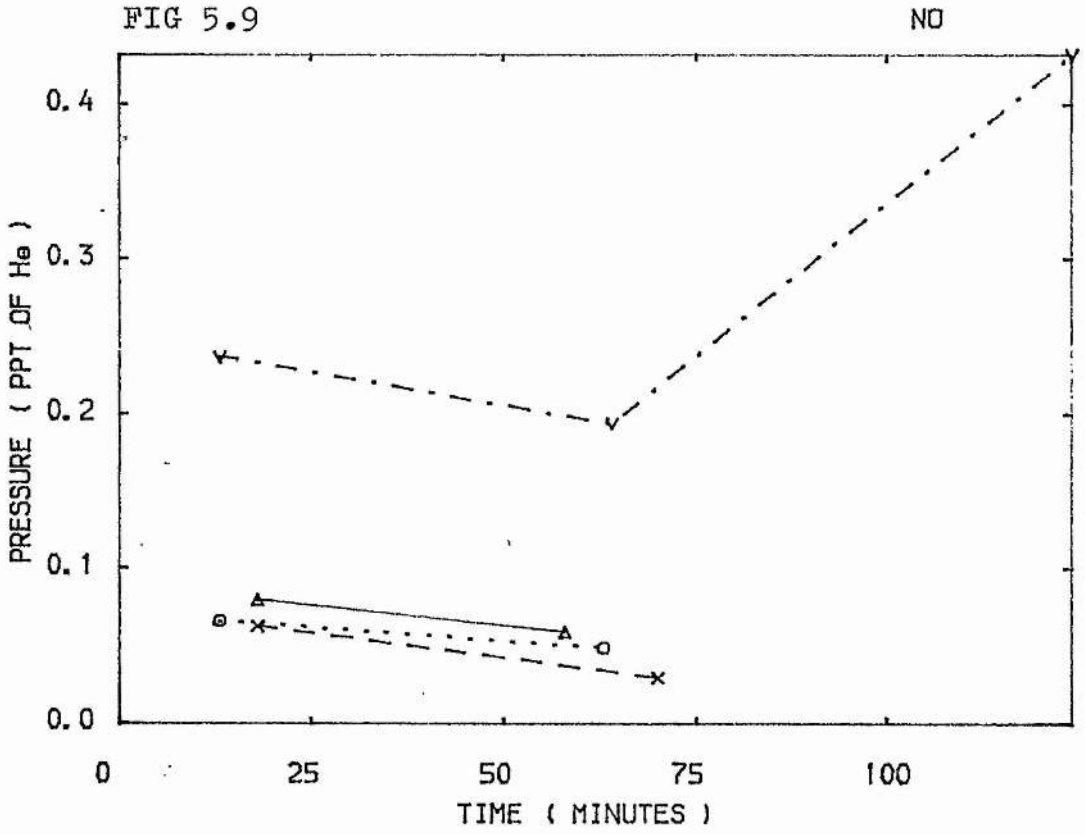

FIG 5.10

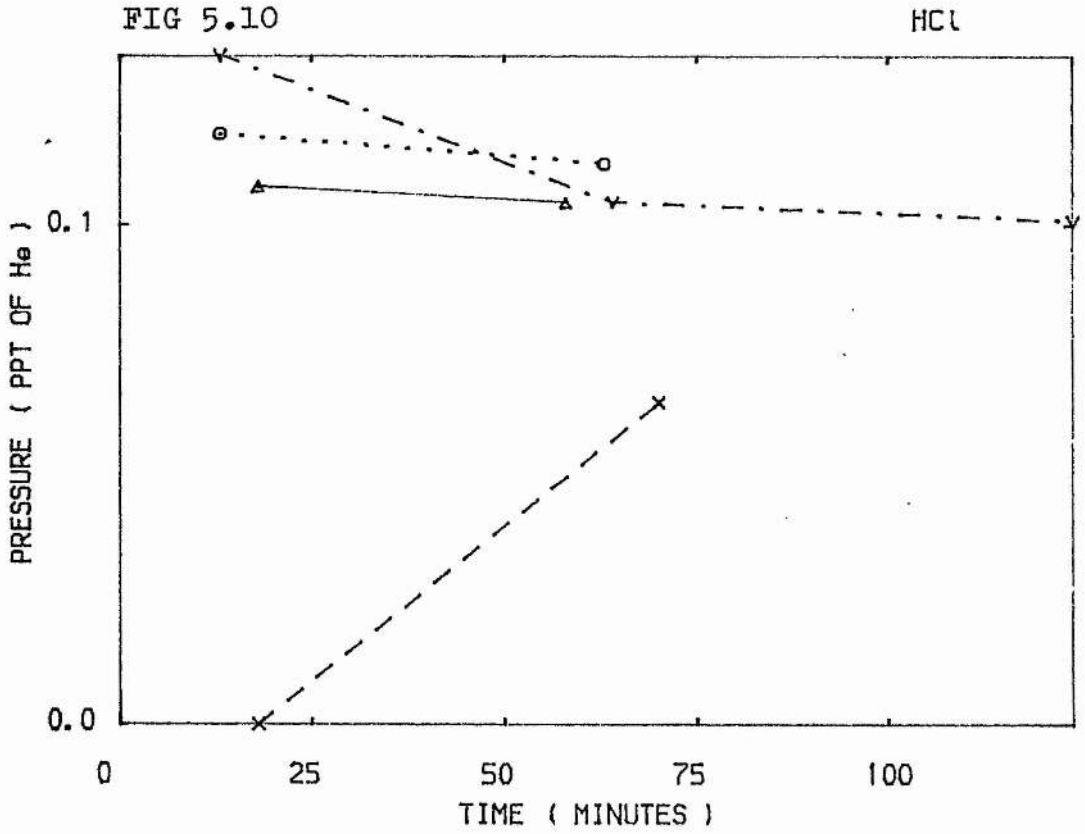

FIG 5.11

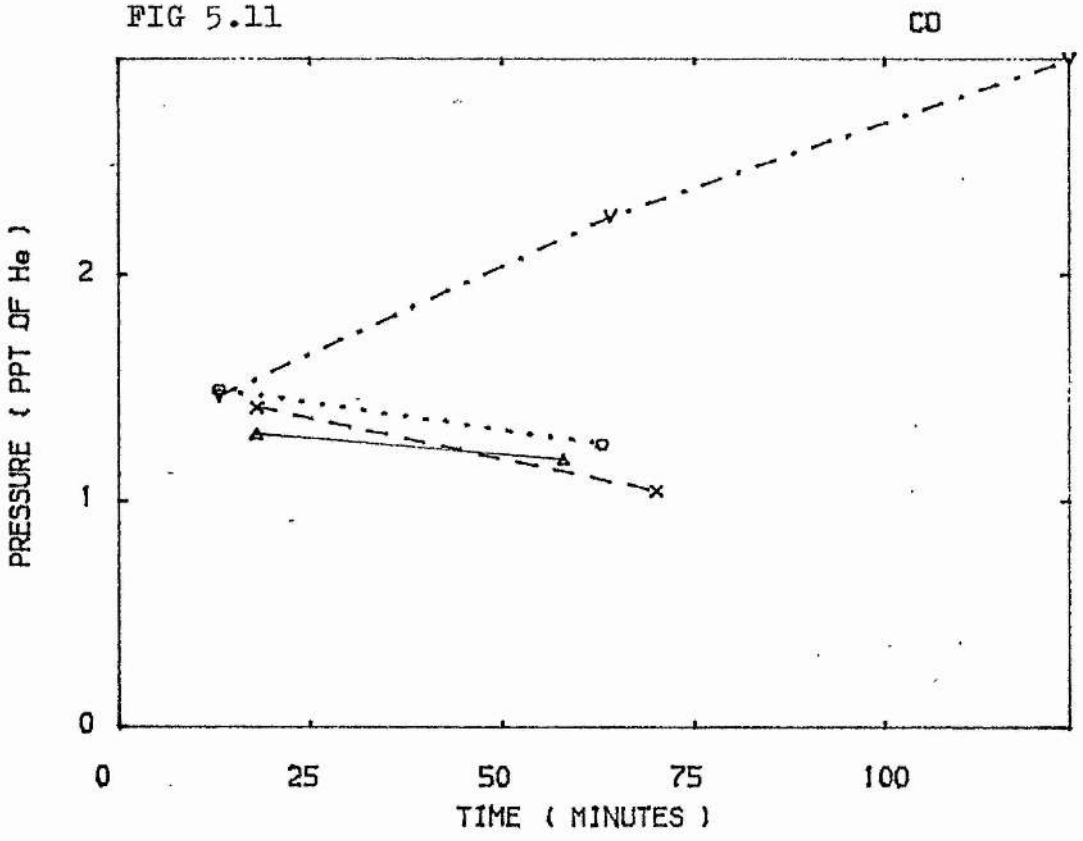

FIG 5.12

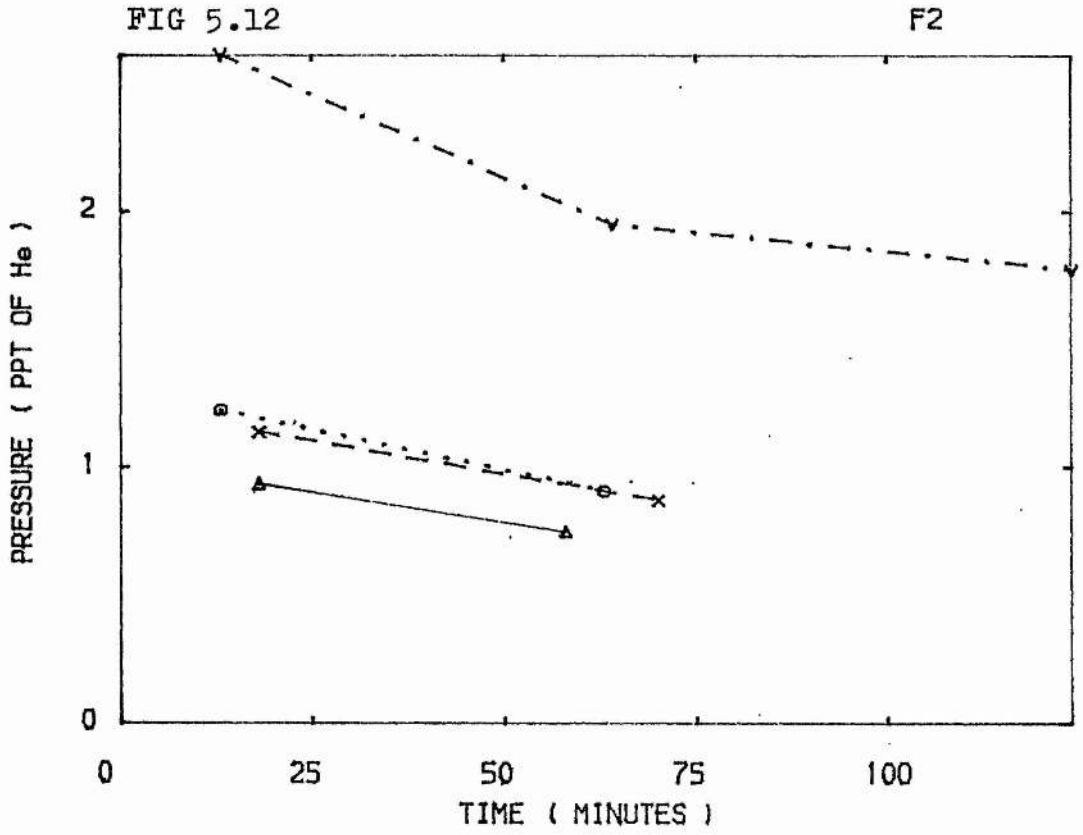

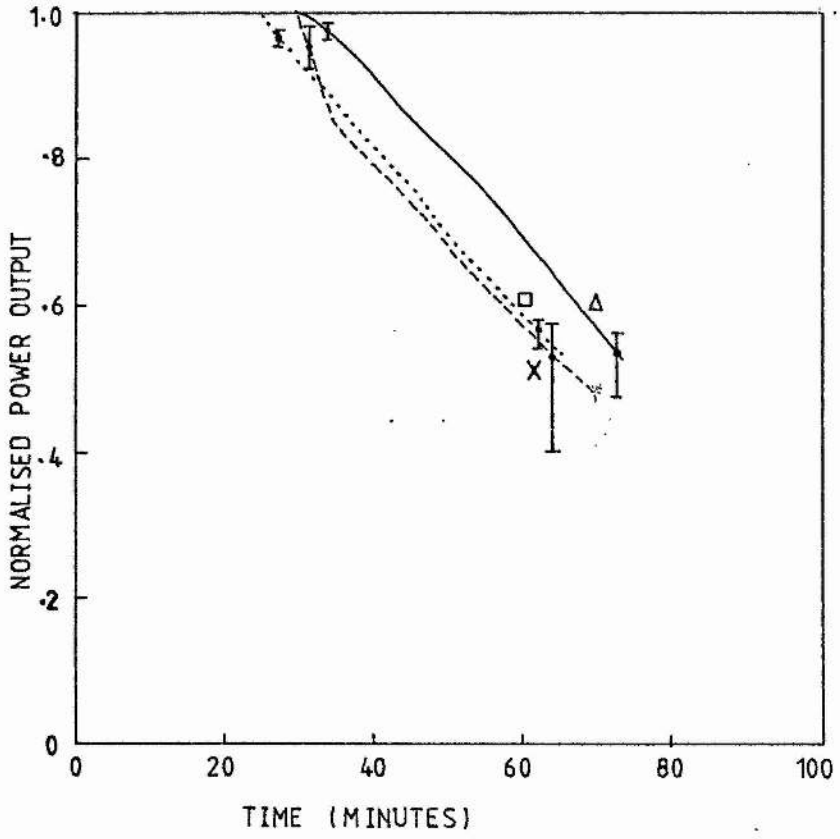

FIG 5.13 KrF laser output for three basic mixes.

Figures 5.14 to 5.25
Effect of cold trap on the evolution of impurities in a KrF mix:

—△— Without cold trap or discharge
--X-- Cold trap at -150°C, discharge on
···□··· Discharge on, Cold trap on at time C
-·-▽-·- No discharge, Cold trap at 100 minutes

Cold trap temperatures given in figure 5.26

FIG 5.14

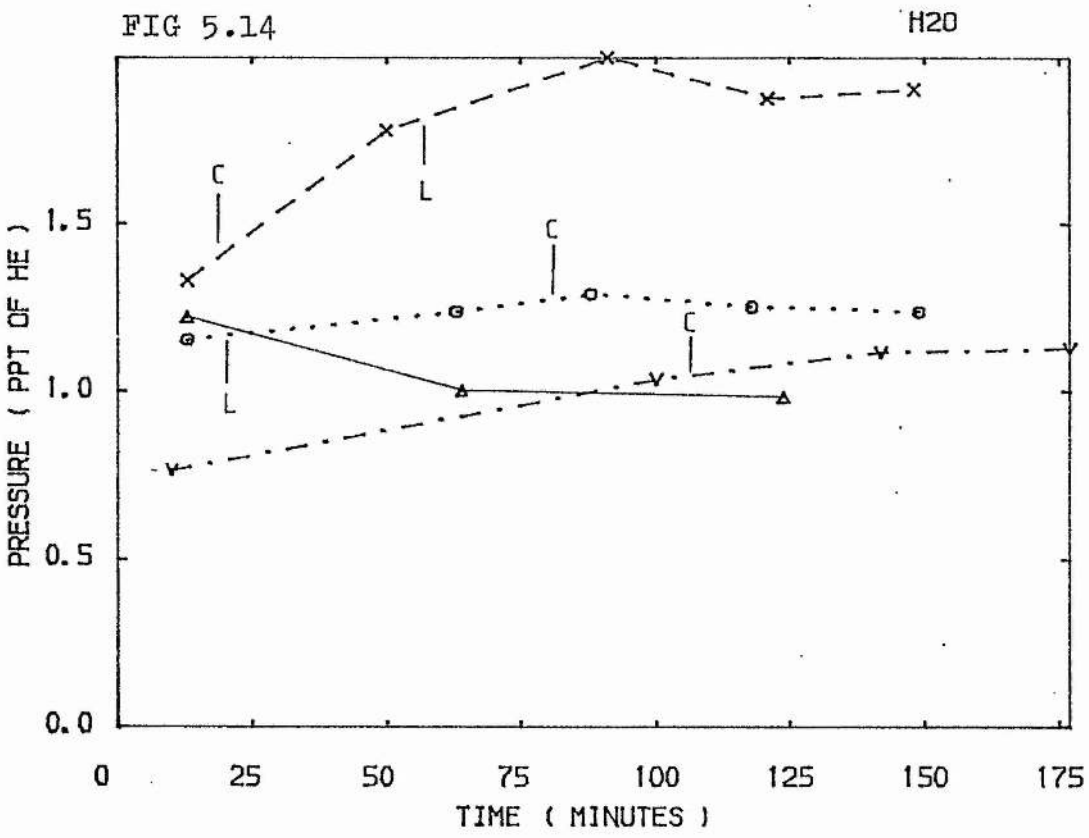

FIG 5.15

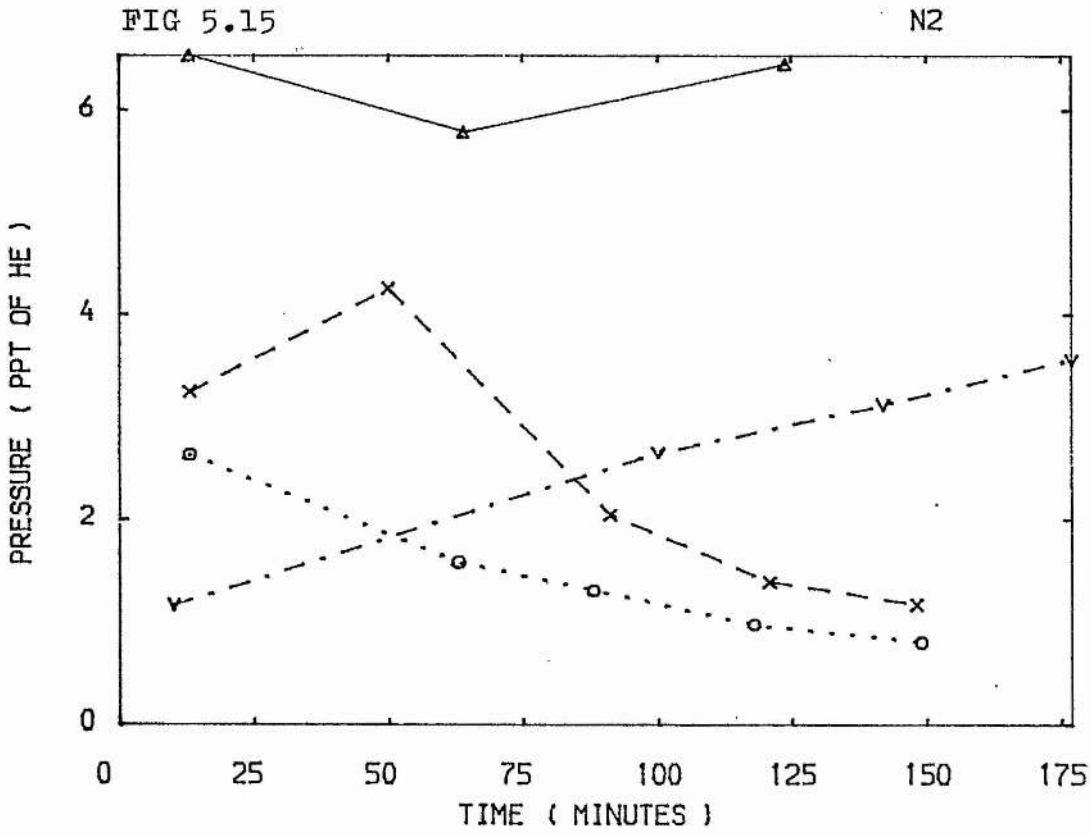

FIG 5.16

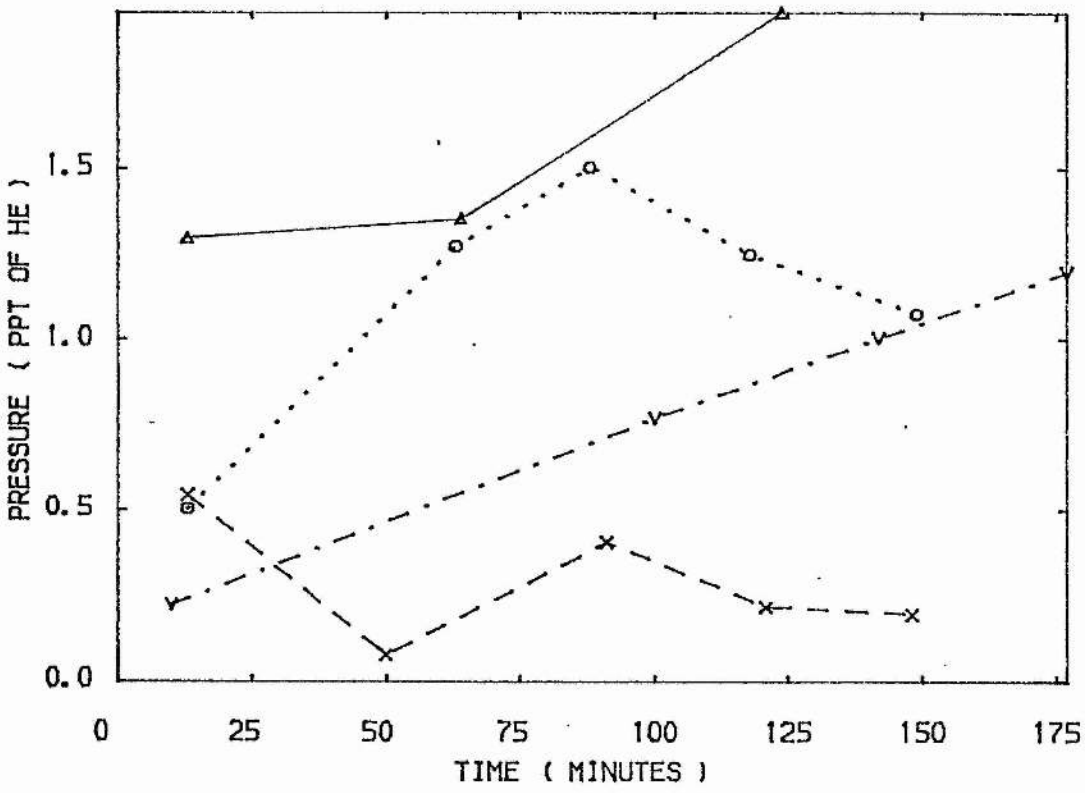

FIG 5.17

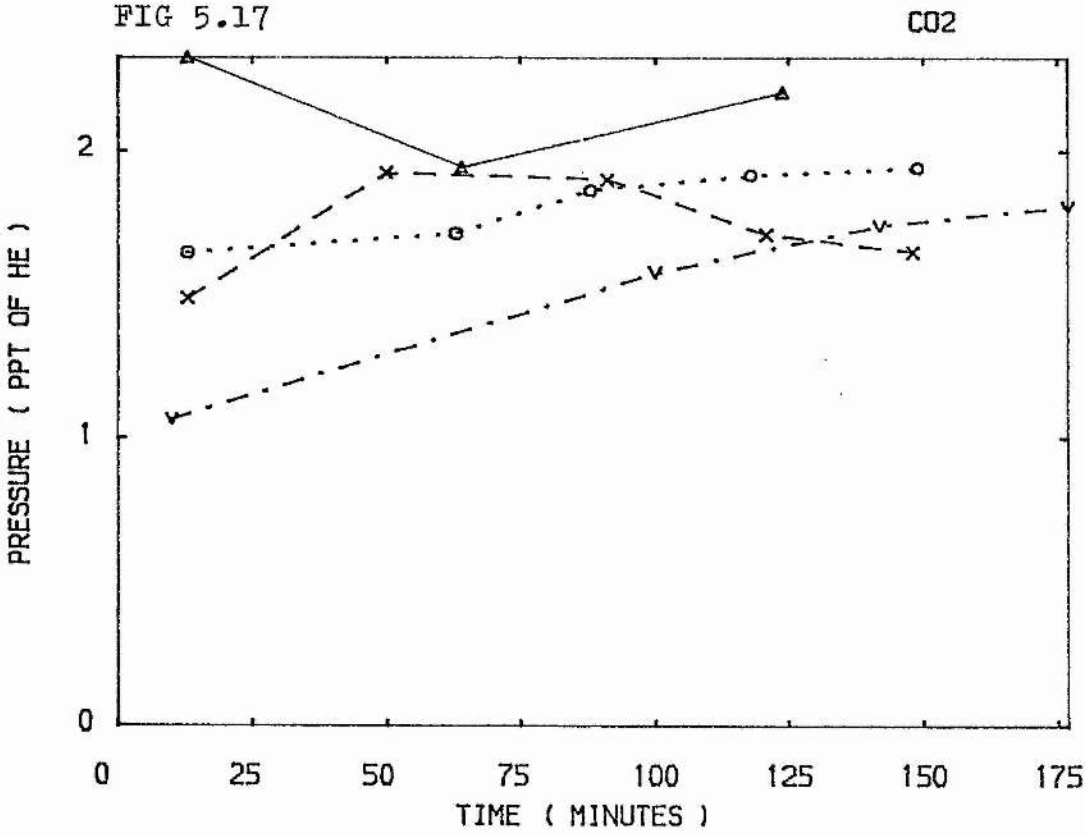

FIG 5.18

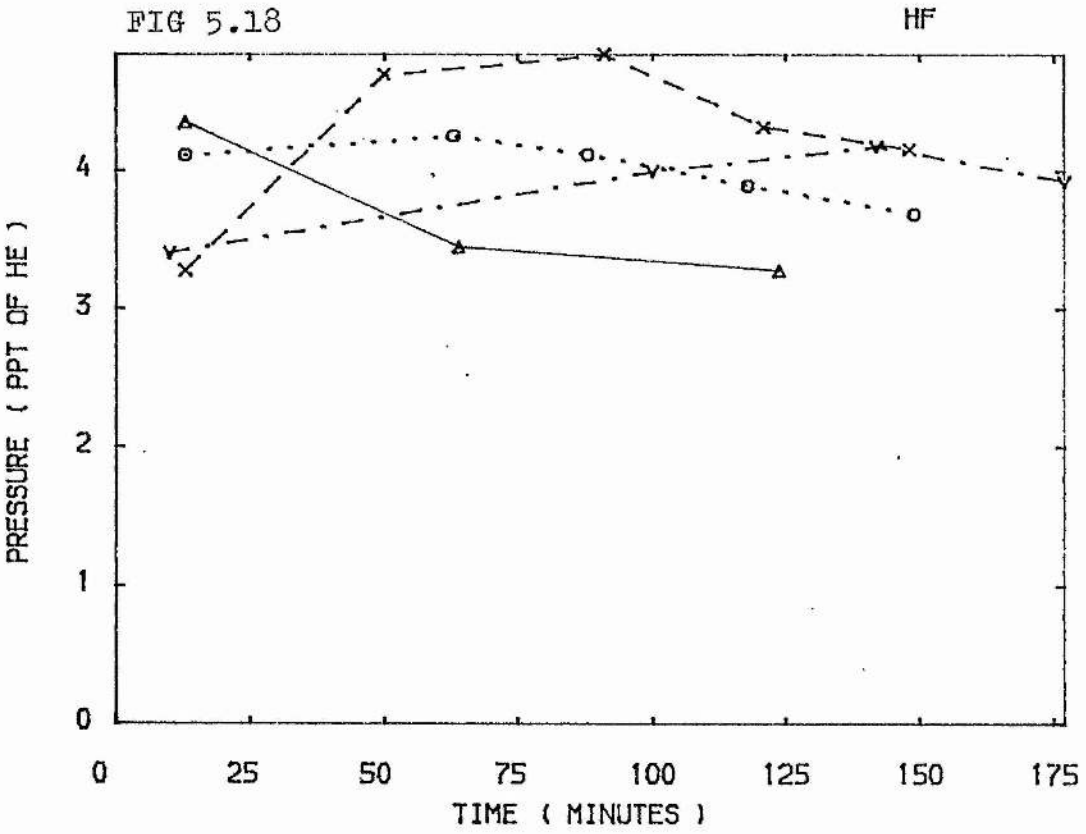

FIG 5.19

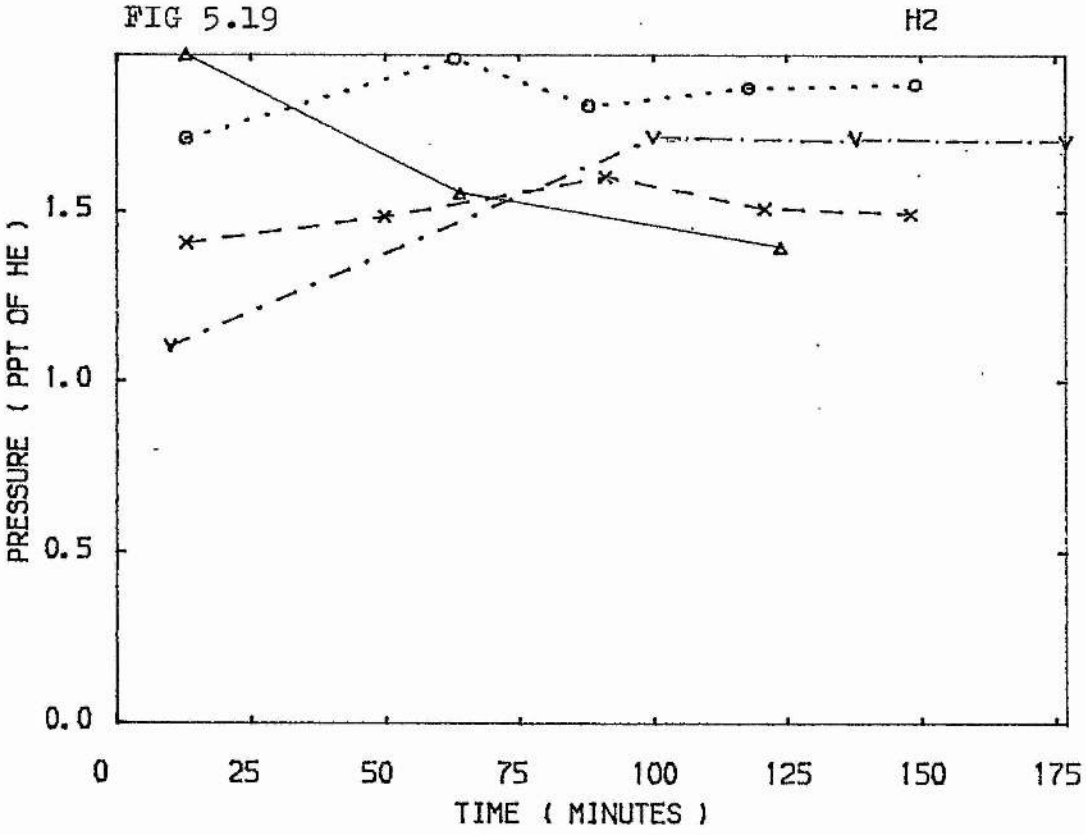

FIG 5.20

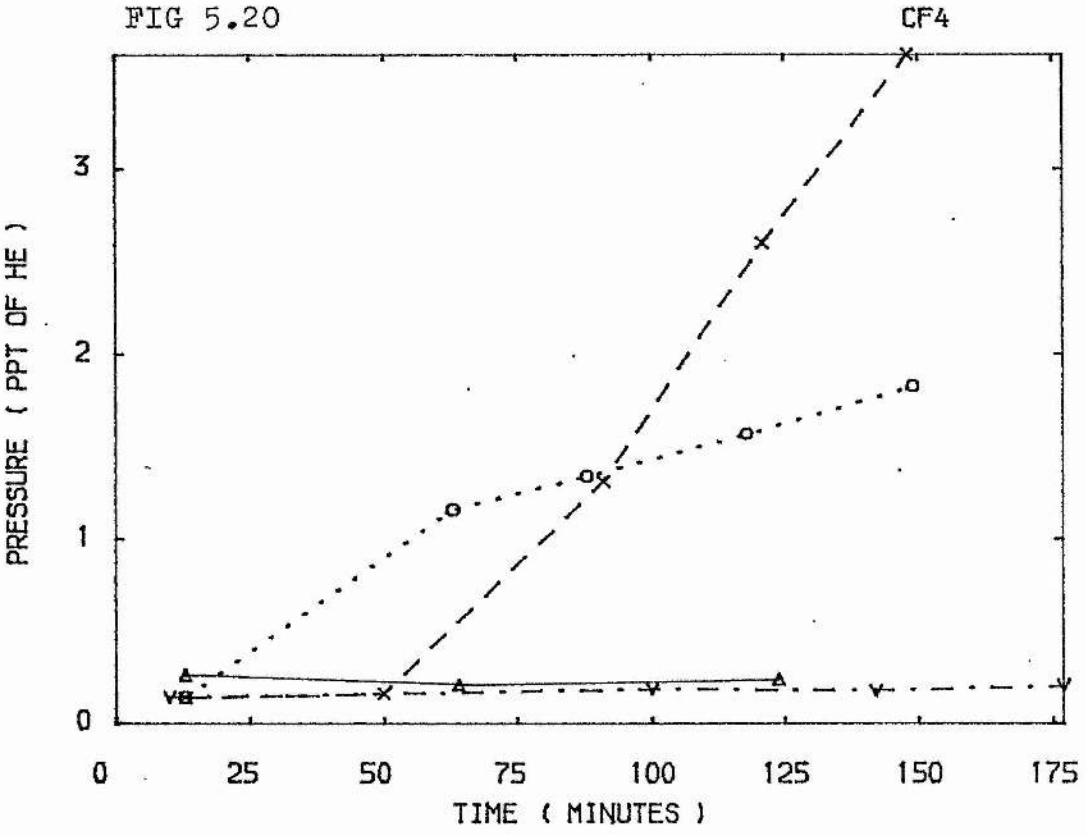

FIG 5.21

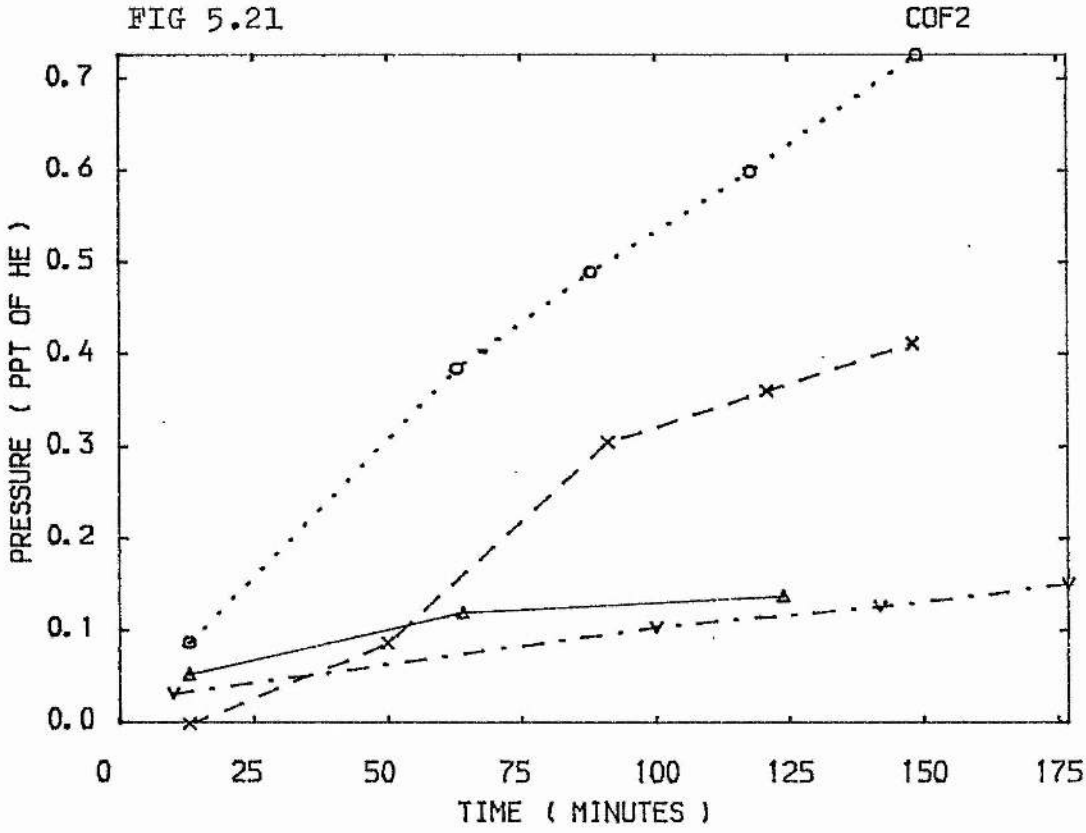

FIG 5.22

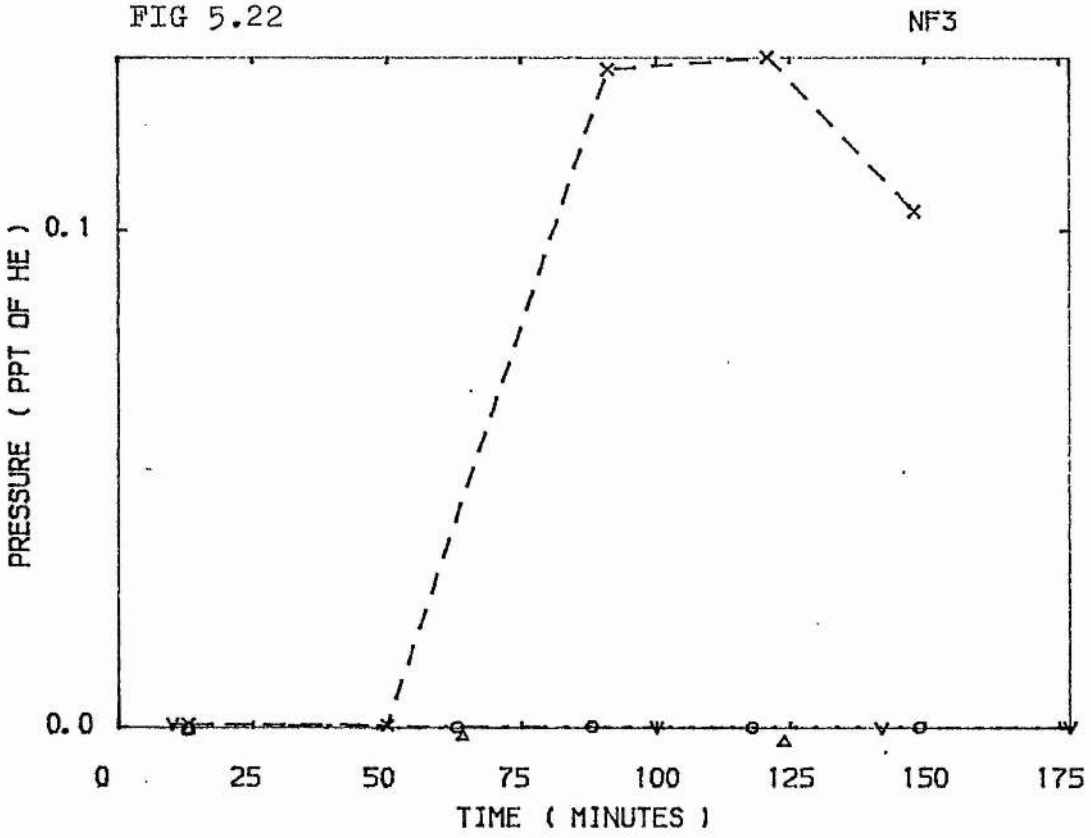

FIG 5.23

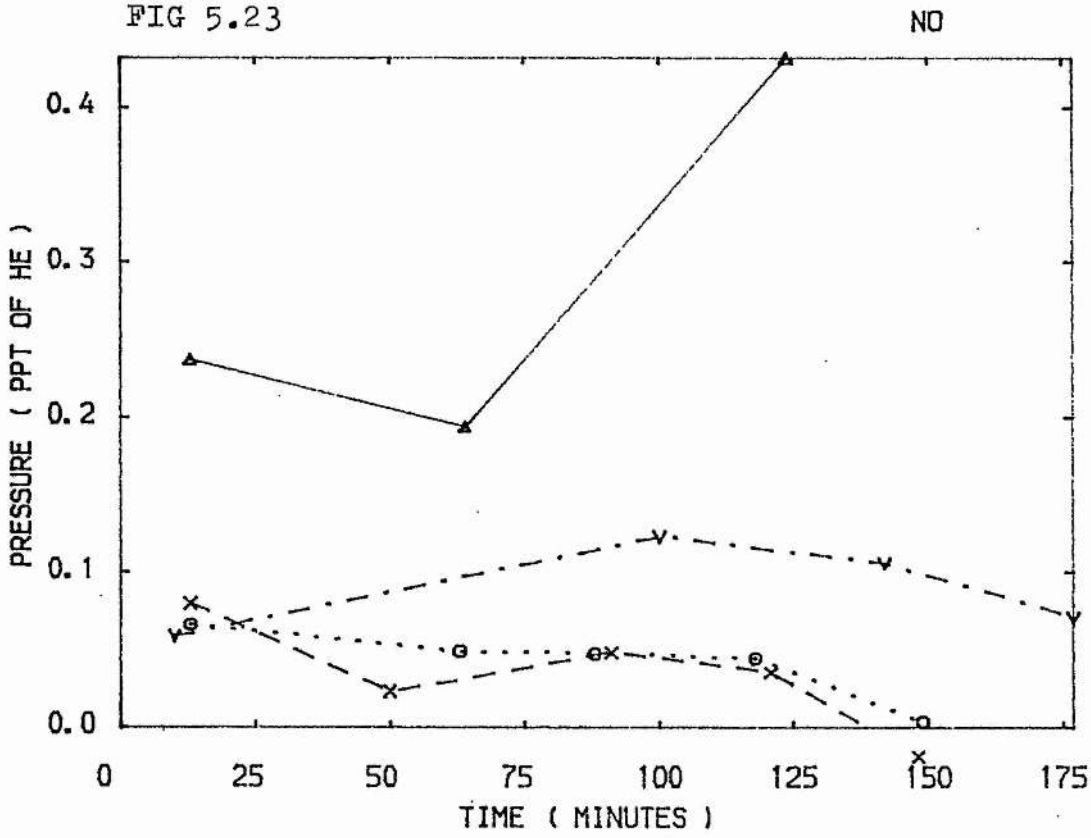

FIG 5.24

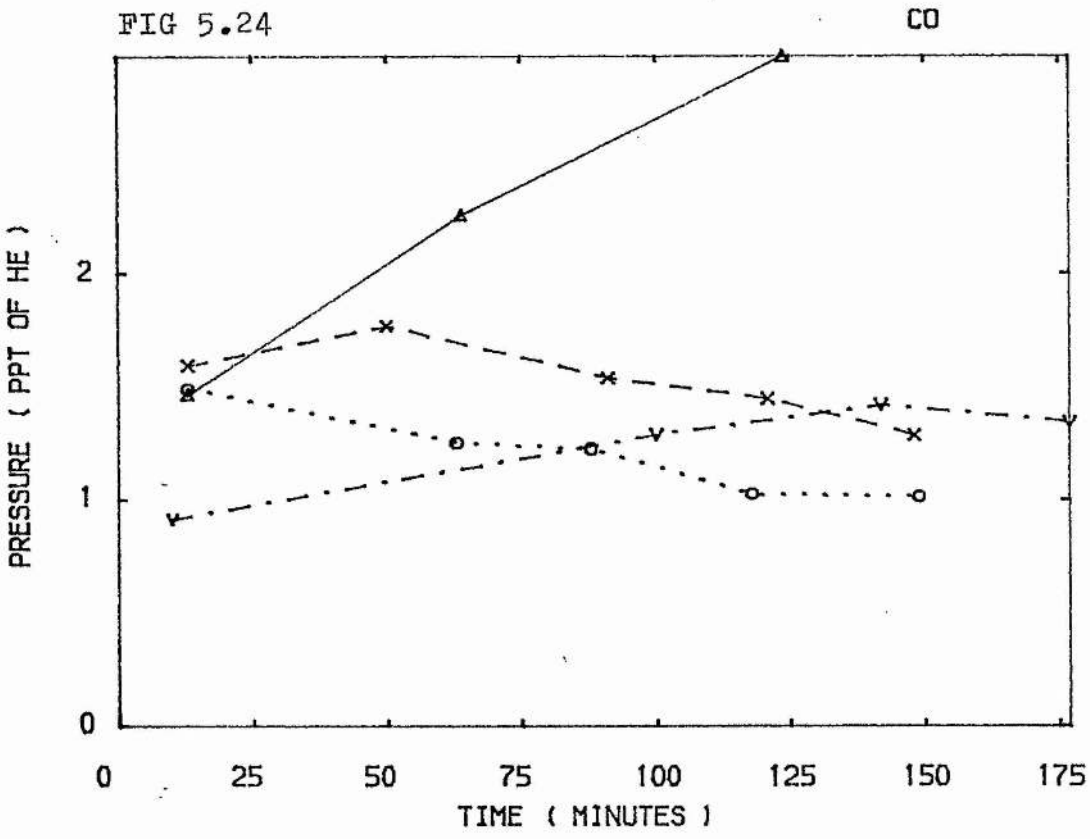

FIG 5.25

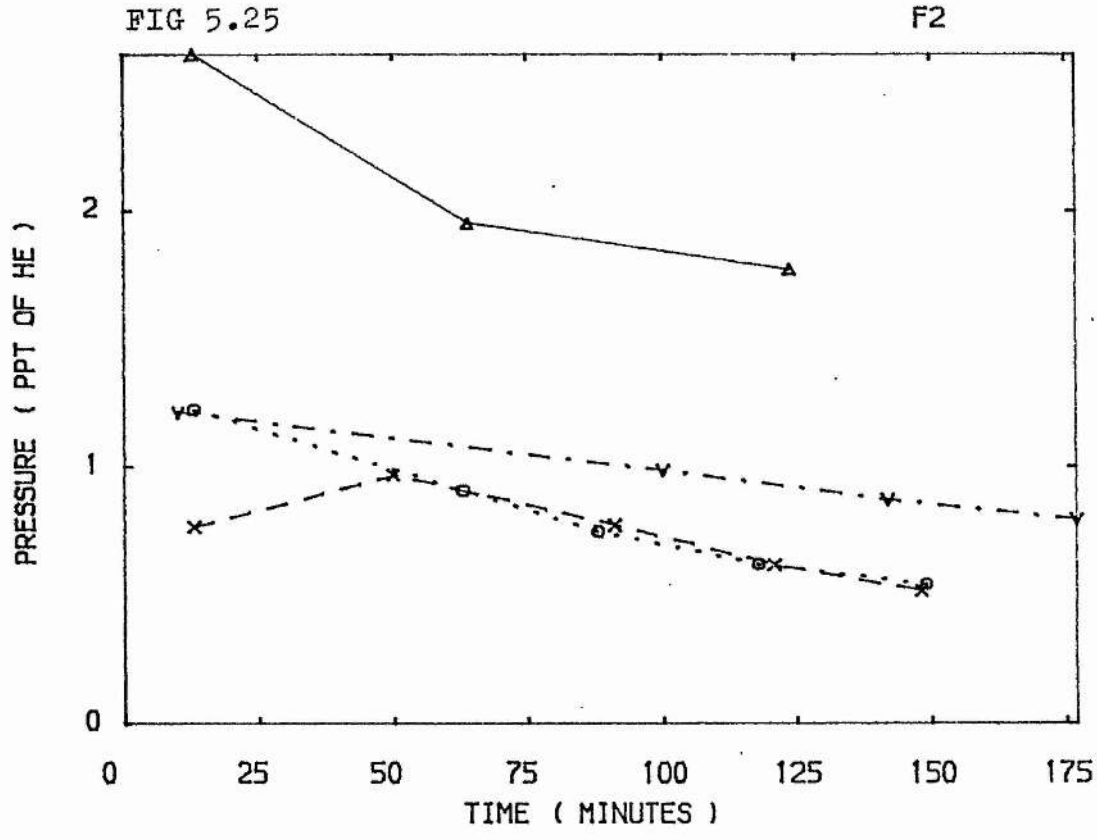

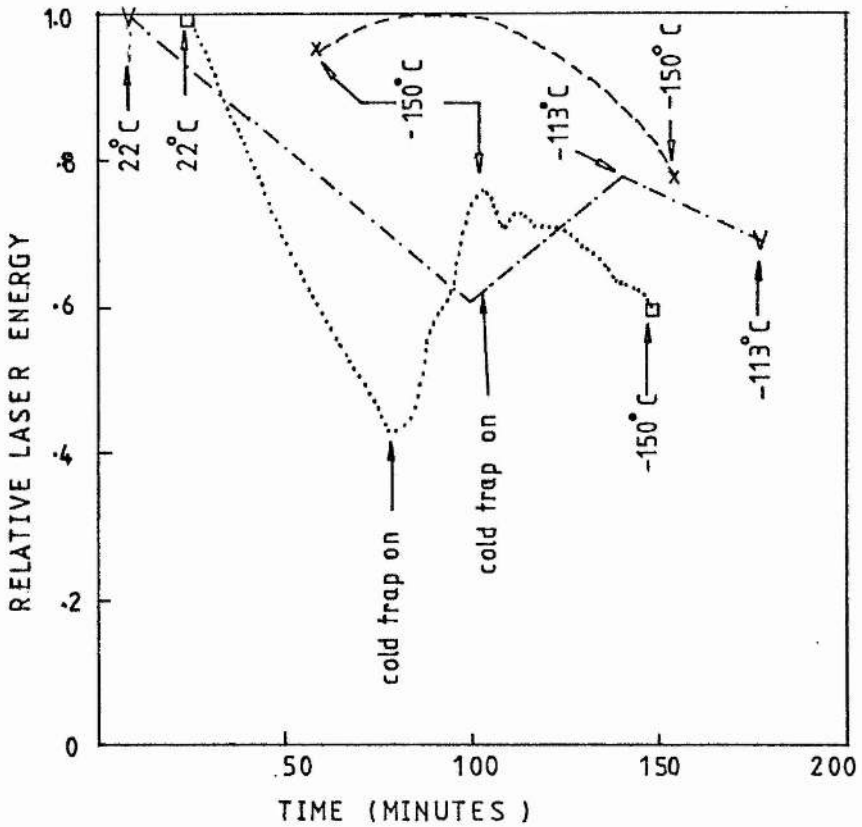

FIG 5.26 Laser output from cold trapped KrF mixes. Arrows indicate cold trap temperatures.

Figures 5.27 to 5.38
Evolution of impurities in a cold trapped
He-Kr-F_2 mix.
—Δ— Without discharge, LV4 version
--x-- With discharge and cold trap at times
indicated by L and C, LV4 version.

FIG 5.27

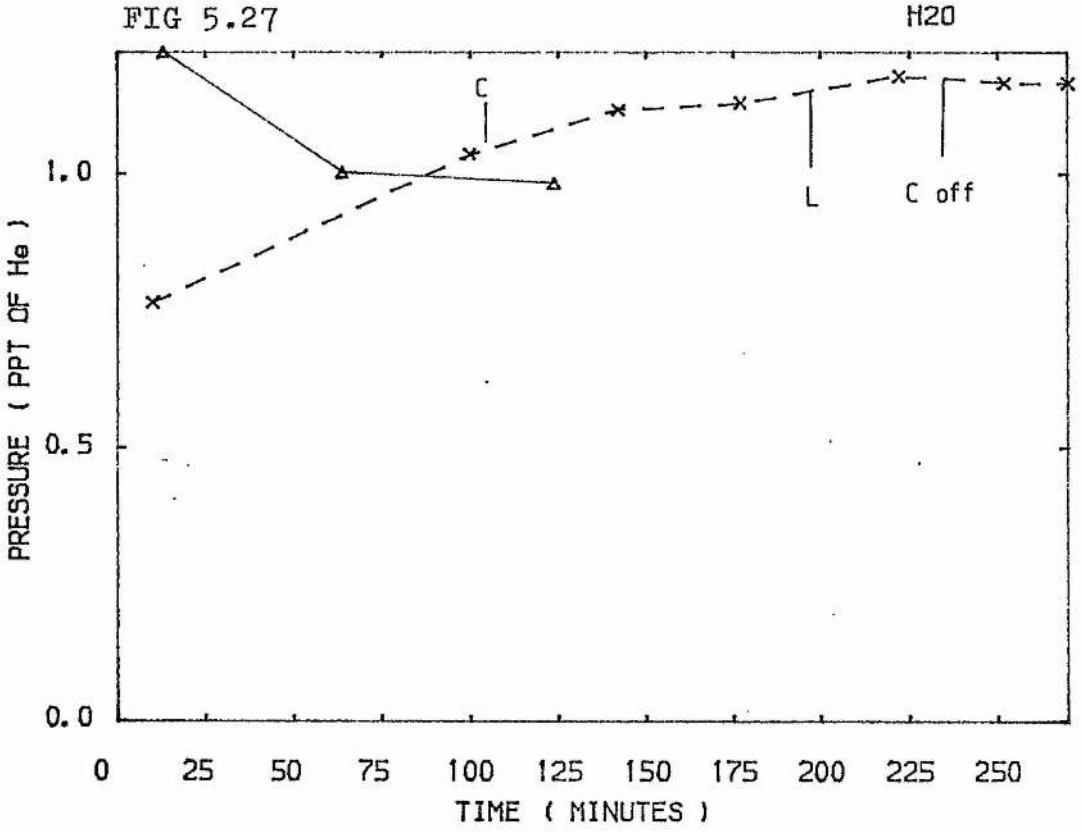

FIG 5.28

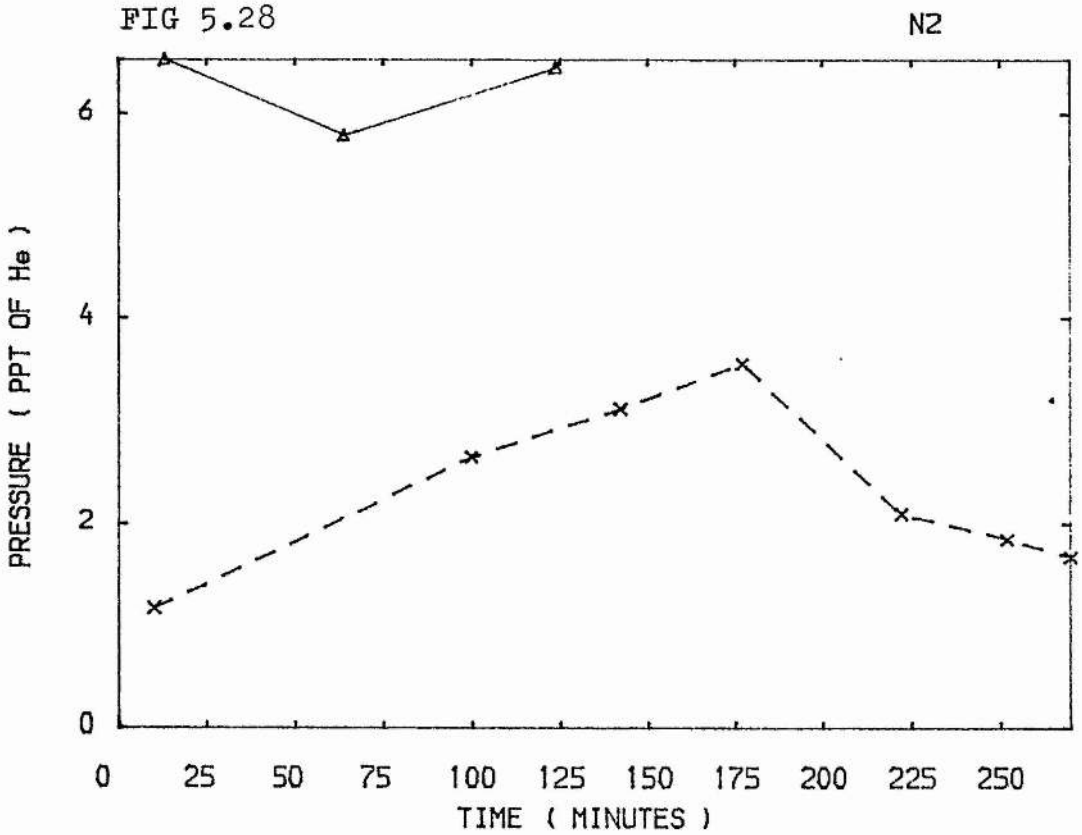

FIG 5.29

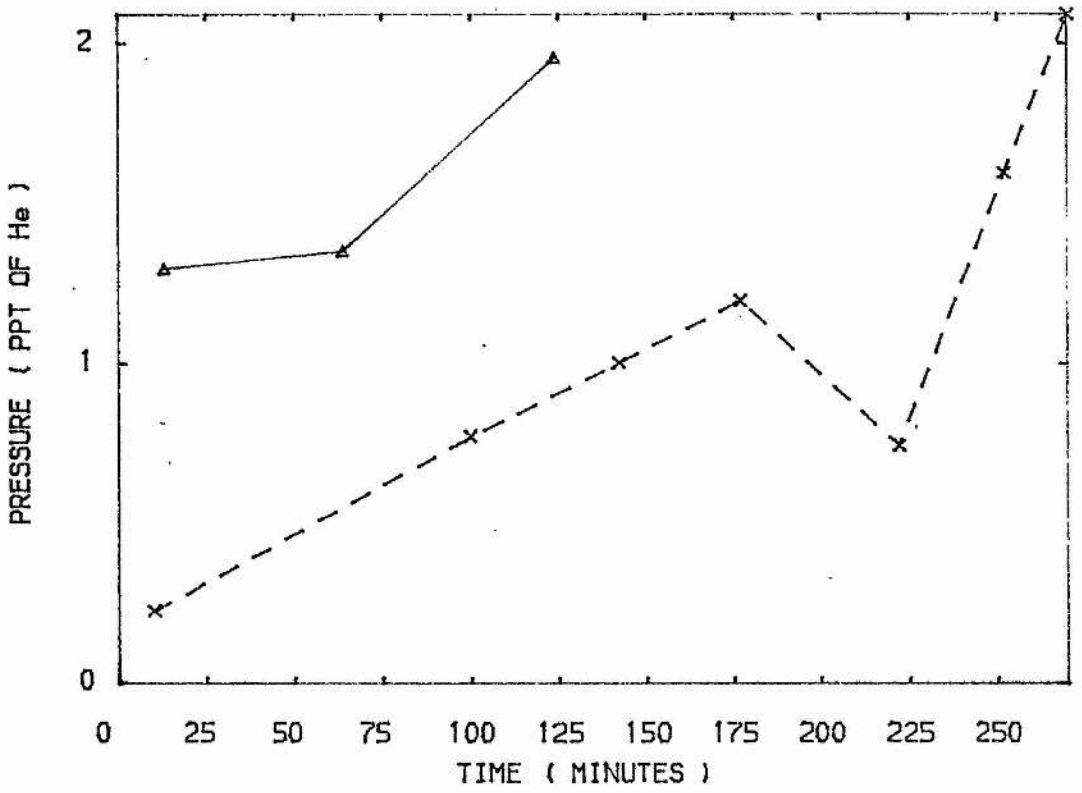

FIG 5.30

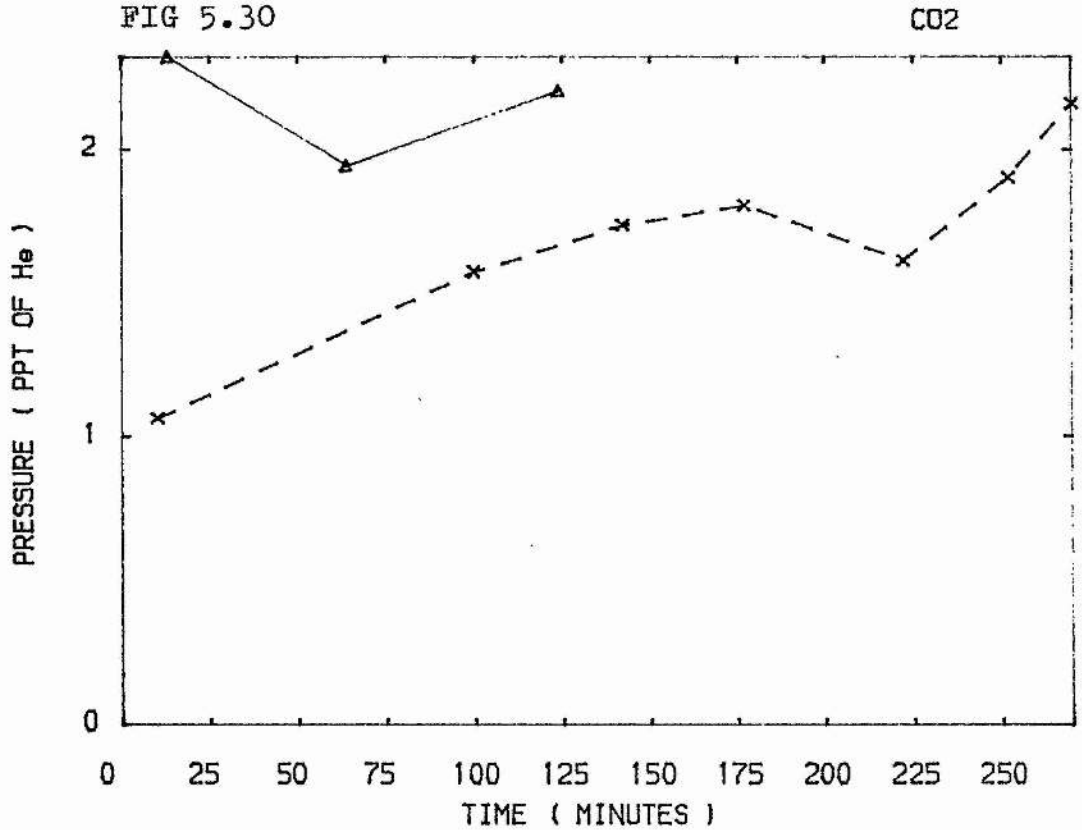

FIG 5.31

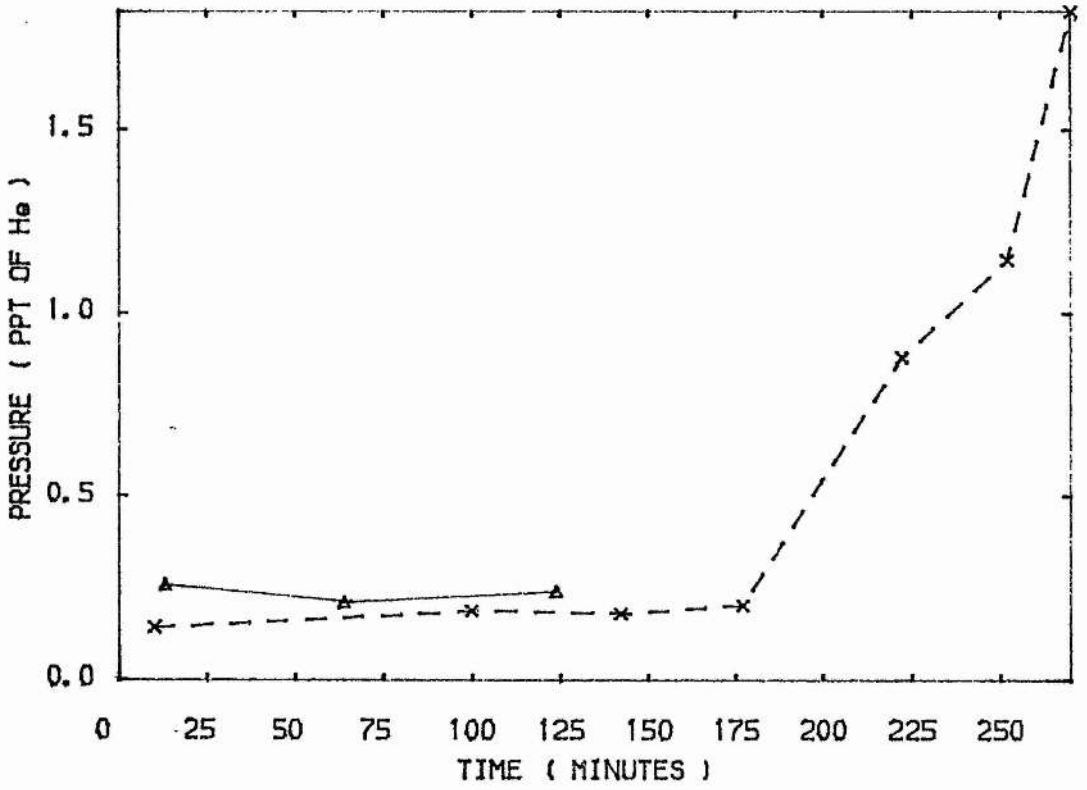

FIG 5.32

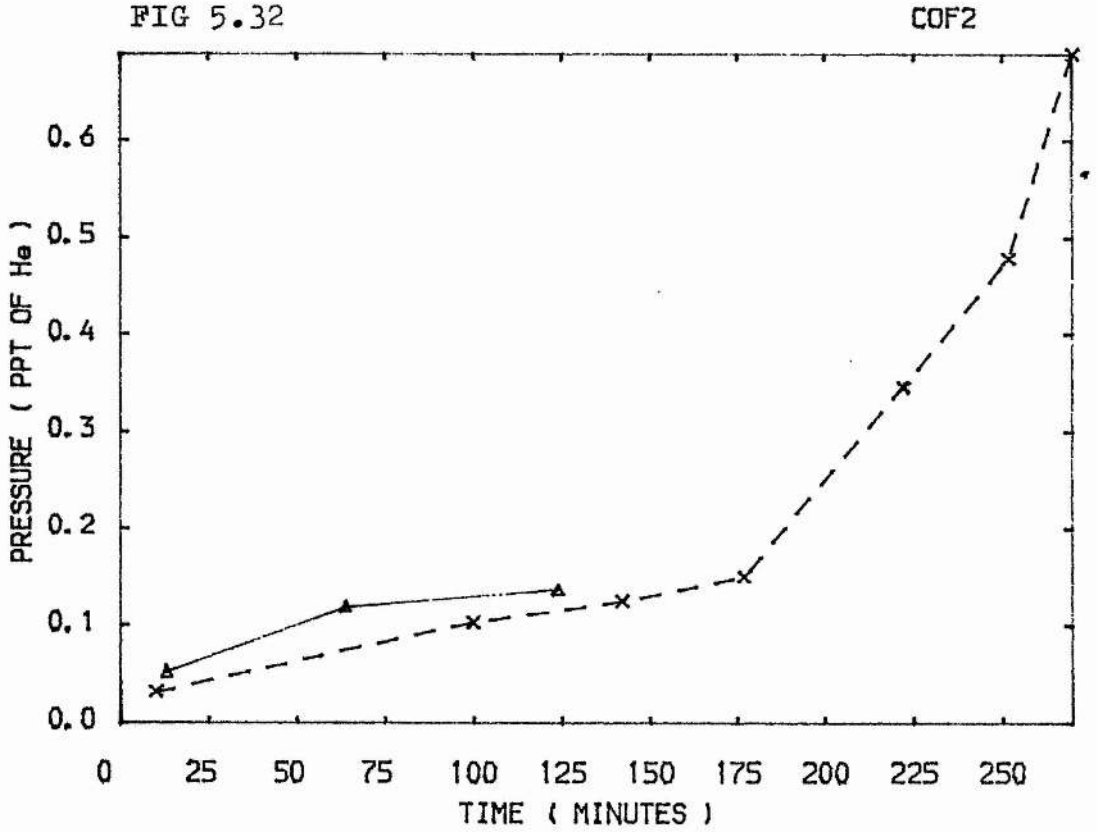

FIG 5.33

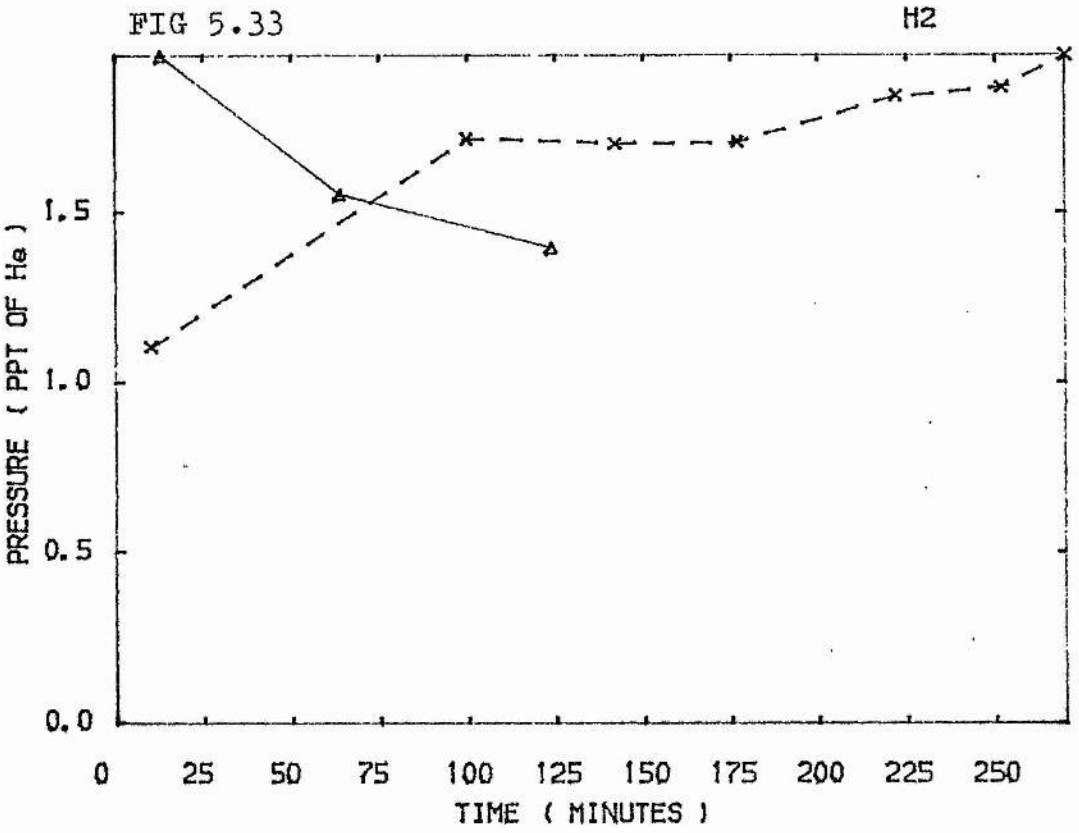

FIG 5.34

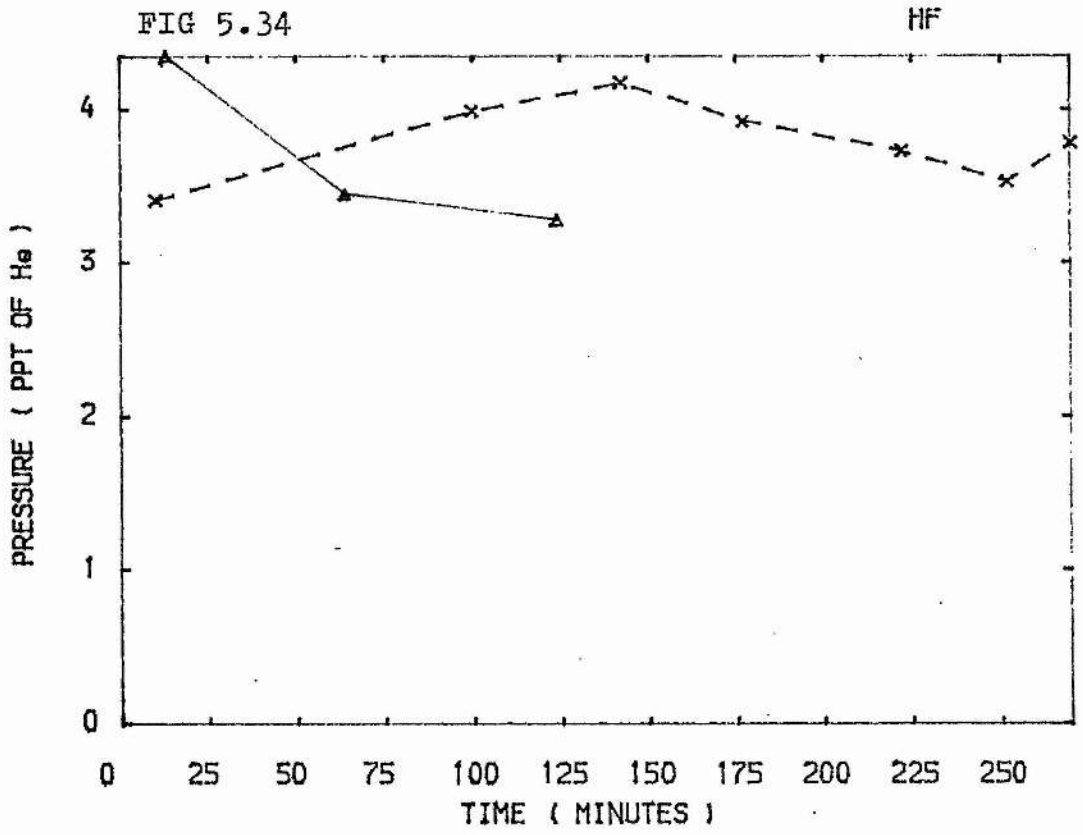

FIG 5.35

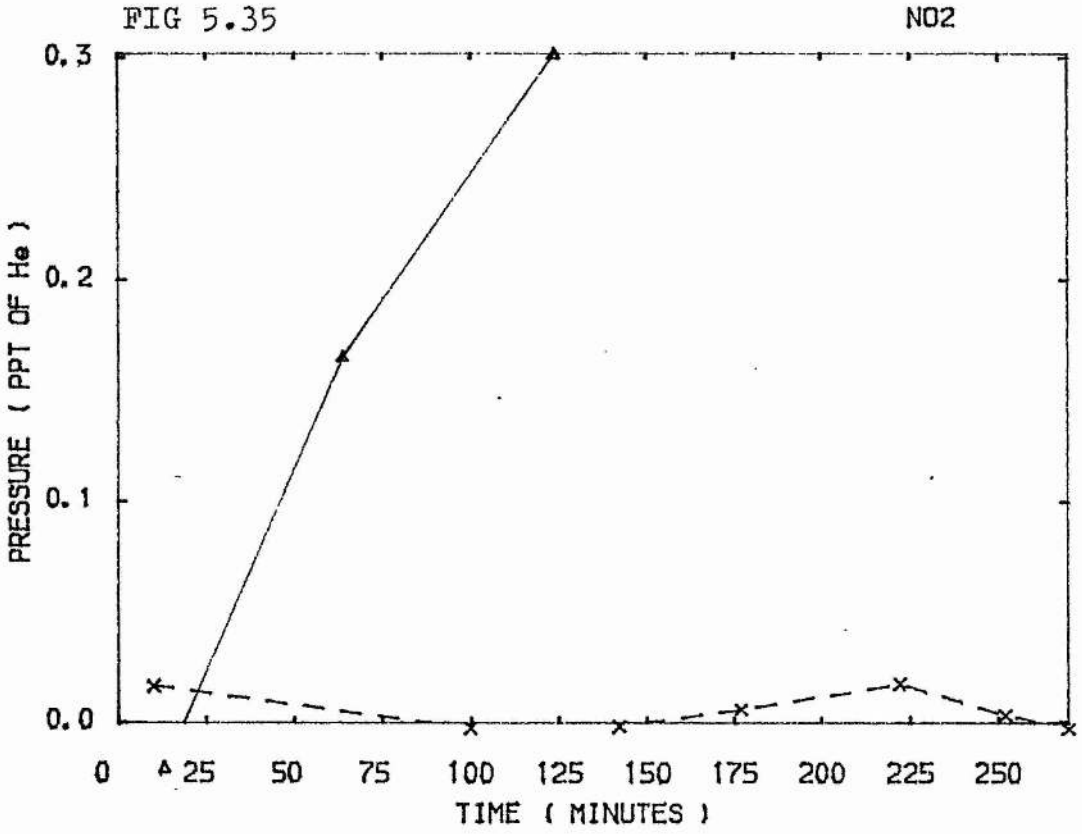

FIG 5.36

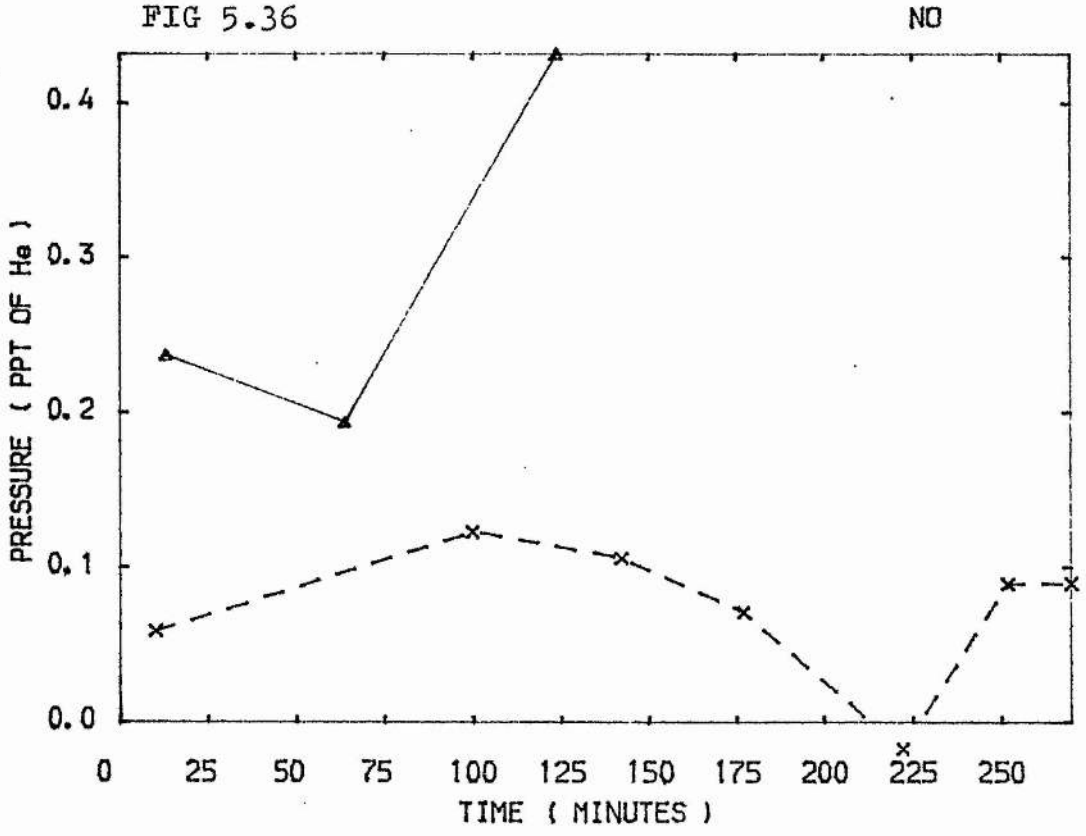

FIG 5.37

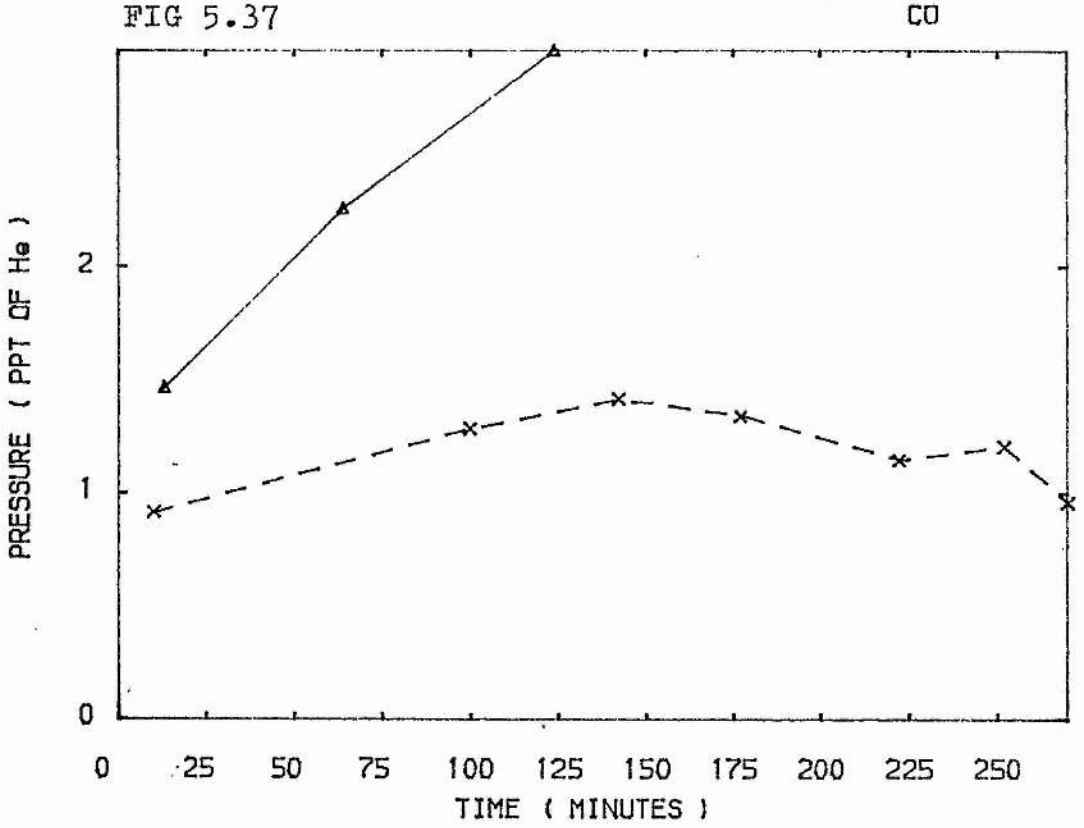

FIG 5.38

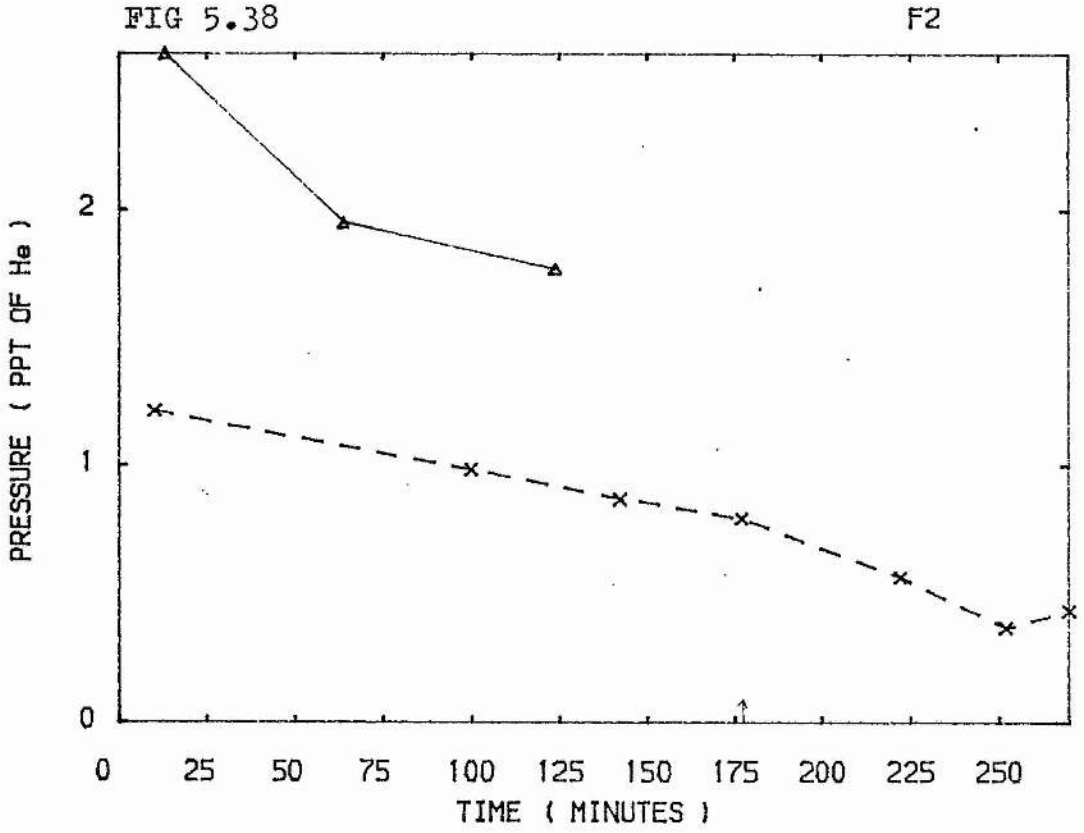

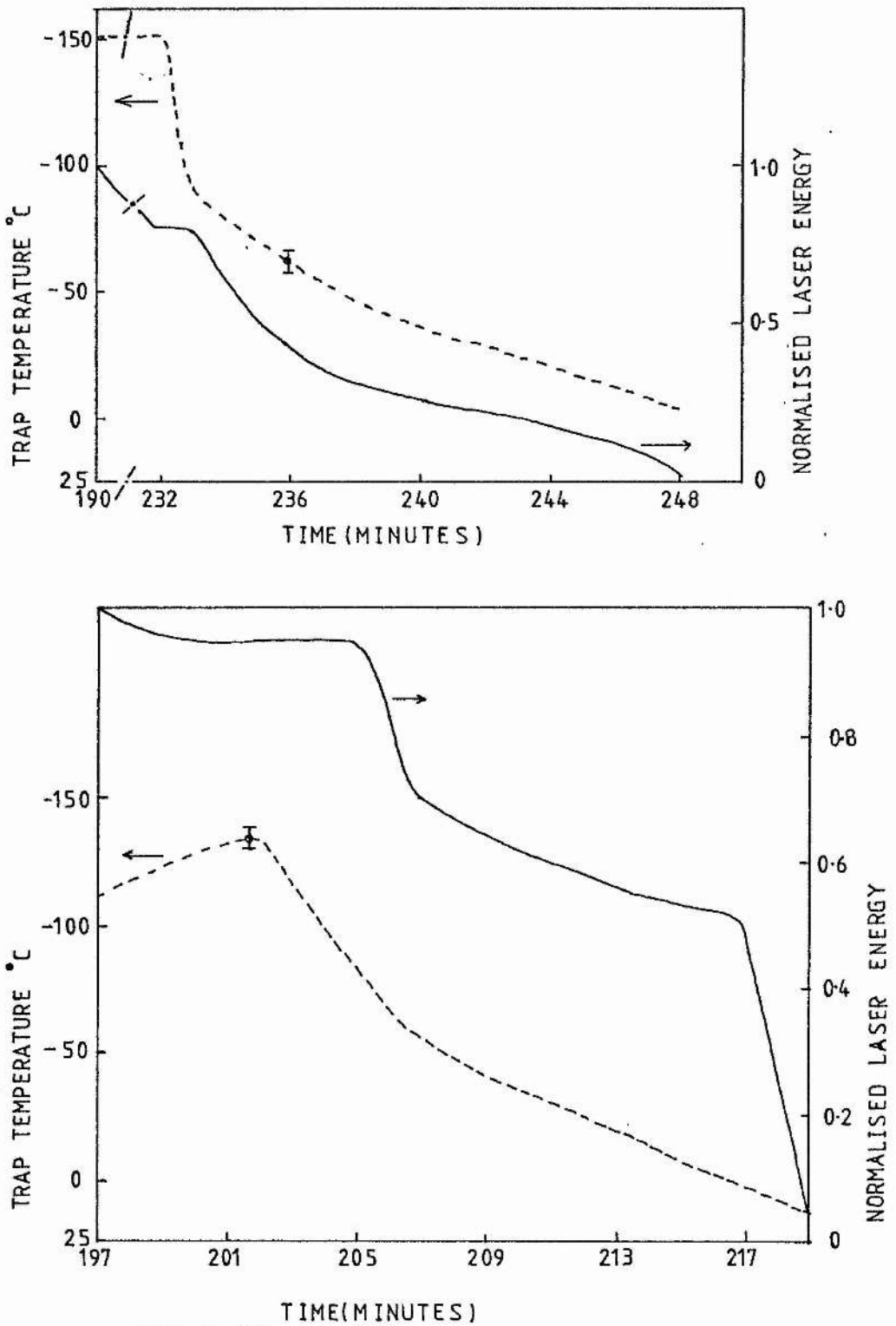

FIG 4.39 a and b
KrF laser output as a function of cold trap temperature.

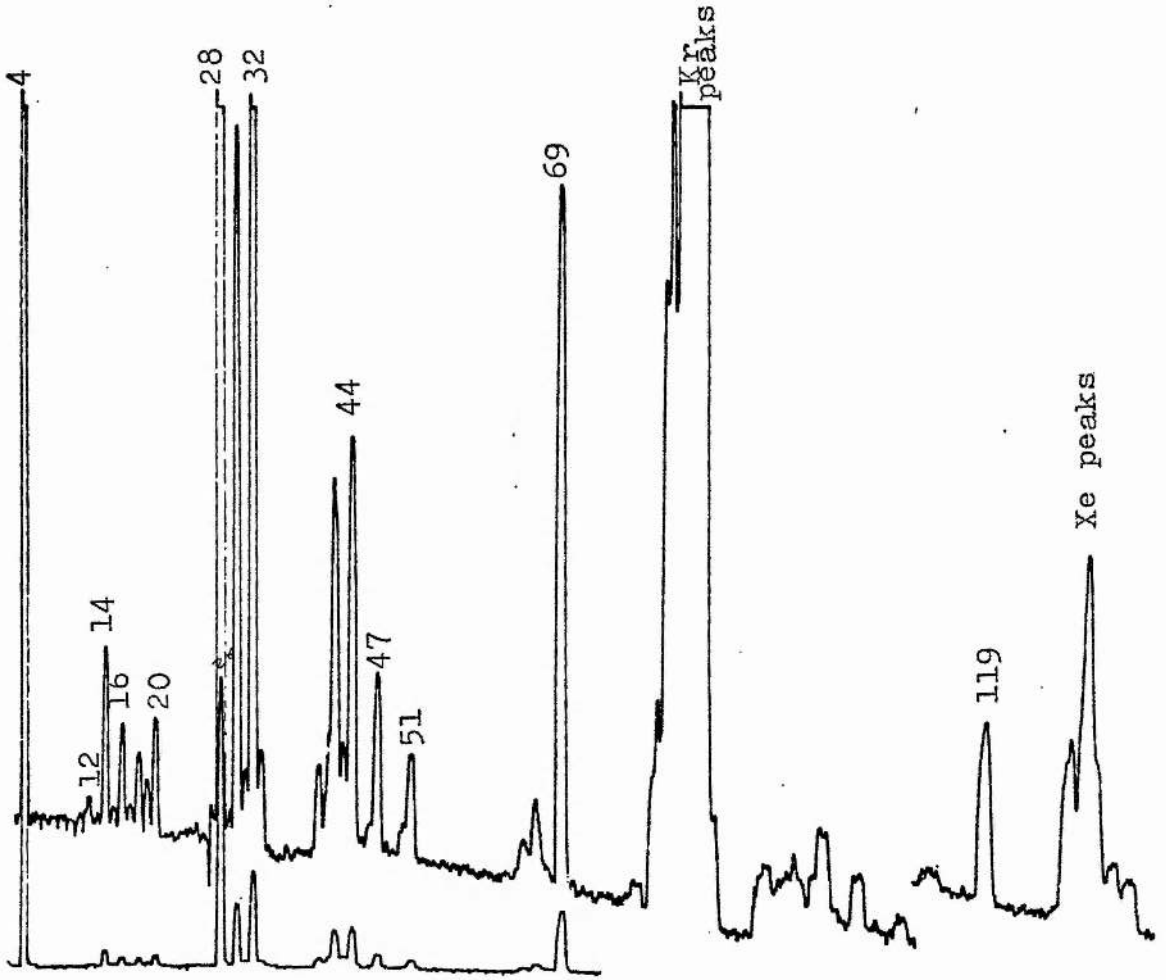

FIG 5.40 Mass spectrum of cold trap contents of a KrF laser.

FIG 5.41:KrF laser output from LV4 and LV5.

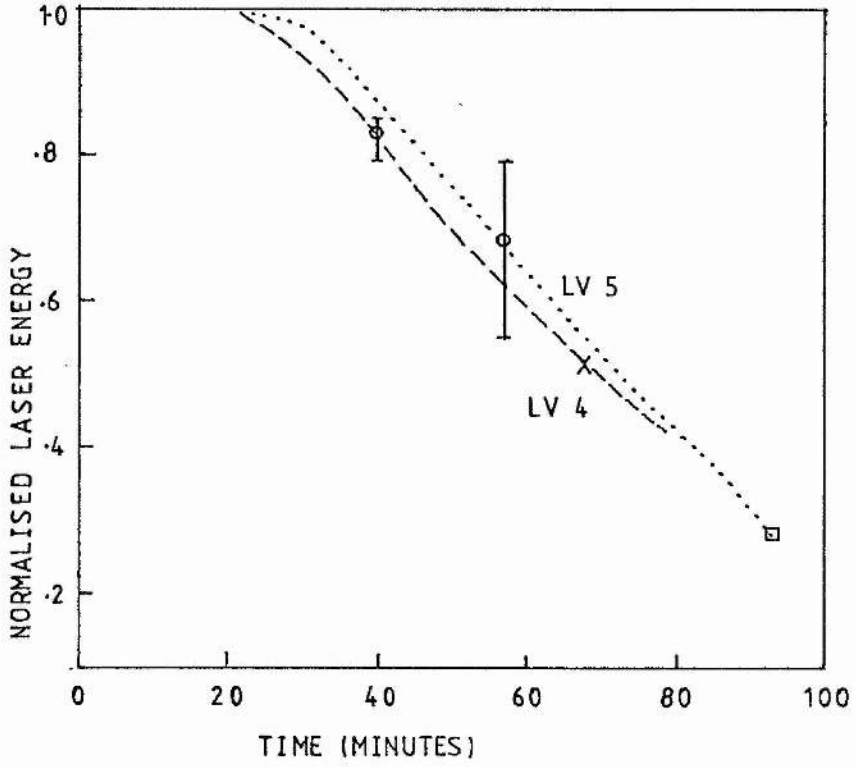

FIG 5.42: Revival of KrF laser by adding F_2.

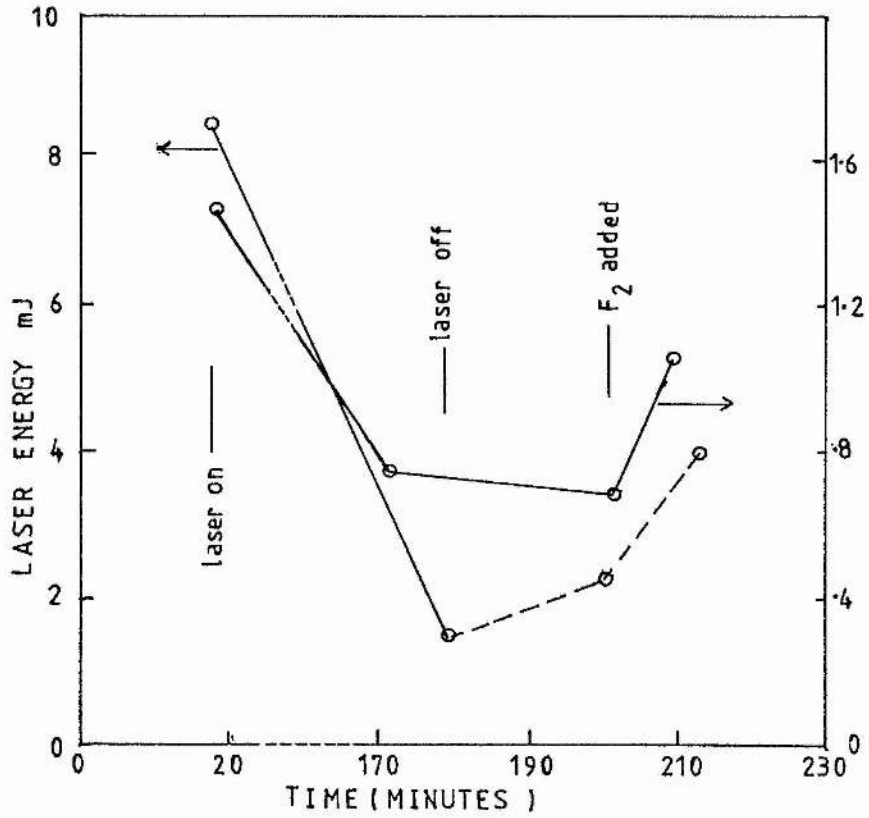

Figures 5.43 to 5.54
Impurity evolution in He-Kr-F_2 mixes:

—△— LV4 without discharge
--X--LV4 with discharge
···□··· LV5 with discharge

FIG 5.43

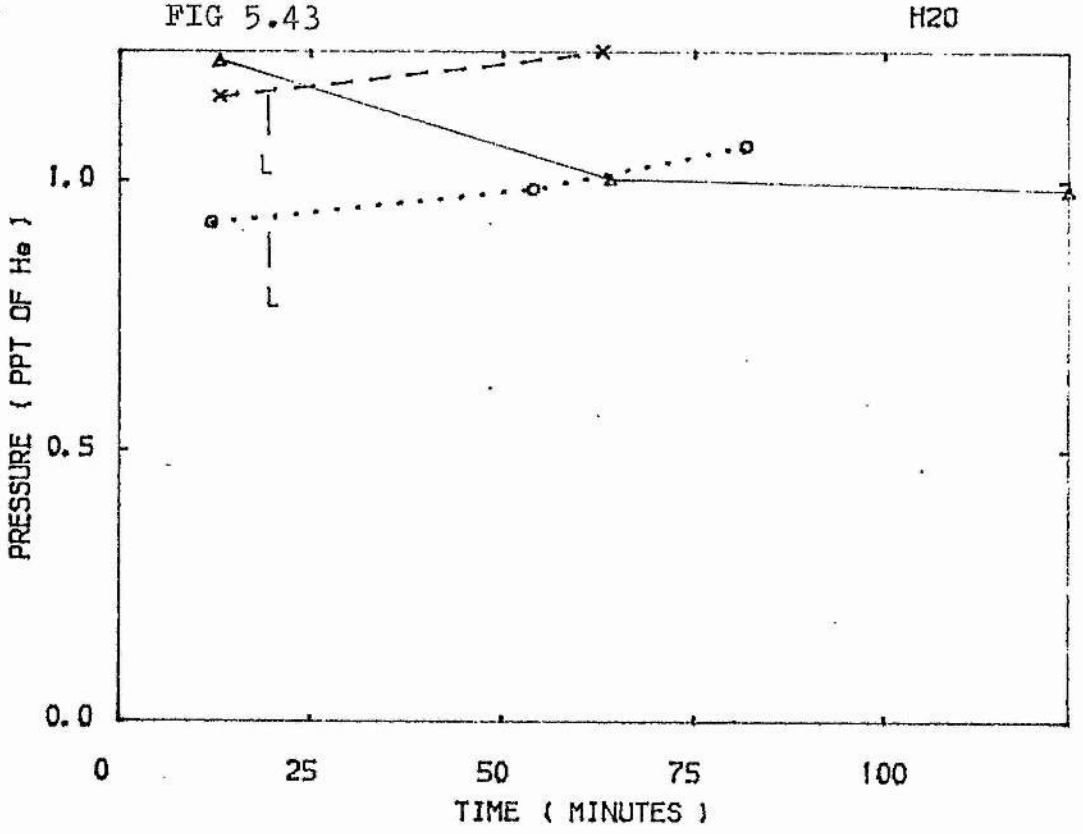

FIG 5.44

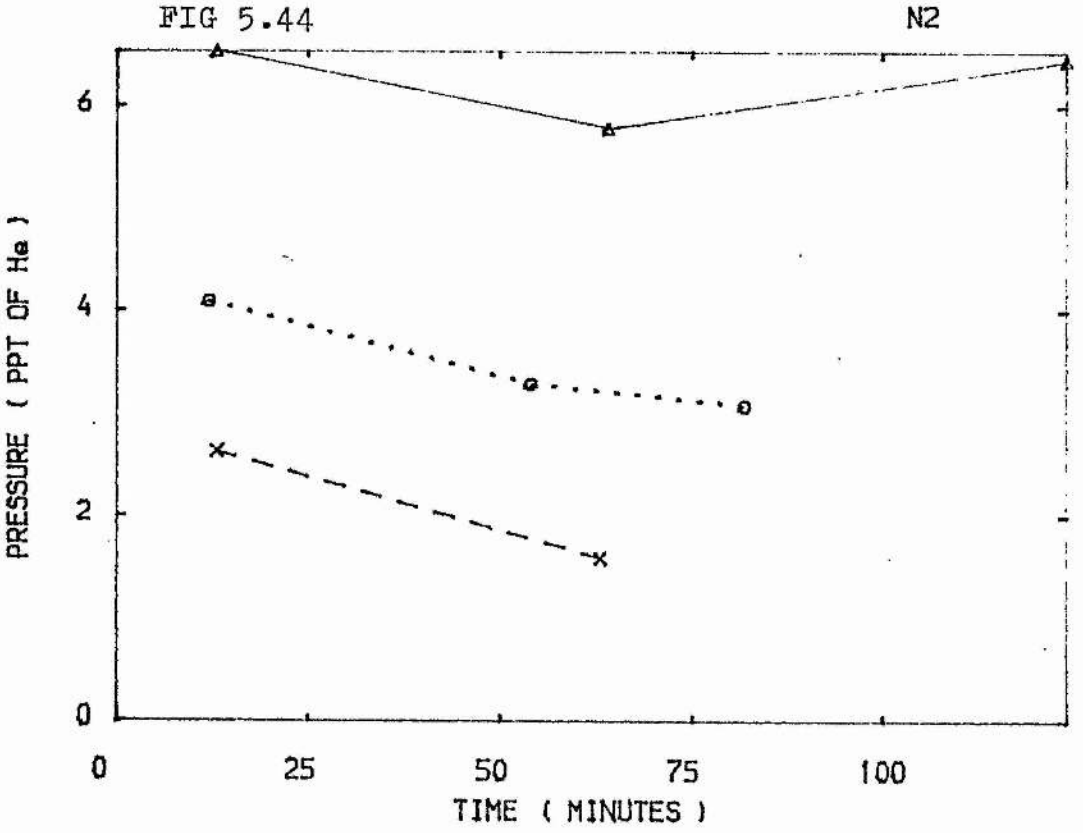

FIG 5.45

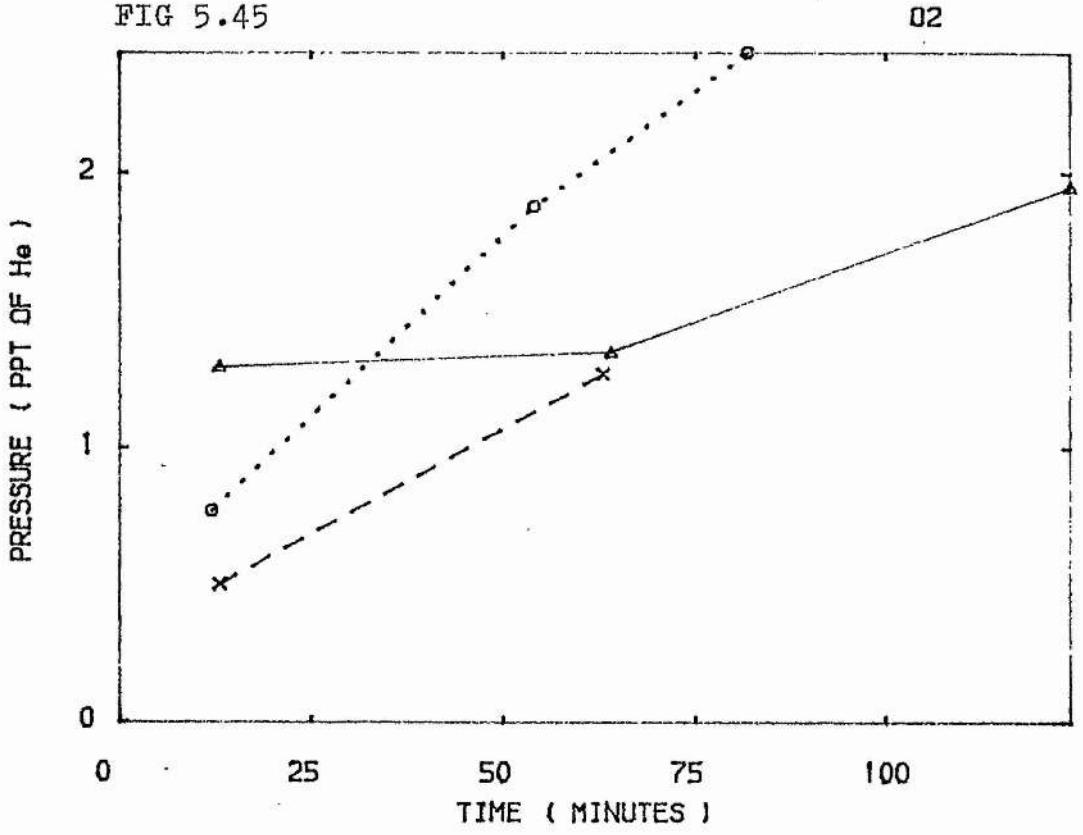

FIG 5.46

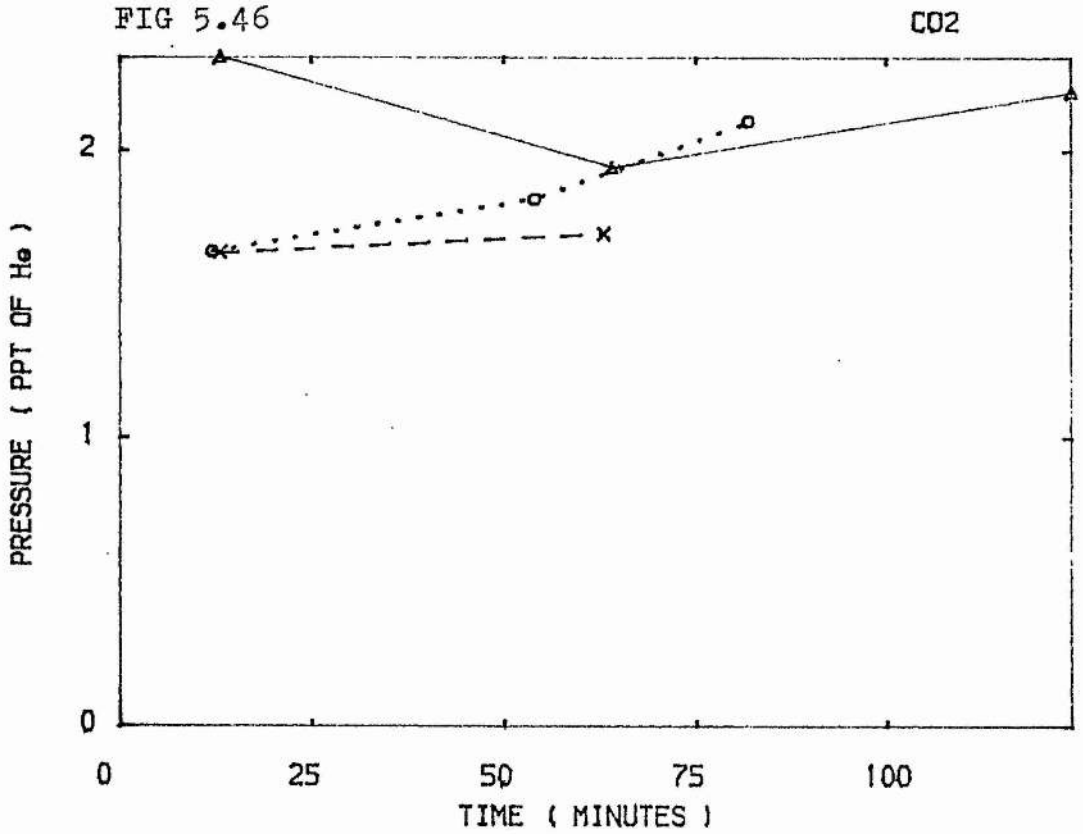

FIG 5.47

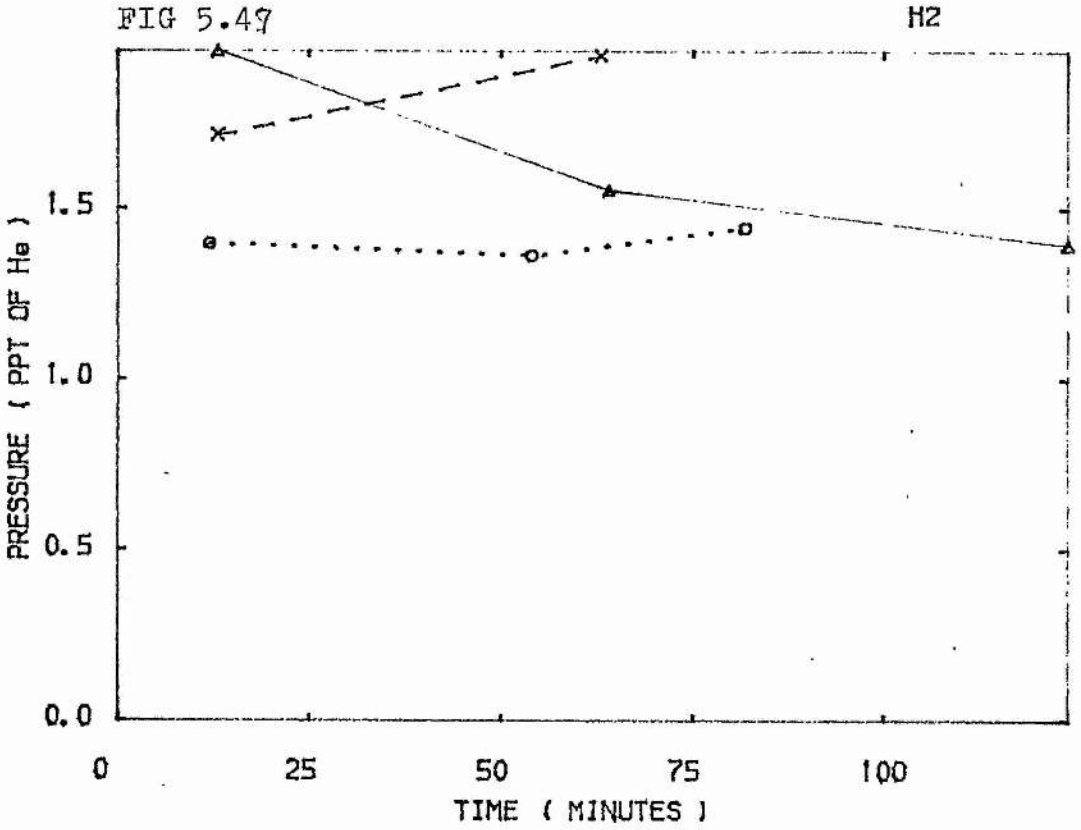

FIG 5.48

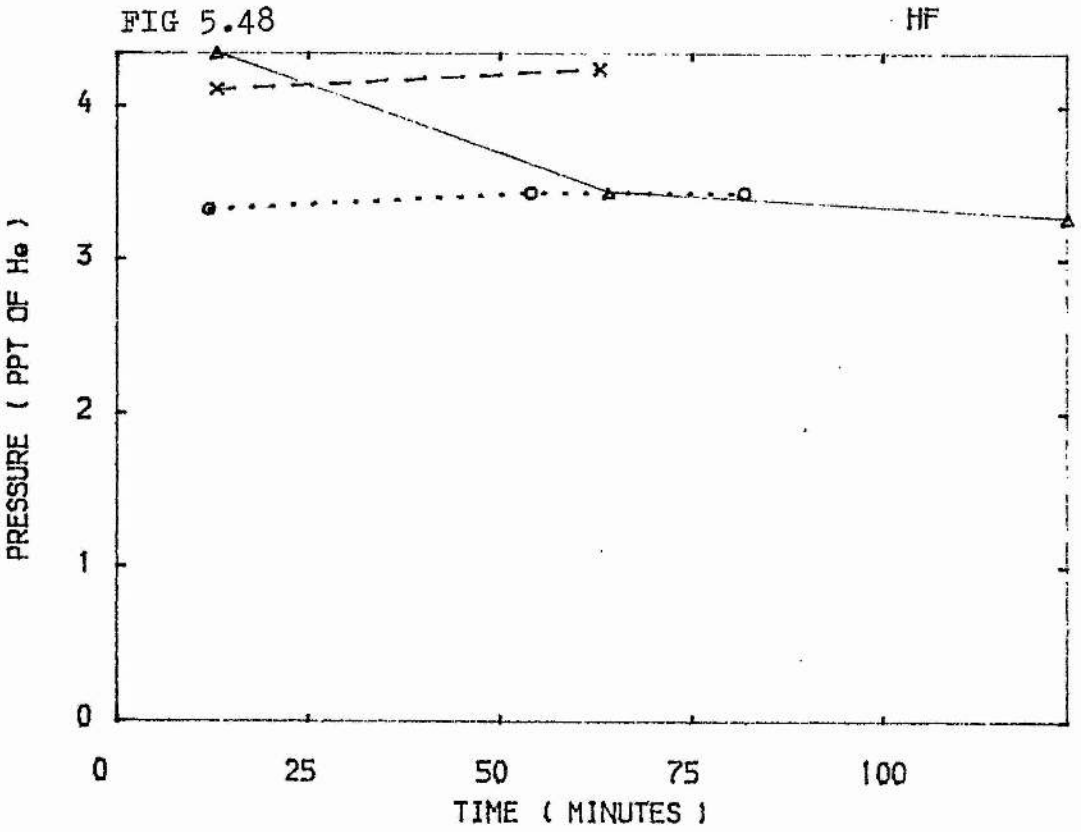

FIG 5.49

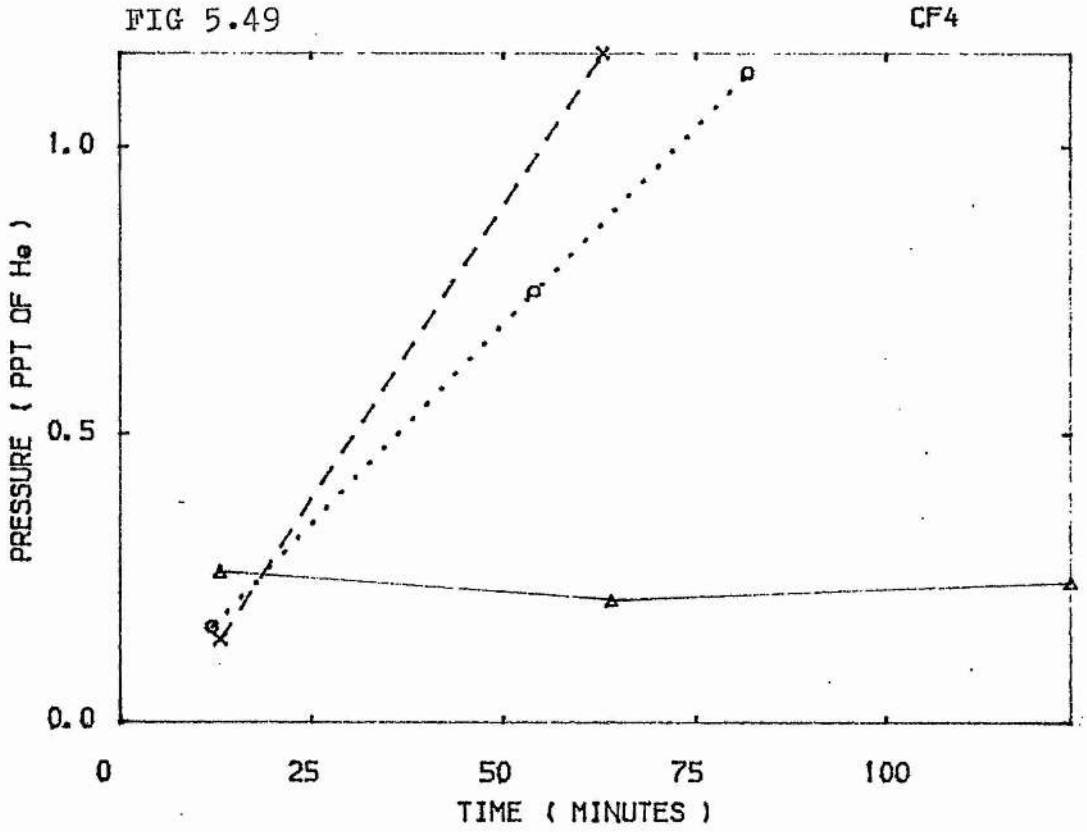

FIG 5.50

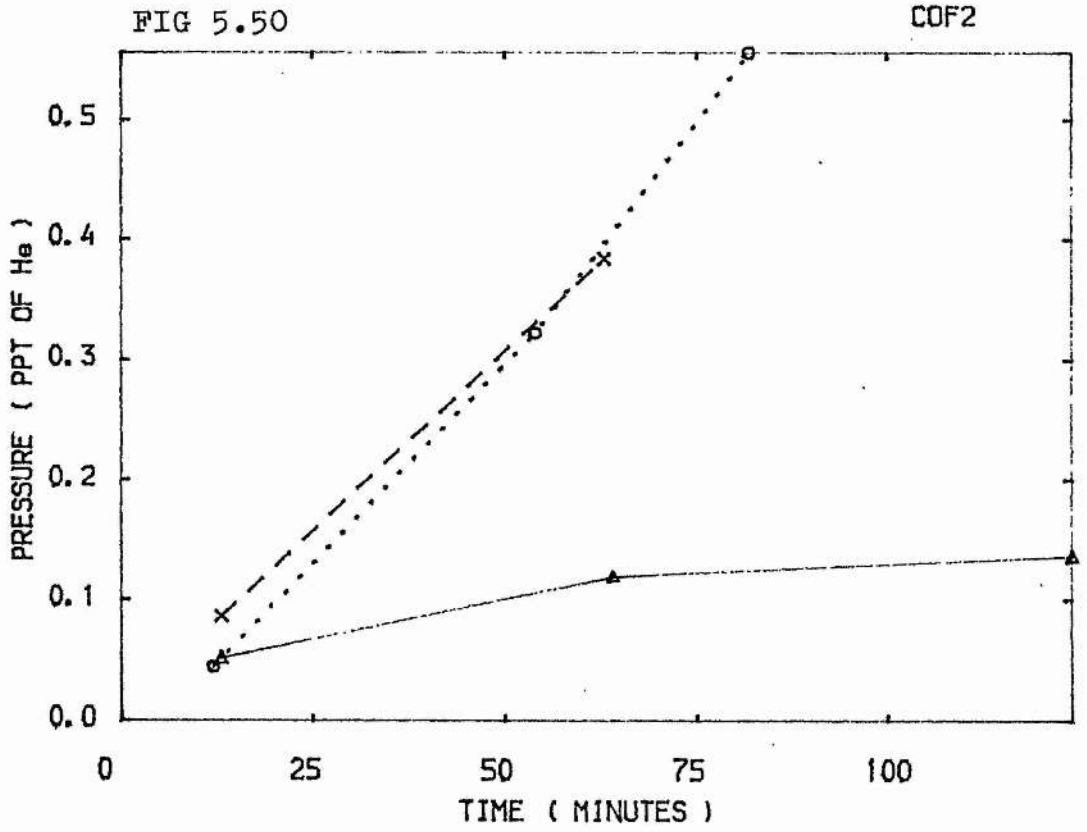

FIG 5.51

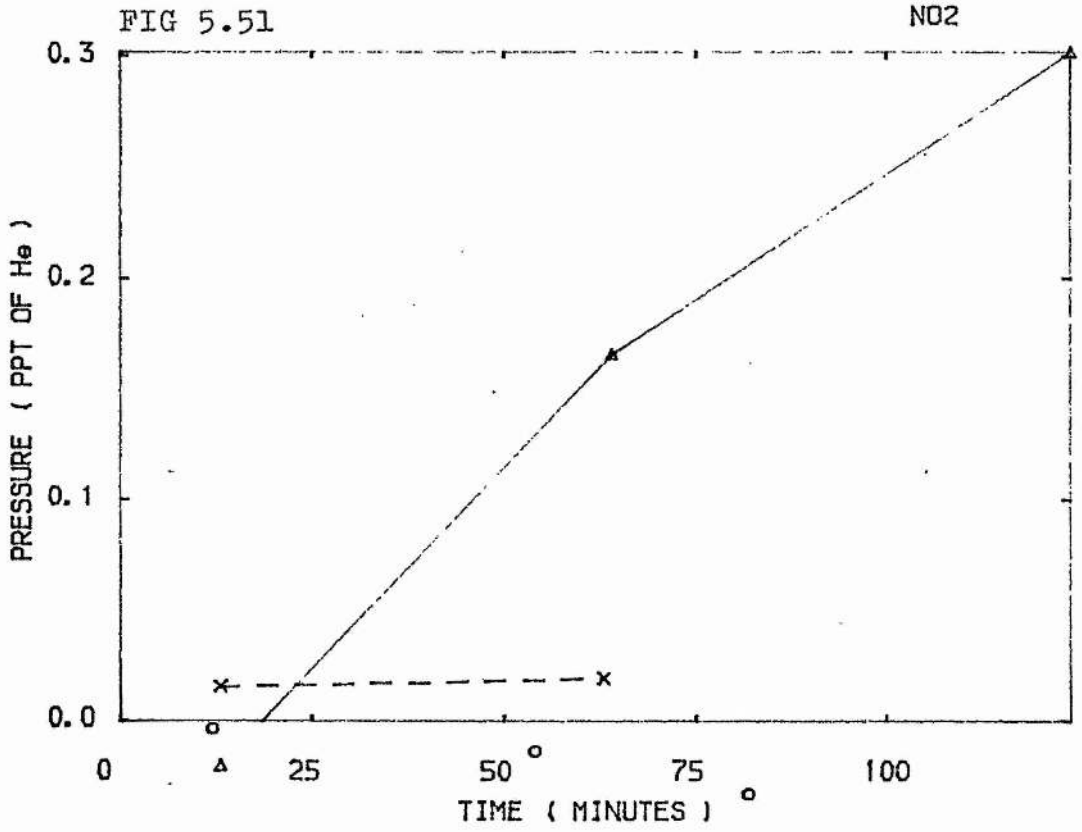

FIG 5.52

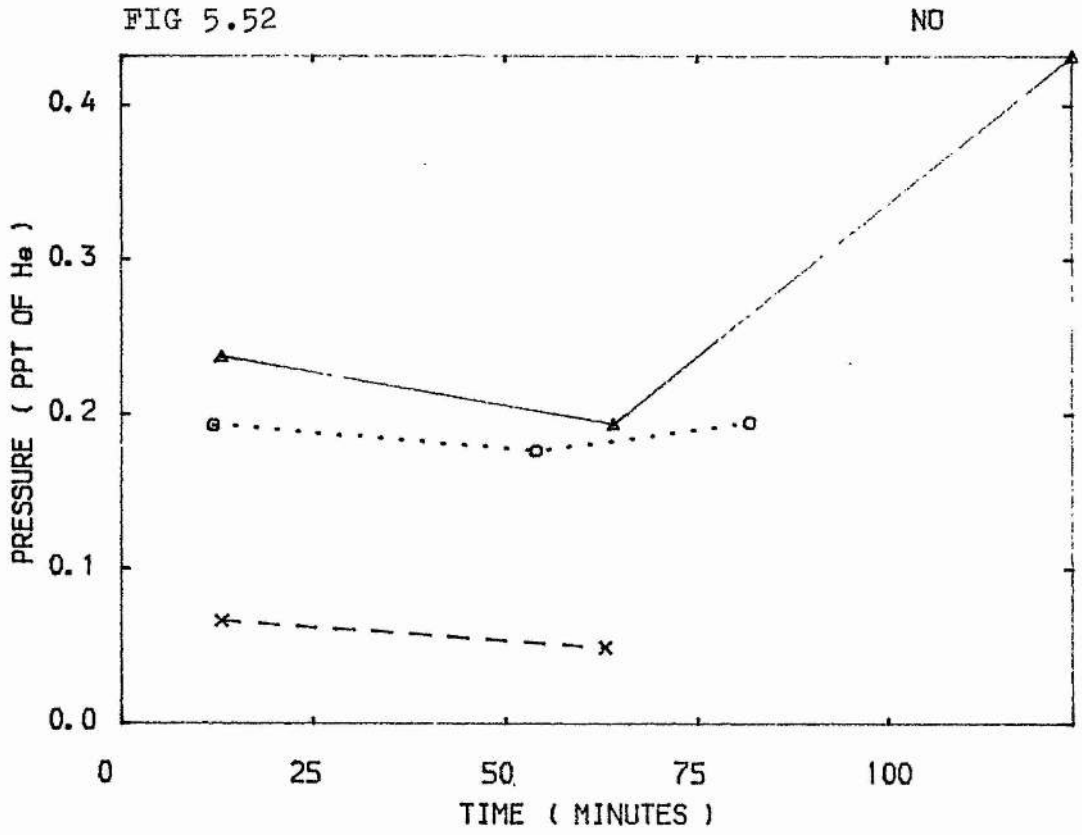

FIG 5.53

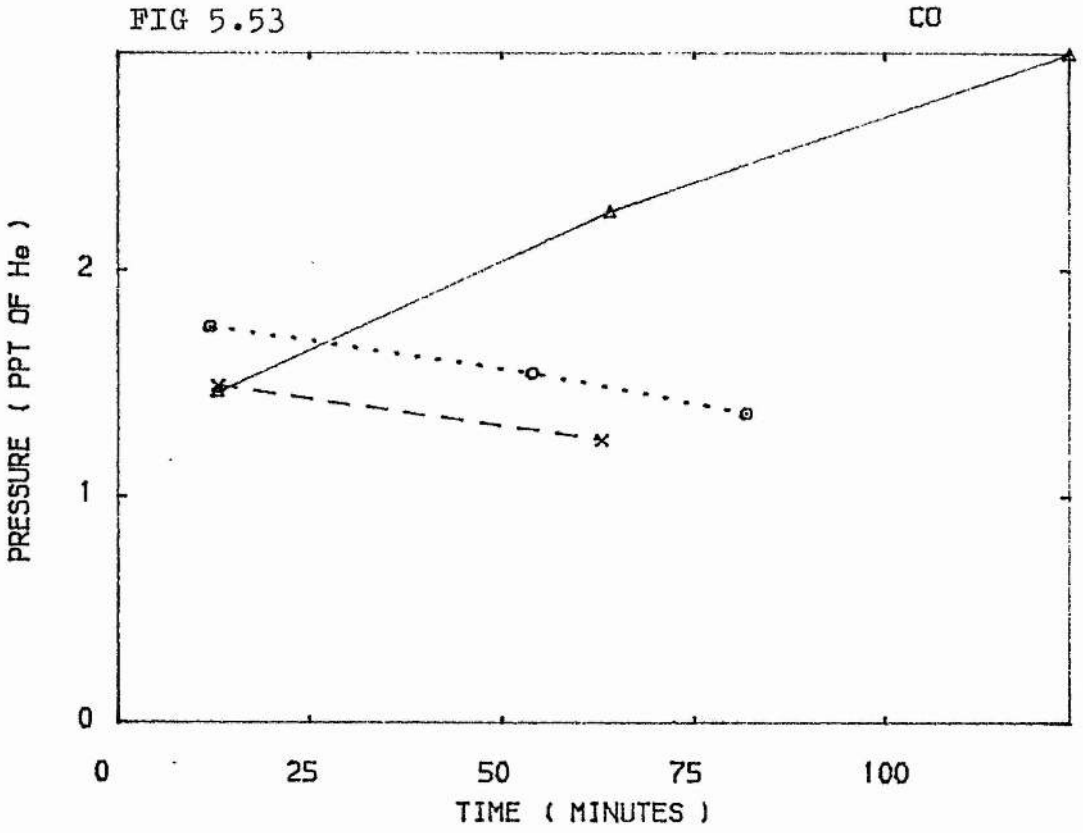

FIG 5.54

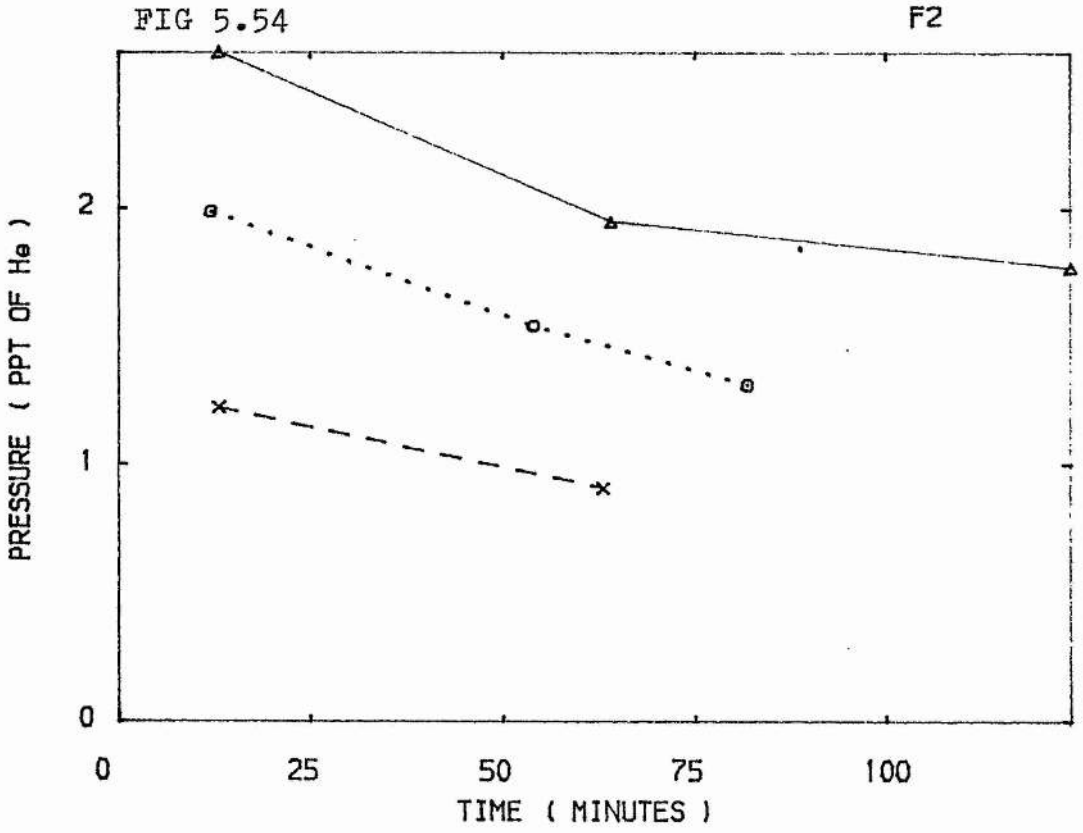

REFERENCES

Johnson P.M, Keller N, and Turner R.E (1978)

Appl. Phys. Lett. 32 291.

Kutschke K.O, Hackett P.A, and Willis C (1981)

Rev. Sci. Instrum. 52 1655.

Mandl A, Slater R, and Appel C.H (1982)

Rev. Sci. Instrum. 53 301.

CHAPTER 6

PERFORMANCE OF FLUORINE AND KrF LASERS WITH ADDED IMPURITIES

Deliberate addition of impurities to the basic gas mixtures of atomic F_2 and KrF lasers can be used as a method to study the effect of individual impurities on the gas lifetime and output characteristics of these lasers. In this way a quantitative evaluation of the effects of impurities can be attempted. We believe this thesis reports the results of such a study for the first time. Controlled addition of individual impurities eliminates complications due to more than one impurity producing effects which are difficult to correlate with the impurities. In this chapter the effects of the following individual additives on fluorine and KrF lasers are reported: CO_2, CO, O_2, CF_4, H_2, SF_6, and N_2. In general about one to three torr of the impurity is added to the basic gas mixture and the mass spectra are taken before, during and after the sequence of discharges, along with measurements of output power. The mass spectra are then analysed as described in chapter 3 to give the partial pressures of various compounds evolving in the laser mixture. The results are then correlated with the power output curves and the rate of loss of F_2.

6.1 Impurity addition to He-F_2 mixtures

The basic mixture used here is the same as was discussed previously (see chapter 4) - 6 torr of F_2 in 850 torr of He in laser version 4. The following 6 impurities are added (amounts given in brackets): CO (3 torr), CO_2(1.5 torr), O_2(2.5 torr), N_2(4 torr), H_2(3.5 torr), and CF_4(3 torr). A mass spectrum of the gas mixture is taken immediately after adding the impurity and then the sequence of discharge pulses is started (25 kV, 1pps). The second, and if needed, a third mass spectrum are taken usually at 30 minute intervals. Of the six impurities, CO and H_2 tended to react with F_2 as expected even without the discharge. The two reactions would be,

$CO + F_2 \rightarrow COF_2$

$H_2 + F_2 \rightarrow 2HF$

The other four impurities did not significantly react with F_2 without the discharges.

6.1.1 Impurity evolution in doped He-F_2 mixtures

Figures 6.1 to 6.30 give the various impurities evolving in the He-F_2 gas mixture after the addition of the six dopant impurities. Each pair of graphs also contains one reference plot for a basic mixture (marked B). The curves are labelled with the names of the dopant impurities. The significant points about these graphs are discussed here for each impurity in turn.

O_2

The growth rate for for O_2 in the basic mix is about 1.5 ppt of He in 80 minutes. When N_2 or CF_4 are dopants the O_2 growth rate is even lower than for the basic mix. For CO dopant O_2 grows slightly faster than in the basic mix. The growth of O_2 when O_2 is the dopant is at about the same rate as for the basic mix. The fastest growth of O_2 is for CO_2 and H_2 dopants. For the CO_2 dopant, this growth slows down as CO_2 gets used up. These two fast growth rates are attributed to the reactions

$CO_2 + F_2 \rightarrow COF_2 + O$

$COF_2 + F_2 \rightarrow CF_4 + O$

$H_2 + F_2 \rightarrow 2HF$

$[H_2 + F_2 + Si + H_2O] \rightarrow [SiF_4 + O_2 + HF + H_2O]$

where the brackets indicate that the actual reaction pathways are not known.

N_2

The partial pressure of N_2 falls slightly over 80 minutes in the same way as in the basic mix, except when CF_4 is added as dopant, in which case, there is a slight increase over the initial value. The amount of N_2 in the trial with CF_4 dopant is also the smallest of the six. The fall in N_2 suggests that it is being used up in some reaction, since without the laser, N_2 partial pressure grows as seen in chapter 4. One product is NF_3, which grows significantly when CF_4, CO, or N_2 are dopants. Since the growth of NF_3 is about 0.1 ppt of He even with 45 ppt of N_2 in He, the growth of NF_3 in the basic mix (about 1.5 ppt of N_2) would be quite

small.

CO_2

When CO_2 is the dopant, the fall in partial pressure of CO_2 is very rapid from about 25 ppt to 10 ppt in 40 minutes. This is accompanied by fast rises in COF_2, CF_4, and O_2. The partial pressure of F_2 also falls more rapidly over this period. These changes indicate that the reaction

$CO_2 + F_2 \rightarrow [COF_2, CF_4, O_2]$

is taking place. When O_2 is the dopant, the CO_2 concentration is higher than in the basic mix, and also grows faster than in the basic mix. There are two possible reasons for this; higher background CO_2 in the mass spectrometer and ion gauge, and reaction at the corona wire site with carbon to produce CO and CO_2. When CO, CF_4, H_2, and N_2 are dopants, the CO_2 partial pressure changes in the same manner as in the basic mix.

CO

The rather high partial pressure of CO when N_2 is the dopant is probably an artefact introduced when solving the linear equations for the partial pressures (see Chapter 3), since the peak at 28 is due to CO, CO_2, and N_2. Neglecting this shift, values and variation of CO is the same as in the basic mix for all the dopants, except for CO. When CO is the dopant, it is used up rapidly, the partial pressure falling from about 6 to less than 1 ppt of He in 20 minutes. This is due to the reaction

$CO + F_2 \rightarrow COF_2$

The rate of fall of F_2 is faster in the initial part when CO is the

dopant; this is compatible with this reaction.

COF_2

In the basic mix COF_2 grows by 0.6 ppt of He in 70 minutes. When CO is added to the basic mix the reaction of F_2 with CO produces a high initial amount of COF_2 of about 3.5 ppt. This reaction continues during the discharge but the rate is apparently slower, since COF_2 is further converted into other compounds, especially CF_4. Addition of H_2, O_2, or N_2 does not change the growth rate of COF_2 compared with the basic mix. The highest rate of growth of COF_2 accompanies the addition of CO_2 and is probably due to the reaction of CO_2 with F_2 in the discharge. Doping with CF_4 also produces a high rate of growth of COF_2, which, along with the less than normal amount of growth of O_2, indicates a reaction of CF_4 with O_2 to yield COF_2 and possibly, F_2 (note the slower drop in F_2 with respect to the other curves when CF_4 is the dopant).

CF_4

The rate of growth of CF_4 is highest when CO is the dopant (about 10 ppt in 35 minutes). With CO_2 dopant, CF_4 grows about 6.5 ppt of He compared with about 3 ppt in the basic mix, in 70 minutes. The growth in CF_4 is suppressed and COF_2 growth is as in the basic mix when O_2 is the dopant, even though a greater than usual amount of CO_2 is present in the trial with O_2 dopant (see CO_2 curves). The growth of CF_4 is less than in the basic mix when H_2 is the dopant and is as in the basic mix when N_2 is the dopant. When H_2 is the dopant the main reaction channels are

$[H_2 + F_2 + Si + H_2O] \rightarrow [SiF_4 + O_2 + HF + H_2O]$.

These are expected to reduce the reaction rate in the reaction channel resulting in CF_4.

H_2O, HF and SiF_4

The variation of partial pressures of H_2O, HF, and SiF_4 cannot be considered significant unless the changes are quite large (of the order of a few ppt of He). The recorded values of HF and SiF_4 are influenced by their production in the mass spectrometer, which in turn depends on the partial pressure of F_2 (see Chapter 3). Since F_2 partial pressure is roughly the same in all the cases except for CO, the large differences in SiF_4 growth when compared with the basic mix are due to changes in SiF_4 partial pressure in the laser itself. From the curves it is seen that the H_2 dopant produces a rapid growth of HF and SiF_4 as expected. When H_2 is the dopant, the H_2O partial pressure is significantly higher than it is with any of the other five dopants or the basic mix. The basic mix shows a growth of SiF_4 of 1 ppt in 70 minutes. All the other dopants have no significant effect on the change in partial pressure of SiF_4. When O_2 is the dopant, the SiF_4 pressure along with that of HF is seen to be higher than normal at the start.

Other impurities

Of the other impurities, SF_6 is present in the mix initially and decreases during lasing (not given in the figures). There is a greater growth in NF_3 when N_2 and CF_4 are dopants (figure 6.25). Nitrous oxide generally decreases during the discharge. It was found that the growth of NO when there are no discharges is highest when H_2 is used as the dopant. This suggests that N_2 reacts with

O released from H_2O in the presence of HF formed in the reaction of H_2 with F_2. With the discharges, NO tends to decrease in partial pressure indicating that other NO depleting reactions are taking place at a faster rate. The two impurities SO_2 and HCl are present in the background at about 0.1 to 0.2 ppt of He in all trials and their concentrations change randomly. Oxygen difluoride (OF_2) is seen to grow in all the trials (figure 6.27 and 6.30). When CF_4 is the dopant there is a greater growth of the 119 peak ($C_2F_5^+$) which shows that the 119 peak is probably due to a product derived from CF_4.

F_2

The depletion of F_2 in the basic mix is 15.4±0.7 ppm (with respect to He) per minute over the lasing period of about 60 minutes as calculated from the three basic mixes (see chapter 4). Table 6.1 below gives the depletion rates of F_2 over the same period for different dopants at different concentrations. For H_2 and CO dopants, the loss includes the initial loss of F_2 without a discharge.

Table 6.1

Depletion rate of F_2 and energy output of F_2 laser for different dopants.

Dopant	Pressure torr					
[1]	[2]	[3]	[4]	[5]	[6]	[7]
CO_2	3.3	94	26	3.9	4	6
	1.5	30	35	--	3	11
	0.8	24	43	--	2	9
H_2	6	>450	0.0	--	--	--
	3.5	45	42	0.50	2	5
CO	3	33	62	0.55	3	18
	5	35	42	0.19	4	56
N_2	6.5	20	(88)	--	(3)	(30)
	4	25	(88)	(3)	(52)	
O_2	2.5	18	34	0.20	1	5
	1.5	14	37	0.16	1	5
	0.8	17	43	0.14	1	5
CF_4	3	10	45	--	(2)	(9)
	1.2	18	47	--	(2)	(11)
Basic mix		16	69			
		14.6	60	0.15	2	4

Column [3] : Depletion rate of F_2 (ppm of He/minute)
[4] : Power at start (micro Joule)
[5] : % drop in energy for 10 minutes at start
[6] : ± % variation in output energy at start
[7] : ± % variation in output energy at end

The effect of the impurities tabulated above is dependent on their partial pressure. One can safely assume that F_2 depletion rates are affected by the above impurities to the same order for low partial pressures (<1 torr of impurity) as for the partial pressures in table 6.1. Under such an assumption we find that the impurities in decreasing order of effectiveness in depleting F_2 are CO_2, H_2, CO, N_2, O_2, and CF_4. In fact CF_4 has a tendency to decrease the depletion rate of F_2 compared to the basic mix.

6.1.2 Effect of dopants on F_2 laser energy output

Energy measurements of the output from the atomic fluorine laser are done using a joulemeter (see chapter 3) which measures the energy in the central portion of the output beam. The output beam has a rectangular cross section of about 30mm x 10mm at the sampling site and the energy meter input aperture is 10mm in diameter. The continuous measurement of energy showed up variations from pulse to pulse, which depended on the dopant used. For the basic mixture, the variations generally increased in time, showing the deterioration of the discharge due to the impurities evolved in the laser.

Figure 6.31 gives the variation in the normalised values of energy for the six dopants discussed in section 6.1.1 along with the drop in energy for a basic mixture. In all cases the dopants decrease the half life of the mixture. When O_2 and CO are the dopants the

energy is highest at the start of the discharge and decreases with time. With CO_2 dopant, the energy output increases with decreasing CO_2 partial pressure. From the graphs we see that as far as the lasing half life of the gas mixture is concerned, CO_2 and H_2 have the worst effect followed by O_2 and CO.

When CF_4 and N_2 are used as dopants, lasing in the ir and uv are observed. This indicates a change in the lasing species and therefore the power output curves are not directly comparable with the others. Lasing in the uv (337.1 nm) is due to the N_2 molecules. At the same time the laser due to atomic fluorine is also visible, at the same intensity as before. However, when CF_4 is added, the red emission is almost completely quenched.

Values of the laser output at the start (table 6.1, column 4) show that CO_2 is the most effective quencher of laser energy, with H_2, O_2, and CO coming next. The values for N_2 and CF_4 are not directly comparable since the corresponding mixtures lase at more than one wavelength. The percentage drop in energy for 1.5 torr and 0.8 torr of CO_2 is not calculated because the energy grows in time as CO_2 is used up. The energies at the start of the discharge can be compared to give the effect of the individual dopants on the discharge. This shows that the quenchers in decreasing order of effectiveness are CO_2, O_2, H_2, and CO. The partial pressures of CF_4 and N_2 are too high to compare since the laser wavelengths are different. However, at smaller concentrations it was found that CF_4 and N_2 have no effect on the output characteristics of the atomic fluorine laser. Thus of the six dopants studied, CO_2 has

the most significant deleterious effect on the output and gas depletion characteristics of the atomic fluorine laser.

The energy output variations (table 6.1, columns 6 and 7) when compared with the basic mix is worst for the mix with CO and CO_2 as the dopant. This is seen to be due to the production of large amounts of COF_2 and CF_4 (see figures 6.23 and 6.24). However, H_2 and O_2 suppress the variations in output power. Production of COF_2 when H_2 or O_2 is the dopant is seen to be as it is in the basic mix.

6.2 Impurity addition to He-Kr-F_2 mixtures

In the last chapter the KrF laser was seen to be more sensitive than the atomic fluorine laser to the impurities present and evolving in the gas mixture. In the next two subsections we investigate the effect of seven dopant impurities on the KrF lasing characteristics. The dopants are CO_2, CO, H_2, O_2, N_2, SF_6 and CF_4. Unlike the He-F_2 mixture, presence of Kr is a disadvantage in the He-Kr-F_2 mixture since the peaks due to Kr are very strong at m/e of 86, 84,82,80, 43, 42, 41, and 40. Thus, for example, peaks due to SiF_4 and SO_2F_2 are masked. However, any large evolution of SiF_4 can be detected by measuring the ion current at m/e of 104. There is a large peak at 102 for SO_2F_2, which can be used to monitor its evolution. Partial pressures of the dopants and the evolved impurities are expected to be lower than in He-F_2 mixes, partly due to the fact that the partial pressure of F_2 is only 3

torr compared to 6 torr in He-F_2 mixes.

6.2.1 Impurity evolution in doped He-Kr-F_2 mixes

The basic mixture used in all the experiments is as given in chapter 5: 3 torr F_2 + 22 torr Kr + 850 torr He in laser version 4. The partial pressures of the various dopants are: CO (0.5 torr), CO_2(0.6 torr), O_2(0.7 torr), CF_4(0.6 torr), H_2(0.6 torr), N_2(2.0 torr), and SF_6(0.6 torr). The mass spectra are taken as described in section 6.1. The evolution of the various identified impurities is given in figures 6.32 to 6.59. Each curve is labelled with the name of the dopant impurity. The impurity evolution in the basic mixture is also given for comparison (curves labelled B).

When these curves are compared with the curves for impurity evolution in He-F_2 mixtures, the trend is seen to be similar with no marked deviations. On the whole the partial pressures of the evolved species are lower since the partial pressure of F_2 and the added impurities are lower in the KrF mixture. The partial pressure of H_2O is highest when O_2 is the dopant as in the case of the He-F_2 mix. The H_2 dopant is expected to be 2.5 ppt of He at the start but because of its reaction with F_2 to form HF even without any discharge, the initial value is lower. The amount of HF formed is lower than in the He-F_2 mix because, in that case, 3.5 torr of H_2 was added to 6 torr F_2 whereas 0.6 torr of H_2 was added to 3 torr of F_2 in the KrF mixture. The values of SiF_4 are not

known but examination of the small peak at 104 shows that SiF_4 increased at a faster rate when H_2 was the dopant; similar behaviour was noted in the He-F_2 mixtures. The other impurities - COF_2, CO, CO_2, CF_4, and O_2 - evolve similarly as in the He-F_2 mixture.

The amount of SO_2 is lower in the KrF mixture - SO_2 like SF_6 is initially present as an impurity in F_2. When SF_6 is added to the KrF mix as a dopant, SO_2F_2 and SOF_2 are produced in the discharge and are accompanied by a decrease in O_2 production relative to O_2 production in the basic mix. It is seen that CF_4, N_2 and SF_6 each suppresses the growth of O_2 compared to that in the basic mix, as in the He-F_2 mixtures. Two reasons for this suppression are suggested: suppression of reaction between CO_2 and F_2 to produce COF_2, and depletion of O_2 in reactions with CF_4 or SF_6 to produce COF_2, SOF_2, and SO_2F_2 respectively.

The depletion rate of F_2, along with the initial output energy of the laser and the number of shots to half power are given in table 6.2.

Table 6.2

KrF laser output and F_2 depletion characteristics.

Dopant	Partial Pressure (torr)	Power at start mJ	Half life pulses	F_2 depletion rate ppm/min
Basic		8.2	2700	4.2
CO_2	0.6	0.3	--	11
H_2	0.6	4.5	2600	7.9
CO	0.5	5.5	1420	6.8
O_2	0.7	7.0	1380	4.5
CF_4	0.6	8.0	2100	2.4
SF_6	0.6	6.0	1260	3.4
N_2	2.0	4.7	1680	4.2

The pattern followed is again similar to that of the He-F_2 mixture, but since smaller quantities of the dopants are used in the KrF mixes, the effects of the dopants per unit dopant partial pressure are more drastic. The worst impurity is seen to be CO_2. Hydrogen and CO come next. When CF_4 and SF_6 are added, the F_2 depletion rate is less than for the basic mix. This could be because CF_4 and SF_6 donate F atoms. Nitrogen impurity does not change the depletion rate of F_2 even at the comparatively high partial pressure of 2 torr.

6.2.2 Effect of dopants on the KrF laser energy and lifetime

From table 6.2 it is seen that CO_2 is the worst impurity of the seven dopants, causing almost complete quenching of laser action at just 0.6 torr (10 ppt of He). The least troublesome impurity is CF_4. The number of shots to half life does not follow the same pattern as the decrease in energy at the start since the half life would depend upon the impurities evolving in the mixture. Thus SF_6 reduces the half life to about 1300 shots compared to 2600 when H_2 is the dopant. This would indicate that the products SO_2F_2 and SOF_2 formed when SF_6 is the dopant are also quenchers of the KrF laser process.

The pulse-to-pulse variation in energy output is greatest (±50%) when CO_2 is the dopant. When CF_4, SF_6, CO, and O_2 are dopants the variation at the beginning is about ±3% becoming about ±20% after 30 minutes. When H_2 and N_2 are added the variation at start is about ±1% becoming ±4% for H_2 and ±10% for N_2 after 40 minutes. The basic mix has a variation of ±3% at the beginning of the lasing period, becoming ±4% after 30 minutes. These variations are similar to those observed for the doped He-F_2 mixtures.

6.3 Role of impurities in the gas mixtures

As mentioned previously, the impurities evolving in the laser can affect the laser performance in the following ways:

(1) They can deplete the active F_2 concentration by irreversibly removing it as stable fluorine compounds. Formation of CF_4, SO_2F_2, and C_2F_6 are examples. This depletion gradually reduces the energy output of the laser unless compensated. If there were no outgassing of CO_2 and other gases from the walls, this fluorine depletion path would not be important. This is because only a finite amount of F_2 will be lost in reactions with the impurities already present. An excess of F_2 can be added at the beginning to compensate for this loss.

(2) The impurities present and evolving in the mixture affect the discharge. The effect of the impurities already present is apparent by a reduction of output energy compared with that of a pure mix as discussed in the previous sections. The evolved impurities could be deleterious, depending upon their nature. Thus CO_2 decreases the output energy initially but after reactions with F_2 to produce COF_2 and CF_4 the laser energy of the F_2 laser actually goes up because of the less pronounced effects of COF_2 and CF_4 on the discharge (see section 6.1.2).

The discharge can be affected in three ways by the impurities: (1) the impurities can absorb at the laser wavelength; (2) the preionizing photons can be absorbed; and (3) the excited states leading to KrF^* or F^* formation can be quenched. Of these three causes the first can be ruled out for the KrF laser for the following reasons. Gower et al(1980) found that in a KrF excimer system made of glass and Al, the absorption at 248 nm (the lasing wavelength) decreased after 1000 pulses, due to a reduction of absorption caused by a depletion of F_2 molecules. Their system had impurities similar to the ones found for versions LV3 and LV4. Similarly, absorption lines in the KrF laser spectrum from a laser constructed out of PMMA and Al could not be attributed to any impurity involving C, F, F_2, HF, CF, CF_2 and noble gas compounds (Shimauchi et al 1978). For the atomic fluorine laser emitting around 730 nm, absorption effects are even less likely since the impurities are simple molecules with no absorption bands in the red region.

Effects on preionization would manifest as an increase in pulse-to-pulse variations due to a decrease in the homogeneity of the discharge. Thus for CO_2 as the dopant the variation in energy is ±50%. For H_2 the variation is quite small, at ±1%. Variations due to other dopants fall in between. Studies of absorption of radiation from spark and corona sources in O_2, CO_2, N_2, and H_2O at pressures less than 5 torr show that they all have absorption coefficients ranging from >200 cm^{-1} for H_2O to 800 cm^{-1} for CO_2 (Meek and Craggs 1978). Therefore one effect of the impurity is the quenching of uv preionizing photons. However, this is probably not the only deleterious effect, since CO_2 is by far the worst impurity, with O_2 or N_2 having much less of an effect, even though their absorption coefficients for short uv corona radiation is about the same (CO_2: 200-800 cm^{-1}, O_2: 500 cm^{-1}, N_2: 750 cm^{-1}). Carbon dioxide is an efficient electron quencher(Nighan and Wiegand 1974). Processes like dissociative attachment and dissociation of the form

$CO_2 + e \rightarrow CO + O^-$

$CO_2 + e \rightarrow CO + O + e$ (reduced energy)

can interfere with the stability of the main discharge.

The excited states of Kr and F, leading to the formation of the upper laser levels, can be quenched by the impurity species in reactions like

$Kr^* + CO_2 \rightarrow Kr + CO_2^*$

$KrF^* + O_2 \rightarrow KrF + O_2^*$

$F^* + SiF_4 \rightarrow F + SiF_4^*$

Unfortunately, we could not get any data on the rate constants for such reactions from the literature.

A better understanding of the effects of the impurities on the discharge needs detailed knowledge of the electron energy distribution and the various rate constants of the possible processes in the discharge under pulsed avalanche discharge conditions. This would necessitate the solution of a system of coupled differential equations taking into account the electrical circuit parameters, the various kinetic processes leading to the formation of the upper laser level, and the quenching effects of the impurities evolving in the laser. The evolution of the impurities would depend upon the outgassing parameters of the laser body and the electron and photon energy distribution in the discharge. An attempt was made to formulate a laser model in such a form for simulation in the computer but was abandoned, mainly because of the rather complete lack of data on the rate constants for reactions involving Kr and fluorine with the impurities. Instead, a black-box model in which the experimental results described in chapters 4,5 and 6 are used is tried out as described in the next section.

6.4 Calculation of effectiveness constants for the impurities

The kinetic processes occurring in the laser gas mixture are numerous and complex. For example, if we assume there are 10 major impurities in the gas mixture, along with the three components of the basic gas mix, this would give rise to 78 two body and 286 three body interactions. On the time scales and energy conditions involved it is difficult to rule out many of these possible reactions. Instead of formulating a comprehensive model to account for so many processes, most of which have unknown rate constants, we shall look at the gas mixture from the outside and assign a 'lumped value' for the effect each impurity has on the energy output of the laser. Each value is then calculated using the experimental results. This approach simplifies the problem enormously and is probably the best first step in the solution of complex problems with many interacting variables such as those we consider here. The method does not assume any knowledge of the actual processes in the laser and therefore does not need a detailed knowledge of the laser kinetics.

In order to set up the model we assume that at any given time, each impurity acts on the lasing mixture independently of the others to quench the laser action (either through absorption or by interfering with the preionization or production of the KrF^* states) and that the quenching action is proportional to the partial pressure (wrt He) of the impurity. At the pressures we have studied, the partial pressure of F_2 can drop to 50% of its initial value before affecting the output power (see chapters 4 and

5). With these assumptions, the variation in the pressure of F_2 can be neglected. If E_o is the output energy when no impurities are present in the laser mixture, the output energy at any time when there are impurities present is then given as

$$E = E_o - [k_1 I_1 + k_2 I_2 + \ldots + k_n I_n]$$

where k_1, k_2,...,k_n are the 'effectiveness factors' for the impurities 1, 2, ..., n present in partial pressures of I_1, I_2,..., I_n ppt of He. The effectiveness constant k_i is a measure of the quenching effect of the impurity i in units of mJ/partial pressure of the impurity(with respect to He). Absolute magnitudes of the effectiveness constants will depend upon the gas mix used, the laser cavity resonator optics, and the discharge geometry. It will also depend upon the characteristics of the mass spectrometer if the partial pressure values are not corrected for the difference in sensitivity of the mass spectrometer to the different gases. However, for a given laser system, the calculated effectiveness constants can be used to work out the expected energy from the gas mix if the partial pressures of the impurities in that laser system are known.

We test the above model by using experimental values for two different cases, that for the atomic fluorine laser and that for the KrF laser. Eleven major impurities were identified for both the lasers, which means that at least 11 equations are needed in each case. We set up 12 equations each for the atomic fluorine and KrF lasers derived from 24 different experiments. Table 6.3 gives

the data for the KrF laser. These 12 equations were then solved on the computer using a least squares method as in the case of the mass spectra equations (see chapter 3). The partial pressures used are uncorrected values but they can be corrected using calibration data given in table 3.3.

The results for the He-F_2 mixture were inconclusive, with large standard errors and random changes of the results with changes in data. This is thought to be due to the small magnitude of the effect of these impurities on the energy output of the atomic fluorine laser. This shows that the atomic fluorine laser is insensitive to the impurities. Since there are more than 10 impurities acting simultaneously to reduce the energy output, the standard error of the calculated constants could be large. However, for the He-Kr-F_2 mixtures the results validate the model, as seen from table 6.3 and figure 6.60. The value of E_o is taken as 10 mJ. When all the 12 trials are included, the best results give a calculated standard error of 2 mJ with the quenching constants as given in column 13. The calculated energy values (row 13) agree remarkably well except for trials 2, 10, and 12. Trial 2 used H_2 dopant which is expected to produce SiF_4 whose effect is not taken into account in the calculation. Trials 10 and 12 are for the basic mixes. This is again because of the smaller partial pressures of the impurities in the basic mix. When these three trials are omitted, the standard error in calculated values decreases to 0.3 mJ. The corresponding quenching coefficients and calculated energy values are given in column 13 and row 13 respectively. Because of their dependence on the data chosen the

calculated quenching constants are not considered to be reliable except for N_2, SF_6, and CO_2. Part of the inconsistency is probably caused by the lack of data on the background values of H_2O, HF, CO, H_2, and SiF_4. However, these calculations show that this technique gives a simple method of determining the quenching constants for the various impurities, provided the assumptions are valid and the partial pressure values of all the quenchers are accurately known. It also shows that, in the case of the KrF laser, the assumptions about the action of the quenching impurities are reasonably valid.

It is difficult to come to definite conclusions about the physical nature of the effects of the impurities since any or all of the processes described in section 6.3 could be taking place for one or more of the impurities. In general, one could write

$E = E_o \exp[-(\bar{\sigma}_1 + \bar{\sigma}_2 + \ldots) I_i]$

for impurity i alone, where $\bar{\sigma}_1$, $\bar{\sigma}_2$,... are quenching cross sections due to the various unknown processes. When I_i is small enough, this would reduce to a linear form

$E = E_o - k_i I_i$, where $k_i = -E_o \sum_i \bar{\sigma}_i$

Therefore, we can consider the quenching constants as the sum (dimensionally adjusted) of the effects due to the various processes described in section 6.3. The linear nature of the quenching effects is thus likely to be due to the small partial pressures of the impurities.

Table 6.3

Impurity effectiveness constants for the KrF laser

Trials	1	2	3	4	5	6	7	8	9	10	11	12	[13]*	[14]*
	Measured partial pressures (ppt of He)													
N_2	1.3	.77	25.	1.4	1.3	1.8	1.1	2.6	2.8	1.1	.77	.86	.12	.15
H_2O	1.2	1.3	.99	1.0	1.3	1.3	1.6	1.2	.79	1.4	.81	1.3	-	-
H_2	1.6	1.8	1.7	1.2	1.8	1.8	1.7	1.7	.28	1.3	.46	1.7	-	-
HF	4.0	4.5	3.5	4.6	4.3	3.8	4.5	4.1	3.5	6.2	4.4	4.0	-.09	.03
COF_2	0.0	.03	.03	.04	.25	.08	0.0	.09	.04	.14	0.0	0.0	.81	9.3
CF_4	12.	.11	.10	.13	.11	.09	.11	.14	.12	.27	.08	.11	-.04	.03
CO_2	1.4	1.4	1.3	1.4	2.1	9.1	1.8	1.6	.92	1.8	.94	1.4	.98	.94
O_2	.27	.16	.31	.13	.22	.30	6.5	0.5	.60	.21	.19	.18	.04	.16
SF_6	0.0	0.0	0.0	13.	0.0	0.0	0.0	0.0	0.0	.01	0.0	0.0	.15	.15
CO	1.6	1.2	1.5	.97	3.0	1.0	1.5	1.5	1.4	1.3	1.1	1.2	.82	-.03
NO	.05	.07	.09	.06	.07	.13	.14	.07	.06	.08	.06	.07	-	-
Energy mJ[12]*	8.0	4.5	4.7	6.0	5.5	0.3	7.0	7.0	8.0	8.2	9.0	10.0		
[13]*	8.0	7.9	4.7	6.0	5.5	0.3	7.0	7.2	7.9	7.5	8.5	7.9		
[14]*	8.0	-	4.7	6.0	5.4	0.3	7.0	7.1	8.2	-	8.9	-		

* Columns 13 and 14 give computed effectiveness coefficients and rows 13 and 14 give the corresponding calculated energies in mJ. The measured energy is given in column 12

6.5 Conclusions

The addition of impurities to pure He-F_2 and He-Kr-F_2 mixtures reveal that CO_2 is by far the most important deleterious impurity for both atomic fluorine and KrF lasers. It is found that He-F_2 systems can tolerate higher levels of impurities than the KrF system. In order of decreasing effectiveness, the impurities are CO_2, H_2, CO, O_2, SF_6, CF_4, and N_2 for He-F_2 and He-Kr-F_2 mixtures. Of these H_2 and CO reacts with F_2 as expected, depleting it, even with no discharges. The pulse-to-pulse variations of a KrF laser are about $\pm 50\%$ when 0.6 torr of CO_2 is the dopant, whereas with H_2 impurity, the variations are less even than those for the basic mix. The rates of formation of various impurity species evolving when the dopants are added clarify the impurity evolution processes in the basic mix discussed in chapters 4 and 5. The impurities are found not to absorb at the laser wavelengths. They seem to quench the preionizing radiation, and in the case of CO_2, act as a sink of electrons in the main discharge. Effectiveness constants have been introduced to describe the effects of the various impurity (contaminant) species on laser output energy. The calculated effectiveness constants show that CO_2 and COF_2 are the compounds with the worst effects on the discharge (energy drop of ~0.9 mJ/ppt wrt He). These calculations are however only an indication of what is possible because of the lack of accurate data for the partial pressures of H_2O, HF, CO and SiF_4.

The results discussed so far in this thesis are summarised in the next chapter. On the basis of the results a design for a compact transverse discharge laser with long lifetime, high efficiency and capable of working at high repetition rates is given in Appendix A.4.

Figures 6.1 to 6.30
Partial pressures of species detected in a $He-F_2$ mixture after the addition of different dopants in version LV4.
Top right hand corner of each figure labelled with name of detected species. Top and bottom figures show results from the same dopants, each pair of curves labelled with the name of dopant. Discharge started within 10 minute of first mass scan.

FIG 6·1

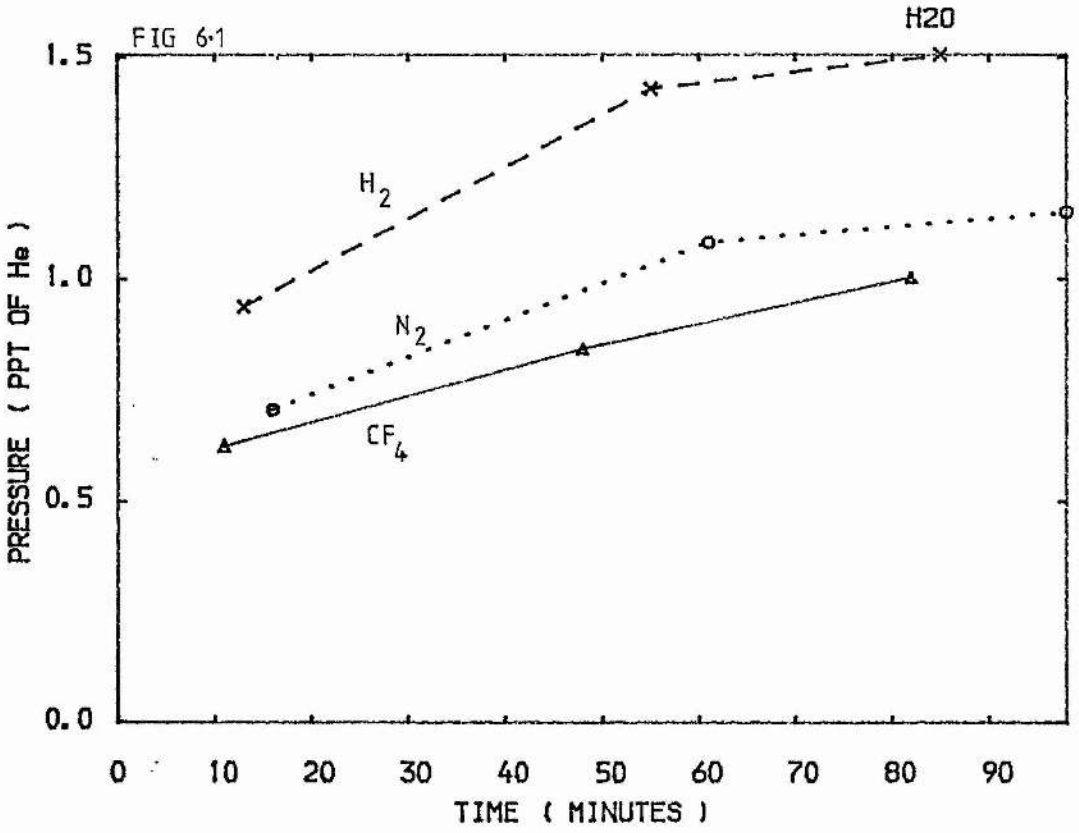
H20
1.5
1.0
0.5
0.0
H_2
N_2
CF_4
PRESSURE (PPT OF He)
0
10
20
30
40
50
60
70
80
90
TIME (MINUTES)

FIG 6·2

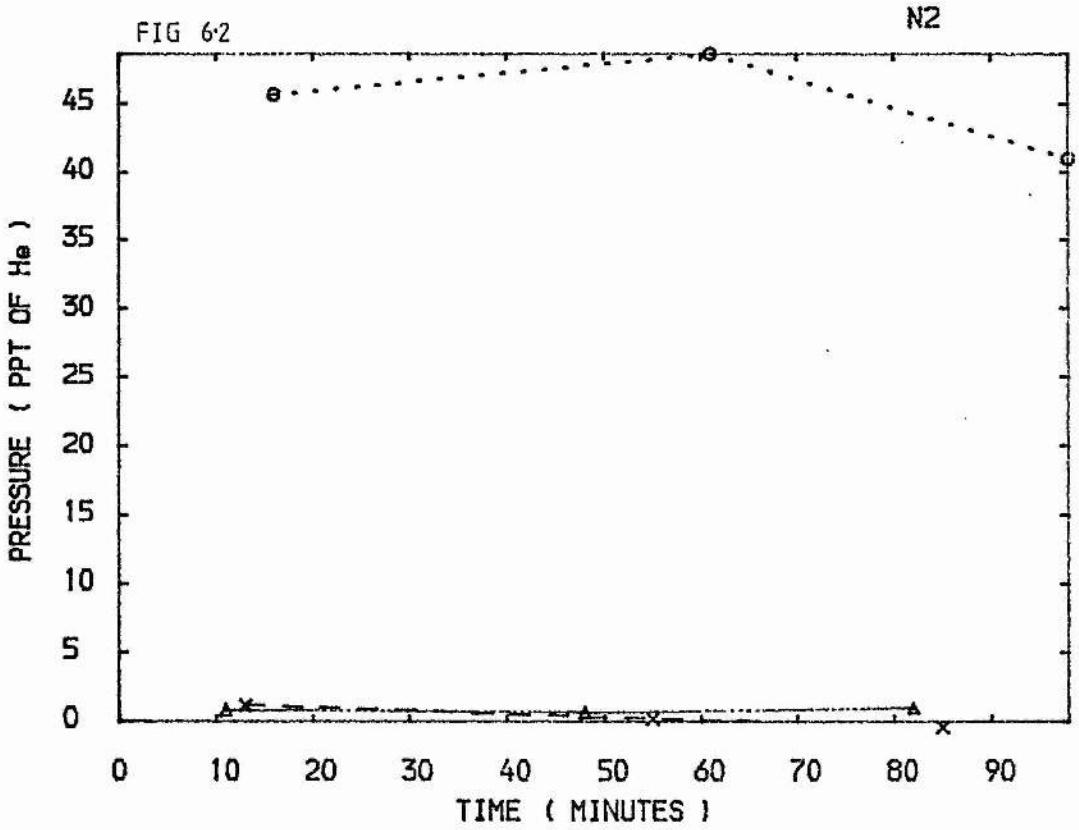
N2
45
40
35
30
25
20
15
10
5
0
PRESSURE (PPT OF He)
0
10
20
30
40
50
60
70
80
90
TIME (MINUTES)

FIG 6·3

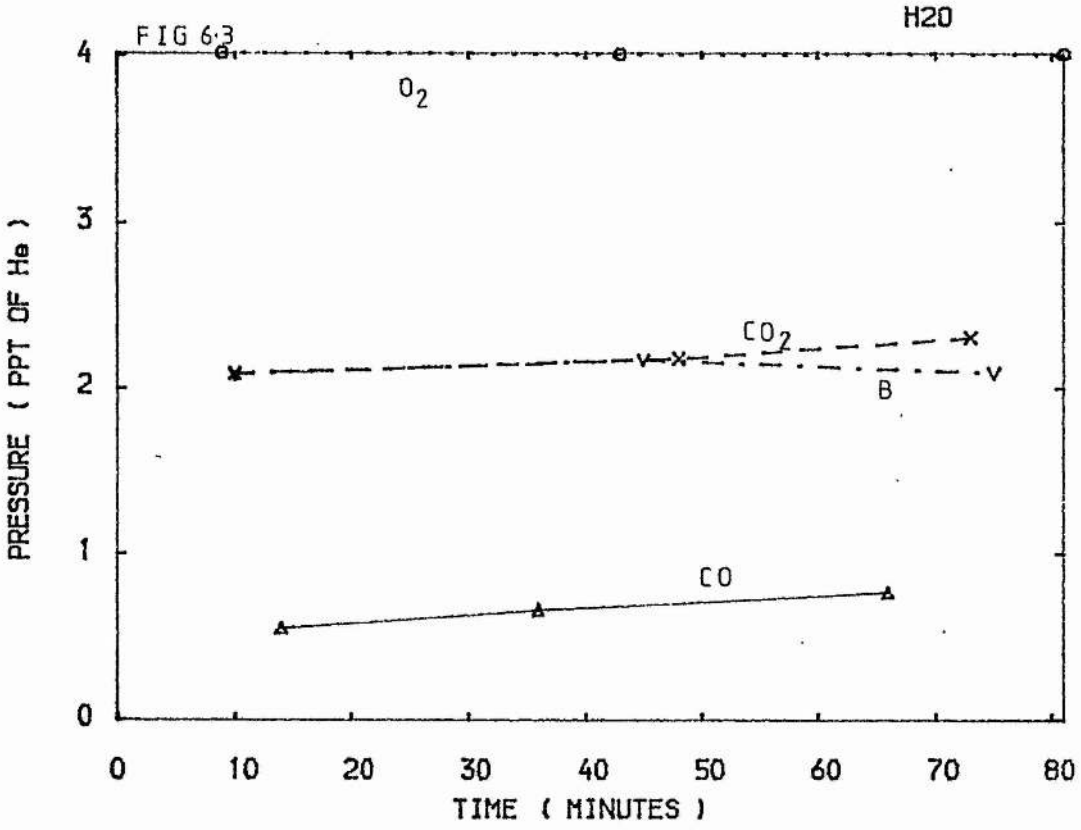
H20
O_2
CO_2
B
CO
PRESSURE (PPT OF He)
TIME (MINUTES)
0
1
2
3
4
0
10
20
30
40
50
60
70
80

FIG 6·4

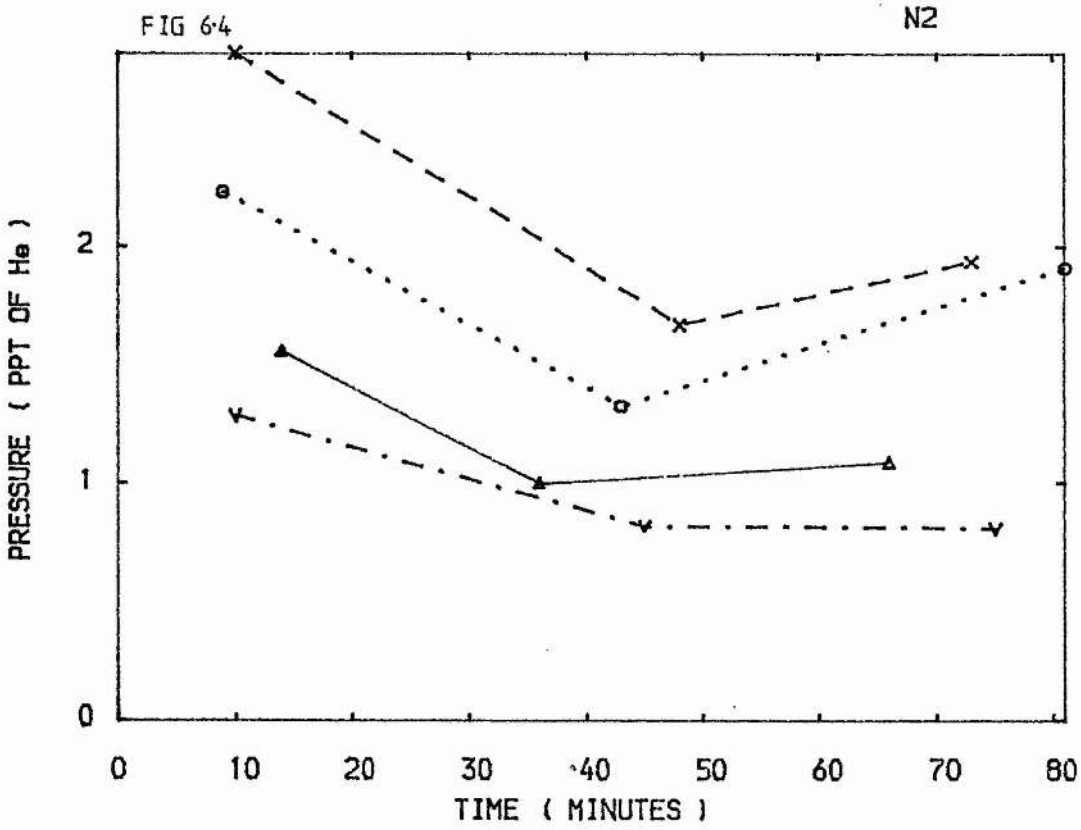
N2
PRESSURE (PPT OF He)
TIME (MINUTES)
0
1
2
0
10
20
30
40
50
60
70
80

FIG 6·5

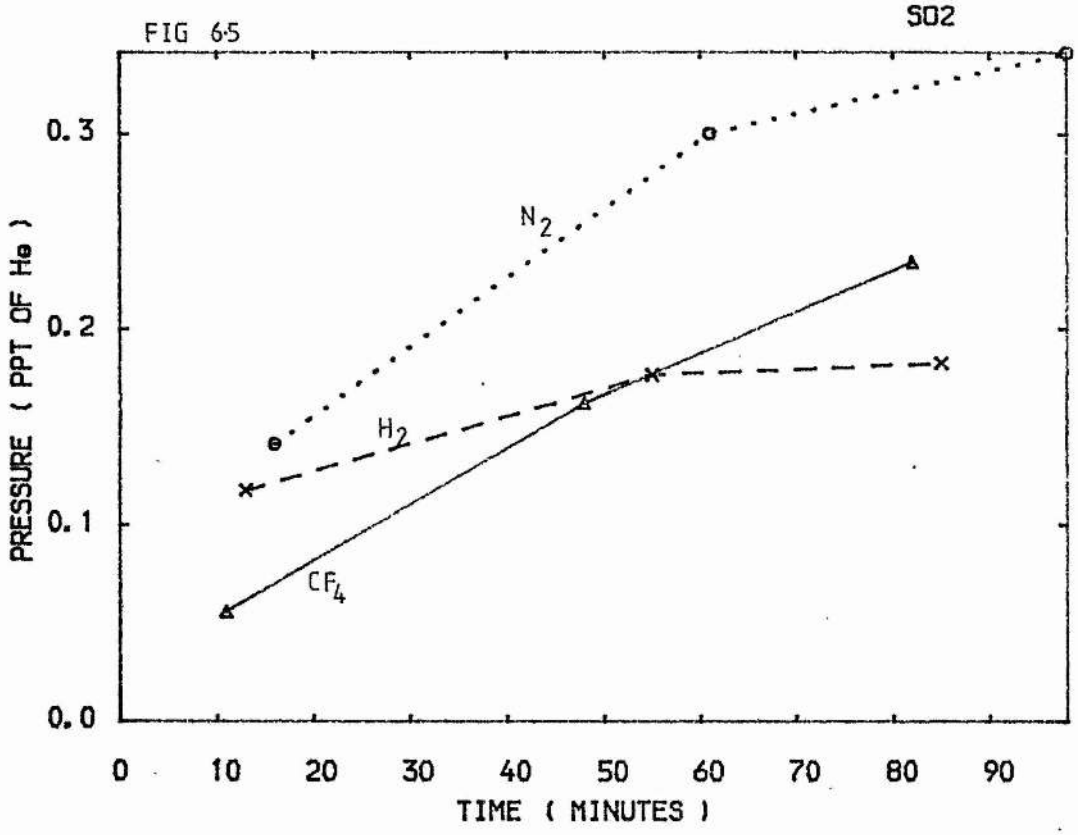
SO2
0.3
0.2
0.1
0.0
PRESSURE (PPT OF He)
N_2
H_2
CF_4
0
10
20
30
40
50
60
70
80
90
TIME (MINUTES)

FIG 6·6

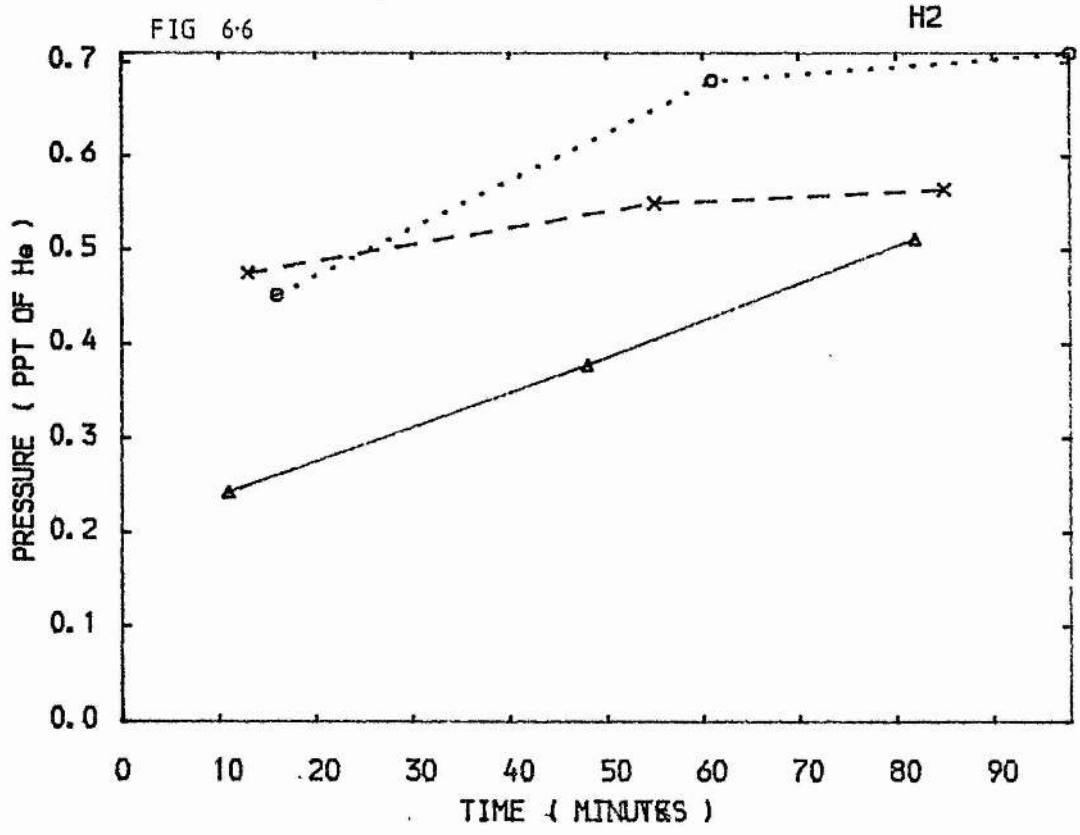
H2
0.7
0.6
0.5
0.4
0.3
0.2
0.1
0.0
PRESSURE (PPT OF He)
0
10
20
30
40
50
60
70
80
90
TIME (MINUTES)

FIG 6·7

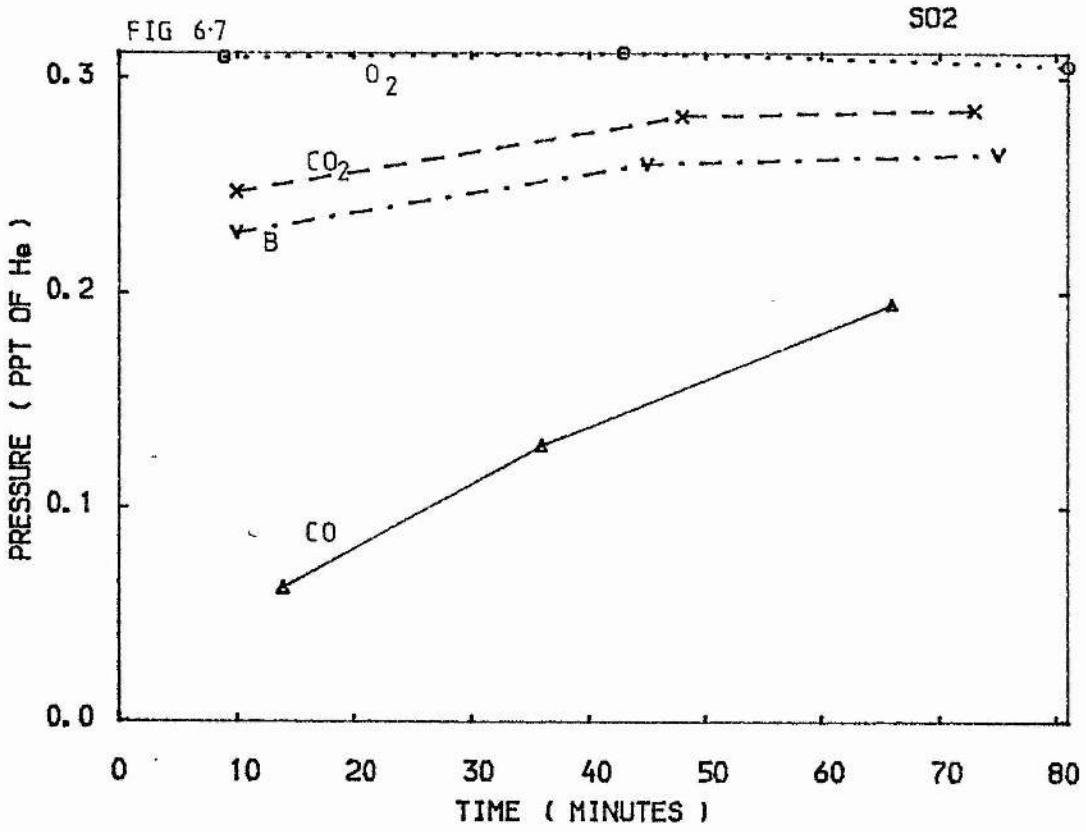
SO2
O2
CO2
B
CO
0.3
0.2
0.1
0.0
PRESSURE (PPT OF He)
0
10
20
30
40
50
60
70
80
TIME (MINUTES)

FIG 6·8

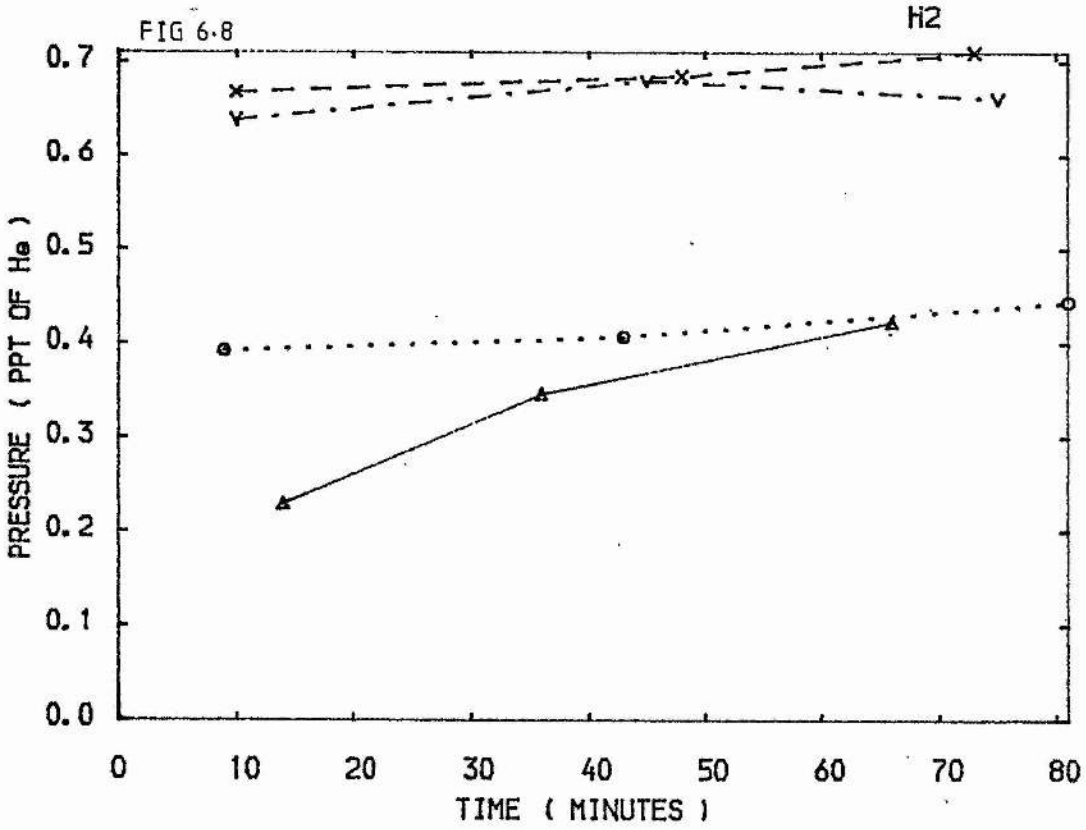
H2
0.7
0.6
0.5
0.4
0.3
0.2
0.1
0.0
PRESSURE (PPT OF He)
0
10
20
30
40
50
60
70
80
TIME (MINUTES)

FIG 6·9

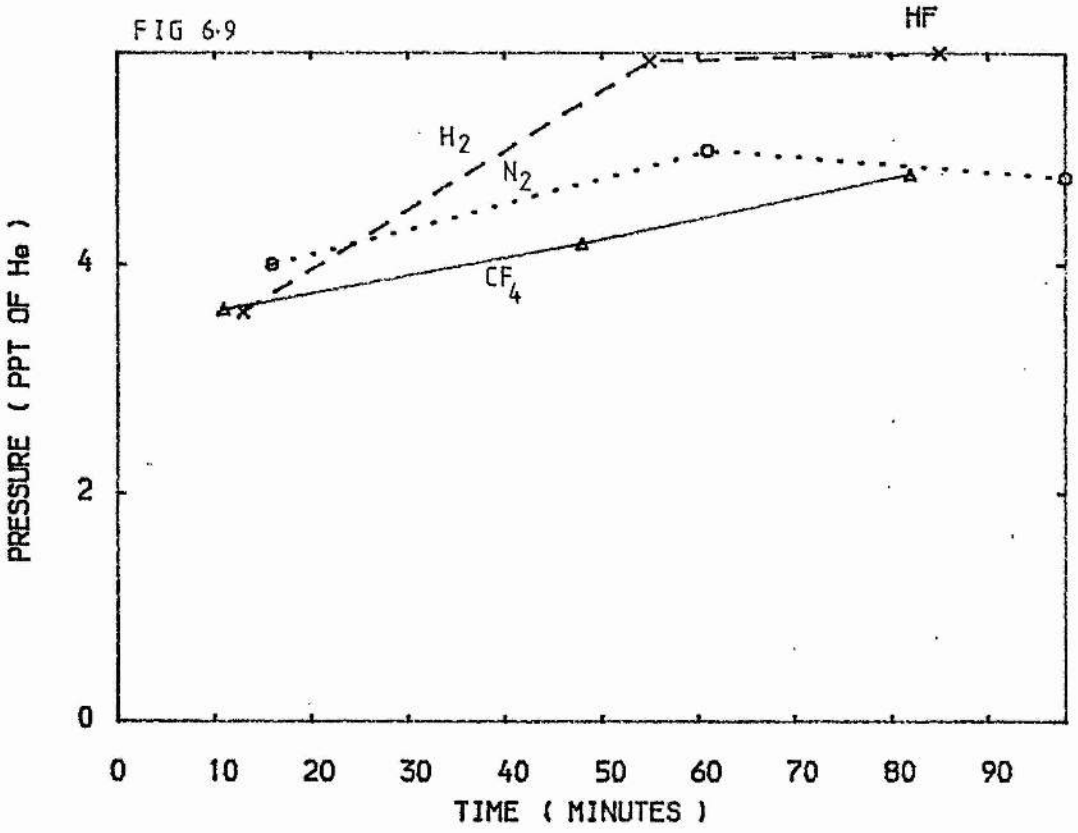

FIG 6·10

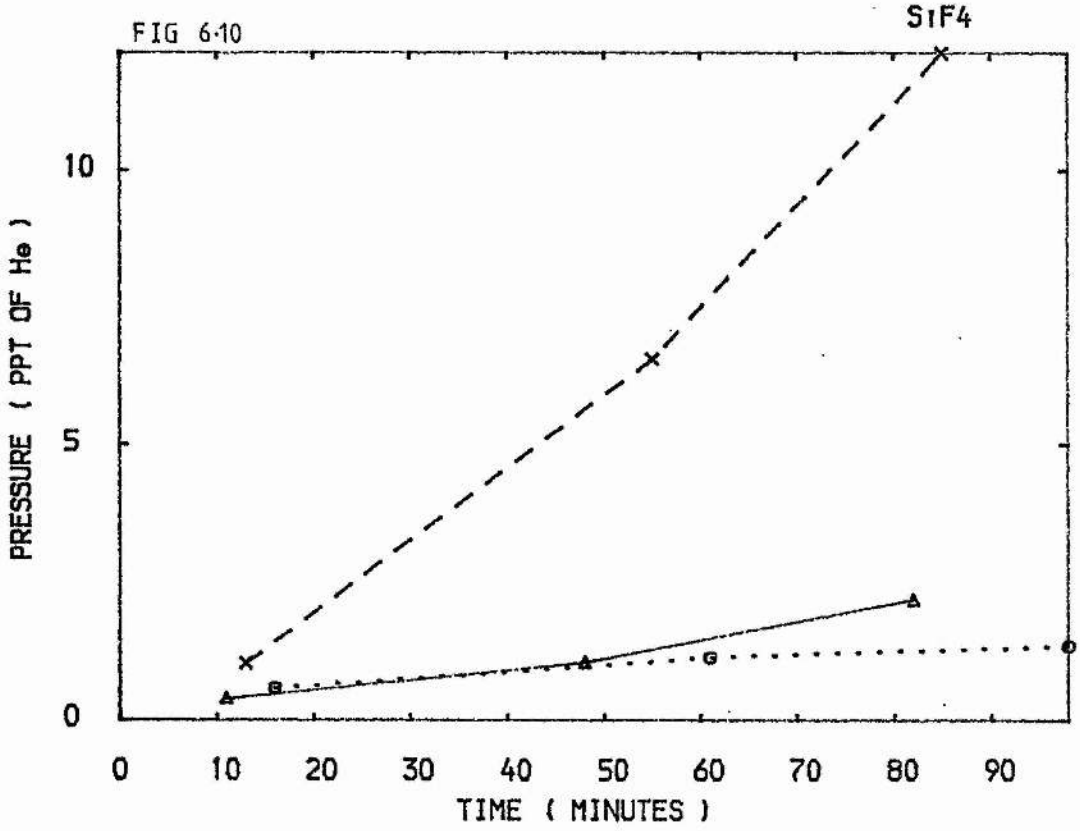

FIG 6·11

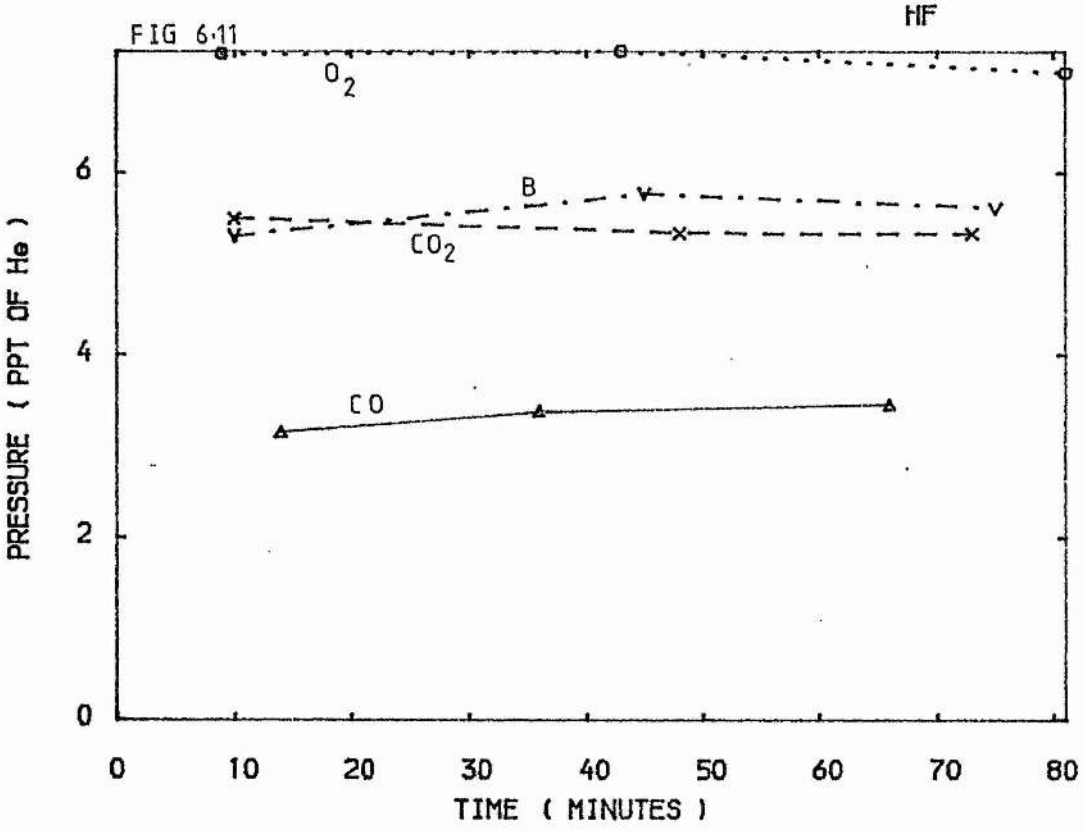

FIG 6·12

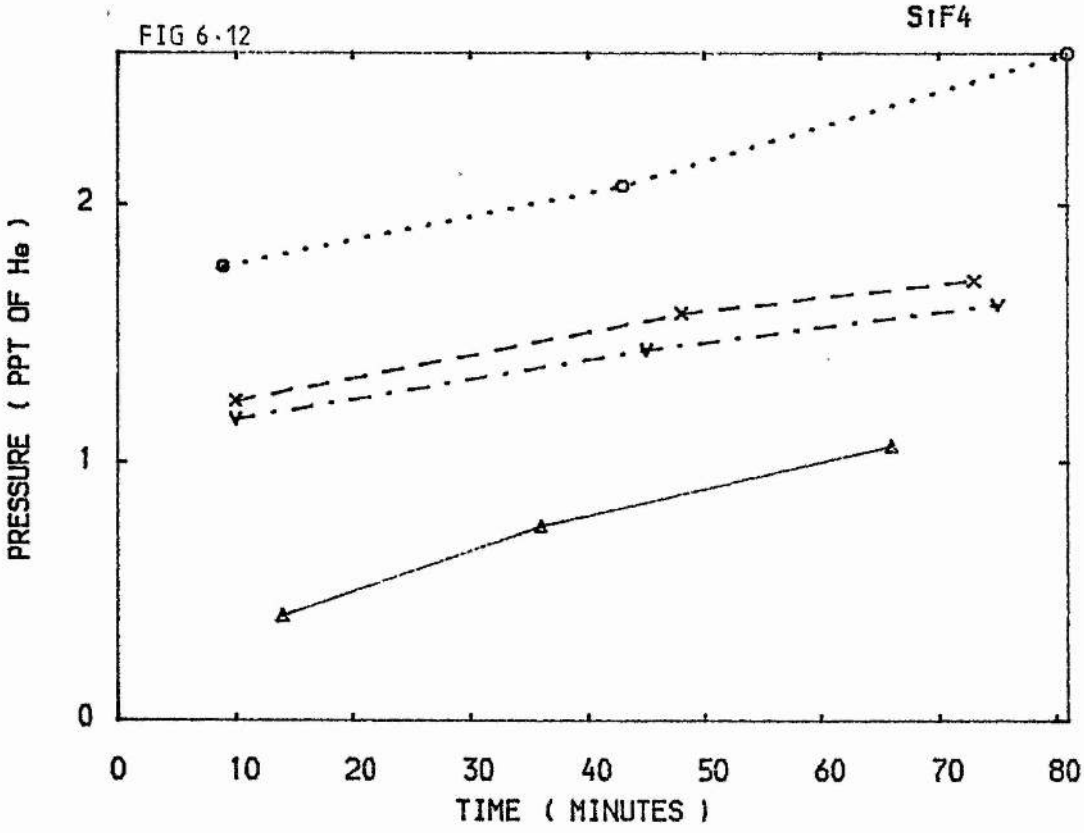

FIG 6·13

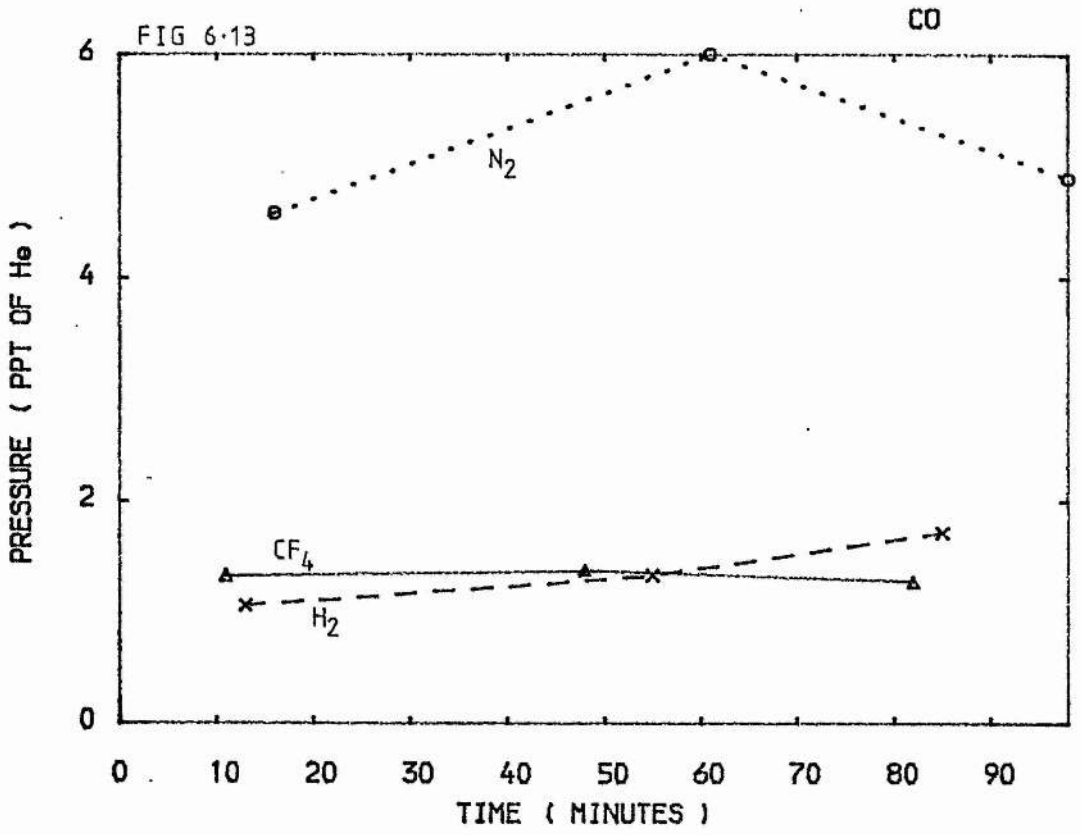

FIG 6·14

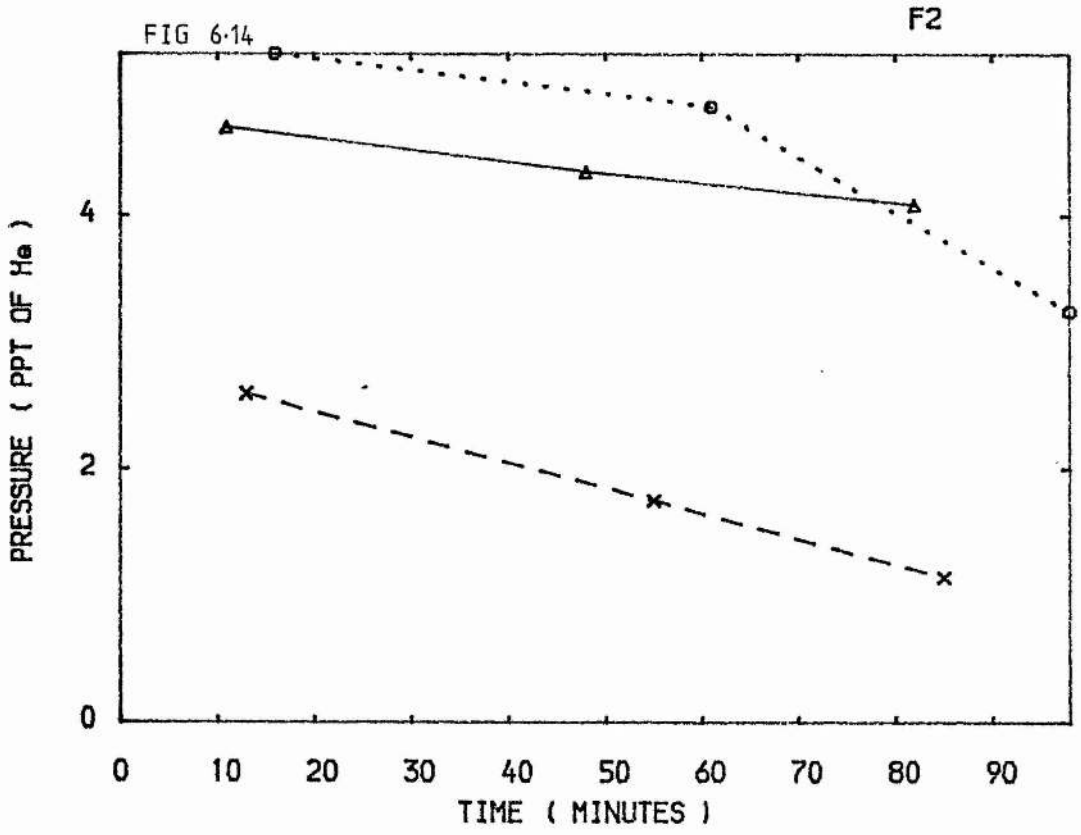

FIG 6·15

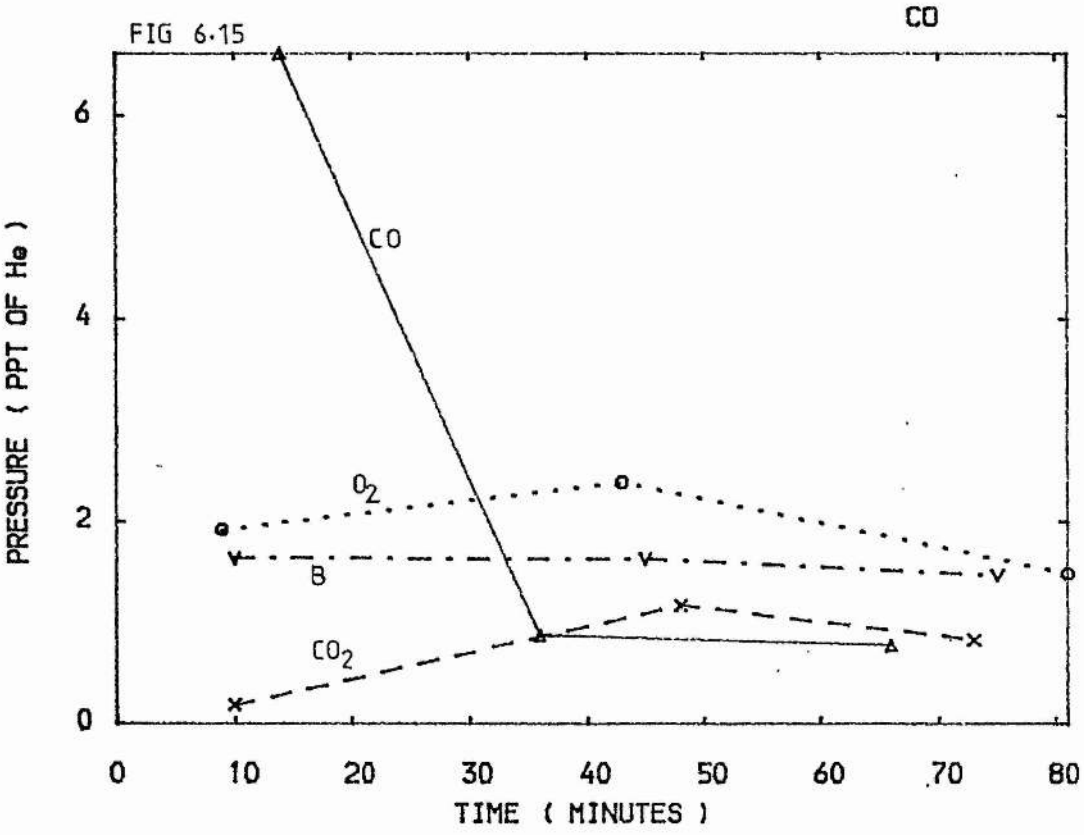

FIG 6·16

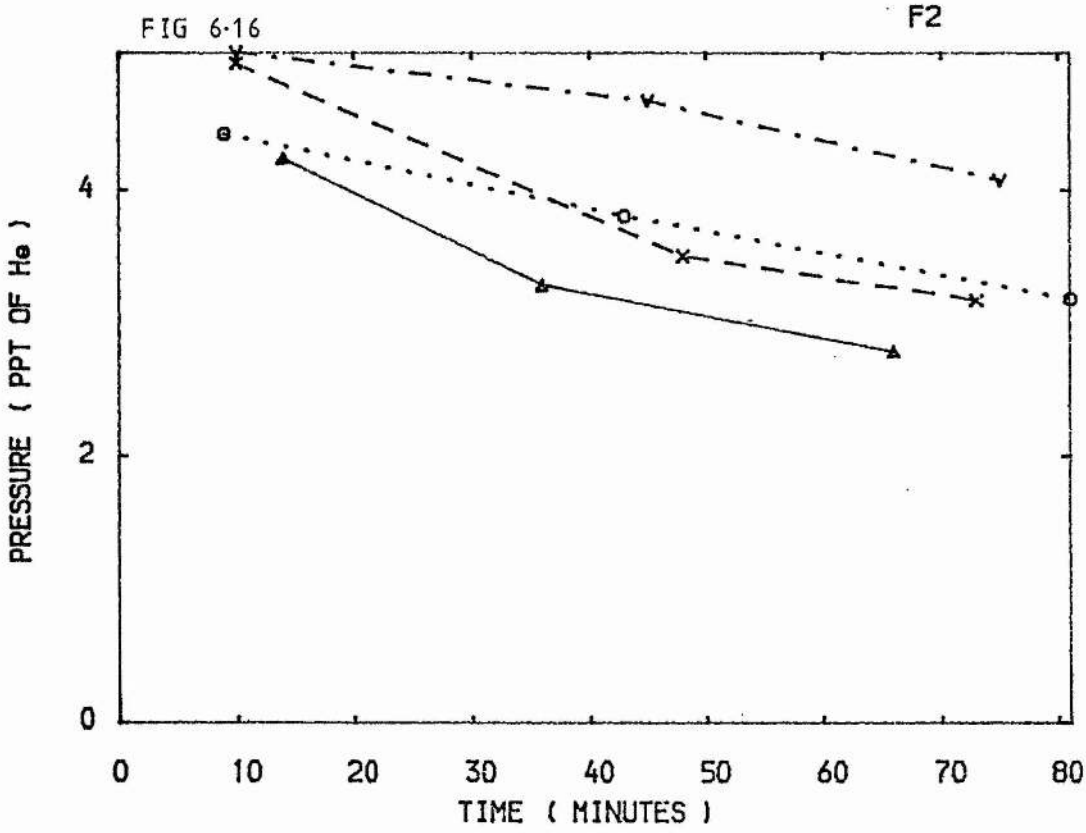

FIG 6·17

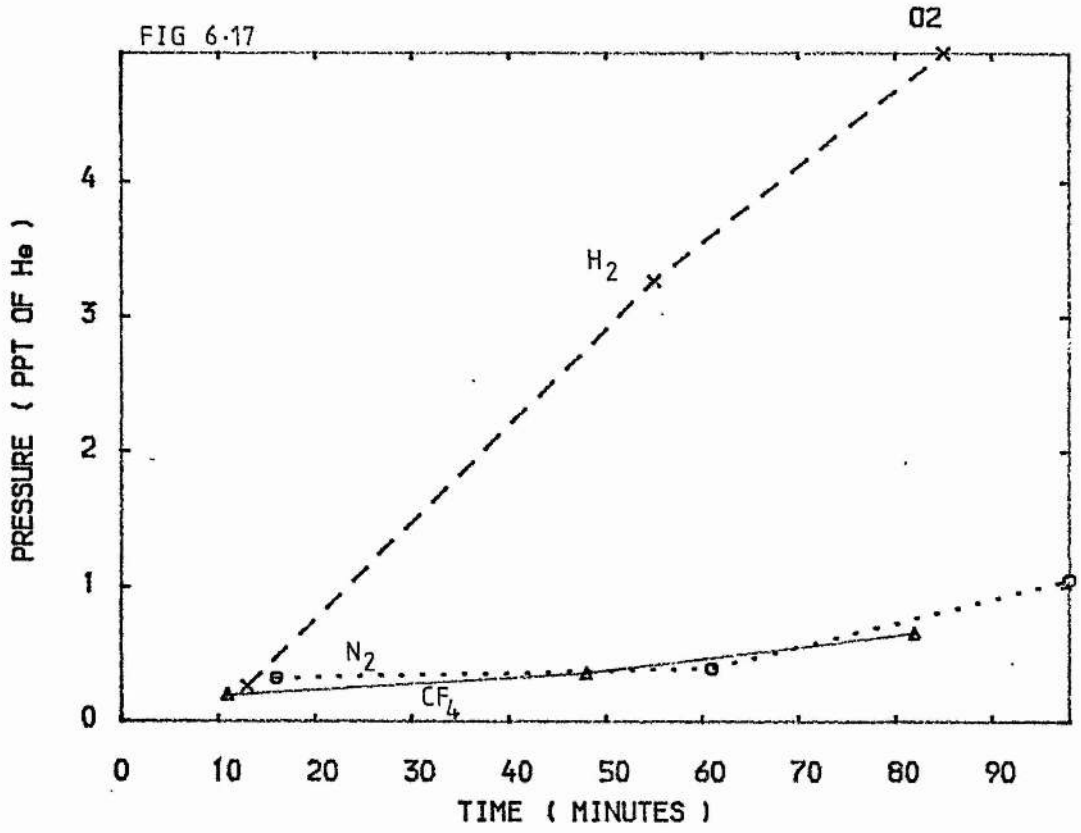

FIG 6·18

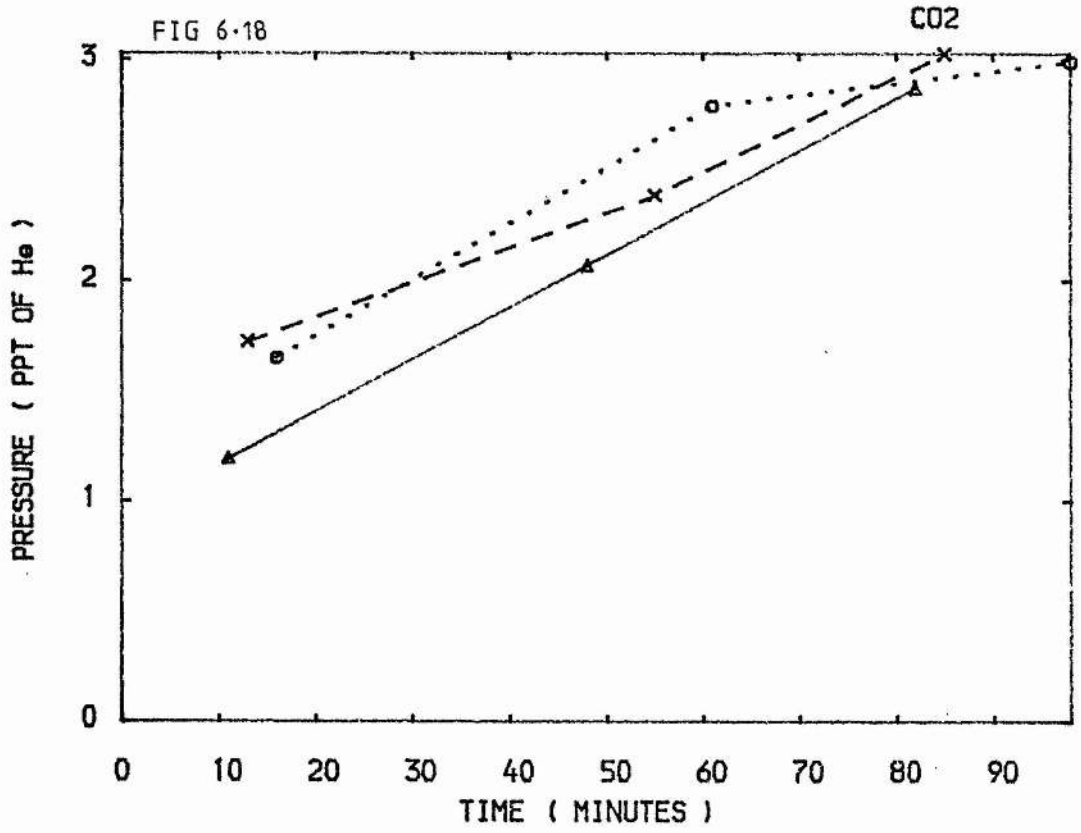

FIG 6·19

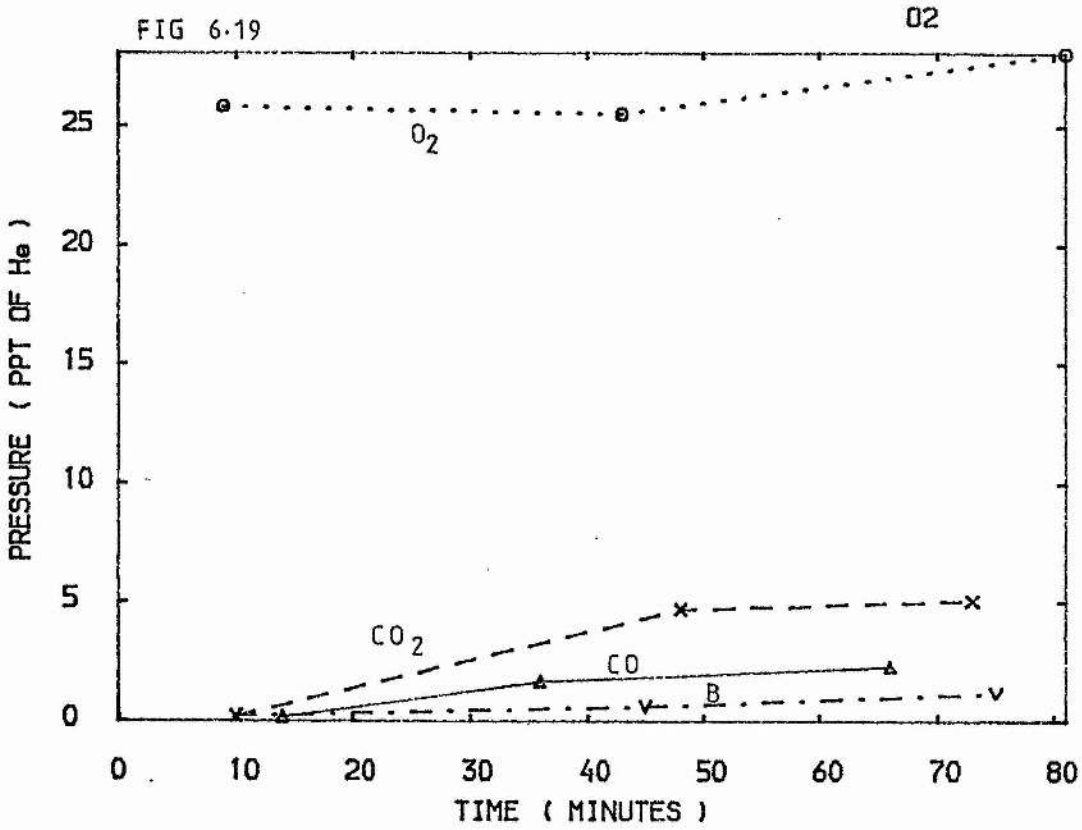

FIG 6·20

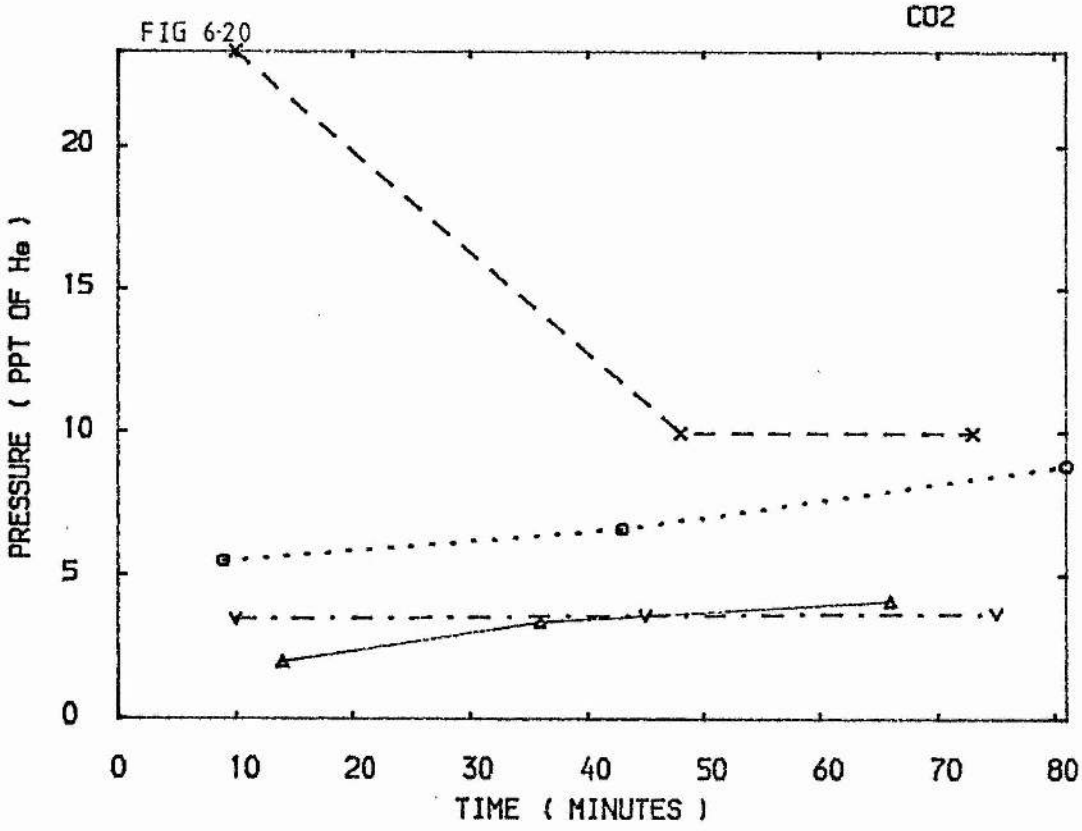

FIG 6·21

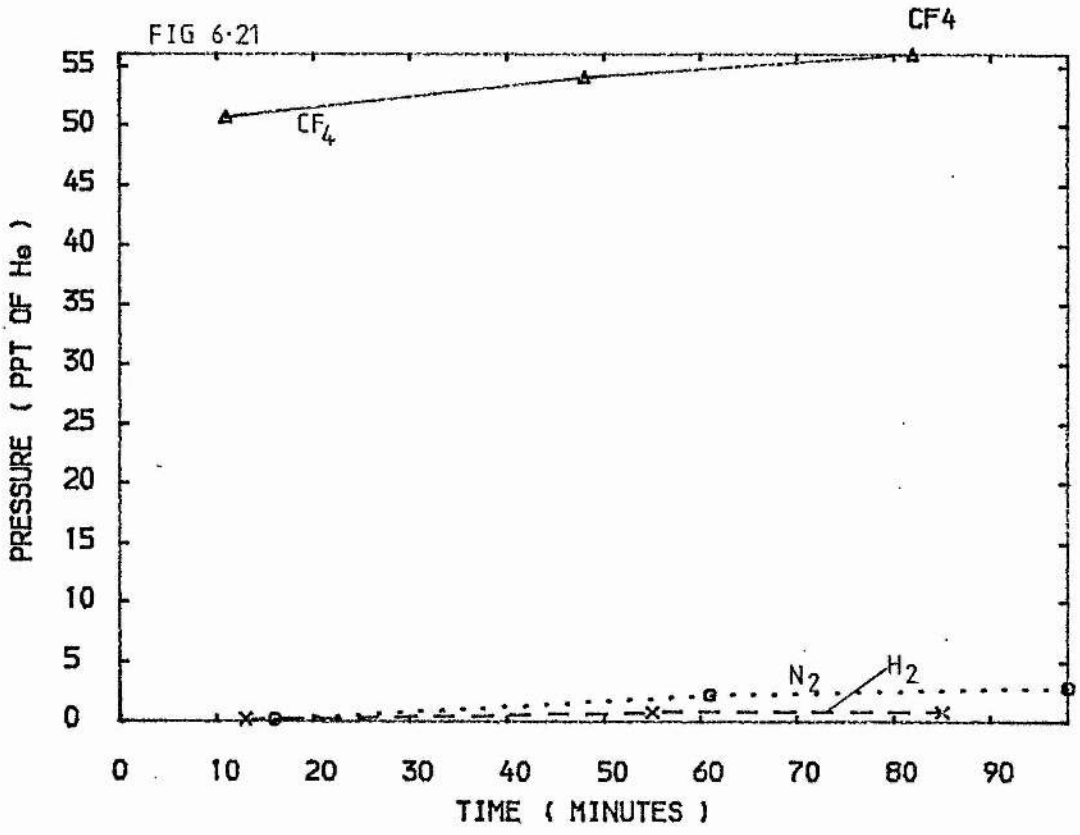

FIG 6·22

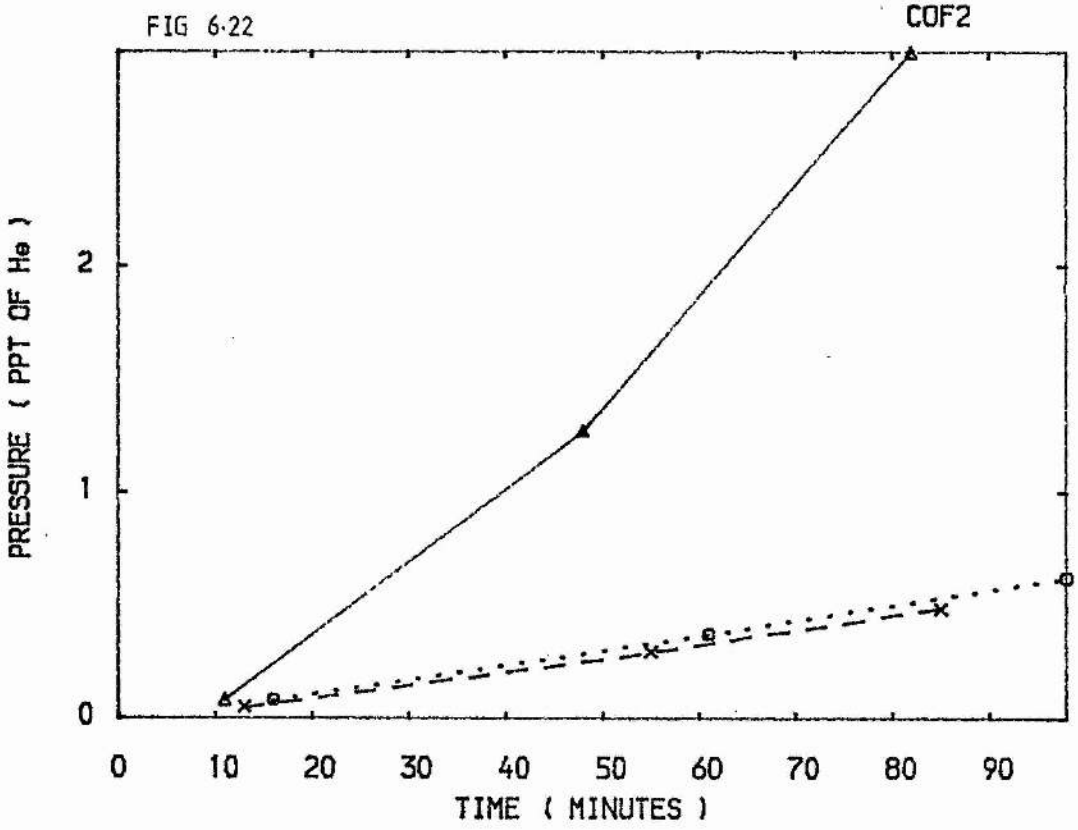

FIG 6·23

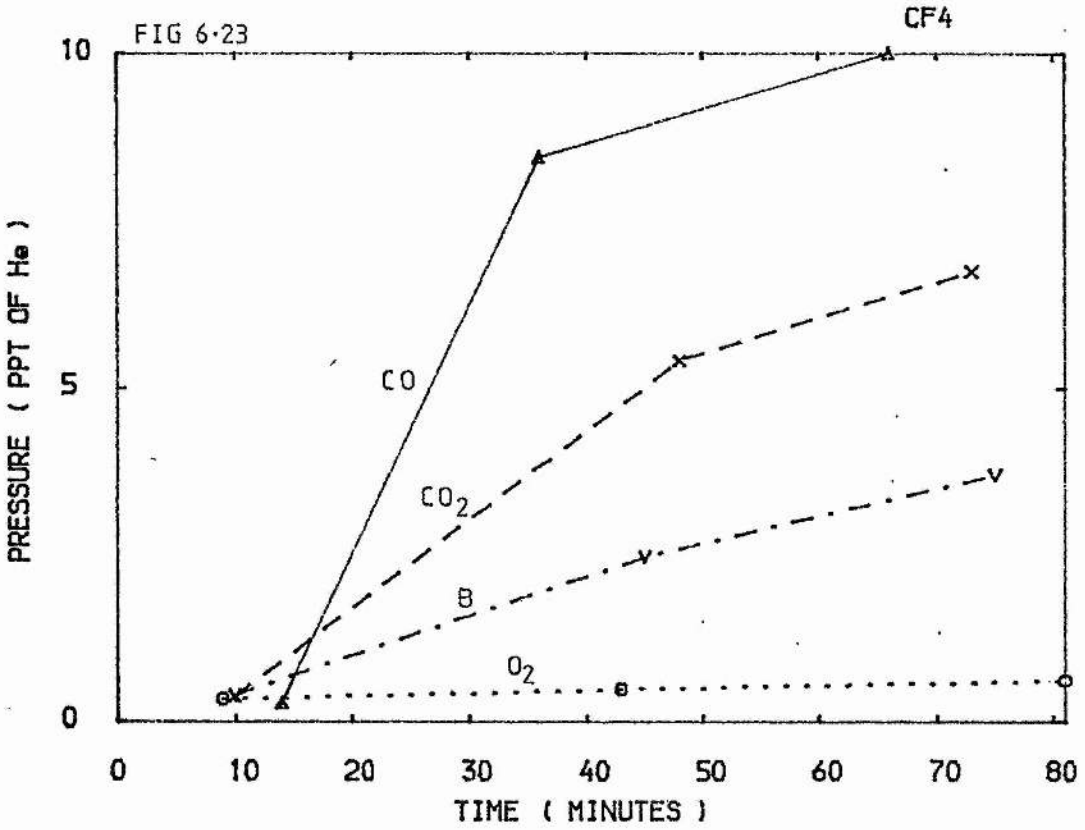

FIG 6·24

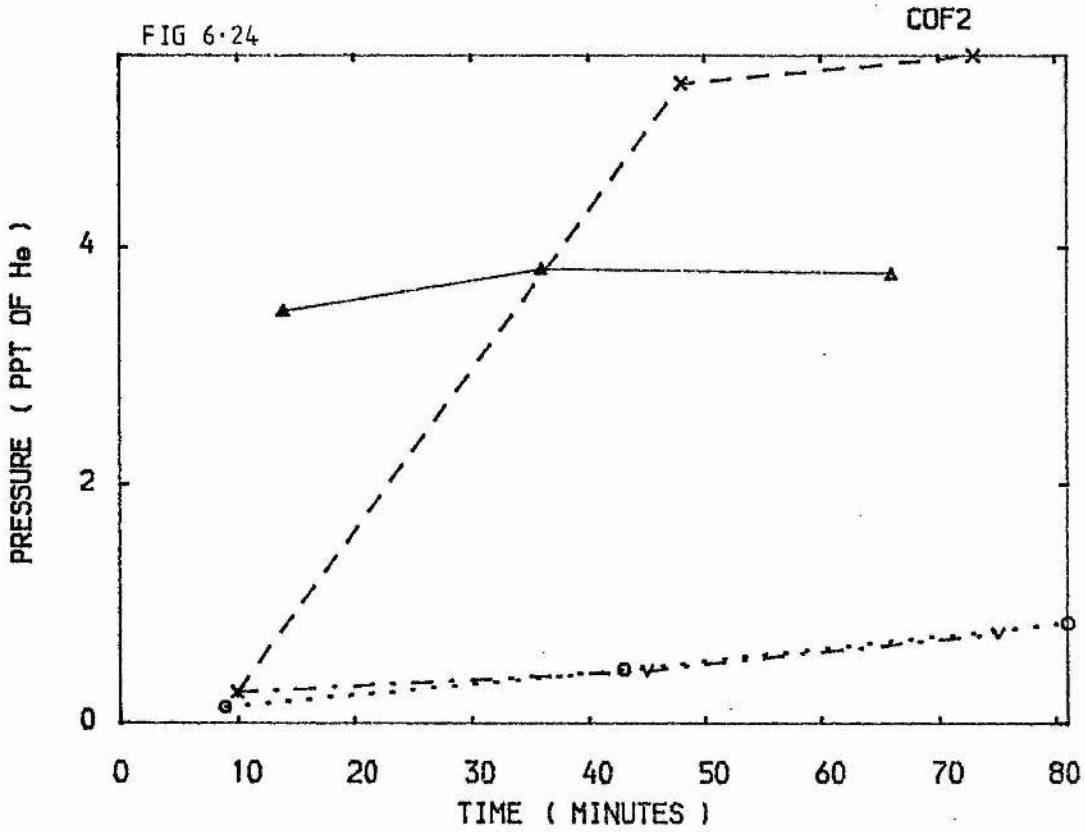

FIG 6·25

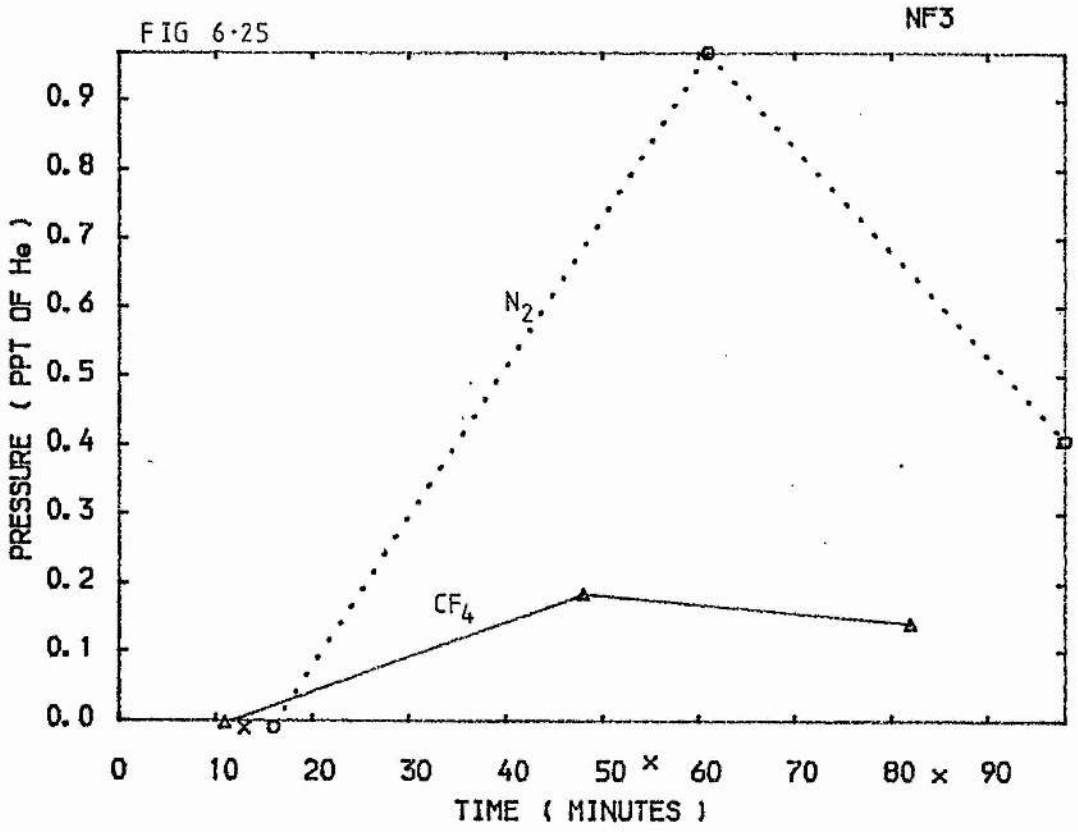

FIG 6·26

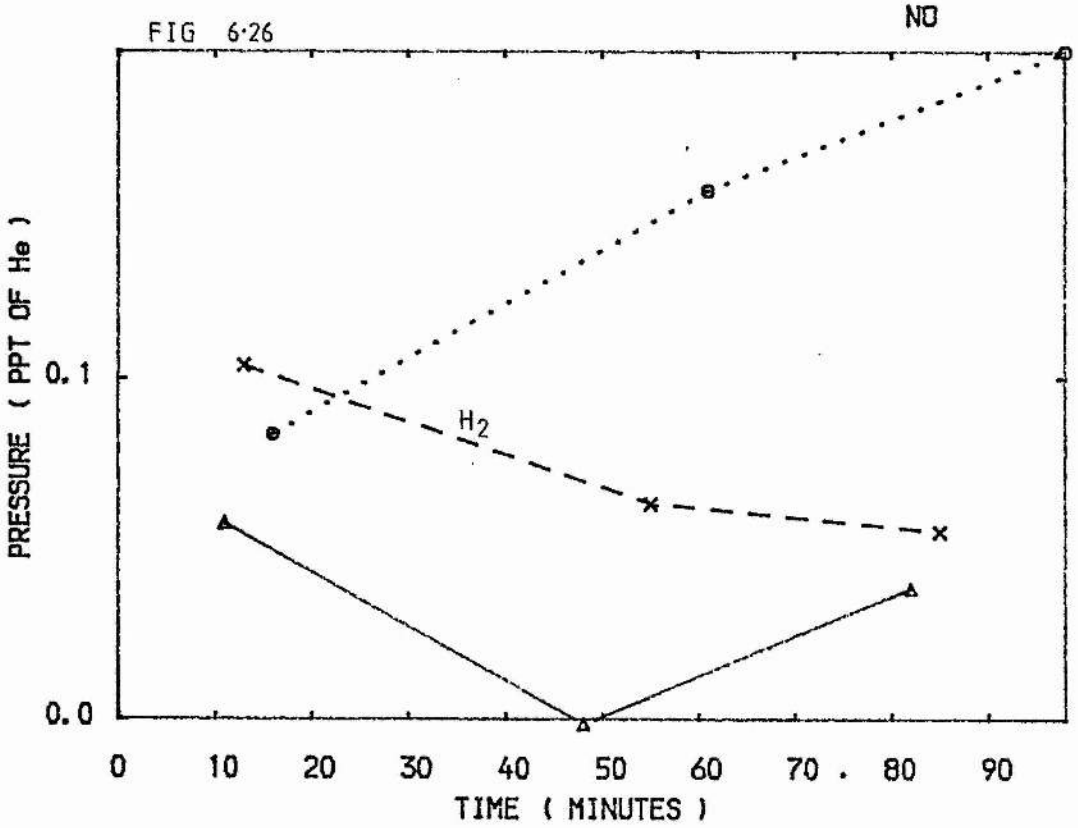

FIG 6·27

OF2

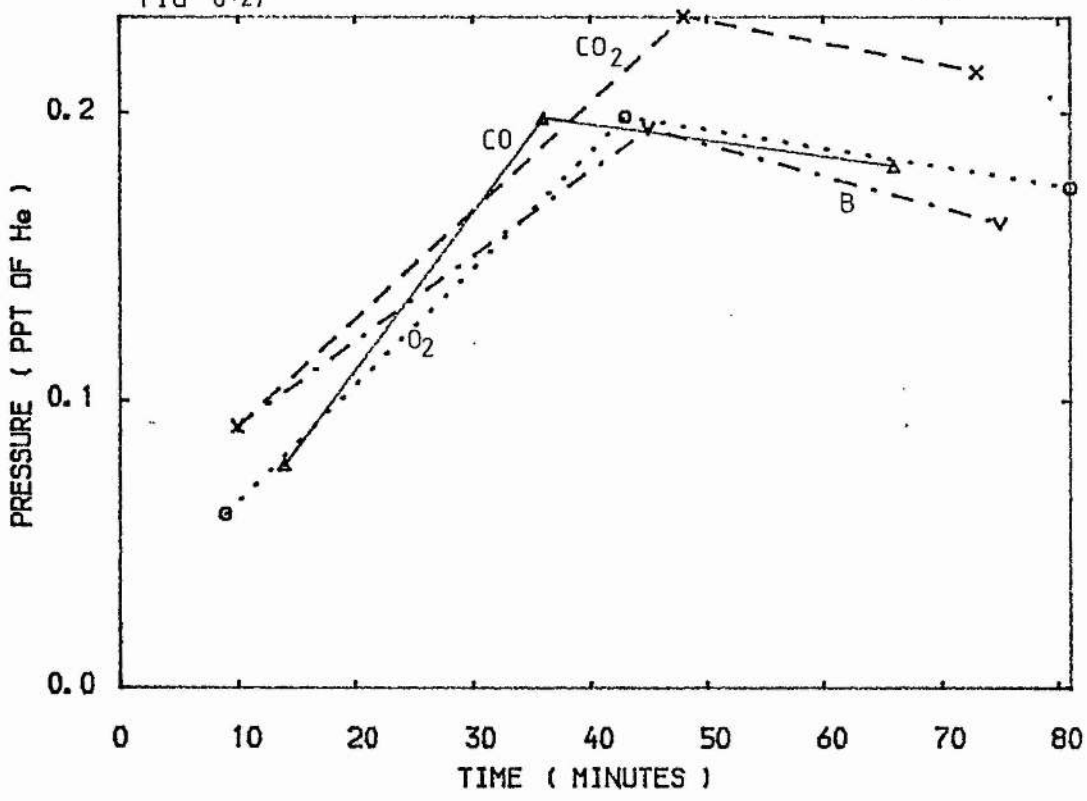

FIG 6·28

NO

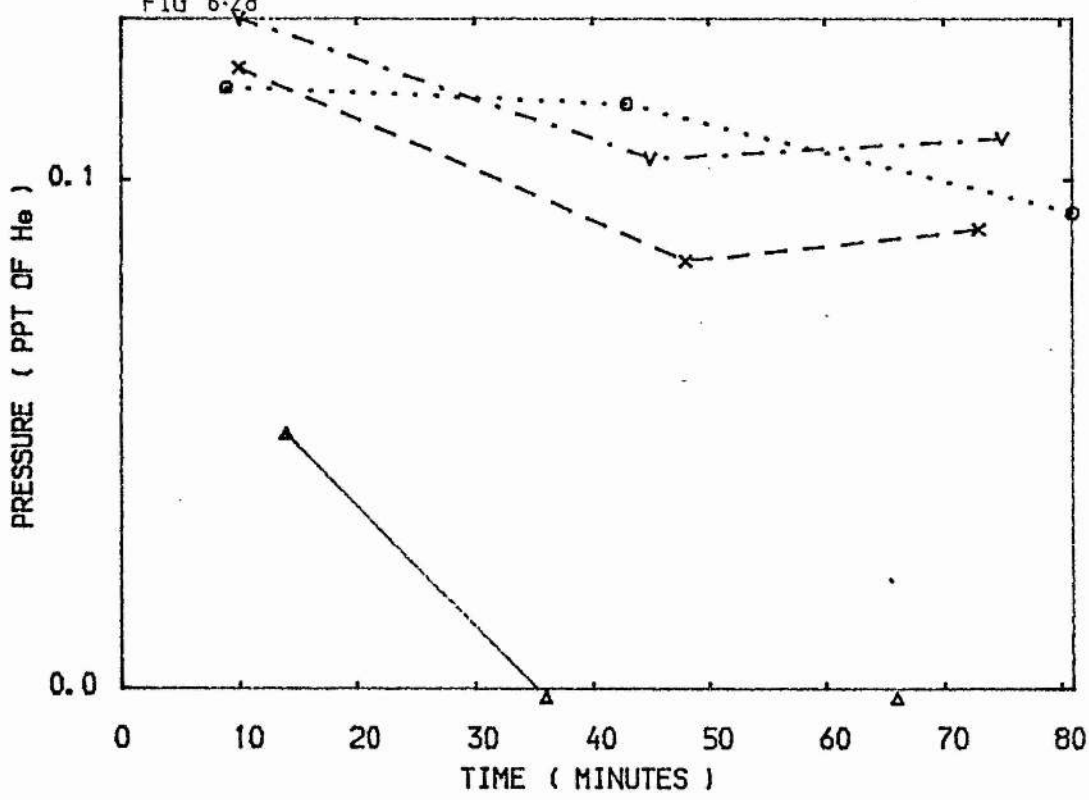

FIG 6·29

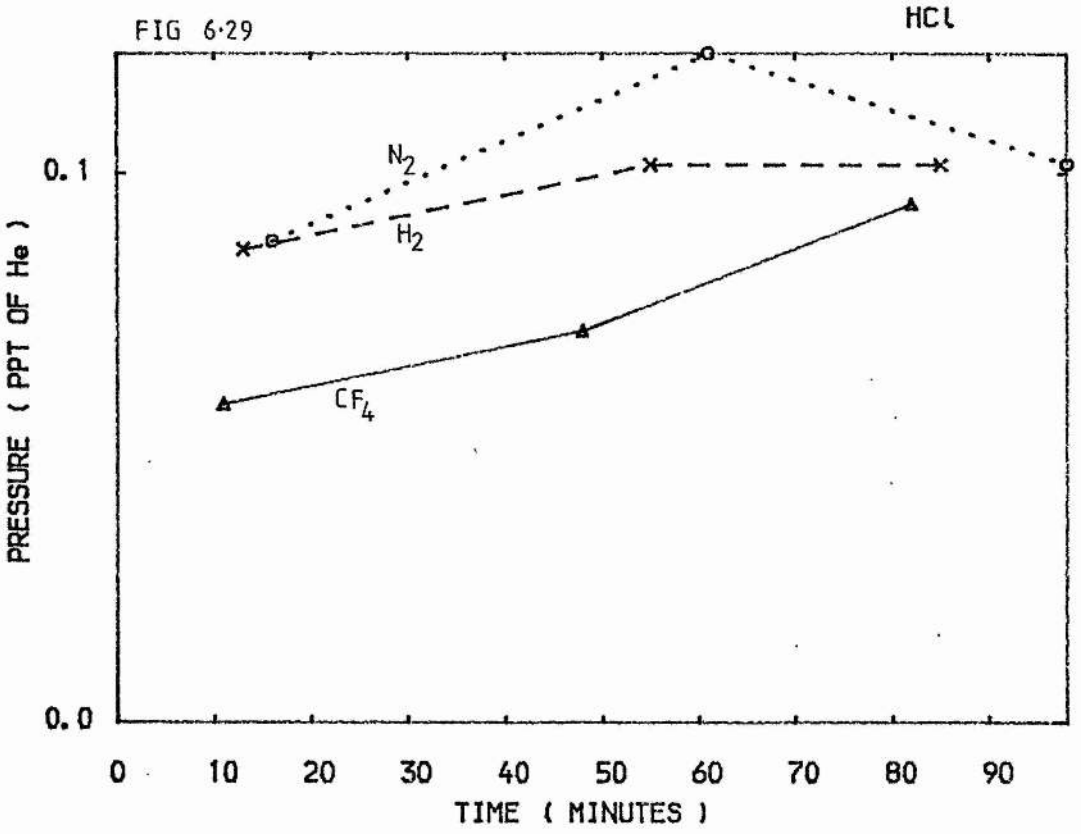

FIG 6·30

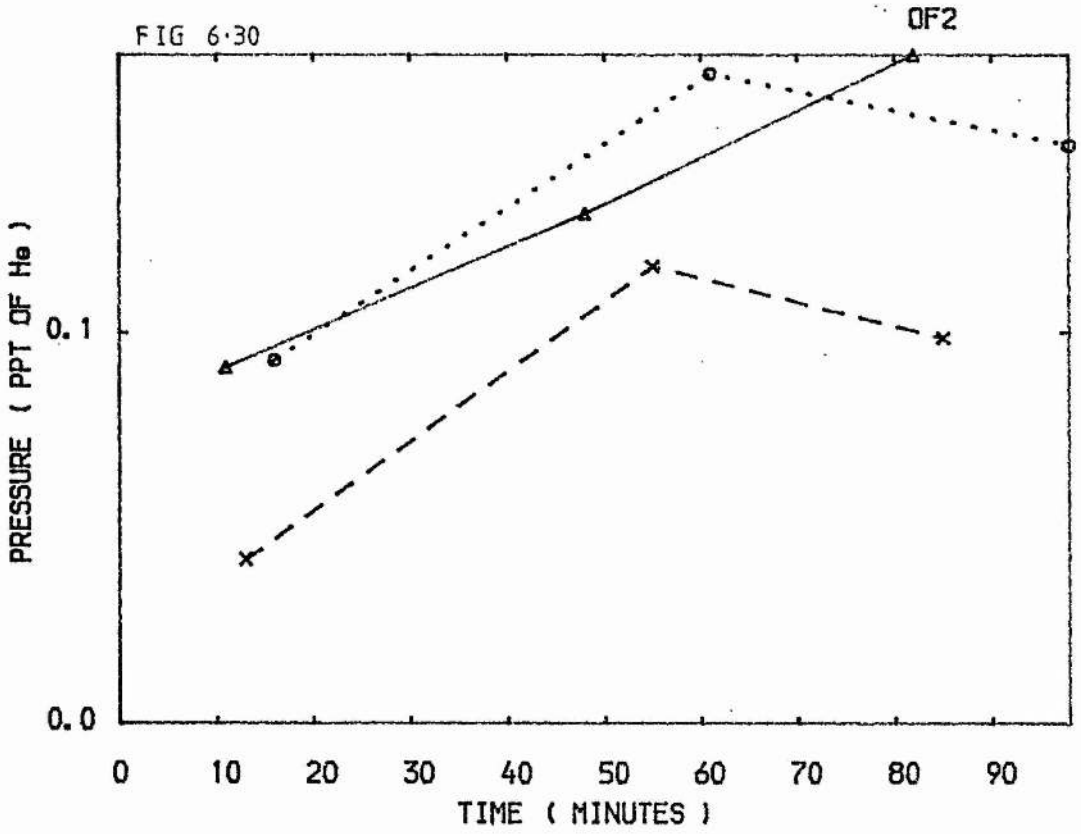

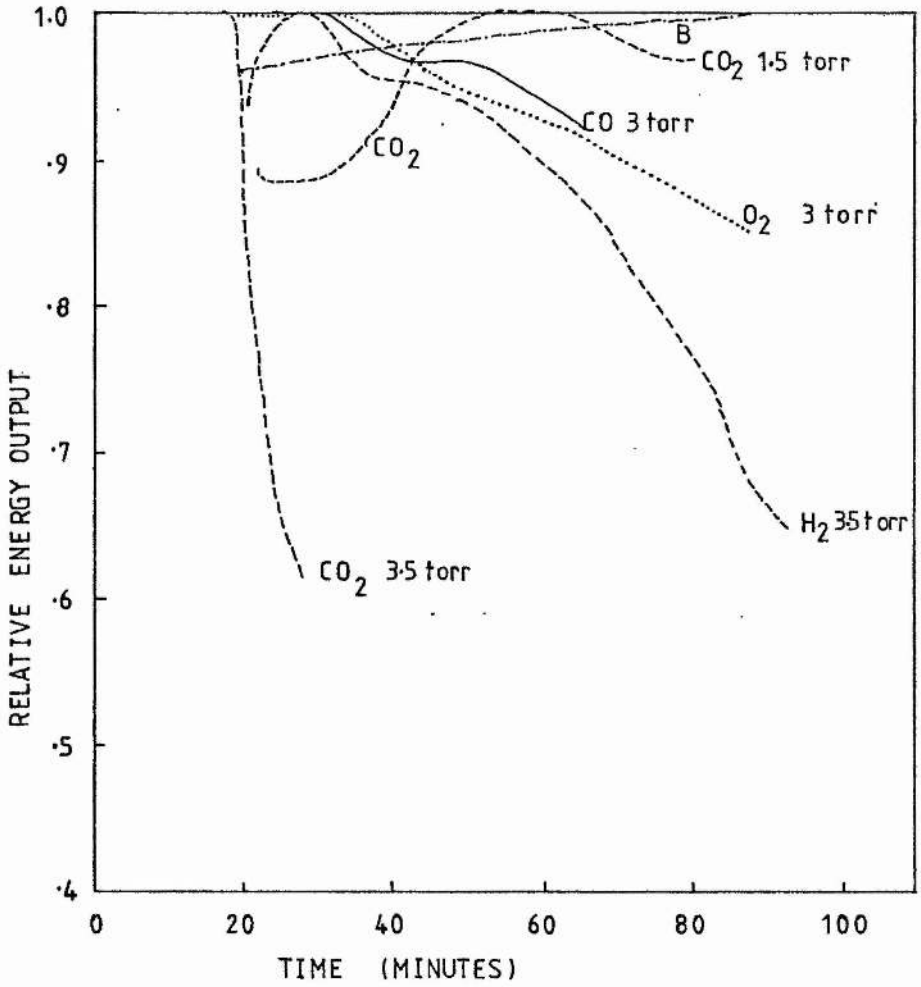

FIG 6.31 Fluorine laser output for different dopants. Dopant name and initial partial pressure as shown.

Fig 6.32 to 6.59
Partial pressures of species detected in a $He-Kr-F_2$ mix after the addition of different dopants. Version LV4 used.
Top right hand corner of each figure labelled with name of detected impurity species. Top and bottom figures show results from the same dopants, each pair of curves labelled with name of dopant.
Discharge started within 10 minutes of first mass scan.

FIG 6·32

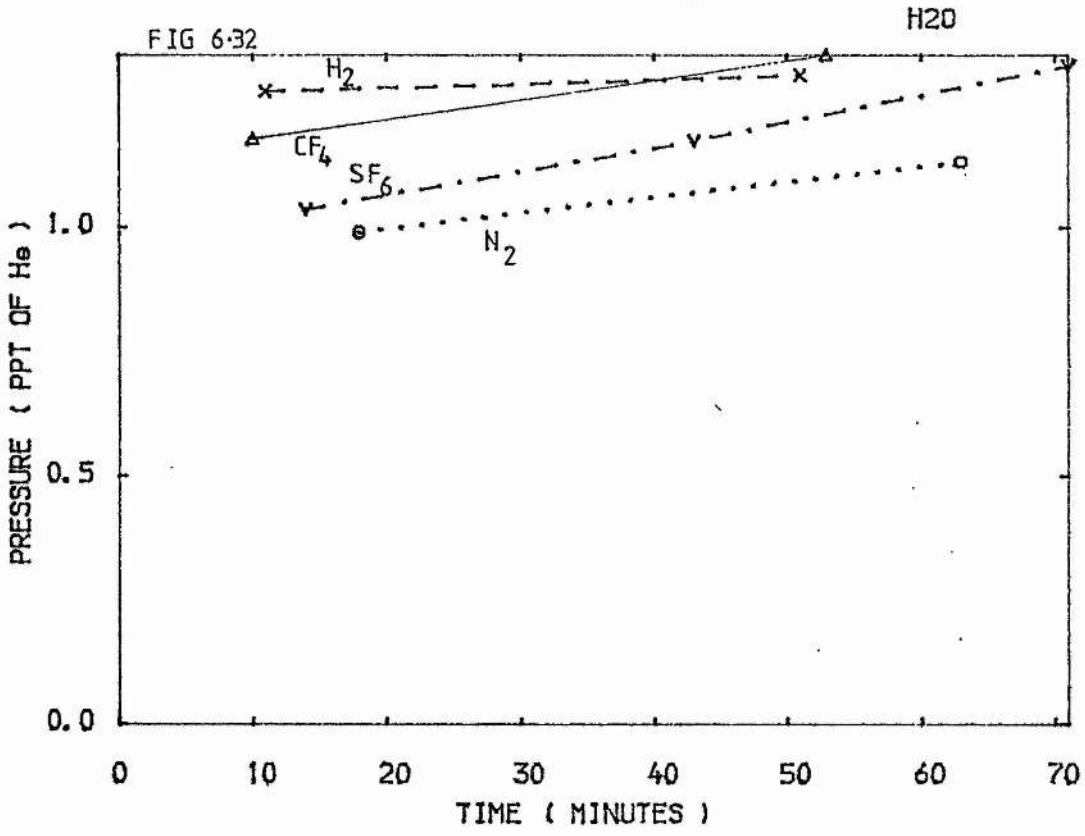

FIG 6·33

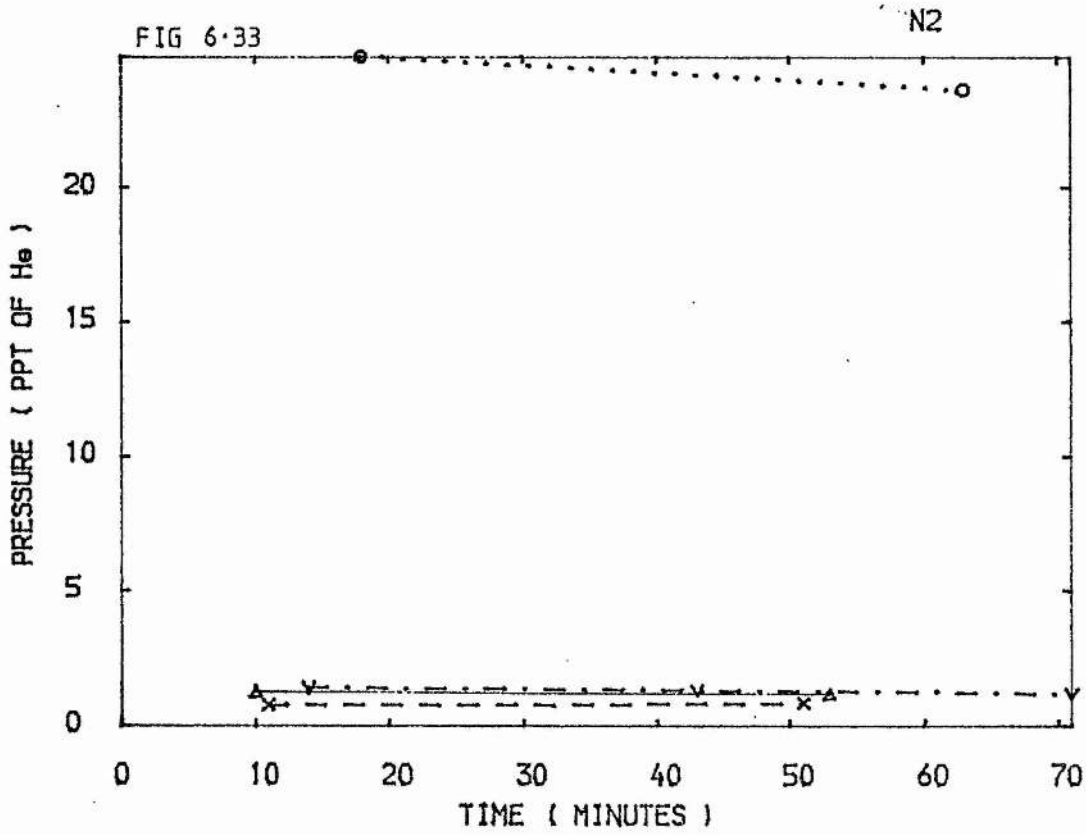

FIG 6·34

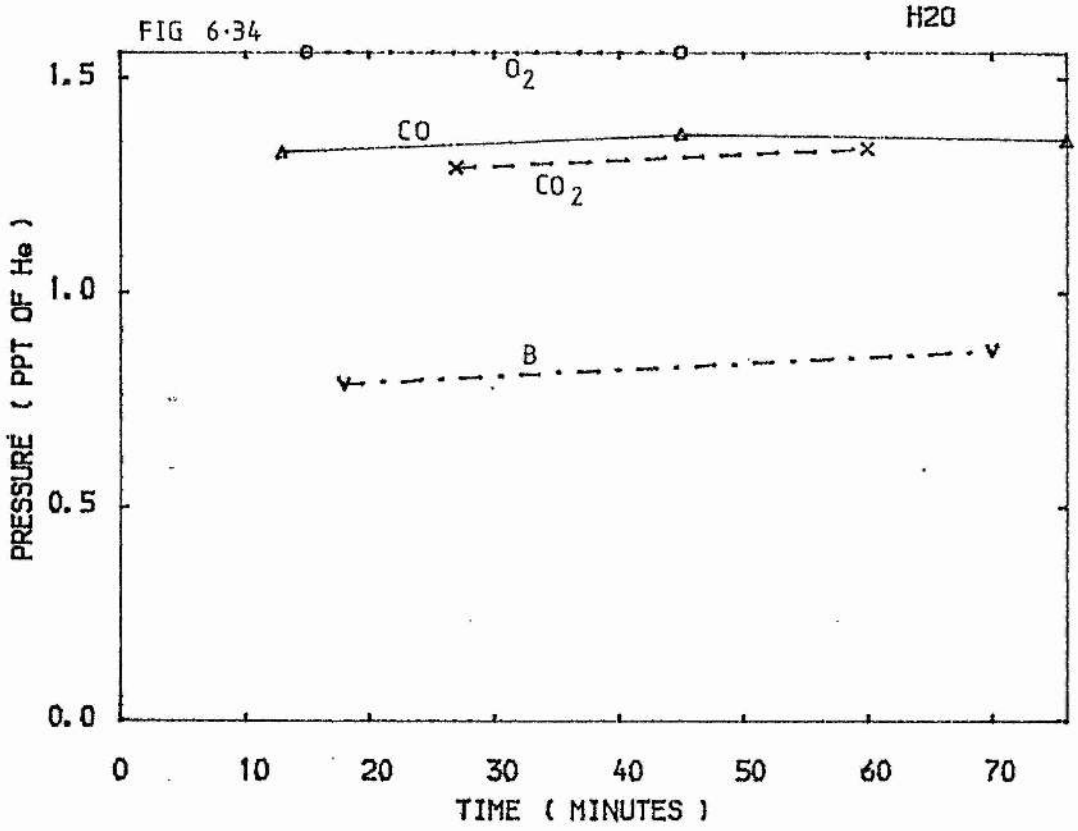

FIG 6·35

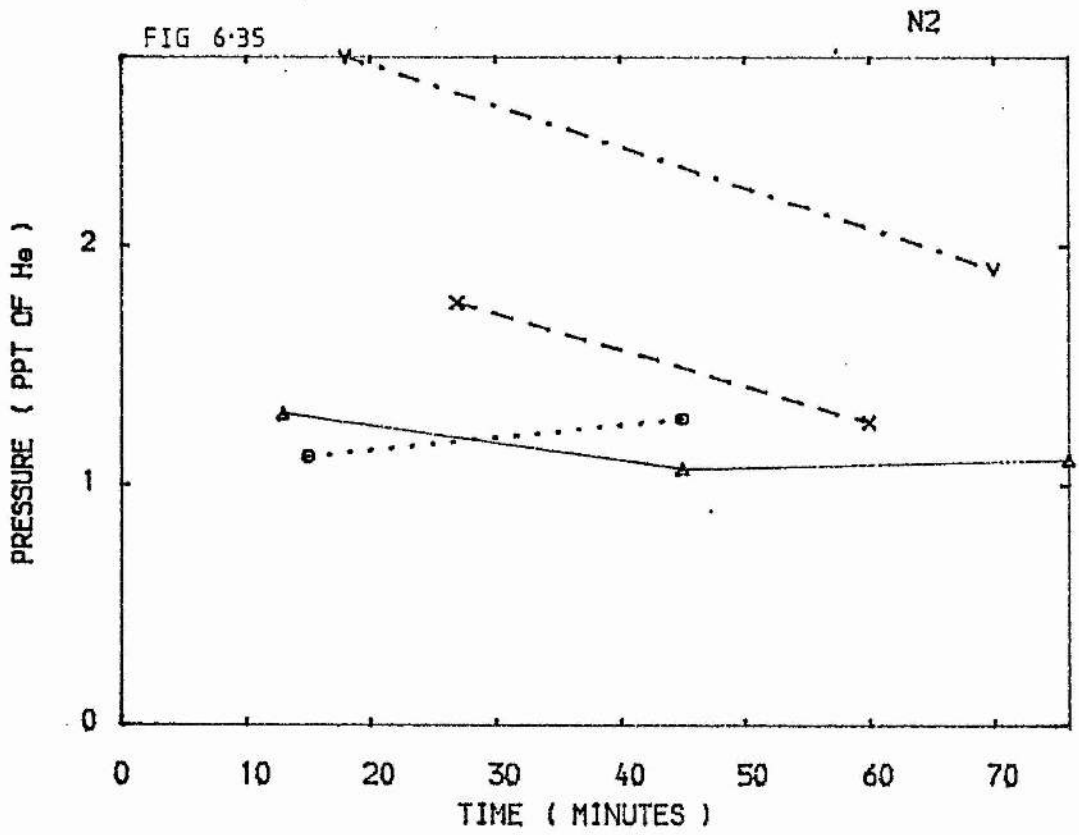

FIG 6·36

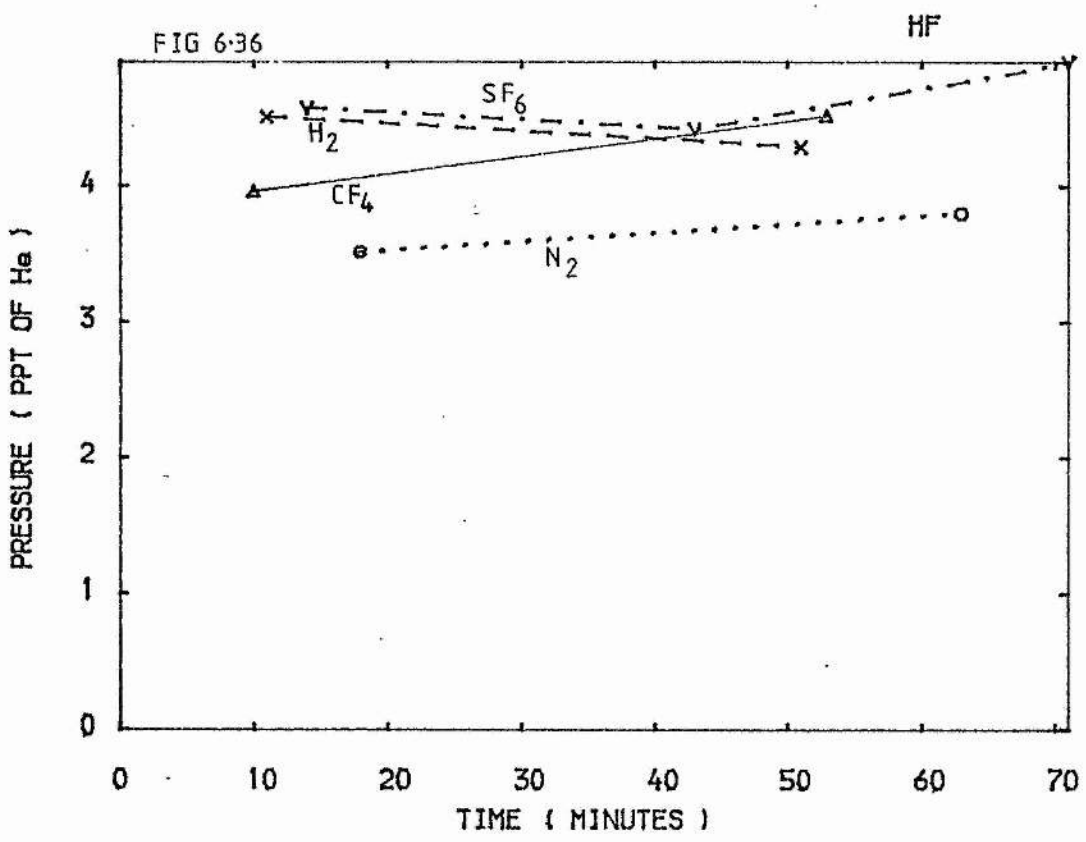

FIG 6·37

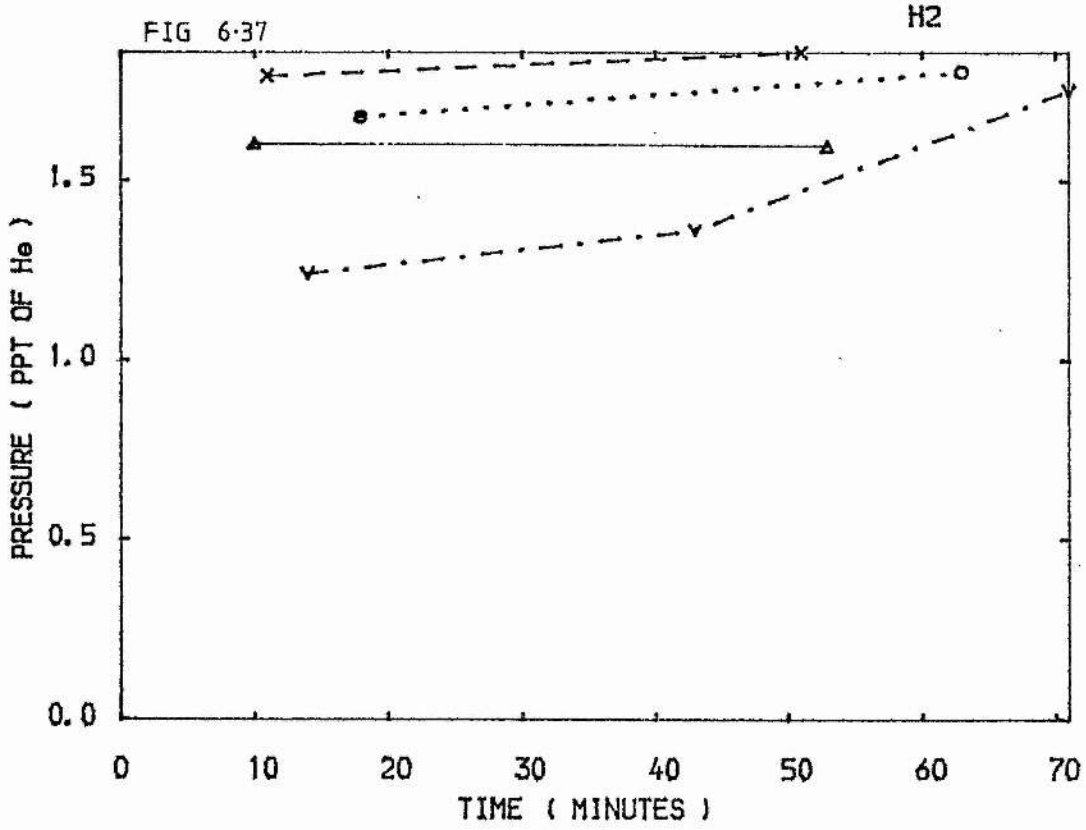

FIG 6·38

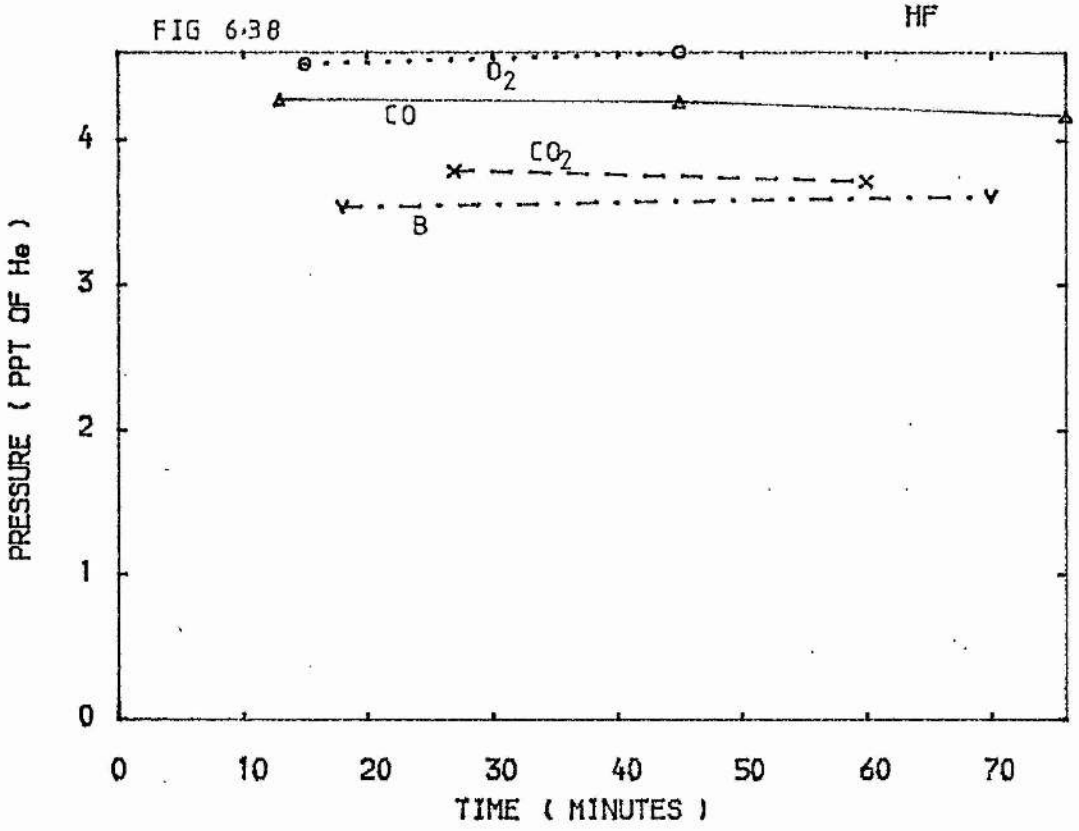

FIG 6·39

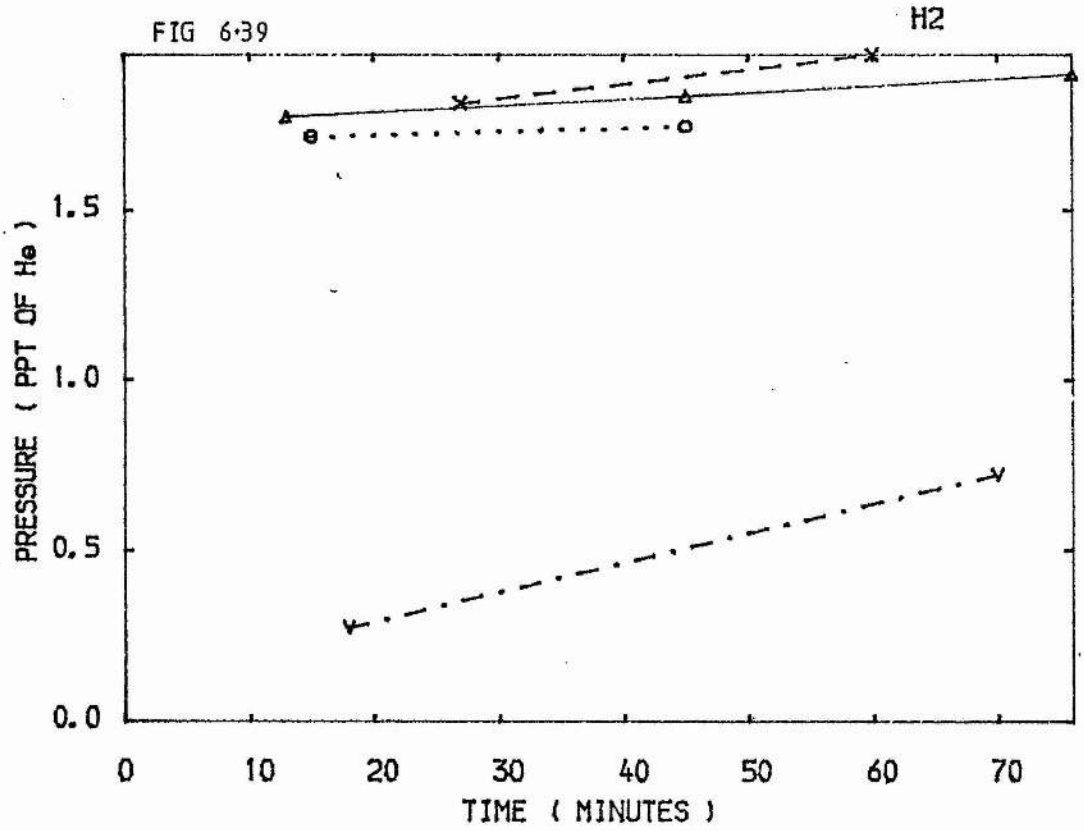

FIG 6·40

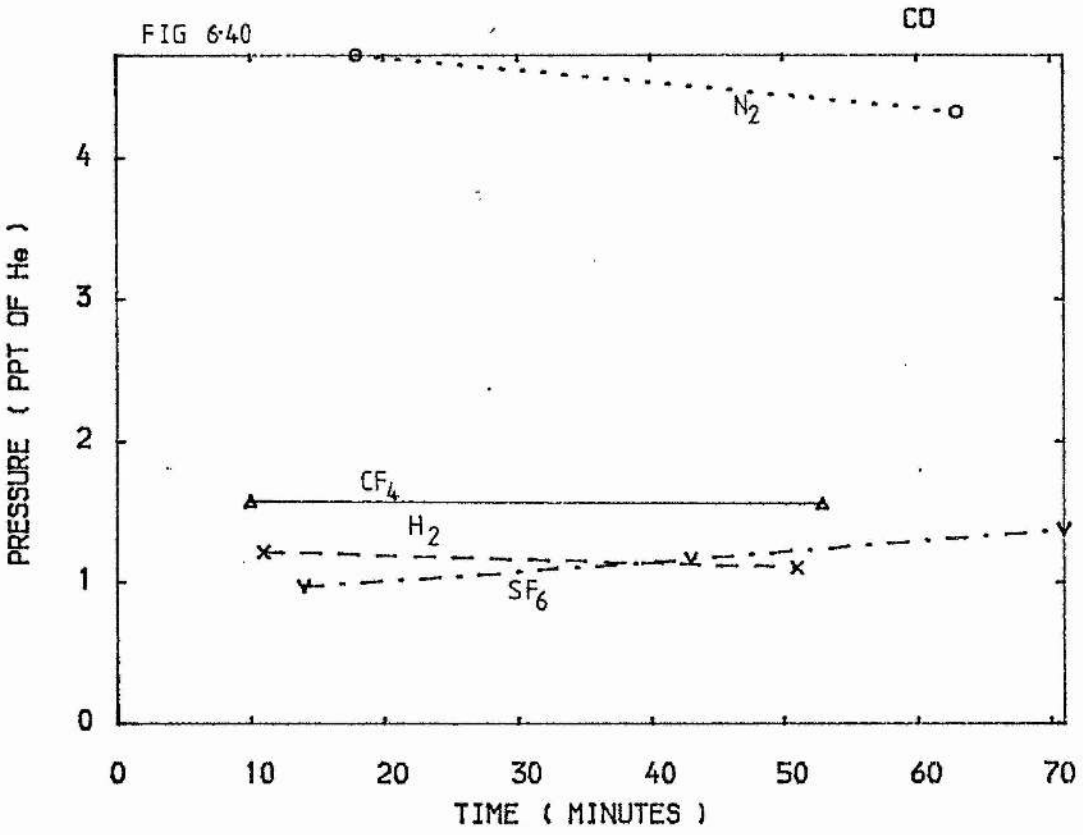

FIG 6·41

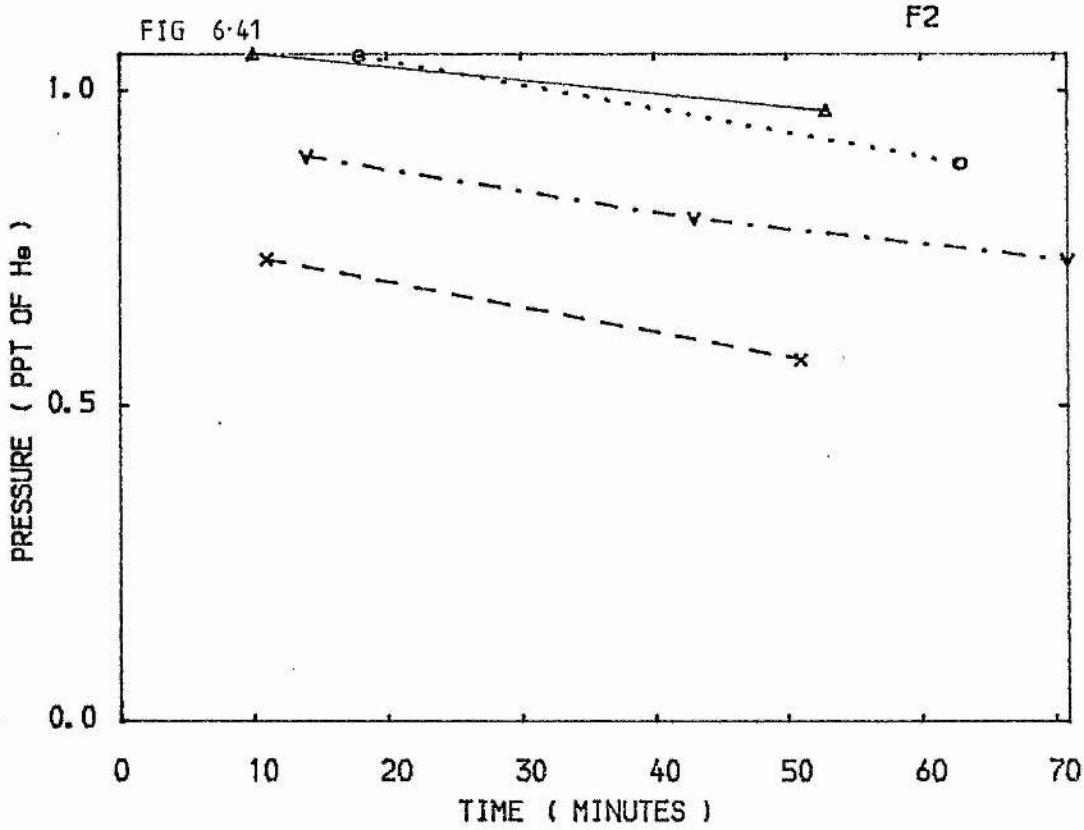

FIG 6·42

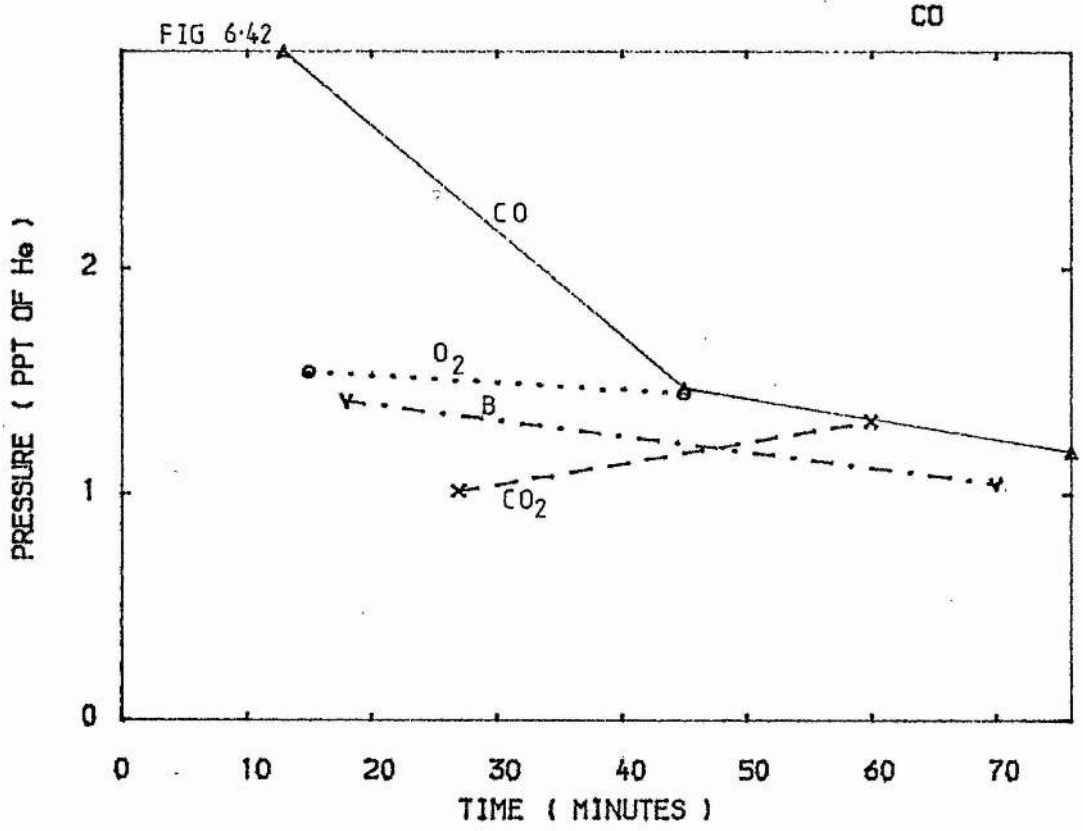

FIG 6·43

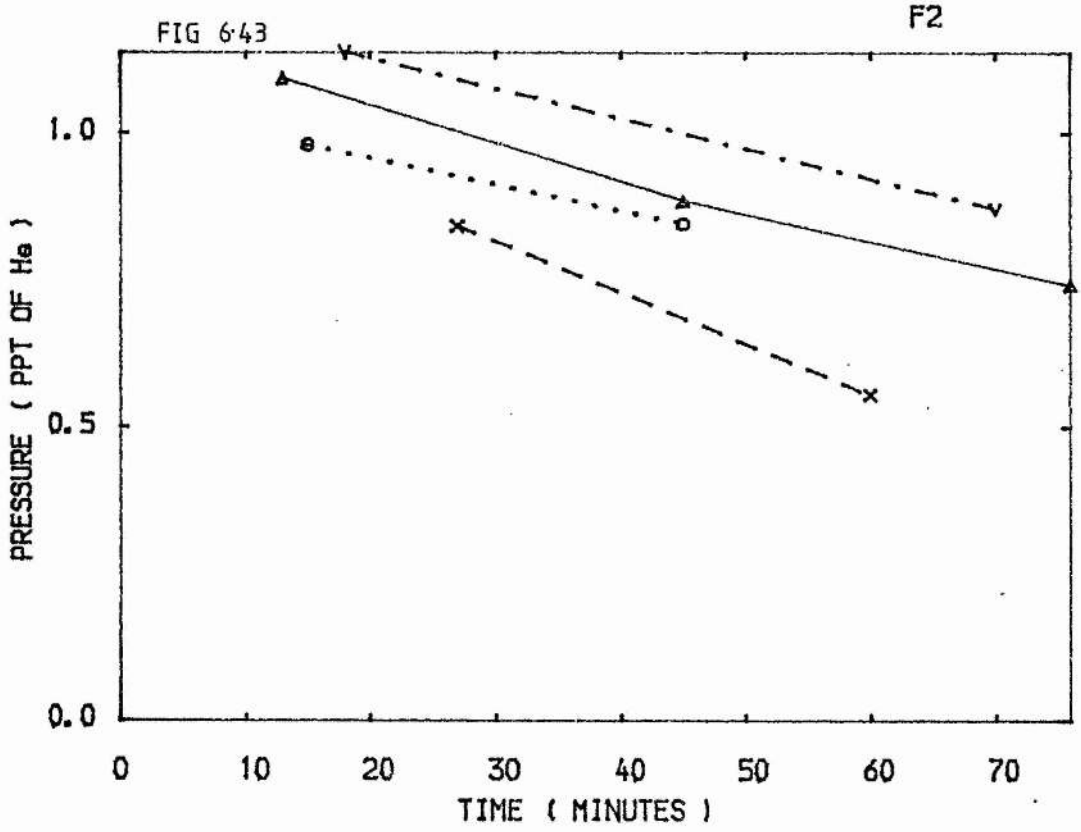

FIG 6·44

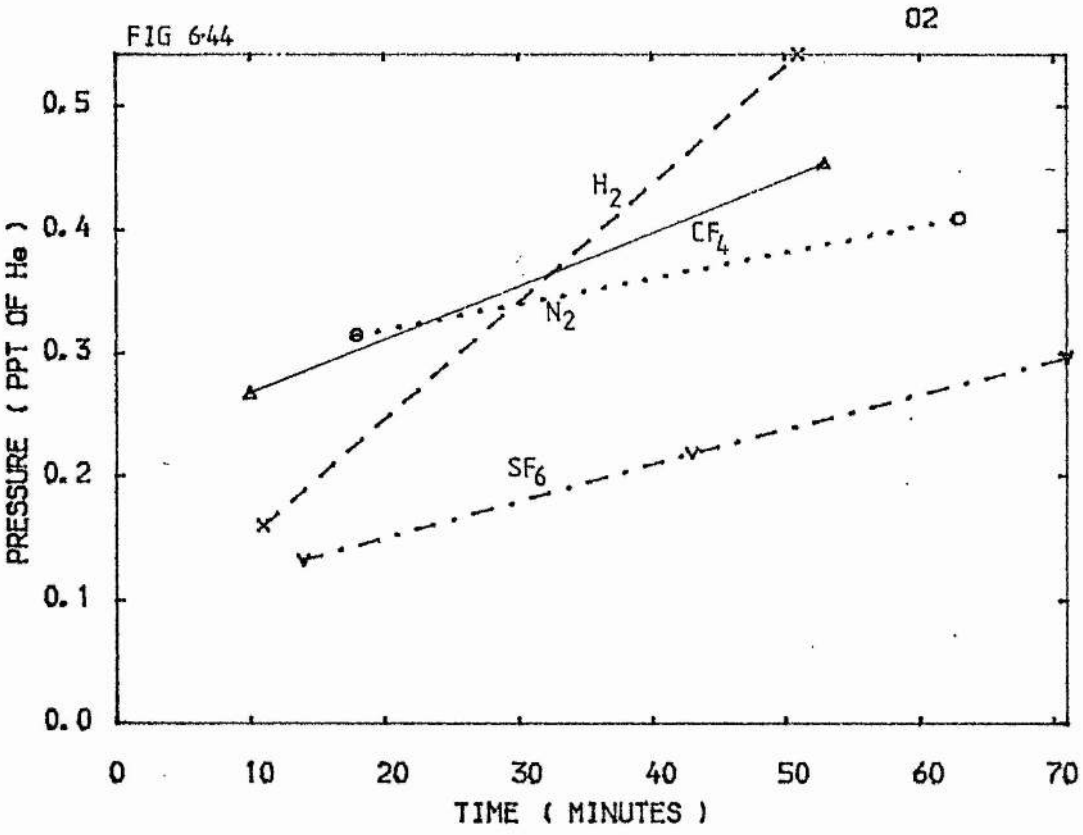

FIG 6·45

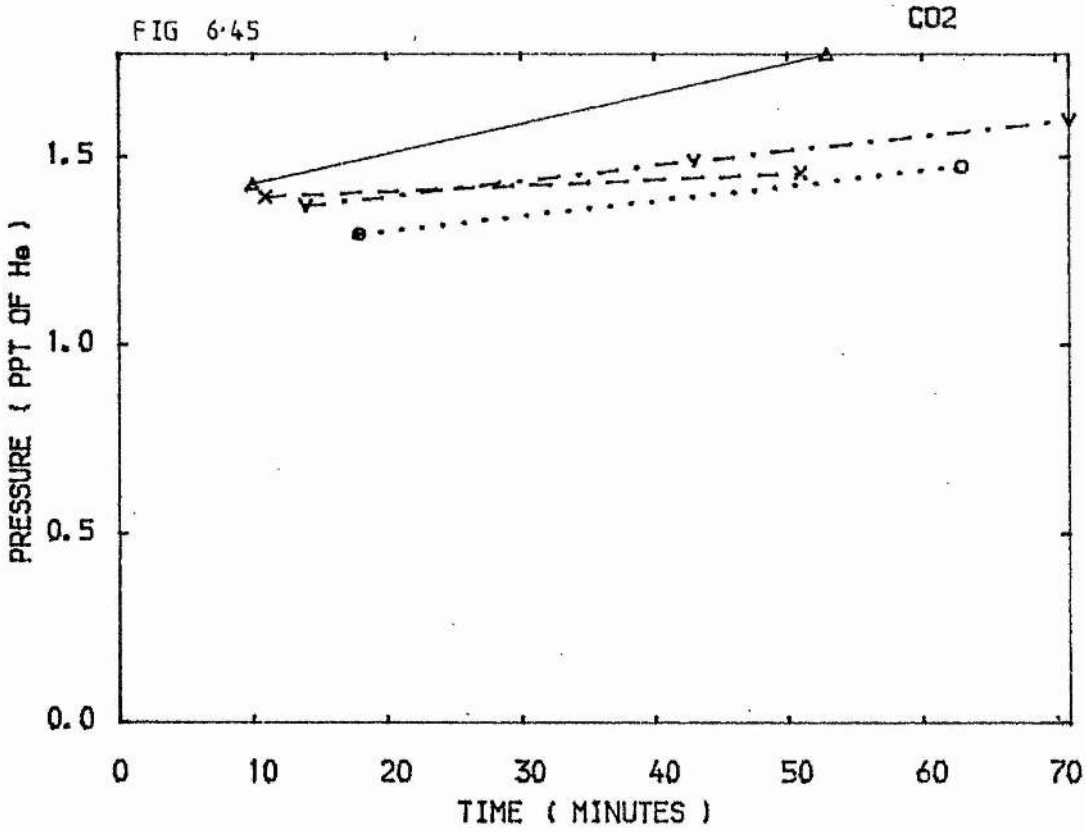

FIG 6·46

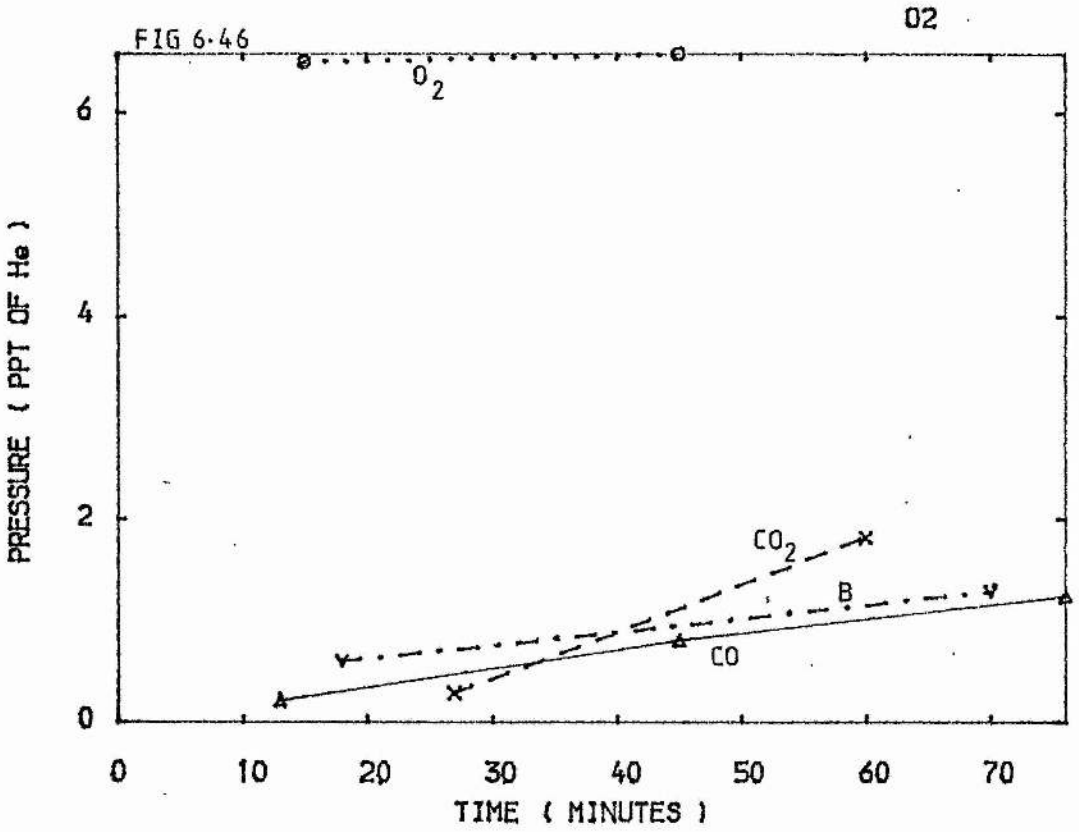

FIG 6·47

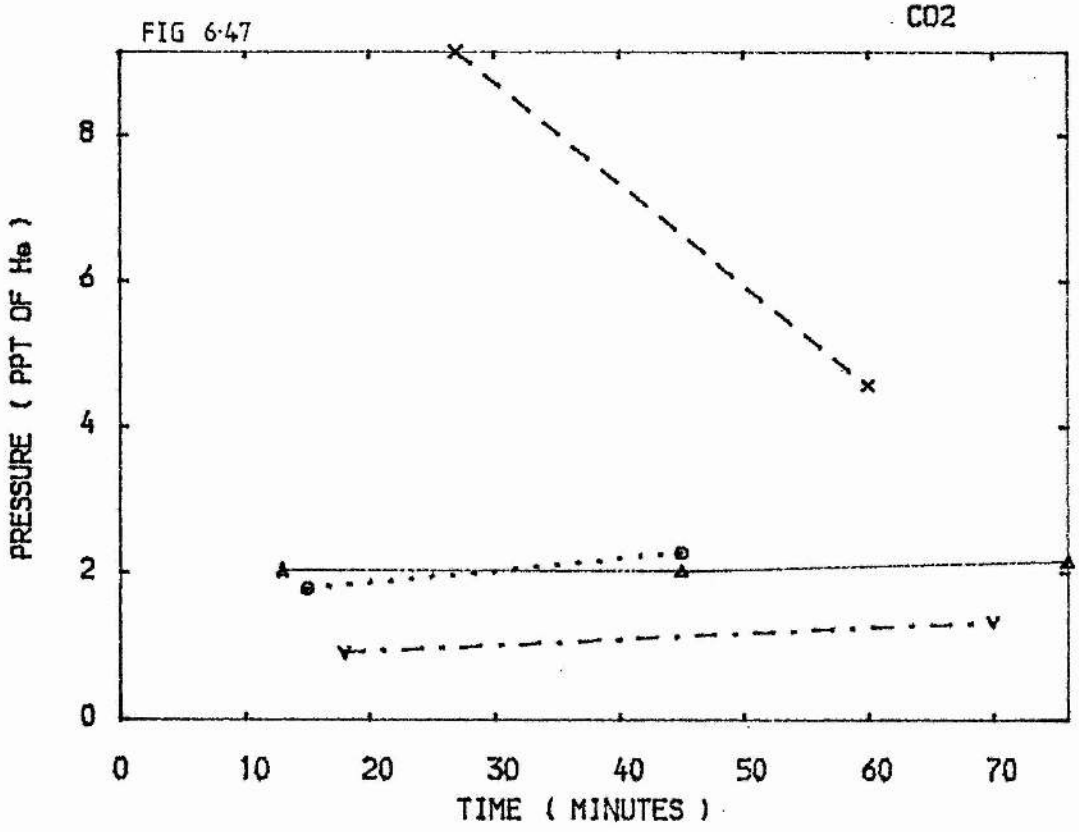

FIG 6·48

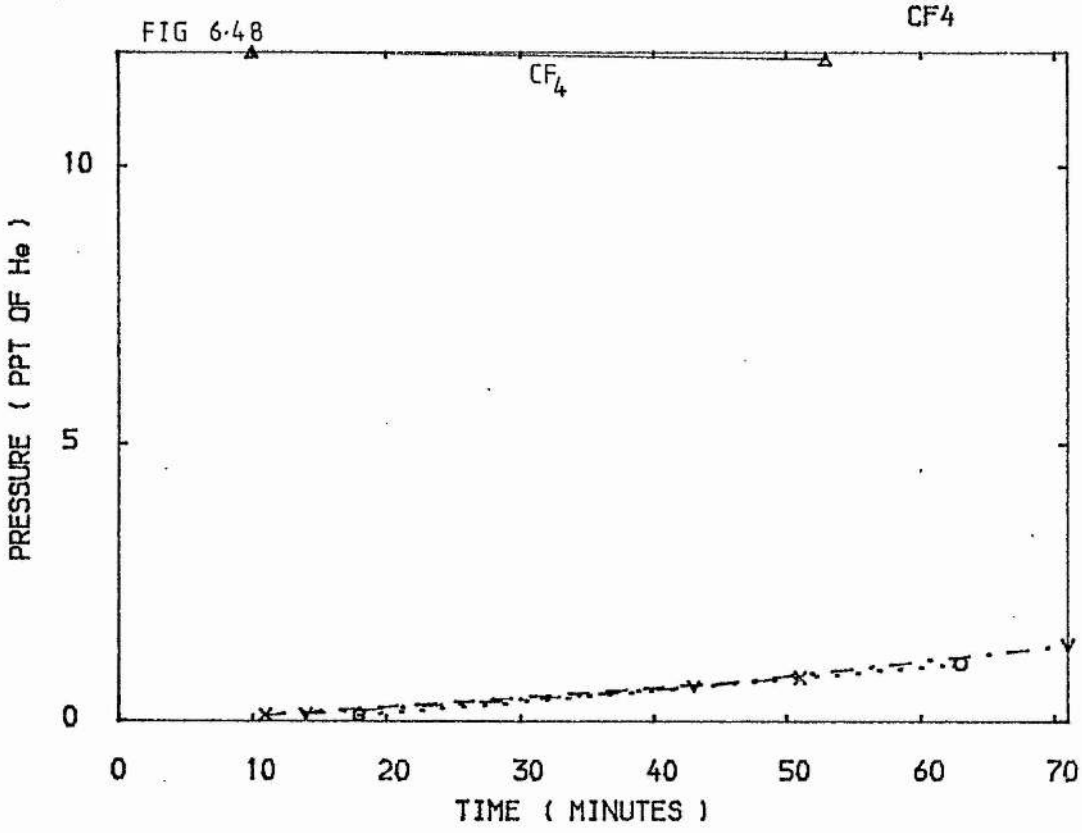

FIG 6·49

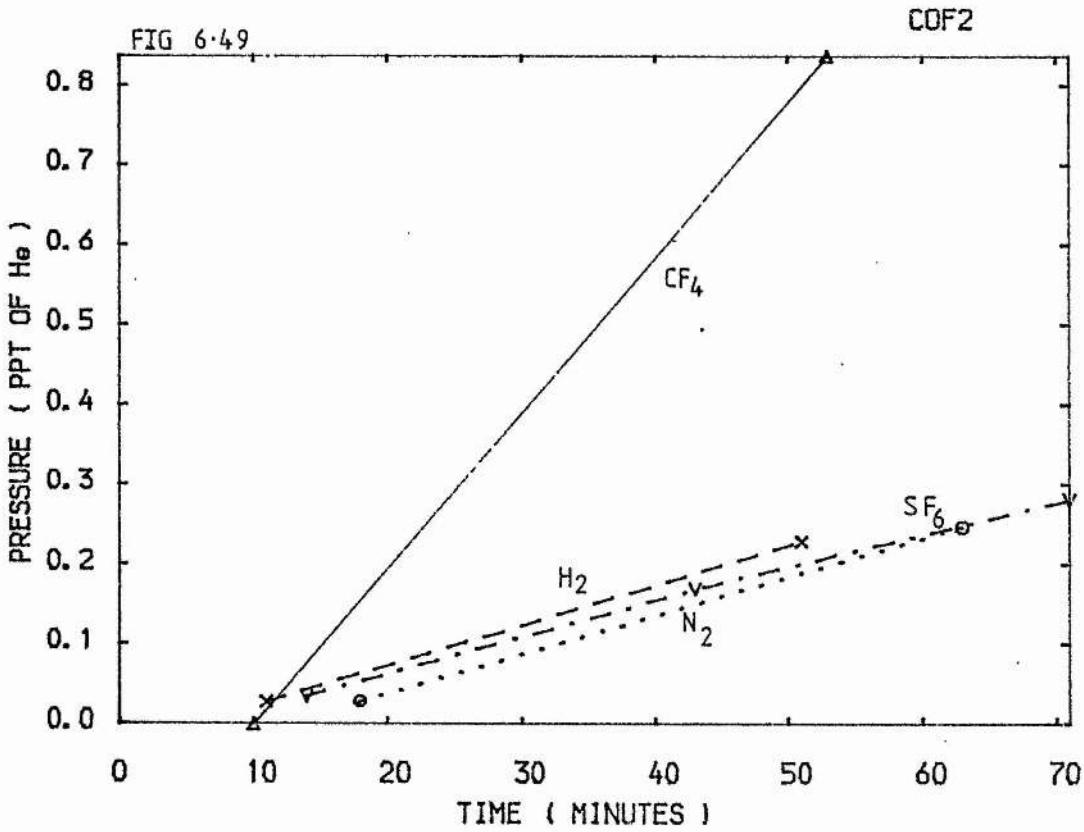

FIG 6·50

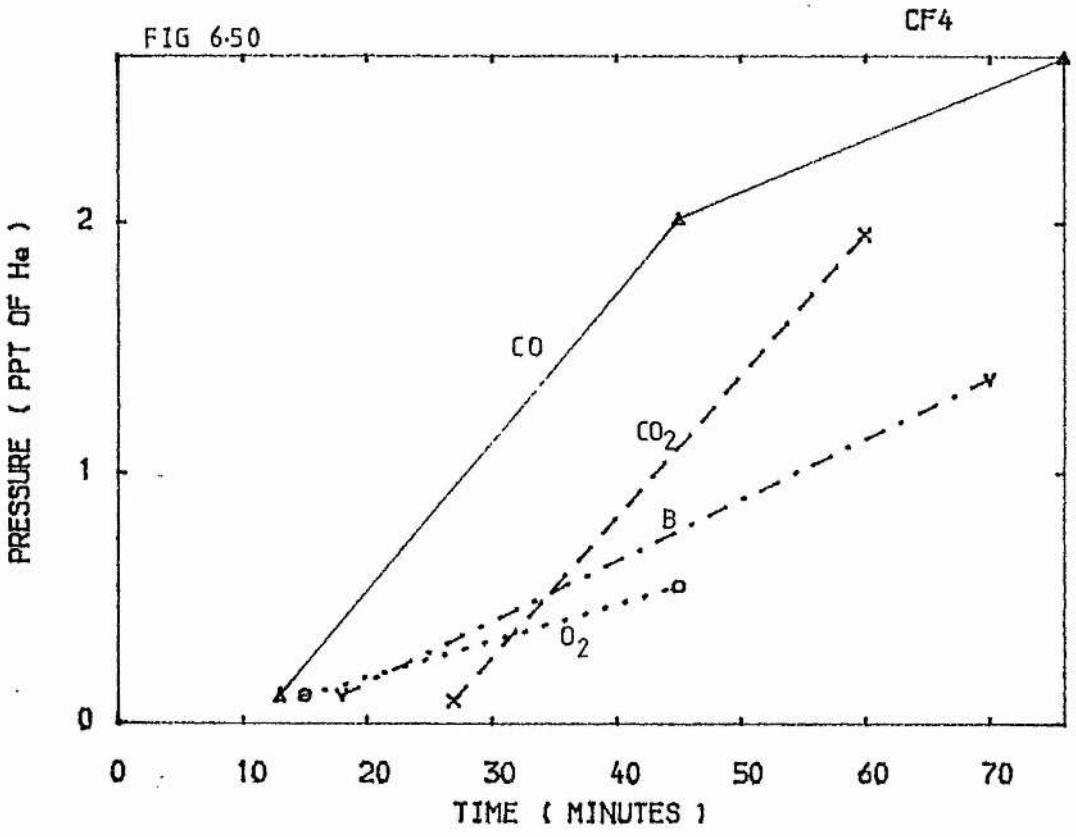

FIG 6·51

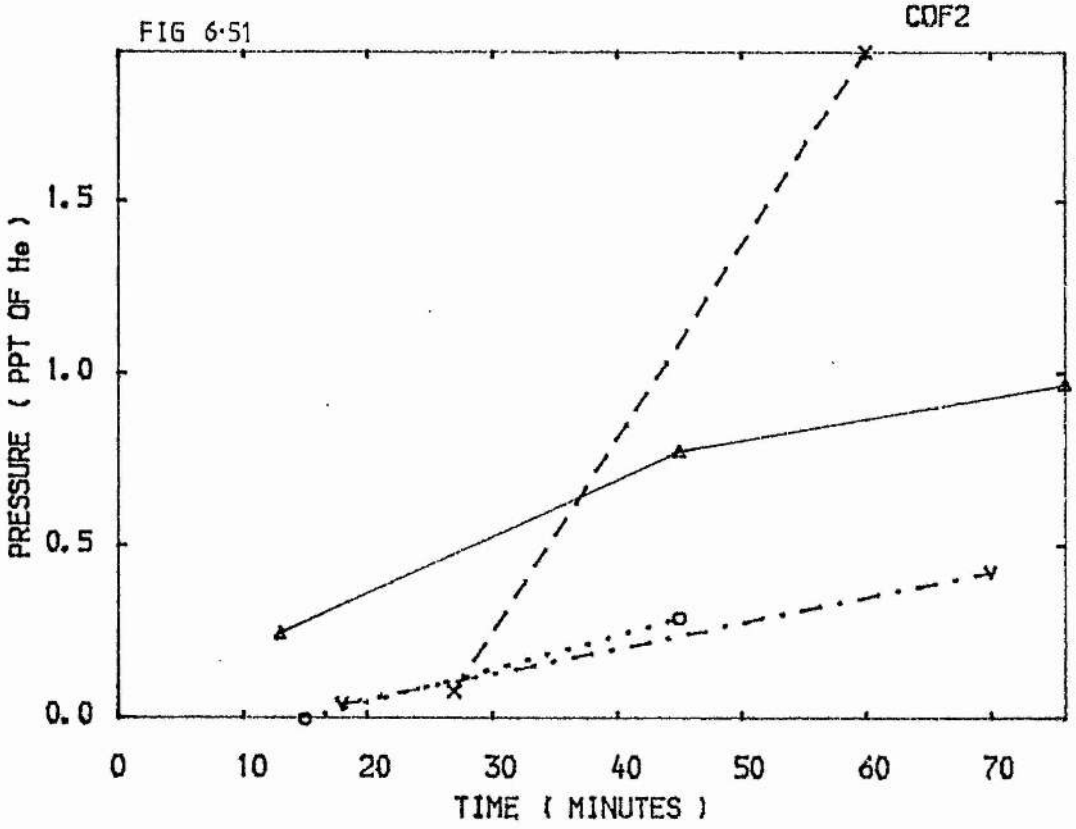

FIG 6·52

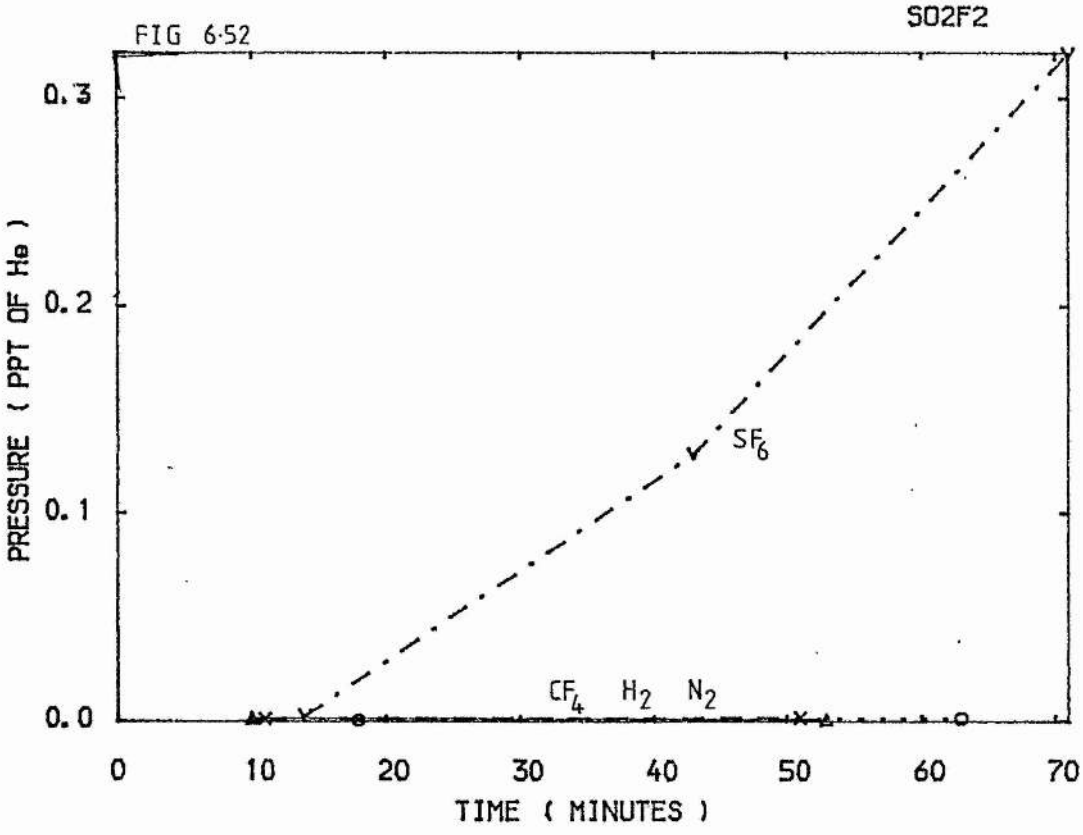

FIG 6·53

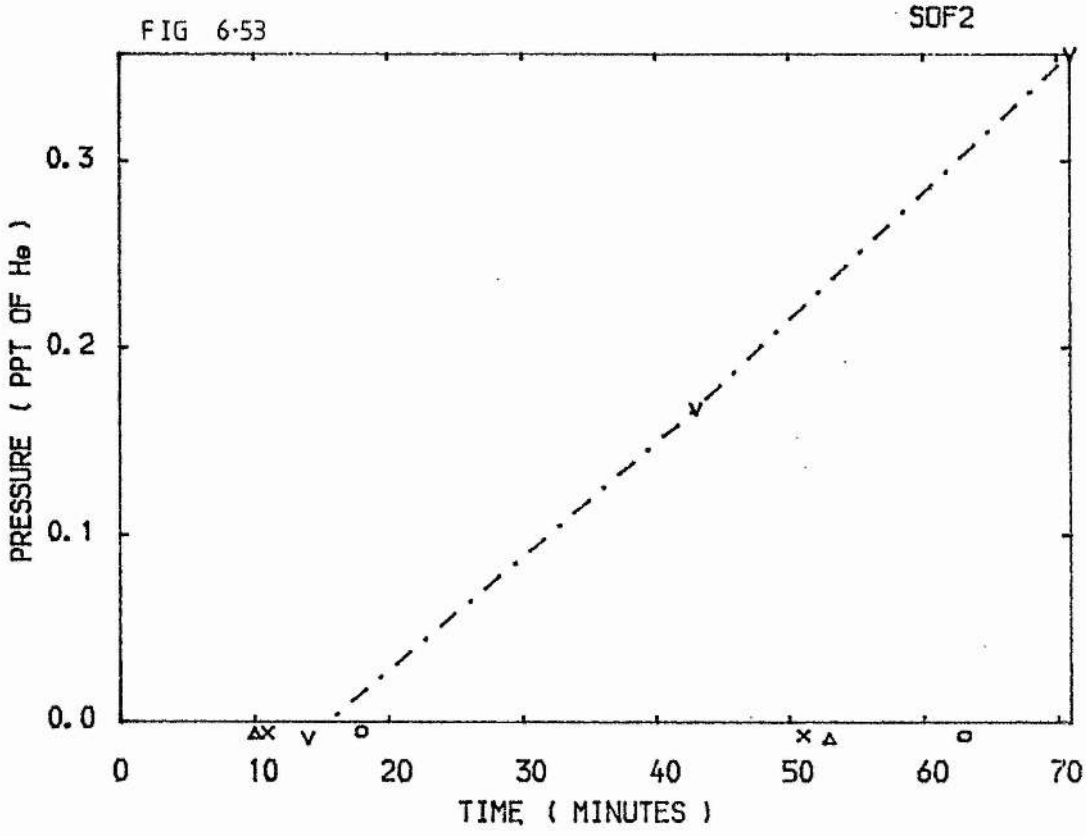

FIG 6·54

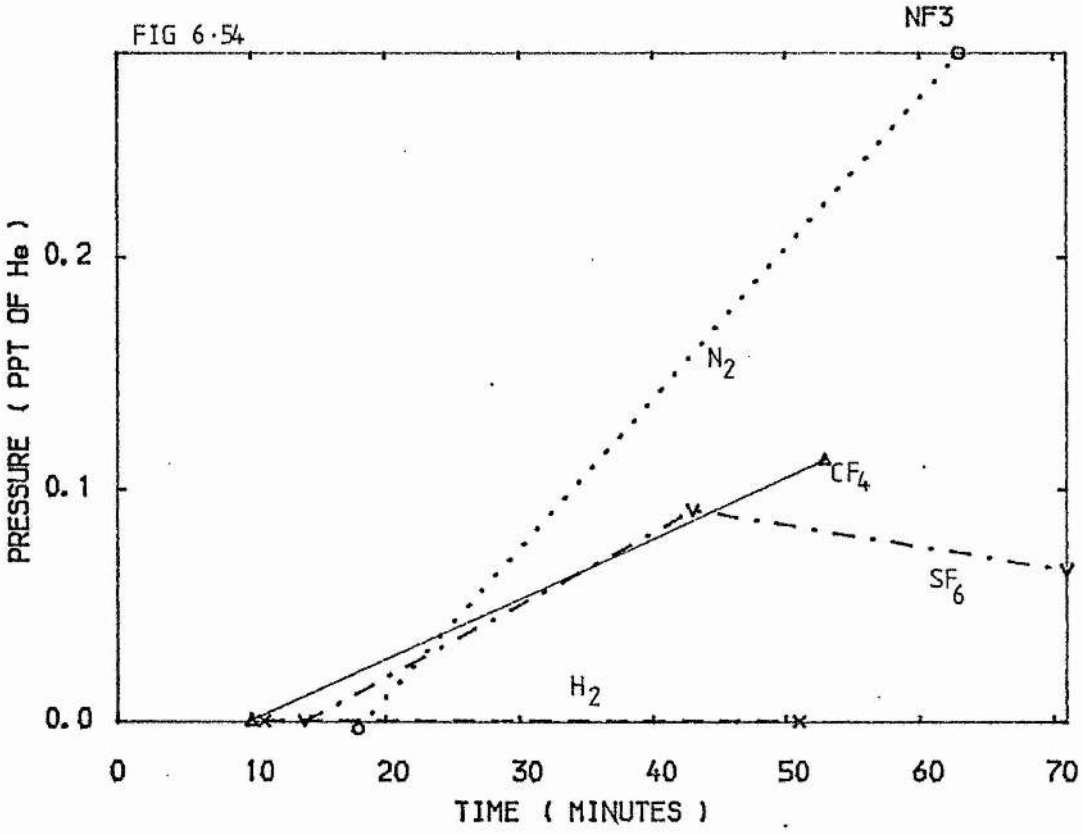

FIG 6·55

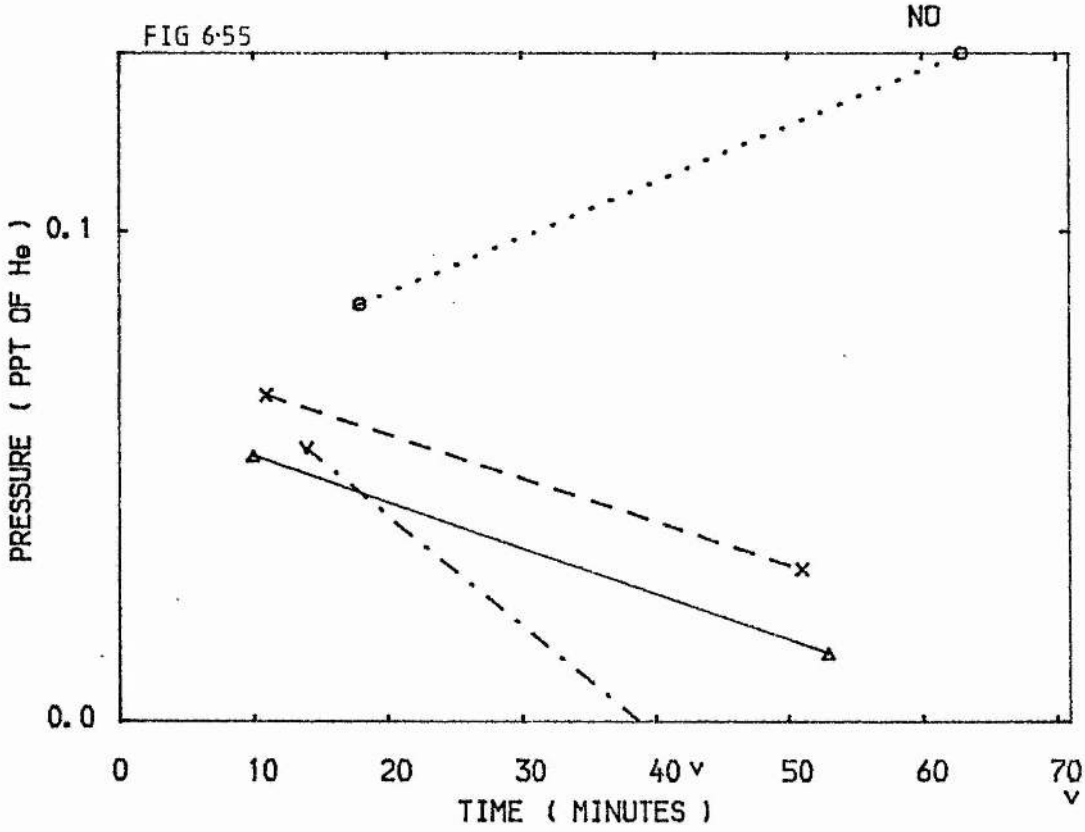

FIG 6·56

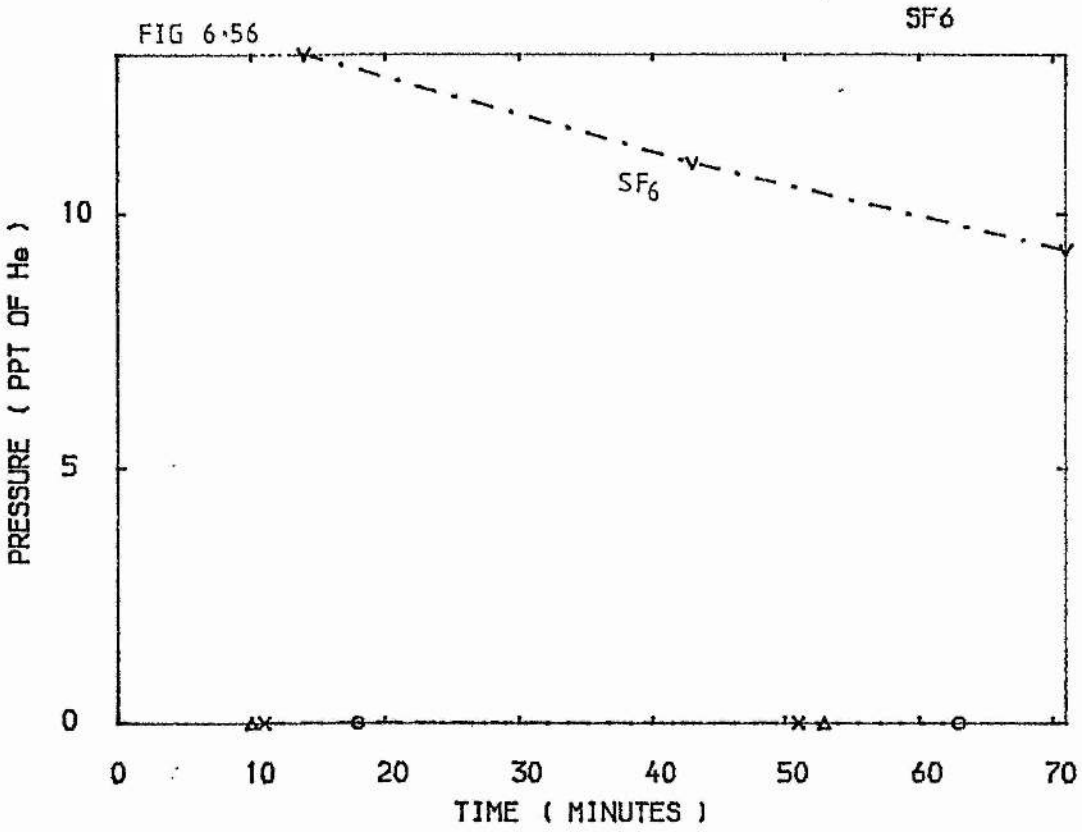
SF6
SF6
PRESSURE (PPT OF He)
0
5
10
0
10
20
30
40
50
60
70
TIME (MINUTES)

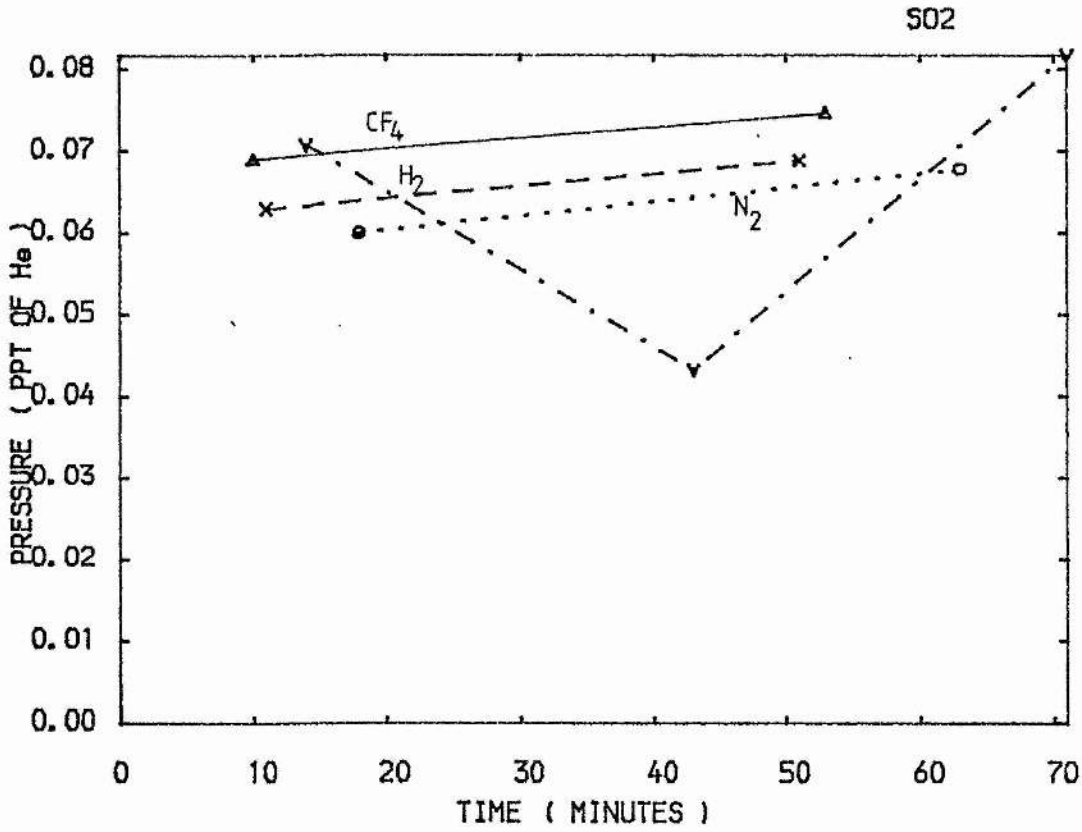
SO2
CF4
H2
N2
PRESSURE (PPT OF He)
0.00
0.01
0.02
0.03
0.04
0.05
0.06
0.07
0.08
0
10
20
30
40
50
60
70
TIME (MINUTES)

FIG 6·58

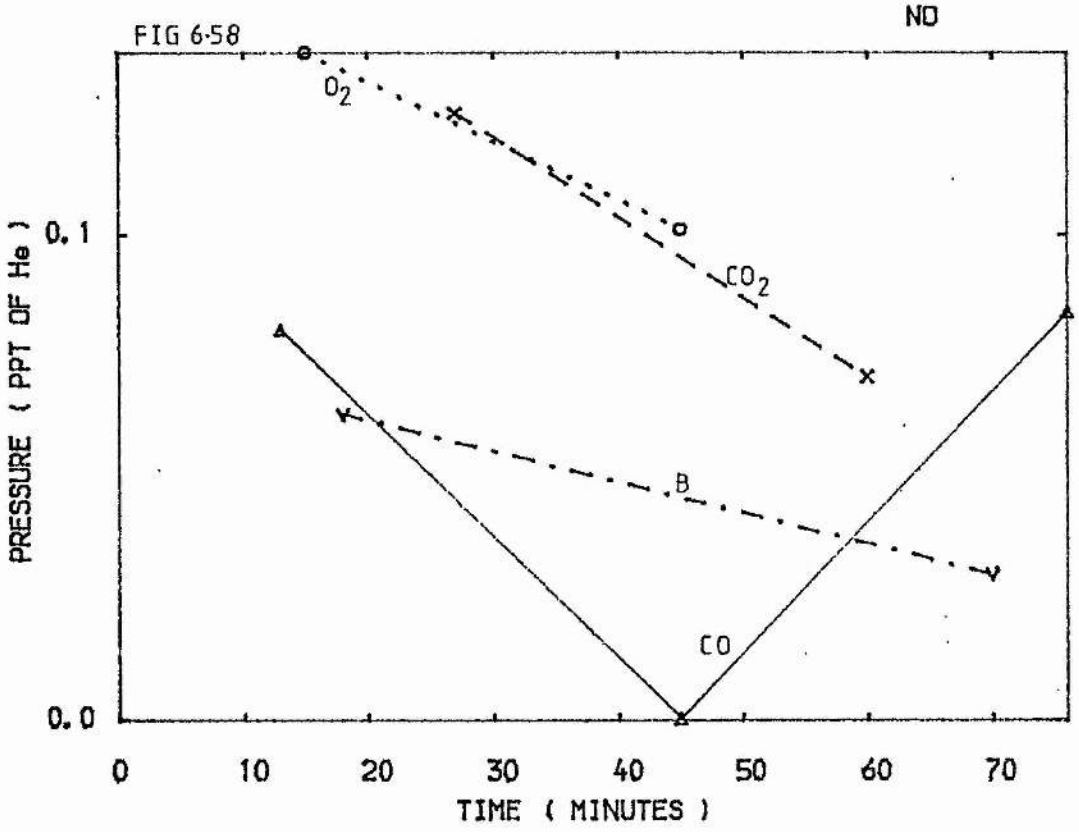

FIG 6·59

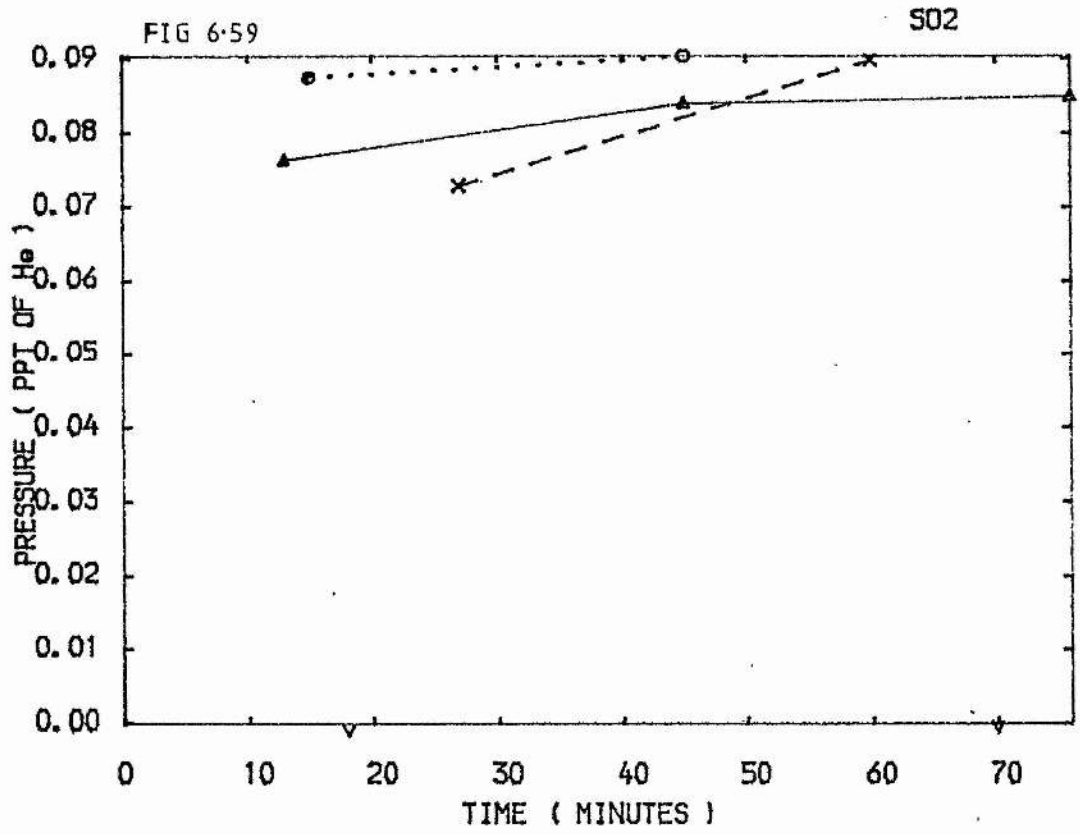

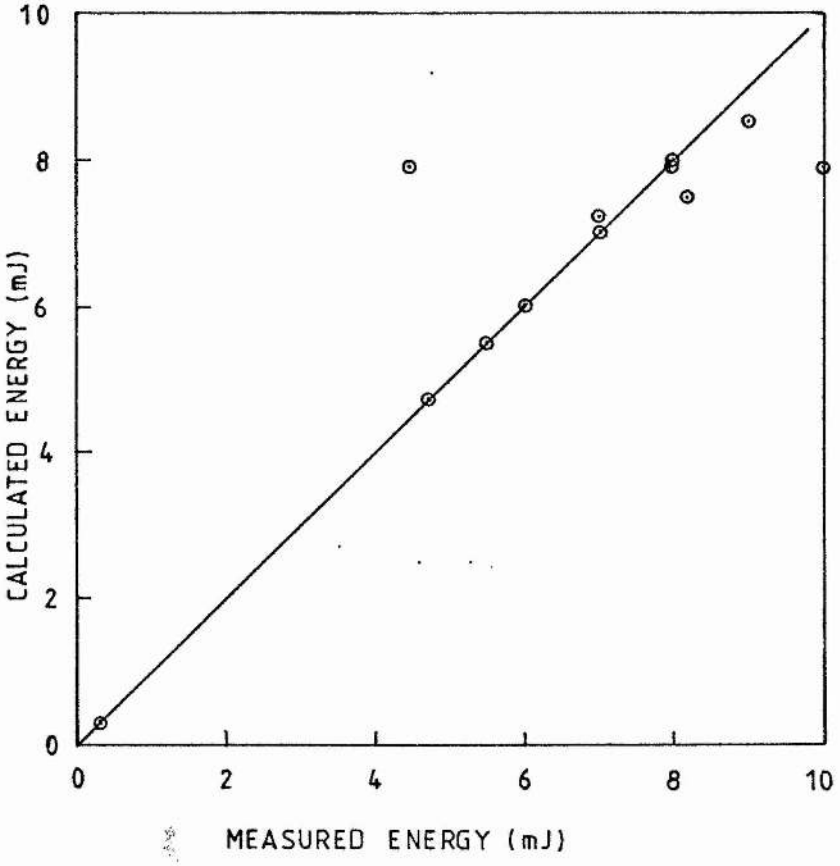

FIG 6.60 Calculated KrF laser output energy using effectiveness constants plotted against measured output energy (see also table 6.3)

REFERENCES

Gower M.C, Kersley A.J, and Webb C.E (1980).

IEEE J1. Quantum Electron. QE16 231.

Meek J.M and Craggs J.D (Ed) (1978)

Electrical Breakdown in Gases, John Wiley and Sons, pp 25.

Nighan W.L and Wiegand W.J (1974) Phys. Rev. A10 922.

Shimauchi M, Karasawa S, and Miura T (1978)

J. Chem Phys. 68 5657.

CHAPTER 7

CONCLUSIONS

The results presented and discussed in the previous chapters are summarised in this chapter, with special attention paid to possible directions of further research. We believe that the results of this thesis lay the foundation for deeper studies of reaction kinetics in the general area of gas laser chemistry and physics of molecular lasers. The nature and scope of the experiments carried out have been rather qualitative and with a broad base. This approach, to what is essentially a complex problem, has brought quick results as far as the design of long lifetime single-fill lasers with fluorine as one of the species is concerned. It has also identified species other than those of the pure laser mixture, the appearance of which is correlated with decrease in laser power output from sealed-off laser systems containing fluorine. The species identified have been found to occur in four systems having quite different geometries and construction materials.

7.1 The mass spectrometer as an analytical tool

One of the important points demonstrated in this thesis is the suitability of the quadrupole mass spectrometer as an efficient and direct analytical instrument to study the evolution of impurities down to the ppm range, especially when corrossive gases are used. Its advantages are summarised as follows:

(1) Fast scan rates. Unlike the magnetic deflection type of mass spectrometer, the quadrupole mass analyser can scan a spectrum in a few seconds with good resolution. The Supavac was able to resolve adjacent peaks with a m/e difference of one at a scan speed of 150 amu/minute. Such scan rates enable the accumulation of more spectra in a given time, leading to greater accuracy and time resolution of peak height measurements.

(2) Higher sensitivity. Comparison of the results reported here with those of Duval (1983) show that the quadrupole instrument has about 10 times more sensitivity to the impurities in the gas mixtures.

(3) The mass spectrometer detects directly and quantitatively the impurity species present in the gas mixture. A very wide range of species can be detected on-line and identified as has been demonstrated in this thesis. The relative errors of measurement of species partial pressures is less than 5% and, once calibrated, the instrument can be used to measure absolute partial pressures within about 10% error. Optical spectroscopic methods are indirect, complicated, and often gives ambiguous results compared to the direct, quantitative, and elegant approach possible with the mass spectrometer. Another defect with the optical spectroscopic

methods is the difficulty in the analysis of O_2, CO_2, N_2 etc due to its presence in air, whereas the mass spectrometer can measure their partial pressures in a gas sample with high accuracy.

(4) The mass spectrometer is highly resistant to F_2 attack. No appreciable deterioration was noticeable either in the sensitivity or resolution after two years of almost daily use with F_2. Since we were initially very concerned about the possibility of deterioration, this result is both gratifying and important to future studies of fluorine systems.

The disadvantages of the mass spectrometer, especially the one we have used, are as follows:

(1) Difficulty in the accurate quantitative measurement of H_2O, HF, SiF_4 and CO. Hydrogen Fluoride and SiF_4 were formed inside the mass spectrometer mainly due to the presence of H_2O and glass. Eliminating the glass ion gauge (which is really not necessary since we measure heights relative to He height and because the Supavac itself can measure total pressures) would solve the problem of SiF_4 production inside the mass spectrometer. Carbon monoxide and CO_2 production inside the mass spectrometer can be reduced by the choice of proper filament material (rhenium instead of tungsten - see Supavac manual). The only way to eliminate the problem of background H_2O in the mass spectrometer is to keep the analyser and inlet system above 100°C during operation. This is feasible, but we did not attempt it. Further work in this area is necessary to find out the extent of inaccuracies created by the presence and production of impurities in the mass spectrometer.

(2) Inability to study fast reactions (ie reactions with time

constants of less than 1 sec). This is beyond the scope of Supavac. However time-of-flight mass spectrometers are available for such studies to complement the kind of long lifetime studies reported in this thesis (McDowell 1963).

(3) Restricted mass range. Again instruments are available which go up to 300 or more amu. They are necessary to study the heavier fluorinated species like C_2F_6 evolving in the laser. However, from the results here, we find that most of the problems are due to the simpler inorganic species like CO_2, COF_2, etc, as far as He, Kr, F_2 mixtures are concerned.

Present day mass spectrometers including the Supavac can be connected to computers, thus enormously increasing the amount of data that can be processed at high speed. We therefore find that the quadrupole mass spectrometer is an appropriate primary tool for the quantitative study of gas laser chemistry.

7.2 Choice of construction materials for a laser

The study of the laser versions made of different materials of construction reported in the last three chapters clearly indicate the direction of choice of materials of construction when F_2 is one of the gas mixture components. Plastics are to be avoided. If they are to be used, PMMA should not be used due to the production of CO_2 in reaction with F_2 and the outgassing of CO_2, H_2O, N_2, and O_2. These impurities, especially CO_2, apart from reducing the laser output, react with F_2 to deplete F_2. The fluorinated polymer

PTFE is a good insulator but it is better kept away from direct uv radiation inside the laser to avoid production of CO_2. The use of corona wires or electrodes made of stainless steel is also to be avoided in order to eliminate production of CO_2. Generation of SiF_4 is avoided by not using Al alloys containing Si. Pure Al or stainless steel is preferred for the metal parts of the laser. The electrodes and corona wires are preferably made of pure nickel. In order to reduce the amount of water vapour, the system is to be made of bakable materials capable of withstanding at least 200°C. The seals are best made of PTFE or its high temperature counterpart, viton. Materials containing S are to be avoided.

Studies of outgassing in metals and plastics under vacuum have been reported in literature (Espe 1966, Beck 1964). But we did not come across any such studies of materials which are to work in an F_2 environment. However the outgassing properties of these materials in vacuum are used as a guide in recommending materials for the construction of a long lifetime laser outlined in section 7.7.

7.3 Use of cold traps to extend laser lifetime

Another result that emerges from the study of the gas mixtures is the use of a simple cold trap to extend the gas lifetime of F_2 containing mixes. When only He-F_2 mixes are used the cold trap is a very simple liquid N_2 on-line cold trap with a slow gas circulator working at about 2 to 4 litres/minute rate. This effectively suppresses loss of F_2 and decrease in energy due to

impurity quenching by condensing out CO_2, CF_4, HF, H_2O, NO, NO_2, COF_2, SiF_4 and extends the number of shots to half power by a factor of 5 to 10. Even though the cold traps used here have not been very efficient, especially for the KrF laser, they can be made with larger capacities by simply increasing the cooled surface area in contact with the gas. Analysis of the cold trap contents is another way of studying the impurity species with <1 ppm partial pressures which would accumulate in sufficient quantities to be detectable. Varying the temperature of the cold trap is found to be an easy way of identifying the impurities that cause laser quenching as discussed in chapter 5. This method showed CO_2 and H_2O as being the prime impurities in a KrF laser mix.

7.4 Impurity addition to study impurity evolution

Once the evolving impurity species in the basic mix are identified, their effects on laser performance can be evaluated by adding small quantities of these impurities to a pure mix and monitoring the energy output and impurity evolution as described in chapter 6. This method has not been used before in the investigation of impurity evolution in excimer lasers. The interaction of impurities can be studied by adding more than one impurity even though it was not done in the present case. We tried most of the main impurities as dopants: CO_2, CO, N_2, CF_4, H_2, and SF_6. The results confirmed that CO_2 is the worst impurity, resulting in the production of COF_2, O_2, and CF_4 in reactions with F_2. Other impurity evolution processes were also clarified, for example, the

increased production of SiF_4 due to the higher partial pressures of HF when H_2 is the added impurity. The study also showed that CF_4 is not a harmful product in small concentrations. The use of SF_6 as a fluorine donor for KrF mixtures is not recommended because the impurities SO_2F_2 and SOF_2 would be produced during discharge.

7.5 Impurity evolution and pulse repetition rate

We used a low pulse repetition rate (one pps) for the discharge mainly to keep the impurity production rate low enough so that no large variations took place during a one minute period for the mass scan. However it was found that for the He-F_2 mix in the PTFE laser versions the lifetime of the gas mix was in excess of several hours, making it difficult to carry out lifetime experiments. This can be overcome by increasing the repetition rate of the laser. However, low repetition rate operation clarifies reaction pathways which might otherwise be masked in a high repetition rate laser because of the decreased time resolution of the mass scans. Thus the evolution of impurity species presented in the previous chapters would be compressed 10 to 100 times in time scale in a discharge pulsed at 10 or 100 pps. Faster repetition rates would also require faster mass scans and faster gas flow rates.

7.6 Theoretical analysis of experimental results

The system studied here is a very complex one with hundreds of reactions taking place on widely varying timescales (from nanoseconds to hours) as was explained in Chapters 1 and 6. This is because the interacting species number more than 10, resulting in about 100 two body and about 300 three body interactions. We have been able to mainly investigate only the experimental side of the problem. The theoretical aspects can be tackled by approaching the problem in two ways.

The black-box approach described and used in chapter 6 evaluates the quenching effects of the impurities in a simple but quantitative way and works remarkably well despite the very simplified nature of approach to the problem. This shows that interaction between the impurities is negligible, and that their effects are roughly in proportion to their partial pressures.

The second way of solving the problem is the exact approach of solving the rate equations relating to all the processes going on in the laser. Such a simulation of the whole system is a very complicated process as shown by the problem of CO_2 lasers (Smith and Thomson 1978). Apart from this, many of the rate constants for reactions involving species like Si, Kr, CO_2 etc are not known and have to be determined before the model can be successfully used. However such simulations would be able to predict long life behaviour of systems much more confidently.

The results reported in this thesis can now be used to design a laser with a long gas lifetime by the choice of appropriate materials of construction. Such a laser is described in detail in Appendix A.4.

REFERENCES

Beck A.H (Ed.)(1964) Handbook of Vacuum Physics, Vol 3, Part 4, Pergamon Press, Oxford.

Duval B (1983) PhD Thesis, University of St Andrews, U.K.

Espe W (1966) Materials of High Voltage Technology, Vol 1, Pergamon Press, Oxford.

McDowell C.A, Ed. (1963) Mass Spectrometry, McGraw-Hill, New York.

Smith K and Thomson R.M (1978) Computer Modeling of Gas Lasers, Plenum Press, New York and London.

Appendix A.1

The computer programme given here can be used to find the partial pressures of individual components in a gas mixture provided the cracking patterns of the suspected components are known. The calculation is done under the assumption that the mass spectrometer has equal sensitivity to all the components. The calculated partial pressures are expressed in relation to the pressure of He in the mixture. The input data is taken from the x-y plot of ion current in mbar units vs m/e output of the Supavac mass spectrometer. The data along with a scaling constant to convert the values to pressure in mbar units is stored in file FOR009.DAT. The output appears on the terminal and is also stored in SPECOUT.DAT. If necessary the programme generates data for the plotting programme given in Appendix A.3. This data is stored in PLOTDATA.DAT.

The subroutine F04JGF solves the system of m linear simultaneous equations in n unknowns using a least square method. (For more details of this subroutine see NAG library documentation prepared by the Numerical Algorithms Group.) The n unknowns are the partial pressures $p_1, p_2, \ldots, p_n$ of the n components in the mixture and the m equations are the heights H_i at each m/e in the range 0-130 expressed as

$$H_i = h_{i1}p_1 + h_{i2}p_2 + \ldots + h_{ij}p_j + \ldots + h_{in}p_n$$

where i takes the value from 1 to m and h_{ij} is the contribution to the height due to the component j at m/e = i with the base peak for

that component taken as 100. This is essentially the cracking pattern for that component.

The programme and output listings are self-explanatary.

```
14-Apr-1983 14:08:50        VAX-11 FORTRAN V3.1-23
14-Apr-1983 14:08:21        USER1:[PHRTG]MSPEC.FOR;6

0001    c  This program fits the given mass spectrum
           for the given compounds
0002    c  using a least square solution of linear
           simultaneous equations.
0003    c  The cracking patterns are stored in f007.dat.
0004       implicit real*8 (a-h,o-z)
0005       integer ticurve
0006       character*6 cname(30)
0007       character*52 title
0008       dimension  height(130,50),b(130),massno(50),xht(10),
0009       1          xmassht(50),lmassno(10),work(200),bx(130),
0010       2       calcht(130),height2(130,50),massout(130)
                      ,outht(130)
0011       logical svd
0012    c
0013    c
0014       write(5,555)
0015    555        format(' data input, return 5 for terminal,
                9 for for009 : '$)
0016       read *, mdata
0017       ngraph=0
0018       write(5,556)
0019    556        format(' return 1 if graph required: ',$)
0020       read *,ngraph
0021       if(ngraph.eq.1)open (unit=3,file='plotdata.dat',
0022       1     status='new')
0023       open(unit=12,file='specout.dat',status='new')
0024    5  write(5,1)
0025    1  format(' Spectrum No.  and time: ',$)
0026       read(mdata,*)title,ticurve
0027       write(5,15)
0028    15 format(' No. of peaks in the sample spectrum:'$)
0029       read(mdata, *) n
0030       write(5,25)
0031    25 format(' Mass nos. and mass heights of sample spectrum:'$)
0032       read (mdata,*) (massno(i),xmassht(i),i=1,n)
0033       y=vmax(xmassht,n)
0034            write (5,111)y
0035    111        format(' Peak value in spectrum:'f8.2/)
0036       write(5,278)
0037    278        format(' He peak height in same units: '$)
0038       read(mdata, *)heht
0039       do 210 i=1,n
0040       xmassht(i)=xmassht(i)/heht*1000.0
0041    210        continue
```

```
0042        write(5,112)title,ticurve,heht
0043        write(12,112)title,ticurve,heht
0044      112       format(//65('+')/1x,a52,2x,'time:',i4,/,
0045        1' Helium height:',2x,1pg10.3/)
0046        if(ngraph.ne.1)go to 558
0047        write(5,557)
0048      557       format(' curveno, pointno: ',$)
0049        read *,ncurve,npoint
0050      558       write (5,279)(massno(i),xmassht(i),i=1,n)
0051        write (12,279)(massno(i),xmassht(i),i=1,n)
0052      279       format(/' m/e and magnitudes as parts per
                  thousand of He hei
0053        1ght'//4(5x,i3,2x,1pg10.3))
0054        do 6 i=1,130
0055        do 6 j=1,50
0056        b(i)=0.0
0057        height(i,j)=0.0
0058      6 continue
0059        do 40 i=1,n
0060        b(massno(i))=xmassht(i)*100
0061        bx(massno(i))=xmassht(i)*heht/1000.
0062      40 continue
0063        jx=1
0064        rewind 7
0065      50 read(7,65,end=100)cname(jx)
0066      65 format(a6)
0067        read(7,375)(lmassno(i),i=1,10)
0068      375       format(10(i3,1x))
0069        read(7,385)(xht(i),i=1,10)
0070      385       format(10(f4.0,1x))
0071        do 300 i=1,10
0072        if(lmassno(i).eq.0)go to 300
0073        height(lmassno(i),jx)=xht(i)
0074        height2(lmassno(i),jx)=xht(i)
0075      300       continue
0076        jx=jx+1
0077        go to 50
0078      100       m=130
0079        jx=jx-1
0080        lwork=4*jx
0081        ifail=0
0082        nra=m
0083        tol=.00001
0084        call f04jgf(m,jx,height,m,b,tol,svd,sigma,irank,
0085        1           work,lwork,ifail)
0086        if(ifail.ne.0)go to 150
0087        write(5,125)
0088        write(12,125)
0089        if(ngraph.eq.1)write(3,1250)ncurve,npoint,jx,ticurve
0090      1250      format(5x,3i3,i4)
0091      125       format(//'   Compound',t15,'Calc value',t30,'Rel
                  value'/t15,
0092        1  'ppt of He'/)
```

```
0093        bmax=vmax(b,jx)
0094        do 130 i=1,jx
0095        if(ngraph.eq.1)write(3,1350)cname(i),b(i)
0096     1350        format(5x,a6,e11.4)
0097        write(5,135)cname(i),b(i),b(i)/bmax
0098        write(12,135)cname(i),b(i),b(i)/bmax
0099     135         format(5x,a6,3x,1pg10.3,5x,1pg10.3)
0100     130         continue
0101        write(12,145)sigma,svd,irank
0102        write(5,145)sigma,svd,irank
0103     145         format(//' Standard error:',1pg10.3,' SVD:',13,4x,
0104        1  ' IRANK:',i3,//65('+')/)
0105        write(5,950)
0106        write(12,950)
0107     950         format(/' Calculated(measured) mass spectrum,
                  heights(in mm) < 5
0108        1  omitted:'//)
0109        do 1156 mx=1,m
0110        calcht(mx)=0.
0111        do 1155 j=1,jx
0112        if(height2(mx,j).eq.0.)go to 1155
0113        calcht(mx)=calcht(mx)+height2(mx,j)*b(j)
0114     1155        continue
0115        calcht(mx)=calcht(mx)*heht*1.0e-5
0116     1156        continue
0117        jcount=1
0118        do 999 i=1,m
0119        massout(jcount+1)=0.
0120        outht(jcount+1)=0.
0121        if(calcht(i).lt.5)go to 999
0122        massout(jcount)=i
0123        outht(jcount)=calcht(i)
0124        jcount=jcount+1
0125     999         continue
0126        write(5,988)(massout(jc),outht(jc),
0127        1bx(massout(jc)),jc=1,jcount)
0128        write(12,988)(massout(jc),outht(jc),bx(massout(jc)),
0129        1jc=1,jcount)
0130     988         format(3(1x,i4,':',f8.3,'(',f6.1,')',2x))
0131              go to 140
0132     150         write(5,175)ifail
0133     175         format(' ifail=',i2)
0134     140         write(5,155)
0135     155         format(' Type 0 to stop,
0136        1  2 for fresh data:'$)
0137        read *, ixx
0138        if(ixx.eq.0) stop
0139        if(ixx.eq.2) go to 5
0140        close (unit=3)
0141        close(unit=12)
0142        stop
0143        end
0001        function vmax(array,n)
```

```
0002        real*8 array(n),vmax,x
0003        x=array(1)
0004        do 10 i=2,n
0005     10 if(x.lt.array(i))x=array(i)
0006        vmax=x
0007        return
0008        end
```

++

Kr1/1:13-9-82(1505) Basic mix before lasing time: 18
Helium height: 6.600E+04

m/e and magnitudes as parts per thousand of He height

2	1.32	12	9.091E-02	14	6.818E-02
16	0.158				
17	0.333	18	1.42	20	6.21
28	2.58				
29	7.576E-02	30	9.091E-02	32	0.212
35	6.061E-02				
36	0.106	38	0.970	44	1.79
47	0.129				
64	0.100	66	0.114	69	0.273
127	7.576E-02				

Compound	Calc value ppt of He	Rel value
H2	1.32	0.212
Kr	7.892E-04	1.270E-04
HCl	0.108	1.737E-02
H2S	1.975E-05	3.180E-06
SO2	8.667E-02	1.395E-02
SOF2	-6.213E-03	-1.000E-03
COS	-2.010E-04	-3.236E-05
NF3	5.130E-04	8.258E-05
OF2	2.876E-02	4.630E-03
SO2F2	1.963E-04	3.160E-05
COF2	0.137	2.205E-02
CF4	0.271	4.359E-02
O2	0.207	3.338E-02
N2	1.07	0.172
Ar	-6.945E-06	-1.118E-06
H2O	1.43	0.230
CO	1.30	0.209
CO2	1.79	0.288
SF6	6.902E-02	1.111E-02
SiF4	-1.473E-05	-2.370E-06
NO	7.980E-02	1.285E-02
NO2	1.166E-02	1.876E-03
HF	6.21	1.00
F2	0.935	0.151

Standard error: 0.845 SVD: F IRANK: 24

++

Calculated(measured) mass spectrum, heights(in mm) < 5 omitted:

2:	87.000(87.0)	12:	5.840(6.0)	16:	9.965(10.4)
17:	19.836(22.0)	18:	94.459(94.0)	20:	410.000(410.0)
28:	170.046(170.0)	30:	6.036(6.0)	32:	14.030(14.0)
36:	7.124(7.0)	38:	64.000(64.0)	44:	118.024(118.0)
47:	9.041(8.5)	64:	5.721(6.6)	66:	6.614(7.5)
69:	17.850(18.0)	0:	0.000(0.0)		

++

Appendix A.2

The programme given in this appendix calculates all the possible combinations of a given list of elements to give compounds of given molecular weights. These compounds can be used as a guide to identify the molecular species giving rise to various unidentified m/e peaks in the mass spectrum.

```
14-Apr-1983 16:55:17       VAX-11 FORTRAN V3.1-23
16:22:23   USER1:[PHRTG]COMPO.FOR;75

0001        character*2 atom(8),element(15),charv(8),charvj,atomx
0002        character cstring*80,letter*1,blank*80
0003        character*24 compound(50,15),comp
0004             dimension mastrial(15),elwt(15),valen(8),
                 v(8),vlist(15),mass(8)
0005        dimension nvalue(15)
0006        data element/'O','Cl','F','N','H','C',
                 'Si','S','Al','Br','I','Cs',
0007        1 'Fe','K','Na'/
0008        data charv/' ','2','3','4','5','6','7','8'/
0009     c  Valency list for the elements
0010        data vlist/4,6,6,3,8,4,4,3,3,4,4,3,3,1,1/
0011     c  atomic weights of elements
0012        data elwt/16,35,19,14,1,12,28,32,27,80,127,133,56,39,23/
0013        data compound /750*' '/
0014        data blank /' '/
0015             integer elwt,valen,vtot,v,vj,vlist,cell
0016     5  write(6,15)
0017     15 format(' No. of elements:'$)
0018        read *,nmass
0019     c  Input element names as in element list
0020        write(6,25)
0021     25 format(' element names:'$)
0022        read *,(atom(i),i=1,nmass)
0023        icount=0
0024        do 40 i=1,15
0025        do 40 nmasx=1,nmass
0026        if(atom(nmasx).ne.element(i))go to40
0027        icount=icount+1
0028        mass(icount)=elwt(i)
0029        valen(icount)=vlist(i)
0030        atomx=atom(icount)
0031        atom(icount)=atom(nmasx)
0032        atom(nmasx)=atomx
0033     40 continue
0034        if(icount.ne.nmass)go to 50
0035        go to 60
0036     50 write(6,55)
0037     55 format(' One or more of the elements not in stored list')
0038        go to 200
0039     60 write(6,35)
```

```
0040    35 format(' No. of compounds:'$)
0041       read *,ntrial
0042       write(6,45)
0043    45 format(' Compound weights:'$)
0044       read *,(mastrial(i),i=1,ntrial)
0045       do 700 i=1,50
0046       do 700 j=1,15
0047    700          compound(i,j)=blank
0048       comp=blank
0049    c
0050    c
0051       nval=1
0052       vtot=1
0053       do 80 cell=1,nmass
0054    80       v(cell)=0
0055              do 70 i=1,nmass
0056    70 vtot=vtot*(valen(i)+1)
0057       do 170 k=1,15
0058    170          nvalue(k)=1
0059       do 120 loop=1,vtot
0060       mtot=0
0061       do 90 nmasx=1,nmass
0062    90 mtot=v(nmasx)*mass(nmasx)+mtot
0063       do 130 k=1,ntrial
0064       cstring=blank
0065       if(mtot.ne.mastrial(k)) go to 130
0066       do 150 j=1,nmass
0067       vj=v(j)
0068       if(vj.eq.0)go to 150
0069       if(vj.eq.1)go to 180
0070       charvj=charv(vj)
0071       cstring=atom(j)//charv(vj)//cstring
0072       go to 150
0073    180          cstring=atom(j)//cstring
0074    150          continue
0075       lcount=0
0076       do 210 i=1,80
0077       letter=cstring(i:i)
0078       if (ichar(letter).eq.32)go to 210
0079       lcount=lcount+1
0080       comp(lcount:lcount)=letter
0081    210          continue
0082       compound(nvalue(k),k)=comp
0083       comp=blank
0084       nvalue(k)=nvalue(k)+1
0085    130          continue
0086       v(1)=v(1)+1
0087       do 110 cell=1,nmass-1
0088       if (v(cell).gt.valen(cell))go to 100
0089       go to 110
0090    100          v(cell+1)=v(cell+1)+1
0091       v(cell)=0
0092    110          continue
```

```
0093    120         continue
0094    c
0095    c
0096       listno=nvalue(1)
0097       do 123 k=2,15
0098    123         if(nvalue(k).gt.listno)listno=nvalue(k)
0099    125         write(6,65)(atom(i),i=1,nmass)
0100    65 format(///' Permuted compound list for the elements:',10A3/)
0101       write(6,75)
0102    75 format(' Mol.wt and Compounds')
0103       write(6,85)(mastrial(j),j=1,ntrial)
0104    85 format(' Mol. wt. :'  /(10(i4,7x)))
0105       do 175 i=1,listno
0106       write(6,135)(compound(i,j),j=1,ntrial)
0107    135         format(1x,10a11)
0108    175         continue
0109    200         write(6,95)
0110    95 format(' want more?   0 for no, 9 for same elements, nonzero
0111       1 for yes: '$)
0112       read *,nans
0113       if(nans.eq.0)stop
0114       if (nans.eq.9)go to 60
0115       go to 5
0116       end
```

```
Permuted compound list for the elements: O  F  N  C  Si
Mol.wt and Compounds
Mol. wt. :
 44          66          69          85          104         119
N2O         N2F2        CF3         N2F3        N2F4        NF3O3
CO2         CF2O        C3NF        CF3O        CF4O        C2F5
SiO         C2N3                    C2N3F       CN2O4       C2N2FO3
            C3NO                    C3NFO       C2N3F2      C3FO4
            SiF2                    SiF3        C3NF2O      C4NF3
            SiC2N                   SiC2NF      SiF4        SiCN2FO2
                                                SiN2O3      SiC2FO3
                                                SiCO4       Si2N2FO
                                                SiC2NF2     Si2CFO2
                                                SiC4N2      Si3FO
                                                Si2O3
                                                Si2C4
```

Appendix A.3

This programme plots the evolution of the partial pressures of various compounds identified in the mass spectrum. The input for this programme is stored in PLOTDATA.DAT. For more details see Appendix 1. A sample output curve is given in figure A.1 . The programme is self explanatory. The GHOST-80 subroutine package is used for plotting. Details on using the package are available at the Computing center of St.Andrews University.

```
15-Apr-1983 12:07:01        VAX-11 FORTRAN V3.1-23
15-Apr-1983 12:01:46        USER1:[PHRTG]APP3.FOR;1

0001        dimension time(7,4,10), prsr(7,4,10),cx(2)
0002        character*6 cname(30),compound
0003        integer ticurve
0004        write(5,111)
0005    111         format(' number of compounds to be
                  plotted(9 max):',$)
0006    c   No. of compounds upto 9.
0007        read *,ncomp
0008        write(5,222)
0009    222         format(' compound names:',$)
0010        read *,(cname(i),i=1,ncomp)
0011        open (unit=11,file='scratch',status='new')
0012        do 1122 i=1,ncomp
0013        write(11,1240)cname(i)
0014    1240        format(5x,6a,2x)
0015    1122        continue
0016    c
0017    c    No. of curves limited to four.
0018    c    No error message given if compound name is not available
0019    c    in list
0020    c    Next read supplies label for the point at time=ticurve.
0021    c
0022    c   ncurve=no of curve,npoint=no of point in each curve,
0023    c   ncomplist=no of compounds in each list in unit 3.
0024    c   No. of points upto 7.
0025    c
0026        rewind 11
0027        open (unit=3,file='plotdata.dat',status='old')
0028        ncumax=1
0029        npoimax=1
0030    970         read(3,70,end=740)ncurve,npoint,ncomplist,ticurve
0031        if(ncurve.gt.ncumax)ncumax=ncurve
0032        if(npoint.gt.npoimax)npoimax=npoint
0033    70 format(5x,3i3,i4)
0034        do 1100 ii=1,ncomplist
0035        read(3,80,end=740)compound,pressure
0036    80 format(5x,a6,e11.4)
0037        do 1000 i=1,ncomp
0038        if(cname(i).eq.compound)go to 990
```

```
0039    1000        continue
0040    990         time(npoint,ncurve,i)=ticurve
0041       prsr(npoint,ncurve,i)=pressure
0042    1100        continue
0043       go to 970
0044    740         nco=1
0045       call paper (1)
0046    750         ncoframe=1
0047       call pspace(.1,.6,.1,.46)
0048    5  xm1=0
0049       xm2=vmax(time,npoimax,ncumax,nco)
0050       ym1=0
0051       ym2=vmax(prsr,npoimax,ncumax,nco)
0052       call map(xm1,xm2,ym1,ym2)
0053       dy=5
0054       if(ym2.lt.10)dy=2
0055       if(ym2.lt.5)dy=1
0056       if(ym2.lt.2)dy=.5
0057       if(ym2.lt.1)dy=.1
0058       if(ym2.lt.0.1)dy=0.01
0059       dx=25
0060       if(xm2.lt.100)dx=10
0061       call scalsi(dx,dy)
0062       call border
0063       read(11,199)cx(1),cx(2)
0064    199         format(5x,2a4)
0065       call pcscen(.5*xm2,-.14*ym2,'TIME ( MINUTES )',17)
0066       call pcscen(.9*xm2,1.05*ym2,cx,8)
0067       call ctrori(90.)
0068       call pcscen(-.1*xm2,.5*ym2,'PRESSURE ( PPT OF He )',22)
0069       call ctrori(0.0)
0070       ncu=1
0071    100         if(ncu.eq.4)go to 33
0072       if(ncu-2)10,20,30
0073    10 n1=0
0074       n2=0
0075       n3=0
0076       n4=0
0077       nochar=224
0078       go to 40
0079    20 n1=10
0080       n2=10
0081       n3=10
0082       n4=10
0083       nochar=248
0084       go to 40
0085    30 n1=1
0086       n2=10
0087       n3=1
0088       n4=10
0089       nochar=229
0090       go to 40
0091    33 n1=10
```

```
0092        n2=10
0093        n3=1
0094        n4=10
0095        nochar=215
0096     40 call broken(n1,n2,n3,n4)
0097        call positn(time(1,ncu,nco),prsr(1,ncu,nco))
0098        call plotnc(time(1,ncu,nco),prsr(1,ncu,nco),nochar)
0099        do 50 i=2,7
0100        if(time(i,ncu,nco).eq.0.and.prsr(i,ncu,nco).eq.0.)go to 54
0101        call join(time(i,ncu,nco),prsr(i,ncu,nco))
0102        call plotnc(time(i,ncu,nco),prsr(i,ncu,nco),nochar)
0103     50 continue
0104     54 if(ncu.eq.ncurve)go to 110
0105        ncu=ncu+1
0106        go to  100
0107    110         call full
0108        if(ncoframe.eq.2)go to 120
0109        if(nco.eq.ncomp)go to 130
0110        nco=nco+1
0111        ncoframe=2
0112        call pspace (.1,.6,.6,.96)
0113        go to 5
0114    120         if(nco.eq.ncomp)go to 130
0115        nco=nco+1
0116        call frame
0117        go to 750
0118    130         call grend
0119        close (unit=3)
0120        close (unit=11,status='delete')
0121        stop
0122        end

0001        function vmax(array,npoint,ncurve,nco)
0002        real array(7,4,10)
0003        x=array(1,1,nco)
0004        do 10 i=1,npoint
0005        do 10 j=1,ncurve
0006     10 if(x.lt.array(i,j,nco))x=array(i,j,nco)
0007        vmax=x
0008        return
0009        end
```

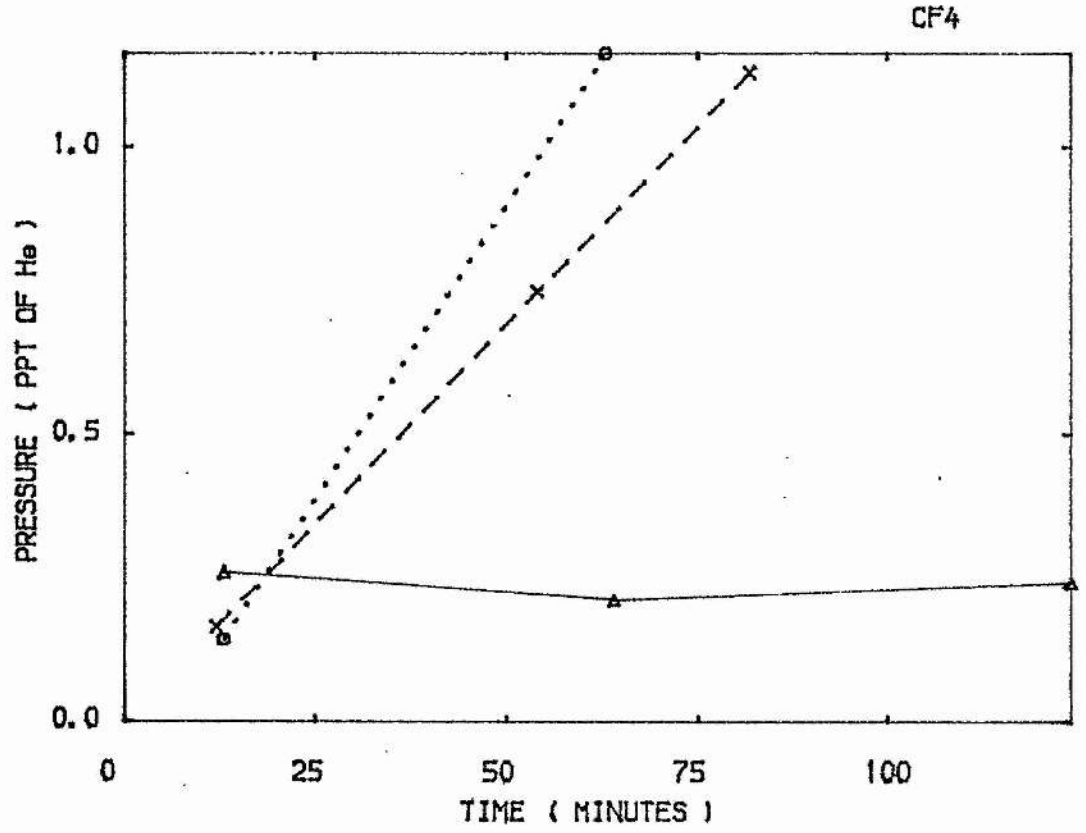
CF4
1.0
0.5
0.0
PRESSURE (PPT OF He)
0
25
50
75
100
TIME (MINUTES)

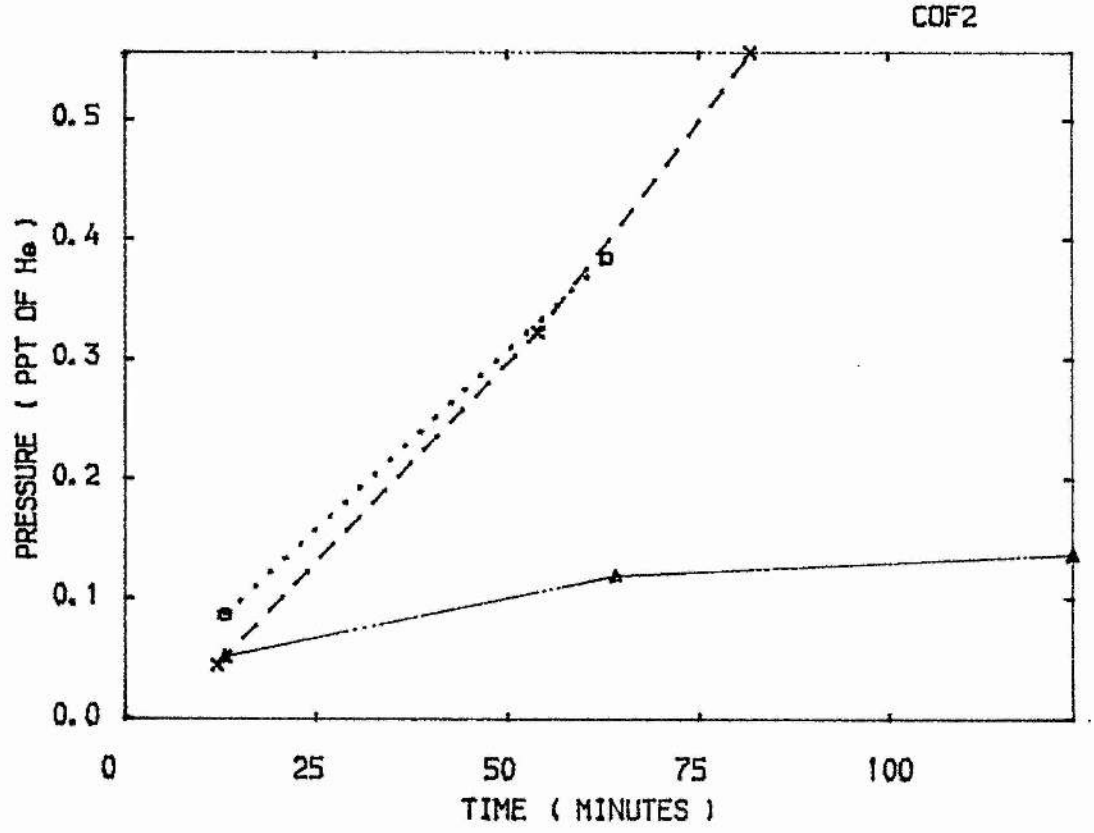
COF2
0.5
0.4
0.3
0.2
0.1
0.0
PRESSURE (PPT OF He)
0
25
50
75
100
TIME (MINUTES)

Appendix A.4 : Design of a long lifetime single fill laser

Using results from the study of the laser versions described in this thesis the following design is proposed for a transverse discharge high pressure gas laser using F_2 as one of the components. A full-size cross sectional view of the laser is given in figure A.1a. The laser consists basically of two metal tubes A and B with a mean diameter of 80 mm and length 500 mm, and separated by 3 mm. This gap is filled with distilled deionized water to form an integral water capacitor of about 30 nf. The material for A can be stainless steel or Al while B is preferably Ni, monel or stainless steel. The type of monel or stainless steel, or nickel chosen is important. They should not contain Si or C, or have dissolved gases. In this respect electrolytic Ni is the best material (Espe 1966). Monel alloy types available commercially are worse than stainless steel in that it contains higher amounts of Si and C than the best stainless steel. The stainless steel alloy Type 304 from Stahl, USA (Type V2A) contains less than 0.08% C and no Si and is the preferred stainless steel for use in the laser. However, for the electrodes and the corona wire, pure Ni is the best choice since it has very little dissolved gases and no Si or C (Espe 1966). Electrolytic coating of the inner tube B and the end plates with Ni might be useful in reducing any residual outgassing from the metal.

The top electrode is insulated from B by the minimum amount of PTFE possible. The PTFE is hidden from uv radiation by being behind the electrode, thus reducing the possibility of reaction with F_2 in the presence of uv photons. Metal plates are used at both ends to seal off the system. The end windows made of CaF_2 are attached to these plates using viton or PTFE O-rings (see figure A.1b). This arrangement has several advantages. The use of a minimum amount of PTFE and viton reduces the possibility of production of CO_2 and other gases and thus reduces F_2 reactions. The metal surroundings help in reducing the radiation of electrical noise from the discharge. The whole system can be baked to at least 200°C if viton is used. If the plastics can be substituted with an alumina ceramic (not containing Si) with proper metal ceramic seals, the baking can be done at temperatures up to 1000°C. Baking under vacuum efficiently outgasses the system, reducing contamination of the gas fill.

The Ni electrode attached to A is properly contoured to avoid arcing to B. The electrode attached to B is made of Ni mesh. The four Ni corona wires behind the mesh are 0.1 to 0.3 mm in diameter and are attached to the two common ceramic feedthroughs on the end plates. The feedthrough plate F attached to B is insulated from A and sealed between A and B using nylon and an appropriate soft seal. (The insulators in the figures are shaded.) The electrode attached to A is sealed using viton O-rings if PTFE is used as shown by the dark circles in the diagram. If ceramic is used, metal-ceramic seals can eliminate the use of O-rings. The water

capacitor electrode spacing is maintained at 3 mm with spacer rings at both ends. They are sealed against A and B using neoprene O ring seals. The gas ports are attached to the end plates.

The electrical circuit for the laser is given in figure A.2 The C-C transfer type of circuit (see section 2.2) is chosen partly because the peaking capacitor uses water as the dielectric and can thus be used only under pulse charged conditions. However this circuit configuration is a minimum inductance low impedence design due to the compact nature of the cylindrical H_2O capacitor. Properly deionized water can take up to 600 kV/cm (Levatter and Bradford 1978) so this laser should work safely up to 180 kV provided the seperators are suitably chosen and the capacitors are spaced properly to avoid air breakdown. Water capacitor lasers have proved to be reliable and efficient in excimer lasers (Levatter and Bradford 1978, Lin and Levatter 1979). The charging capacitor array is connected to the water capacitor in a minimum inductance loop through a thyratron switch using copper plates bolted on to the feedthrough plate attached to B (not shown in the figure). Use of the thyratron increases the reliability in switching and the repetition rate of the laser compared to a spark gap switch used for results reported here. The whole assembly is compact and easily demountable. The corona wire is pulsed using two cables of about 2 nf capacitance, each connected to either end of the corona wires and switched by the same thyratron. This avoids jitter and the use of a separate switch (see section 2.3). Use of coaxial cables, because of their low inductance and high impedence, decreased the risetime of the corona pulse and prevents

arcing from the corona wire to the mesh electrode. We chose the mesh electrode design since it was found to be best for uniformily preionizing the discharge gap (see section 2.3). The distance between the electrodes is smaller than between the electrodes and the walls. This along with the preionization would confine the discharge to the region between the electrodes (Hasson and Bergmann 1980).

The gases used are to be as pure as possible. Helium should be the purest, since it is used in the largest quantity. Helium and Kr can be obtained with >99.999% purity. The purity of F_2 obtained commercially is only about 98% and so has to be purified further. This, as seen from the cold trap experiments is best done by using a liquid N_2 cold trap to trap out CF_4, COF_2, SF_6, SO_2, H_2O, HF, SiF_4 etc. The laser is first evacuated and baked before filling with the purified gases. A gas reservoir made of the same metal as the inner tube B can be used to increase the gas volume and thus decrease time between fills.

This proposed design, based on the results reported in this thesis, is expected to give a greatly improved lifetime and a greater number of pulses without fall in energy for the He-F_2 and He-Kr-F_2 gas mixes. The same design can also be probably used for other excimer lasers using F_2 or HCl as the halogen donors.

Figures.A.1a and b

Constructional details of a long-life KrF and F_2 laser.

a. Full scale cross sectional view

b. Full scale cross section along axis. Electrodes not shown in b.

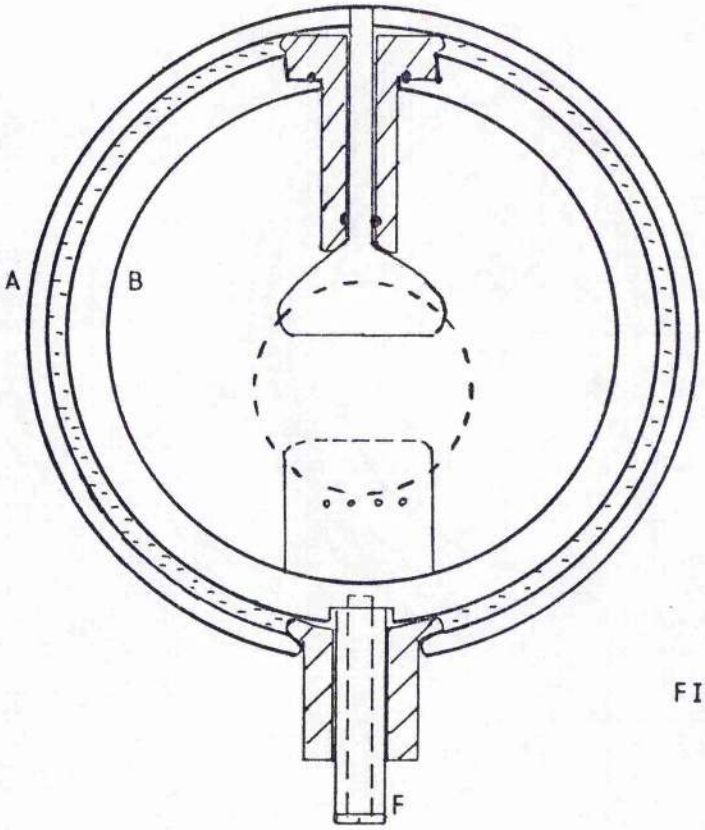

FIG A.1a

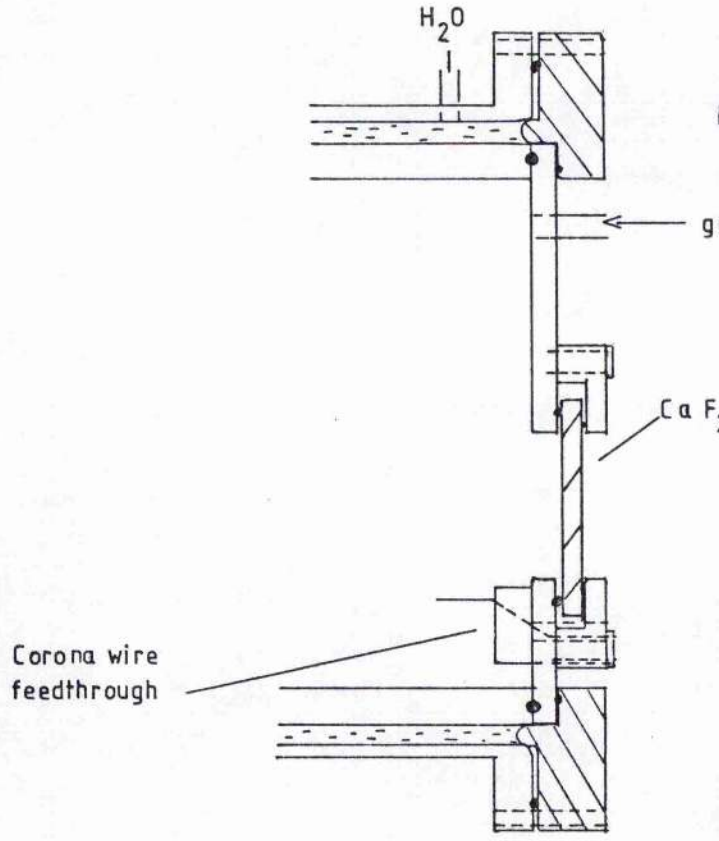

FIG A.1b

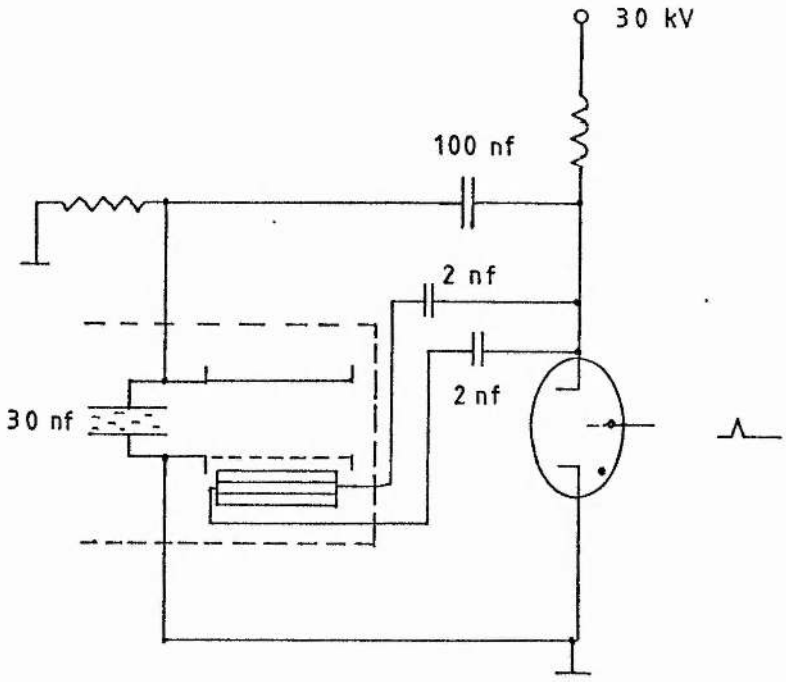

FIG A.2 C-C transfer laser excitation circuit for the long-life laser using a thyratron switch.

REFERENCES

Espe W (1966) Materials of High Voltage Technology, Vol 1,
Pergamon Press, Oxford.

Levatter J.I and Bradford Jr. R.S (1978)
Appl.Phys.Lett. 33 742.

Lin S.C and Levatter J.I (1979)
Appl.Phys.Lett. 34 505.